The interpretation of magnetic anomalies between Iceland and Scotland

Alan David Ingles

THE INTERPRETATION OF

MAGNETIC ANOMALIES BETWEEN

ICELAND AND SCOTLAND

A Thesis submitted for the Degree of

Doctor of Philosophy

in the

University of Durham

BY

ALAN DAVID INGLES

Graduate Society

September, 1971.

ABSTRACT

The collection of data and the results of a detailed magnetic survey on the crest of the Iceland-Faeroes Rise are described.

A matrix method is developed to transform gravity anomalies to magnetic anomalies, and vice versa, to determine the ratio of magnetism to density in an equivalent layer, to solve for the angle of magnetisation of a body causing a magnetic anomaly and to separate magnetic anomalies caused by different types of source body.

The data from the detailed survey area are interpreted as supporting the conclusions of previous authors that the crustal structure of the Iceland-Faeroes Rise is highly anomalous for an oceanic setting, and is similar to that of Iceland, with at least two magnetic layers which contain central intrusive complexes; granitic rocks may also be present.

The matrix methods developed in the first part of this work are used to interpret gravity and magnetic data from a previous Durham survey on the Iceland-Faeroes Rise. Results indicate that the magnetic anomalies are controlled by seismic structure on NE - SW profiles, but include a component which is independent of seismic structure which is of greater significance on NW - SE profiles. The latter component is identified as magnetisation changes as a function of time.

Magnetic and gravity anomalies from the Scottish Continental Shelf region are used to demonstrate further the scope of the matrix methods for combined analysis of gravity and magnetic anomalies.

ACKNOWLEDGEMENTS.

I would like to thank Professors G.M. Brown and M.H.P. Bott for providing facilities for this work, and Professor M.H.P. Bott for his supervision.

I am grateful to the officers and crew of m.v. Arran Firth and R.R.S. John Murray, and to the members of the geology department, University of Durham, for their help during survey work. I am also grateful to Dr. U. Fleischer for providing bathymetric, gravimetric and magnetic contour maps for the southern part of Iceland - Faeroes Rise, which were obtained from the survey work of the Deutsches Hydrographisches Institut at Hamburg.

The work was financed by a N.E.R.C. Research Studentship.

CONTENTS

CHAPTER 1.

INTRODUCTION ....1.

1.1 Marine magnetic anomalies, sea-floor spreading and the North Atlantic ....1.

1.2. The setting of the Iceland-Faeroes Rise ....4.

1.2.1 Sea-floor spreading histories ....4.

1.2.2 Magnetic anomalies ....7.

1.2.3 Bathymetry and seismic reflection profiling ....9.

1.2.4 Age dating and petrology ....10.

1.2.5 Seismic refraction and gravity measurements 13

CHAPTER 2.

COLLECTION, REDUCTION AND DESCRIPTION OF SURVEY DATA 17

2.1 Collection of data, survey procedure ....17.

2.2 Correction and reduction of data ....18.

2.3 Presentation and description of survey results ....28.

2.3.1 Stacked total field profiles ....29.

2.3.2 The contour maps ....32.

2.3.3 Summary and discussion of trends ....36.

CHAPTER 3.

METHODS FOR THE INTERPRETATION OF MAGNETIC DATA 40

3.1 Methods developed by previous workers 40

3.1.1 The indirect method ....41.

3.1.2 Non-linear optimisation, a direct method ....42.

3.1.3 The linear inverse method, a direct method ....44.

3.2 The development of methods for the joint analysis of gravity and magnetic anomalies by the linear inverse technique ....49.

3.2.1 The Poisson formula and its application ....50.

3.2.2 Development of the linear inverse method to perform Poisson type analyses ... 53.

3.2.2.1. The transformation of anomalies ... 55.

3.2.2.2 The direct calculation of the ratio p/J or J/p ... 57.

3.2.2.3 Calculation of the angle of magnetisation ... 59.

3.2.3 The programmed versions of the methods and their application to test models ... 63.

3.2.3.1 Basic transform programs TR/GM and TR/MG ... 64.

3.2.3.2 Direct calculation of J/p and p/J by use of programs JG/RAT and GJ/RAT ... 79.

3.2.3.3 Calculation of the angle of magnetisation program SBETA ... 80.

3.2.4 Application of the transform programs to separate magnetic anomalies ... 84.

3.2.5 The importance of the regional field ... 88.

3.3 The two-dimensional approximation in quantitative interpretation ... 89.

CHAPTER 4.

INTERPRETATION OF DATA FROM THE ICELAND-FAEROES RISE 91

4.1 Interpretation of magnetic data from the survey of m.v. Arran Firth, 1969 ... 91.

4.1.1 The regional magnetic high in the west of the survey area ... 92.

4.1.1.1 An interpretation in terms of body geometry ... 98.

4.1.2 The interpretation of high amplitude, relatively isolated anomalies ... 104.

4.1.3 The eastern section of variable magnetic anomalies ... 108.

4.1.4 Discussion ... 111.

4.1.5 Summary of conclusions ... 116.

4.2 Interpretation of data from the survey of R.R.S. John Murray, 1967 ..117.

4.2.1 Interpretation of line K ..117.

4.2.1.1 Transformation of anomalies and the ratio p/J 119 .....

4.2.2 Interpretation of data from line C ..125.

4.2.3 Conclusions ..126.

4.3 General discussion and recommendations ..127.

CHAPTER 5.

GRAVITY AND MAGNETIC ANOMALIES OF THE SCOTTISH CONTINENTAL SHELF AREA. 130

5.1 The Faeroes-Shetland Channel ..130.

5.2 The Hebridean-Shetland Shelf gravity high 'A' ..133.

5.3 Gravity low 'F', south-west of Shetland ..137.

REFERENCES ..140.

APPENDICES .....

CHAPTER ONE

INTRODUCTION

The subject of this thesis is mainly that of the presentation and interpretation of magnetic anomalies on the Iceland-Faeroes Rise. Data used in the interpretations were collected during two geophysical surveys conducted by the Geology department of the University of Durham: the first, in July, 1967, was based mainly on widely spaced NW - SE tracks, along the crest of the Iceland-Faeroes Rise and into the Norwegian Sea, covered by R.R.V. John Murray; the second survey was conducted in July, 1969, from m.v. Arran Firth, and consisted of closely spaced E - W tracks in a small area on the crest of the Iceland-Faeroes Rise. During the first survey, gravimetric data were also recorded, and the first phase of the second survey was devoted to seismic refraction lines, on the Rise and in deeper water to the south of Iceland. Interest in the origin of the Iceland-Faeroes Rise is due to its obscure significance in the evolution of the northeast Atlantic Ocean by sea-floor spreading.

1.1 Marine magnetic anomalies, sea-floor spreading and the North Atlantic.

The spreading history and age of an ocean basin are usually determined from a study of the typical linear magnetic anomalies which were first observed in the northeast Pacific by Mason and Raff (Mason, 1958; Mason and Raff, 1961) and, subsequently, by other authors in all the major oceans (Pitman and Heirtzler, 1966; Heirtzler et al., 1966; Pitman and Heirtzler, 1968; Dickson

et al., 1968; Godby et al., 1968; Avery et al., 1968; Le Pichon and Heirtzler, 1968). Use of these anomalies in the study of ocean basin evolution depends on the assumption that they are caused by the presence of positive and negative remanent magnetisations (Vine and Matthews, 1963). The hypothesis of Vine and Matthews states that the linear strips of positive and negative magnetic anomalies form a record of geomagnetic field polarity reversals, from the time of the initial opening of an ocean to the present day. The record is built up as a sequence of thermo-remanent magnetisations within basaltic additions to the oceanic crust as they cool through the Curie temperature point. Thus, the linear magnetic anomalies of the Raff-Mason type are isochrons, with a strike direction perpendicular to the resultant direction of spreading of a particular region of the ocean floor.

The linear magnetic anomalies themselves have been recognised to exhibit symmetry in distribution about the axes of mid-ocean ridge systems on profiles perpendicular to the strike of the ridges. Each major component of this symmetry is identified by a number based on a convention established by Pitman et al. (1968), and each number has been assigned an age on the time scale of Heirtzler et al. (1968), or modifications of this time scale. Thus, the determination of the spreading history of a particular oceanic area depends on the recognition of the numbered sequence of anomalies, or by correlation of the magnetic anomaly pattern with that of an area for which a spreading history has been established.

In relating the evolution of an ocean basin to the concept of sea-floor spreading it is often necessary to consider the effects

of various disturbing phenomena which complicate or obscure the magnetic pattern. The offsets in the pattern caused by transform faults (Wilson, 1965) can produce anomaly configurations of great complexity, such as the series of sigmoidal patterns noted off the west coast of North America (Menard and Atwater, 1968). A global pause in spreading activity may have occurred from 40 mybp to 10 mybp (Ewing and Ewing, 1967) which would cause juxtaposition of magnetic anomalies caused by volcanic material of significantly different ages. Migration of the spreading axis itself has been proposed (Johnson and Heezen, 1967; Vogt et al., 1970) and also two active spreading axes may have existed simultaneously in a single ocean basin (Godby et al., 1968). In addition, much information on the initial spreading rates and directions for parts of the north Atlantic, as determined from magnetic anomalies, is obscured by the magnetic quiet zone, the boundary of which is sub-parallel to the continental slope (Heirtzler and Hayes, 1967).

Complexity in the marine magnetic anomaly pattern is often associated with marginal transformations between areas that differ in spreading history. Such marginal complexity can effectively obscure the relation between adjacent ocean basins which, individually, exhibit a magnetic anomaly pattern of relative regularity.

A situation of this type exists in the northeast Atlantic, of which a physiographic map is shown in fig. 1.1; a residual total field magnetic anomaly map, from the aeromagnetic survey of Avery et al. (1968) over the northern part of this area, is shown in Fig. 1.2. The area may be divided into three sub-areas, based on a classification by magnetic anomaly patterns and strike

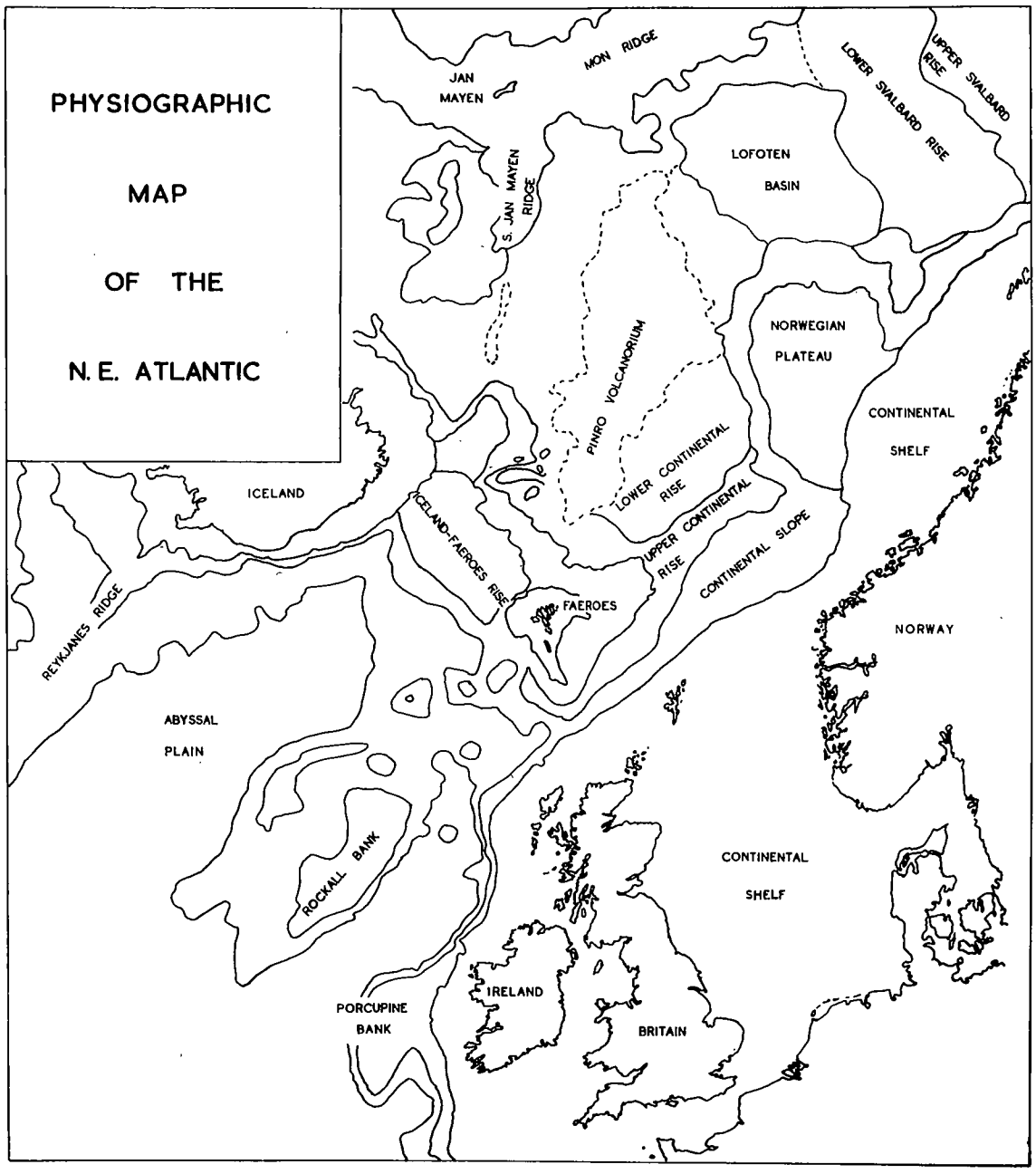

Fig 1.1 Physiographic map, location of relevant features.
(after Dobinson, A., 1970)

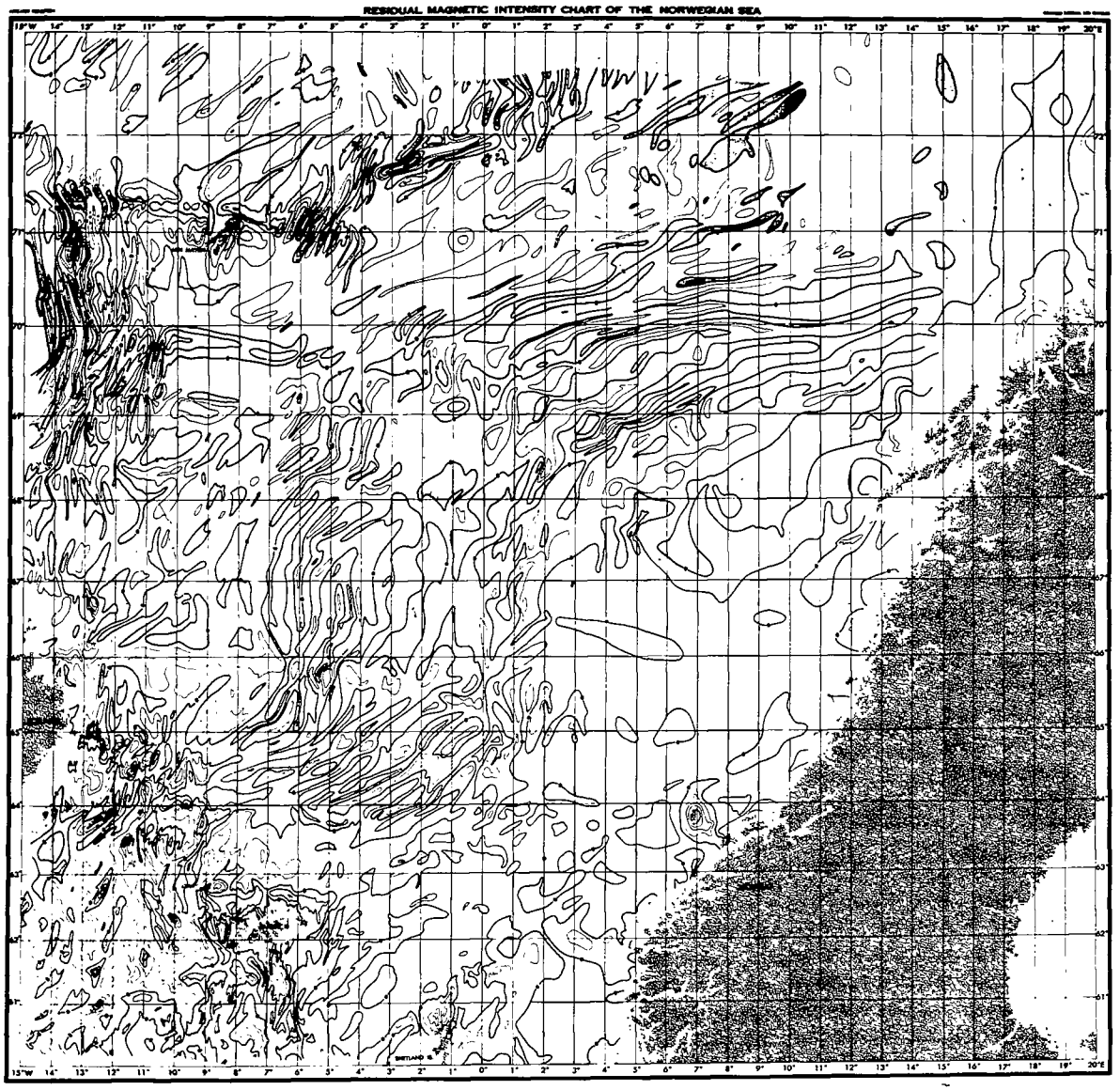

Fig 1.2

Residual aeromagnetic anomaly trends in the Norwegian Sea (after Avery et al., 1968).

directions. North of the WNW - ESE trending Jan Mayen Fracture Zone, a system of anomalies, of general trend NE - SW, is associated with the spreading axis of the Mohns Ridge (Vogt et al. 1970). South of the Jan Mayen Fracture Zone, in the Norwegian Sea and on the Icelandic Plateau, the main anomaly trend is N - S with shorter wavelength anomalies to the west of the aseismic South Jan Mayen Ridge. Finally, the southernmost sub-area, in the Atlantic basin south of Iceland, is characterised by NE - SW trending anomalies associated with the active Reykjanes Ridge section of the main Mid-Atlantic Ridge (Heirtzler et al., 1966; Godby et al., 1968; Talwani et al., 1971). The two marginal zones between these sub-areas exhibit different magnetic anomaly characters: the Jan Mayen Fracture Zone is associated with a N - S change in the principal strike direction of the anomalies, from N - S to NE - SW; the southern marginal zone includes the Iceland-Faeroes Rise and is of great complexity.

1.2 The setting of the Iceland-Faeroes Rise.

The Iceland-Faeroes Rise forms part of a NW - SE trending aseismic ridge which extends from the east coast of Greenland to the European continental shelf north of Scotland. In turn this ridge system, which reaches topographic culminations in Iceland and the Faeroe Islands, is intimately associated with the concept of a Thulean igneous province, of extent from Baffin Island, through Greenland to northwest Scotland and Antrim and of predominantly Tertiary age.

1.2.1 Sea-Floor spreading histories.

Southwest of this ridge system, spreading is based on the

Reykjanes Ridge and its relation to the opening of the main Atlantic Ocean. The spreading history of this region appears to be relatively simple, but to be based on several stages, during which the openings between Labrador and Greenland, and Europe and Rockall were also developed. The following sequence is taken from Le Pichon et al. (in press) who proposes that the initial opening of the north Atlantic occurred in the late Cretaceous:

1) Before anomaly 32 (76 mybp) there was opening between Rockall and Europe.

2) Between anomalies 32 and 24 (76 to 60 mybp) the first two thirds of the Labrador Sea were created.

3) Between anomalies 24 and 20 (60 to 49 mybp), there was a triple junction of active ridge axes in the North Atlantic, with spreading in the Labrador Sea, continued spreading in the main Atlantic Ocean and spreading from the newly formed Reykjanes Ridge.

4) After anomaly 20 (49 mybp), spreading in the Labrador Sea is much reduced, and finally ceases, while that from the Reykjanes Ridge continues.

Laughton (1971) states essentially the same sequence, with the exception that this author considers the Rockall trough to be the site of a complex transform fault system associated with the Iceland-Faeroes Rise as a fossil mid-ocean ridge, and not as the site of an extinct spreading axis.

Spreading rates on the Reykjanes Ridge have been subject to fluctuation (Vogt et al., 1970), but direction has remained essentially constant at 095°T since at least 40 mybp, ~~a direction which is somewhat southeast of a normal to the axis.~~

The latest period of spreading began about 18 mybp (Vogt et al., 1970) at a rate which has been constant for at least the last 10my (Talwani et al., 1971), at 1.13cm/yr in the direction 095°T or 0.98cm/yr in a direction perpendicular to the axis (Vogt et al., 1970). While the spreading configuration associated with this axis appears to be relatively simple, it has been suggested that two dormant spreading axes are located symmetrically about the Reykjanes Ridge and parallel to the present active axis, at a distance of 260km on either side (Godby et al., 1968).

North of Iceland and the Greenland-Scotland ridge system, the history appears to be more complicated. Vogt et al. (1970) consider that Norway and Greenland began to separate approximately 60 - 70mybp, and that the location of the Mohns Ridge, in a median position with respect to the opposite continental shelf areas, suggests a single spreading axis for the whole opening north of the Jan Mayen Fracture Zone. Between the Jan Mayen Fracture Zone and Iceland, Vogt et al. (1970) showed that the distance between the South Jan Mayen Ridge and the edge of the Norwegian continental shelf (fig. 1.1) is approximately equal to the total width of spreading generated by the Mohns Ridge from 60 to 42mybp. The active Iceland-Jan Mayen Ridge is located west of the aseismic South Jan Mayen Ridge and thus, lies much closer to Greenland than to Norway. A shift of spreading axis has been postulated from the east to the west side of the South Jan Mayen Ridge (Johnson and Heezen, 1967; Vogt et al., 1970). The extinct axis is marked by a line of seamounts in the Norwegian Sea (Vogt et al., 1970) known as the Pinro Volcanorium (Fig. 1.1), from which spreading ceased at about 42mybp. The present activity on the Iceland-Jan Mayen Ridge has been continuous

since at least 10mybp (Vogt et al., 1970). The South Jan Mayen Ridge is now regarded as a sliver of Greenland left between the present position of the spreading axis and the extinct axis (Johnson and Heezen, 1967).

Within this configuration of sea-floor spreading, the Greenland - Scotland ridge is a lateral ridge of the type defined by Wilson (1963), who considered that both the Greenland - Scotland and the Rio Grande - Walvis ridge systems represented sections of the oceanic crust formed at and spreading from 'hot spots' on the active axis. The 'hot spot' is a section of the mid-ocean ridge where volcanic activity is more intense.

1.2.2 Magnetic anomalies.

The total field aeromagnetic map of Avery et al. (1968) over the Iceland-Faeroes Rise (fig. 1.3) shows the complexity in the magnetic structure over the crestal plateau. The regular NE - SW Raff-Mason type of anomalies in the ocean basin to the south of Iceland realign over the crest of the Iceland-Faeroes Rise into a N - S trend, with a marked shortening of wavelength in the E - W direction and an increase in amplitude. Off the north - east flank of the Rise, the dominant trend is again NE - SW until the N - S anomaly pattern of the Norwegian Sea is developed at about 65°N.

Within the N - S pattern of anomalies on the crest of the Rise, complexity is increased by the presence of some NW - SE trending anomalies, particularly towards the south and on the Faeroes shelf area. Towards the north, the zone of high wavenumber N - S anomalies narrows and peters out by about 65°N. Anomalies of the type that characterize the crest of the Iceland-Faeroes

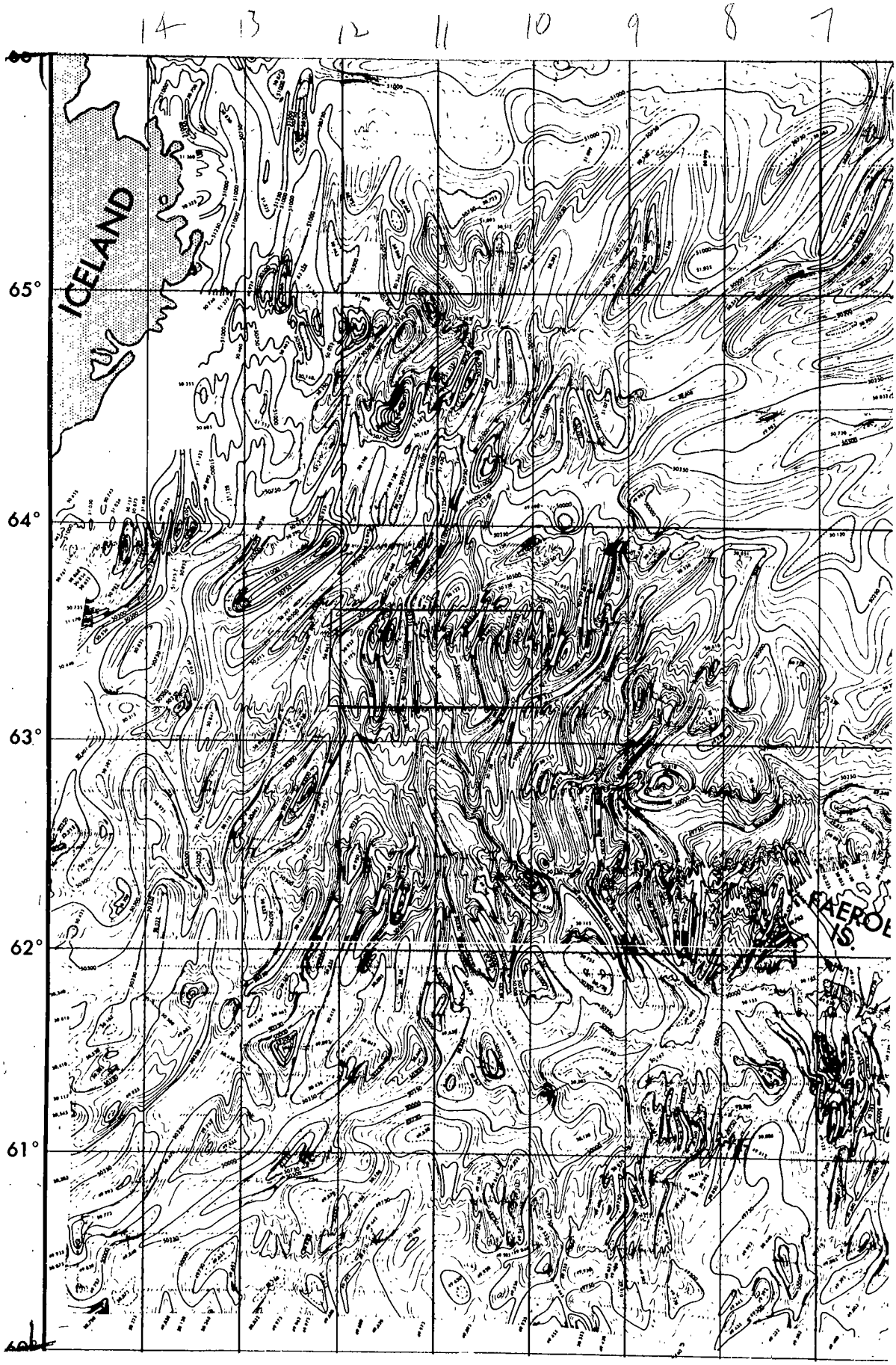

Fig 1.3 Total field aeromagnetic, Iceland-Faeroes Rise.
Area of detailed survey, 1969, outlined.

Rise are found also on the Wyville - Thompson Ridge, between the Faeroes and Scotland, and have been confirmed, from the results of a detailed shipborne survey, on the Faeroes Bank (Dobinson, 1970).

Over Iceland itself, Serson et al., (1968) noted a large positive magnetic anomaly associated with each branch of the Neovolcanic Zone in southern Iceland. The trend of local anomalies is NE - SW in the southern half of Iceland, but becomes N - S in the north after an abrupt change in direction at 65°N.

The widely spaced flight lines of Avery et al., (1968) did not permit full resolution of local trends and continuities in the magnetic pattern on the crest of the Iceland - Faeroes Rise, and it was to enable a more complete investigation of these local features that the detailed survey from m.v. Arran Firth was conducted in 1969.

A detailed magnetic survey, conducted by the German Hydrographic Institute (Hamburg) from FS Meteor in 1968, showed great irregularity in the magnetic pattern over the southern half of the Iceland-Faeroes Rise (Fleischer, personal communication), with N - S, NE - SW, NW - SE trending features. There are also local anomalies of circular or elliptical form, with amplitudes up to 1500 gamma. Johnson and Tanner (1971) have discussed the results of a semi-detailed shipborne survey over the northern half of the Iceland - Faeroes Rise, and these authors take note of a NW - SE trending feature within the limits of the area covered by m.v. Arran Firth.

1.2.3 Bathymetry and seismic reflection profiling.

The Iceland-Faeroes rise is in the form of an elevated, gently domed plateau, rather than the 'range and valley' sea-floor topography of the Mid-Atlantic Ridge. On the crest of the Rise, bathymetric relief is low (fig. 1.4); the sea floor is generally at a depth of 500 - 600m, with local features and scarps rising to 100 - 150m above the general level (Fleischer, personal communication). This smooth crestal topography is not usually associated with a complex system of magnetic anomalies in the absence of faulting; such high wavenumber anomalies are observed over ocean ridges of rough topography, and in the presence of rifting (Vogt et al., 1969). To the north-east, the Rise is bounded by steep flanks descending to 2500m in the basin of the Norwegian Sea, while to the south-west, the bathymetric gradient is more gentle towards the Atlantic basin south of Iceland. The junction of the Rise with the two 'shelf' areas of Iceland and the Faeroes is marked, in each case, by a steep scarp of about 200m (fig. 1.4).

The presence of high wavenumber magnetic anomalies indicates that 'basement', of presumably igneous origin, outcrops at or close to the sea floor over most of the Iceland-Faeroes Rise. A short air-gun seismic reflection profile, recorded during the 1969 survey of m.v. Arran Firth, was unable to detect any sedimentary cover in the crestal region (Peacock, private communication). Subsequent reflection profiles (Jones et al., 1970; Johnson and Tanner, 1971) have shown that the north-east flanks are covered by a thick wedge of sediment, while over the crestal region and the more gentle south-west slopes, the sedimentary cover is present only locally, where it is very thin.

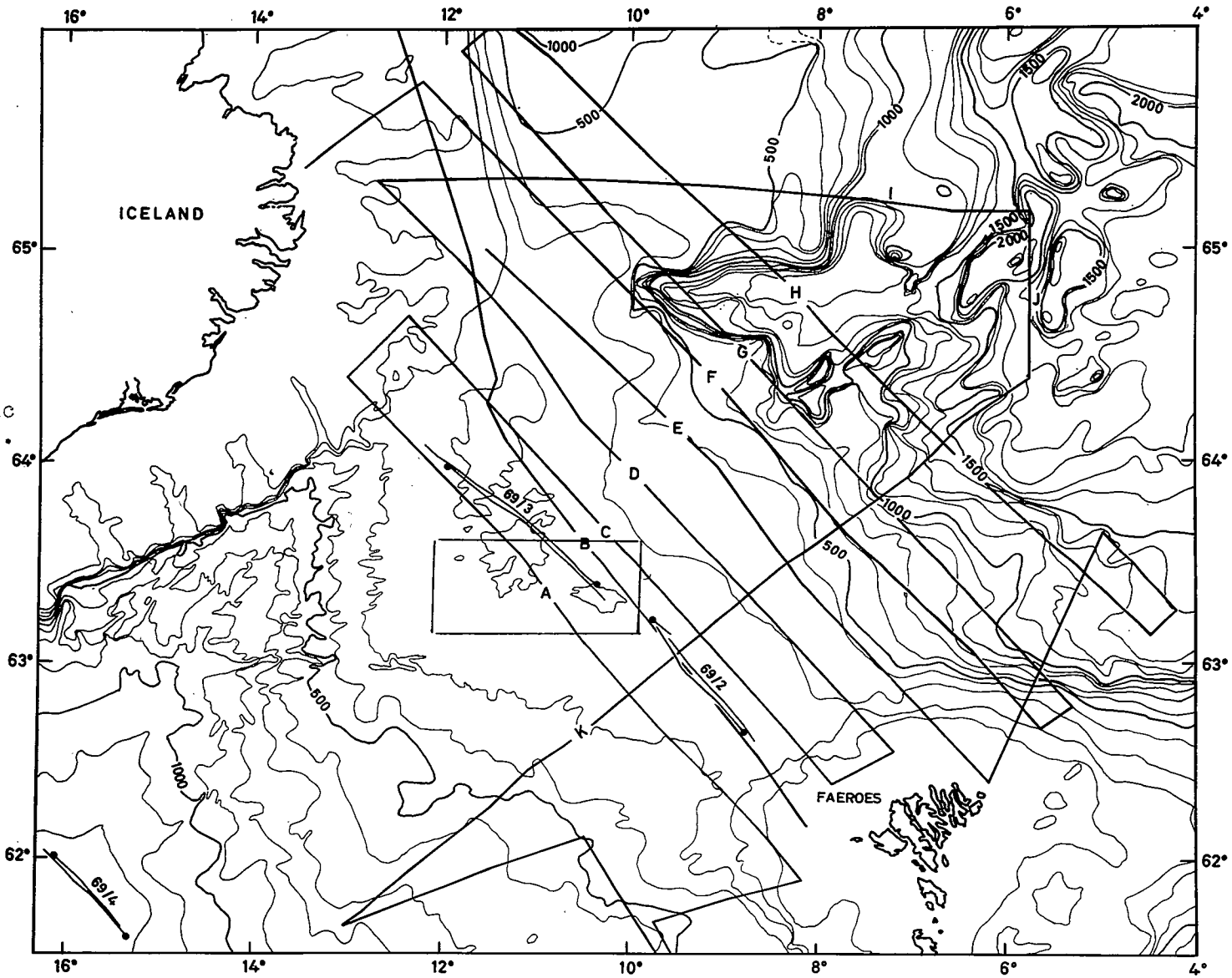

Fig 1.4

Bathymetry(fathoms), gravity and magnetic lines(1967) and seismic refraction lines(1969).

Core samples obtained during the survey of FS Meteor in 1968, from the south-west section of the Iceland-Faeroes Rise contained only rock and shell fragments; this content was considered to be due to overflow of water from the Norwegian Sea, which results in the removal or non-deposition of fine material (Sarginson, 1969). The same mechanism was invoked by Jones et al. (1970) to explain the asymmetrical distribution of sediment on the Rise.

1.2.4 Age dating and petrology.

The concept of a Tertiary British-Arctic, or Thulean, igneous province, once of wide extent but now restricted to Antrim, north-west Scotland, the Faeroes, Iceland and parts of Greenland due to differential subsidence, has been modified since the general acceptance of sea floor spreading and as isotopic dating has shown that Iceland represents a much younger phase of activity.

It is generally accepted that detectable movement between Greenland and Europe was initiated at about 60mybp (Vogt et al., 1970; Le Pichon et al., in press), although the initial split was somewhat earlier. An age of 60my has also been recorded for a number of features of igneous origin which are probably associated with the development of a spreading axis. The basalt pile of the Faeroes has been dated on K/Ar ratios at 50 - 60my (Tarling and Gale, 1968), a date that is consistent with the Lower Eocene age obtained from palynological studies; a similar age has been obtained for Rockall (Moorbath and Welke, 1968). Both of these seem to have been contemporaneous in formation with the Tertiary activity in north-west Scotland

if the Island of Skye is a representative area (Moorbath and Welke, 1969). However, Iceland represents a much younger phase of activity; the eastern part of the country, which includes the oldest exposed rocks, has been dated at 15my (Moorbath et al., 1968). Thus the age of the Iceland-Faeroes Rise falls within the range 15 - 60my if it forms part of the evolution of the north-east Atlantic by sea floor spreading. The geometry of its location is in favour of the Rise being formed during the spreading process, and argues against its presence as a pre-existing feature.

The Iceland-Faeroes Rise is terminated to the north-west and to the south-east by land areas in which the geology has been investigated quite extensively.

To the north-west, Iceland has been shown to consist of Tertiary-Recent lavas, pyroclastics and intrusives. Ages increase in approximately an E - W direction from the so called 'central graben', containing exposed Quaternary Volcanic material, outwards to the wholly Tertiary areas. The Tertiary area of eastern Iceland has been shown to consist of two types of igneous activity (e.g. Walker, 1963); fissure controlled eruptions have produced vast quantities of flood basalts in which are set central volcanic intrusive complexes associated with magma reservoirs at a high level in the crust and a wide variety of rock types due to extensive differentiation of the parent magma (Carmichael, 1964). Further petrologic variation in Iceland is provided by the presence of an alkali - basalt trend, possibly in association with the tapping of a deeper magma source along fracture zones (Sigurdsson, 1970).

To the south-east, the exposed rocks on the Faeroe Islands

consist of a thick sequence of basalts (Noe - Nygaard and Rasmussen, 1968) which generally become more basic up the succession, from quartz-tholeiites to olivene-tholeiites. The graduation in composition has been explained (Noe - Nygaard and Rasmussen, 1968) in terms of an increasing depth for magma segregation with decreasing age, an explanation that is in accordance with a continuous increase in distance from an active spreading axis.

The compositions of the Thulean volcanics are anomalous in an oceanic area; Chayes (1964) omitted the lavas of the Jan Mayen and the whole of the Thulean group, including Iceland, from his oceanic classifications as they were considered to be of continental type. The proportion of acid lavas and intrusives in eastern Iceland associated with centres such as Thingmuli (Carmichael, 1964) is at about the limit of that obtainable by fractionation from a parent basaltic magma, but the results of ~~K/Rb~~ isotope ratio determinations show no difference between Icelandic acid and basic rocks (Sigurdsson, 1967), and the Icelandic acid rocks show no sign of contamination assimilation of an ancient crustal source of lead, as shown from isotope studies on the intrusives of Skye (Moorbath and Welke, 1969) and from Rockall (Moorbath and Welke, 1968). Thus the acid rocks of Iceland seem to be derived from a basaltic parent by a process of differentiation that is anomalously extensive and efficient in an oceanic environment.

The quartz-normative tholeiitic lavas of the Faeroe Islands are also unusual, when compared to similar rocks from active ocean ridges, in their consistently higher iron and titanium content (Noe - Nygaard and Rasmussen, 1968).

1.2.5 Seismic refraction and gravity measurements.

The anomalous character of Iceland is evident also in its variable crustal structure, with a total thickness of 10 - 15km (Palmason, 1970) which is greater than that of typical oceanic crust. Palmason (1970) has presented a review of the crustal structure of Iceland based on the results of previous workers in refraction seismology (e.g. Bath, 1960; Palmason, 1967) and surface wave studies (Tryggvason, 1962), and on the results of recent refraction experiments. An average crustal structure, as recognised from refraction seismology, has been presented by Palmason as follows:

Layer	Average P - velocity (Km/s)	Average density (gm/cc)
0	2.8	2.1 - 2.5
1	4.2	2.6
2	5.1	2.7
3	6.5	2.9
4	7.2	3.1

Layer 0 has been identified with Quaternary lavas and pyroclastics which form the surface layer in the Neovolcanic Zone of Iceland. P - velocities in this layer are very variable and so is the total thickness which is up to 1000m on the active Reykjanes Peninsula. Layers 1 and 2 are composed mainly of Tertiary flood basalts of the same rock type. In most locations, layer 1 forms the outcropping layer away from the Neovolcanic Zone, but layer 2 is the surface formation in

south-east Iceland. Layer 3 is not exposed; it may be equivalent to the main oceanic layer, but on Iceland it has considerable variation in thickness and depth to its upper surface. The fifth refractor, layer 4, is considered to be the uppermost mantle, but of the anomalous low-velocity type that has been detected beneath active ocean ridges (Le Pichon et al., 1965). The crust of Iceland is thus defined by the depth to layer 4 which varies from 10 - 15km where detected in refraction data.

The basalt pile of the Faeroes has been correlated on P - wave velocities with layers 1 and 2 in Iceland (Palmason, 1965). A velocity corresponding to layer 3 in Iceland was also recorded, and again this layer is not exposed at the surface.

Seismic refraction measurements on the Iceland-Faeroes Rise were made as part of the geophysical survey in 1969 when the detailed magnetic data was collected. The locations of two reversed lines, 69/2 and 69/3 on the Rise, and of the reversed line 69/4, shot in deeper water, are shown in Fig 1.4. Results from the refraction survey (Bott et al., 1971) demonstrate the presence of a crustal structure of layering and variability on the Rise similar to that in Iceland, and of total thickness equal to, or greater than that of the Icelandic crust. Layers with velocities corresponding to layers 1, 2, 3 and 4 have been identified on the Iceland-Faeroes Rise, but in most cases each velocity is slightly higher than its average equivalent in Iceland. However, in Iceland the velocity in layer 1 is higher in the south than it is over the rest of the country and is of the same order as that recorded by Bott et al., (1971).

The free air gravity map presented by Bott et al.(1971), compiled from data collected during the 1967 survey of RRV John Murray, is shown in fig. 1.5. Local anomalies on the original data profiles have been related by Bott et al., to variability in upper crustal structure which was shown to be present from the results of the refraction survey. In broad structure, Bott et al., have shown that the Iceland-Faeroes Rise is approximately in isostatic equilibrium, with compensation provided by crustal thickening to 20km. These authors have interpreted a change in level of the Bouguer anomaly, from +110mgal on the Rise to -35mgal in the bowl-shaped anomaly field of Iceland (Einarsson, 1954), as being caused by lateral change in density from the normal upper mantle beneath the Rise to Anomalous upper mantle beneath Iceland. Thus, Bott et al., conclude that the Iceland-Faeroes Rise has been formed by an anomalous type of sea floor spreading due to the presence of a 'hot spot' on the Mid-Atlantic Ridge, and that the Rise is related to Iceland in the same way that more typical oceanic crust is related to a typical active mid-ocean ridge. In contrast, Bott et al., distinguish a possible change, at the southern end of the Iceland-Faeroes Rise, to a crust of continental type beneath the Faeroe Islands, and suggest that the northern and north western edges of the whole Rockall-Faeroes plateau mark the site of a true continental edge. This hypothesis receives support from the inclusion of the Faeroes 'shelf', as well as Rockall, in a pre-drift reconstruction of the north-east Atlantic (Bott and Watts, 1971) to produce a better overall fit than that produced by the

reconstruction of Bullard et al. (1965).

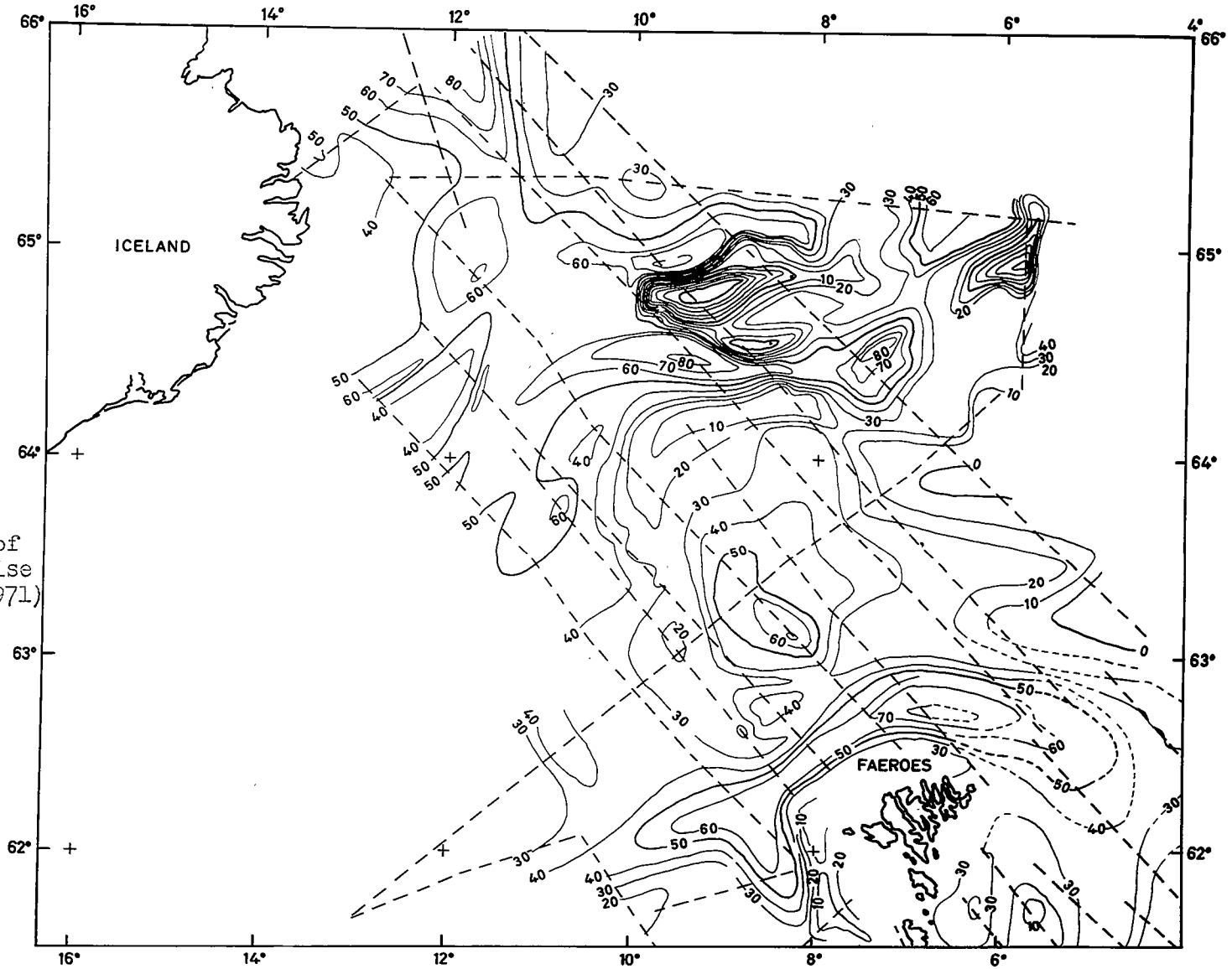

Fig 1.5

Free air gravity map of the Iceland-Faeroes Rise (after Bott et al., 1971)

CHAPTER TWO

COLLECTION, REDUCTION AND DESCRIPTION OF SURVEY DATA.

The area of the detailed magnetic survey was covered during the period 8th - 13th July, 1969 from mv Arran Firth, and was contained by geographical coordinates 63°09'N, 63°35'N; 09°50'W, 12°10'W (fig. 1.3).

2.1 Collection of data, survey procedure.

The detailed magnetic survey on the plateau of the Iceland-Faeroes Rise was conducted on a grid of twelve E - W lines. The lines were approximately of 100km length and with an average spacing of 5km; the actual spacing distance between adjacent lines varied locally between 2km and 6km due to moderately high seas and tracking failures of the Loran - C navigation equipment.

A Varian proton precession magnetometer, on loan from the National Institute of Oceanography at Wormley, was used for recording magnetic data. The theoretical resolution of this instrument is one gamma. The cabinet containing the recycling, counting and visual display units of the magnetometer was located in the forward cargo hold of mv Arran Firth, and produced an analogue paper record of total field variations. An adequate recycling period was determined at 10 seconds, and this value was used throughout the survey. After a study of the total field version of the aeromagnetic map (fig. 1.3), the full scale deflection of the pen recorder was set at 1000

gamma to accommodate the expected steep gradients. During the survey period, the ship's speed was either 5 knots, while an airgum seismic reflection profiling system was being tested, or 8 knots, when the guns were out of the water; thus, values of magnetic field were recorded at intervals of 20m or 35m along the lines. An additional pen on the display unit of the magnetometer was used to write time marks on a side trace of the analogue record, at intervals of 10 minutes. These time ticks were produced by a manual D.C. switch located near the navigation equipment on the bridge of mv Arran Firth. The magnetometer unit and paper record were checked hourly when day, time and the first two figures of field strength were written against the sixth time tick.

The sensing head 'fish' of the magnetometer was towed 150m astern to reduce the disturbing effect due to the survey ship. This effect was also minimized by the east-west configuration of the survey lines (Bullard and Mason, 1963).

Navigational coordinates were recorded at intervals of 10 minutes, by use of a continuous tracking Loran - C receiver, for which a fix accuracy of 300m is claimed. Time marks were entered on the magnetic record for each navigation fix. The Loran receiver required resetting on occasions due to temporary tracking failures. Other interruptions were caused by failures in the power supply, which also accounts for some gaps in the magnetic record.

2.2. Correction and reduction of data.

The treatment of magnetic data must include a consideration

of the 'noise' level introduced by time dependent variations in the earth's field. This noise includes the two main types of disturbance due to short period daily variation (measured in hours) and the longer period secular variation (measured in months). Magnetic storms, of more random occurrence, consist of higher amplitude, higher frequency fluctuations, and can render magnetic data too unreliable for interpretation. As the survey lasted only five days, the disturbing effect of secular variation is negligible.

In treatment for the effects of the daily variation, which is influenced by local geographic and atmospheric conditions, surveys over land make use of corrections derived from the magnetograms of the observatory nearest the survey area. For marine surveys in areas well away from land, the application of corrections for the daily variation is more uncertain. If the facilities are available, a recording station on a moored buoy in the survey area can be used as a source of data on local variations (Cann and Vine, 1966). Alternatively, information from peripheral land observatories may be used to indicate the reliability of magnetic data, by use of K indices. The K index describes the range and rate of change of a field component, as measured at a particular observatory (Bartels, 1957), and is a quantitative measure of the tolerability of time dependent magnetic variations.

In order to assess the effect of these variations for the period of the survey in 1969, magnetograms were obtained from observatories at Leirvogur, in Southern Iceland, and Lerwick,

Shetland. The magnetograms indicated the absence of magnetic storms for the period of the survey, but were studied to determine also the degree of correlation between the records from the two observatories.

There is quite good phase agreement between Leirvogur and Lerwick for variations of 8 - 10 hours, in both the vertical and horizontal components, although the amplitude of variation is lower at Lerwick. Fig. 2.1. shows the daily variation for a typical 24 hour period during the time of the survey. In the vertical component, relative maxima occur at 18 - 19 hours (universal time) at both observatories, and both recorded a minimum at 04 hours. Peak to trough ranges of the 8 - 10 hour variations at Leirvogur were generally of the order 30 - 100 gamma in the vertical component. The most intense activity occurred in the interval 00 - 07 hours of 12th July, when oscillations of 50 gamma amplitude, and periods of 10 - 30 minutes were superimposed on 4 - 6 hour variations. Maximum amplitudes of the latter were 100 gamma for the vertical component and 200 gamma for the horizontal component at Leirvogur. Throughout the entire survey period, the amplitude of variation in the vertical component was lower than that of variation in the horizontal component. In the high latitudes of the survey area (field inclination of 75^{o}) Leivogur and Lerwick, the magnitude of the vertical component of the earth's field is four to five times that of the horizontal; base values for the components at Leirvogur in June, 1969, were:

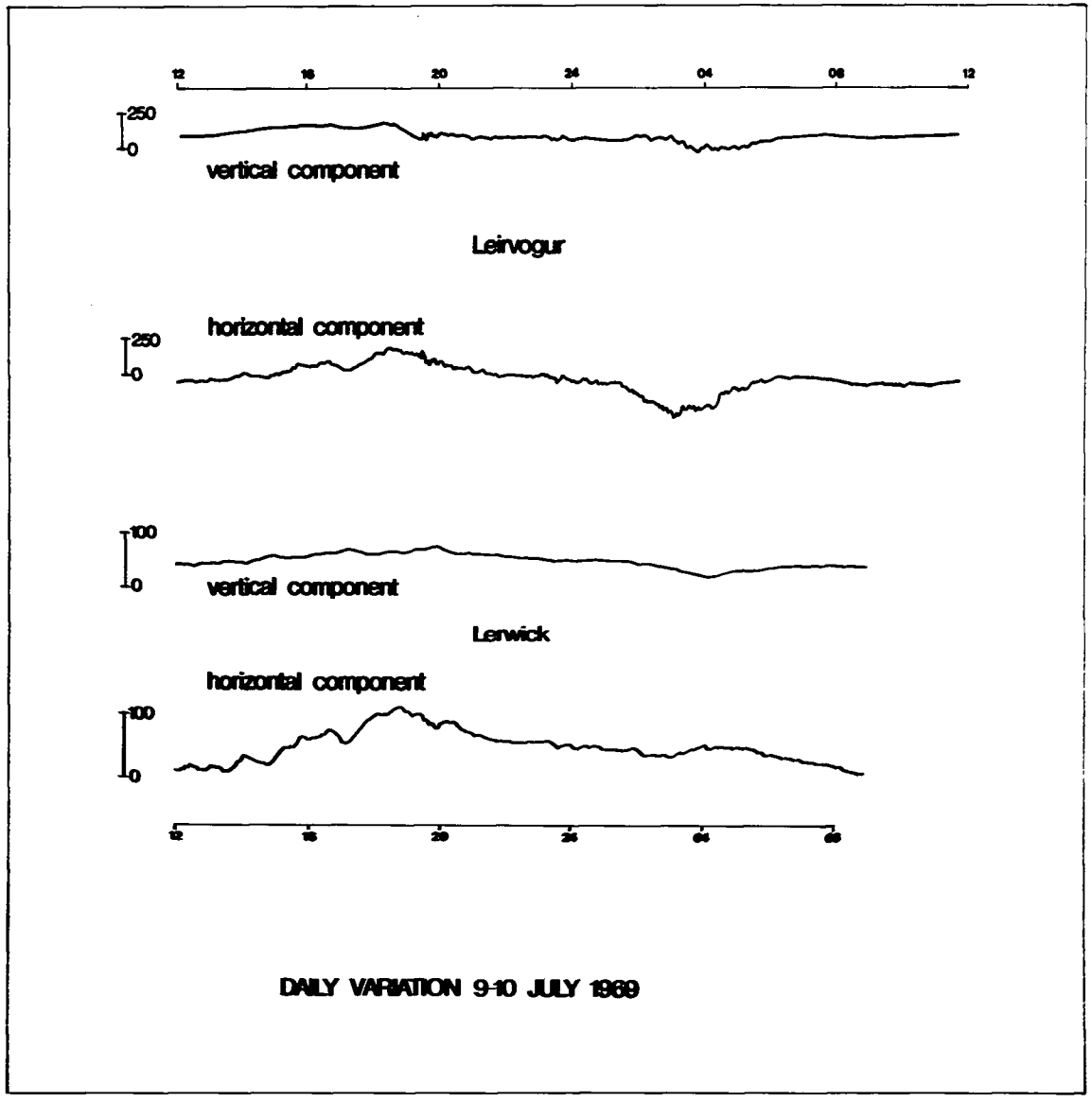

Fig 2.1

Observatory magnetograms, variation in gamma with universal time.

Zo = 49390 gamma

Ho = 12045 gamma

Thus variation in the horizontal component has a much smaller effect on the total field values than does variation in the vertical component.

The daily variation as observed at Leirvogur represents a root-mean-square error of 40 gamma in the total field measurements for the survey area; the corresponding error calculated from the Lerwick magnetograms is 20 gamma. These error estimates were calculated from magnetogram values at intervals of 8 hours.

A correction was applied to the survey data from the Leirvogur magnetograms, and was based on a hand-smoothed representation of the longer period (4 - 10 hours) variations for both field components, related by an inclination of 75°. These corrections were applied within the main reduction program, SPHEL (see below). The main uncertainty in applying corrections in this way, even with the assurance of some correlation between flanking land observatories, is a lack of knowledge of the behaviour of field variations in the conditions of the open ocean.

No correction was made for the lag of the magnetometer sensing head relative to the Loran receiving antenna on the stern superstructure of mv Arran Firth. Neglecting slight divergences from parallelism in adjacent ships' tracks, the maximum spurious phase difference, due to this lag, on adjacent magnetic profiles is two cable lengths, or 300m. This does not

affect quantitative interpretation as this was performed on single profiles, and the induced error in anomaly trends on the total field and residual maps is well within the accuracy of hand contouring.

Further processing of the data was conducted in five main stages, during which the data was converted to a form suitable for interpretation, and regional field constants were calculated:

i) Conversion of Loran - C navigation readings to geographical coordinates of latitude and longitude (a Decca program).

ii) Conversion of latitude and longitude to grid coordinates of km north and km east from a false origin (program GRID).

iii) Calculation of regional field values for each navigation fix (program REGMAG).

iv) Conversion of the analogue record of total field magnetic data to a digital sequence.

v) The assignment of geographical coordinates to each station point in the digital data, the calculation of distance and azimuth between successive stations and reduction to residual anomalies. This stage was performed by use of the main magnetic reduction program SPHEL.

All reduction and interpretation programs were written for use on the Northumbrian Universities Multiple Access Computer IBM 360/67 at Newcastle, unless otherwise stated, in which case computations were performed on the IBM 1130 at Durham.

i) Conversion of Loran - C Readings to Geographical Coordinates.

Readings of day, time, Loran - C data and ship's heading and speed, from the geophysical log book of the survey, were transferred onto punched cards for processing on the IBM 1130. This stage in the reduction makes use of a program, developed by the Decca Navigation Company, to solve for the intersection of two sets of hyperbolae which are the loci of constant time difference in the reception of Loran master and slave signals. The program produces a punched card output containing the input data plus latitudes and longitudes. The output form of day and time is that of an integer and decimal fraction of a day. This set of output provides the basic calibration and library record for the survey.

ii) Conversion of Geographical to National grid Coordinates.

This stage of the reduction was included as a preliminary step in the preparation of a contour map, and makes use of a program written by A. Dobinson (Dobinson, 1970).

iii) Calculation of the International Geomagnetic Reference Field.

The program to compute values of the IGRF was written at Cambridge and is based on the work of the International Association of Geomagnetism and Aeronomy (IAGA), Commission 2, Working Group 4. Values of a reference field, represented by a series of spherical harmonics, are computed at the corners of full degree squares on the ellipsoid surface of the earth (IAGA, 1969). Stations which fall within the degree squares are assigned a reference field value by interpolation. The final

values obtained are those calculated by an extrapolation from epoch 1965.0 to the date of the survey, by a harmonic representation of secular variation. The user of the program is required only to write a computer routine for specific input and output formats, and for calling the main operating procedures.

The punched card output from this program contains time and geographical coordinates, as well as the regional field values, and forms one section of input to the main magnetic reduction program.

iv) Conversion of Analogue Magnetic Records to Digital Form.

A digital sequence was obtained on punched paper tape by use of a D - Mac pen follower. The records were prepared for digitisation by dividing the data into sections, or blocks, contained within known time intervals, as defined by the ticks entered during the survey. Block length was usually 30 minutes, but some longer or shorter blocks were necessary to cover gaps in the navigation record, or for the end points to coincide with changes in speed or major heading changes. The time of start and finish of the block, calibration coordinates for the full scale reading of the record and the first two figures of the total magnetic field were punched onto the tape at the start of each block.

As the field over the Iceland-Faeroes Rise contains a mixture of anomalous magnetic features, with a wide range of spectral composition, and also the analogue record was a function of time during which there had been a number of changes in the ship's speed, it was decided to use a varying digitisation

interval. The analogue record was covered by a sequence of digitised points to divide the wave forms into linear sections of varying lengths. Supplementary points were inserted over sections of very long wavelength. Due to the nature of the magnetic field, even short profiles contain a sufficient number of station points, and a coverage of sufficient uniformity to ensure adequate conditioning of the data for use in least-square technique.

A computer program (SMAG), written by A. Dobinson (1970), was used to convert the D-MAC coordinates of each station point into a total field value and an abcissa representing a decimal fraction of the total duration of the block in increasing time. The output from this program was edited 'manually', and individual blocks were separated by the insertion of header cards containing times of start and finish and corrections for daily variation. This raw data formed the second input section to the main reduction program.

v) Main Magnetic Reduction Program (SPHEL).

SPHEL is a general purpose reduction program for marine magnetic data in profile form. The programming language is PL/1, and a complete listing with input specification for the IBM 360 is contained in appendix A.

The first section of the program assigns geographical and grid coordinates, and a value for the magnetic regional (IGRF) to each digital station point. Assignment is by a process of linear interpolation based on the time of each controlling navigation fix, the times of start and finish of each data block and the position of each station within its block as

represented by the fraction of the total duration of the block. The correction for daily variation is also made in the same way, by assuming a linear gradient between the values assigned to the ends of each block. As the average block duration was 30 minutes, the interpolation was made over distances of 6 - 9km, involving 30 - 50 stations. Within this distance the change in value of the IGRF depends on the azimuth of the line, but is generally less than 10 gamma, and a linear interpolation is quite adequate. The IGRF is subtracted from the total field value at each station point to produce a residual anomaly.

The second section of SPHEL computes the distance between successive station points and sums these values to produce cumulative distance along the profile. The national grid coordinates could be used to compute distances in areas close to the centre of the grid system where distortion is small. In the area of the Iceland-Faeroes Rise, and especially for long profiles, distances are preferably calculated from latitude and longitude and the formulea of geodesy. For this purpose the program DISAZ, written by M.A. Hutton (1970) was included in SPHEL as a subroutine. This subroutine uses coefficients derived from the International Gravity Formula to calculate the distance and azimuth of a second pair of latitude and longitude coordinates relative to a first pair; the azimuth is calculated in the form of a back-bearing.

A third section of SPHEL computes an additional set of residual anomalies by least-squares regression to a polynomial.

In the standard version of the program (appendix A), the data are used to derive a linear regional (first order polynomial), but with slight modification, curves of second or third order can be used. The least-squares procedure is performed by use of LLSQ, a standard routine of the IBM 360 systems library, and included in the special batch of programs of the Scientific Subroutine Package (SSP)(IBM, 1968).

The coefficients produced by fitting a line to the data consist of a regional magnetic value at a false origin, which may be at one end of the line or elsewhere, and a regional field gradient along the line with increasing distance. Thus, a set of residual anomalies is derived by subtraction of the values of the dependent variable in the regional equation.

The final output of SPHEL consists of all or some of the following for each digitized point:

a) day and time.

b) distance and azimuth.

c) latitude and longitude.

d) grid coordinates.

e) total magnetic field.

f) residual anomaly based on the IGRF.

g) residual anomaly based on least-squares.

In a typical performance of SPHEL, with 1055 station points and 60 navigation fixes, the operation occupied a core space of 115k and ran for a total time of 84 seconds, including input and output.

For the purposes of comparison an additional reduction procedure was followed for the data of the detailed survey area. The total field data was summed over intervals of 10km

to produce an average value for this interval, and the average values were used in a least-squares process to produce a plane-fitted regional for the whole survey area. For this procedure, the sequence and program (MMRED - B) of A. Dobinson (1970) were followed exactly.

Magnetic data from the Durham survey of 1967 were digitised and processed by SPHEL; gravity data from the same survey and from the survey of 1968 (Watts, 1970) were digitised by hand.

For certain types of interpretation it was necessary to have the data in the form of a regularly spaced array of station points; this form is also more efficient for input. To obtain this form, a Fortran program written by P.J. Gunn (personal communication), and based on the cubic spline method of Bhattacharyya (1969), was translated into PL/1.

2.3 Presentation and description of survey results.

For the purposes of data presentation and qualitative interpretation, a plotting program written by A.B. Watts (1970) was used to prepare data sheets for hand contouring. Positions with associated gamma values were plotted by an automatic graph plotter on line to the IBM 1130. Hand contoured maps of total field (fig. 2.3)and IGRF residual anomalies (fig. 2.4) were prepared in this way. The IGRF residual map was produced to show the general distribution of positive and negative anomalies, and contouring is based on plotted values at intervals of 1km to 1.5km and was drawn without special reference to the contours of the total field map. The main

features and trends are similar on both maps. An additional plotting program was written to convert the digital data back into an analogue record as a function of distance (fig. 2.2).

2.3.1 Stacked total field profiles.

In the presentation of total field profiles (fig. 2.2), projection onto true east-west lines or correction for non-parallelism of ship's tracks was not attempted; thus, slight spurious differences in wavelength are to be expected across corresponding sections from north to south. The profiles were stacked about 11°30'W, the average centre point for each line, a correlation of even short wavelength anomalies should be reliable in the region of this longitude. Towards the profile ends, only large anomalies may be followed across adjacent tracks with confidence. Finally, a loss of navigation for part of the western end of line 4 required that digitisation be based on long blocks between uncertain fixes. The affected section has been moved a 'token' distance away from the reliable data in the stacked profiles, but the gap was closed for contouring.

In fig. 2.2 correlation across profiles has been indicated for some of the larger anomalies where this was considered to be reliable. Upper case letters denote relative magnetic highs, and relative lows are indicated by lower case letters. Corresponding anomalies have been labelled by the same convention on the contour maps.

In the following description of the magnetic field, the stacked profiles (fig 2.2) should be consulted as they show

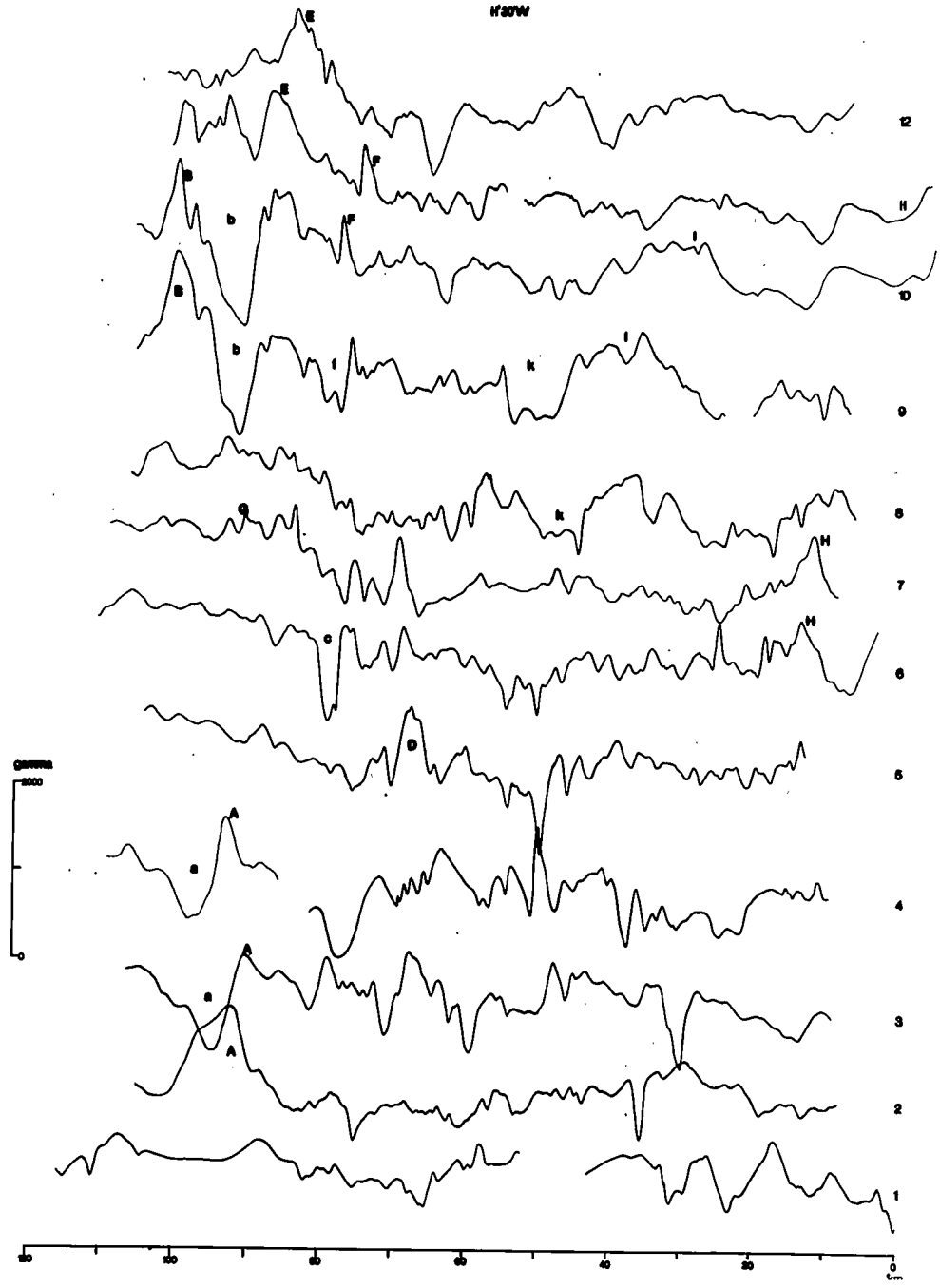

Fig 2.2 Stacked total magnetic field profiles.

graphically the true amplitudes, and the total field contour map (fig 2.3) shows the geographical relation of the anomalies. Specific description of the contour maps will be made below to emphasise anomaly trend directions.

An important feature of the detailed survey data is an increase in the field values to the west of the area. For convenience, this will be referred to as 'the regional high' as it forms an apparent background field for shorter wavelength, high amplitude anomalies such as B, b, E, A and a. Within this western section, the high amplitude anomalies stand in relative isolation, while to the east, distinction of individual anomalies is more difficult due to a greater degree of interference between anomalous features containing a wide range of frequencies.

The regional high represents an increase of 500 - 600 gamma in the total field for much of the western part of the survey area, but there is a decrease in this amplitude towards the south, and it may be as little as 200 - 300 gamma on lines 1 and 2. The effect is difficult to distinguish in the south due to the dominance of anomalies A and a. This east-west change in magnetic field level takes place over a distance of 10km to 15km on lines 7 through 12, but south of these lines the gradient is more gentle and the change in level takes place over a distance of about 20km; here, again, the separation of different components is uncertain. On line 6, and possibly on all lines to the south of this, the main gradient of the regional high may occur further to the east; the change in level seems to take place just to the west of low k on line 6.

An indication of this is the presence of the steep high amplitude low c (900 - 1000 gamma) which has a relative simplicity and dominance that is rare in the central and eastern sections of the survey area, but is more typical of anomalies such as a and b.

Of the high amplitude anomalies in the west of the area, the double feature Bb, on line 9, has the greatest gamma range, with a peak to trough difference of over 2000 gamma. The corresponding difference for Aa is 1000 - 1200 gamma from line 4 on the stacked profiles, but a maximum value of about 1600 gamma is observed in a northwest - southeast direction on the contour map (fig 2.3). Taken individually, the amplitudes of anomalies A, a, B, b and E lie in the range 800 - 1100 gamma, relative to an estimated background field represented by the regional high. The widths of these anomalies lie in the range 5 - 12km. Smaller field variations, such as those forming the broad area of high G on line 8, are of relative amplitude 300 - 400 gamma, and of width 3 - 4km. It is possible that the narrow high F continues across lines 8, 9, 10, and 11.

Over much of the central and eastern sections of the survey area, the anomaly content is more varied with respect to both amplitude and frequency. Amplitudes are generally in the range 300 - 700 gamma and anomaly widths vary between 3km and 8km. Longer wavelengths become more obvious to the north, for example at high I of width 15 - 16km, and on the eastern edge of the survey area high H has a width of 12 - 15km, with a full amplitude of 900 - 1000 gamma.

Steep gradients and moderate to high amplitudes are found in all sections of the survey area, even for short wavelength anomalies, and this supports the inference that magnetic basement outcrops at the sea floor.

2.3.2 The contour maps.

The interrelation of features described above is seen on the total field map (fig 2.3), and the IGRF residual map (fig 2.4). The residual map is in effect a filtered map (see beginning of section 2.3).

The onset of the regional high is marked in the east by gradients with a N - S or NNE - SSW trend, although, in places this is obscured by the presence of anomalies F, f and c. The regional high forms a broad positive anomaly of 400 gamma average amplitude (fig 2.4). On the extreme western margin of the survey area, there appears to be a NE - SW striking system of anomalies which alternate between highs and lows in the range 50900 - 51400 gamma (fig 2.3). These are all positive on the IGRF residual map, but may continue across the regional high in continuity with such positive and negative systems as F, f where the magnetic effect of the broad structure is diminished. This continuity may be represented on both maps by the area of high G which is characterised by relatively gentle field gradients between the two main anomaly clusters to the north and south, and has a NE - SW strike direction for its minor components.

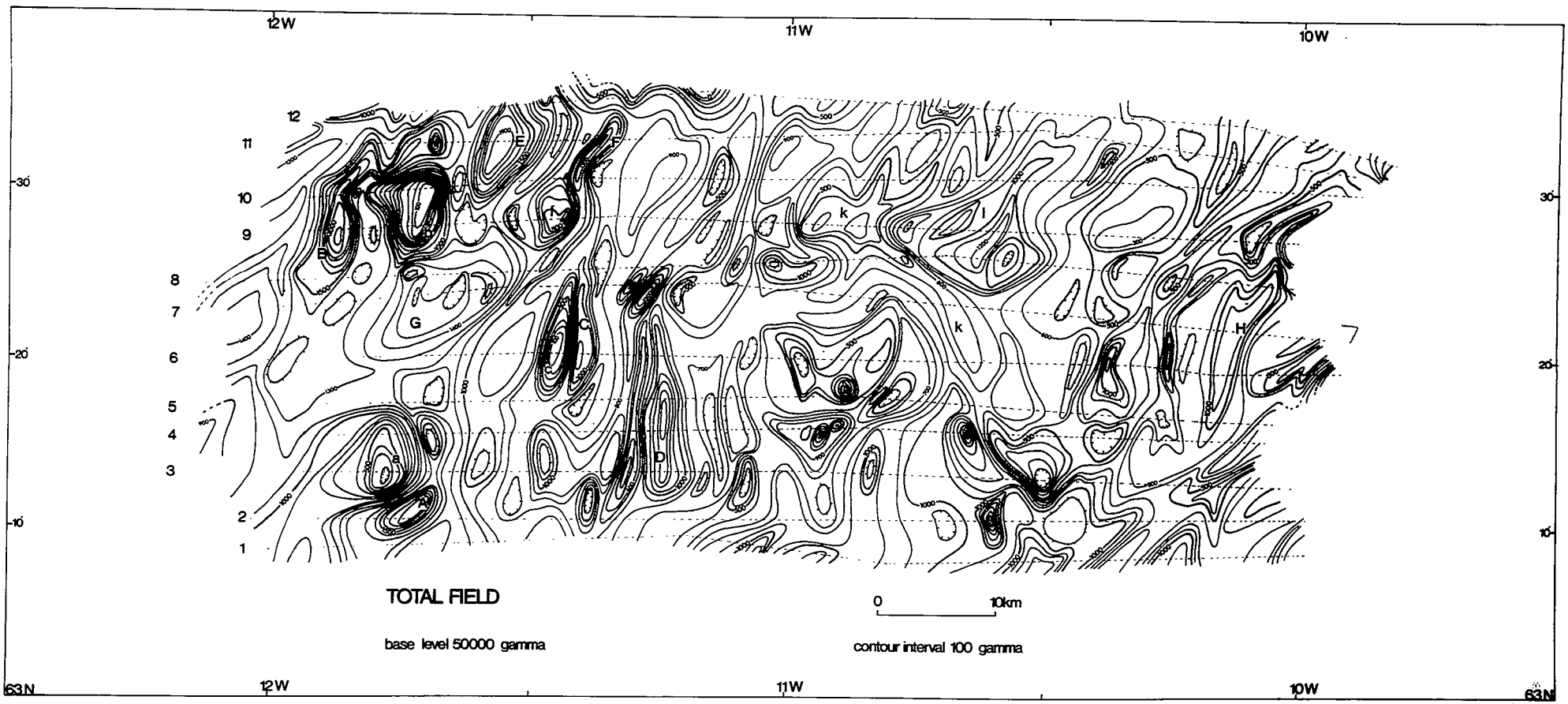

Fig 2.3 Contoured data from the survey of 1969; tracks of mv Arran Firth indicated by dashed lines.

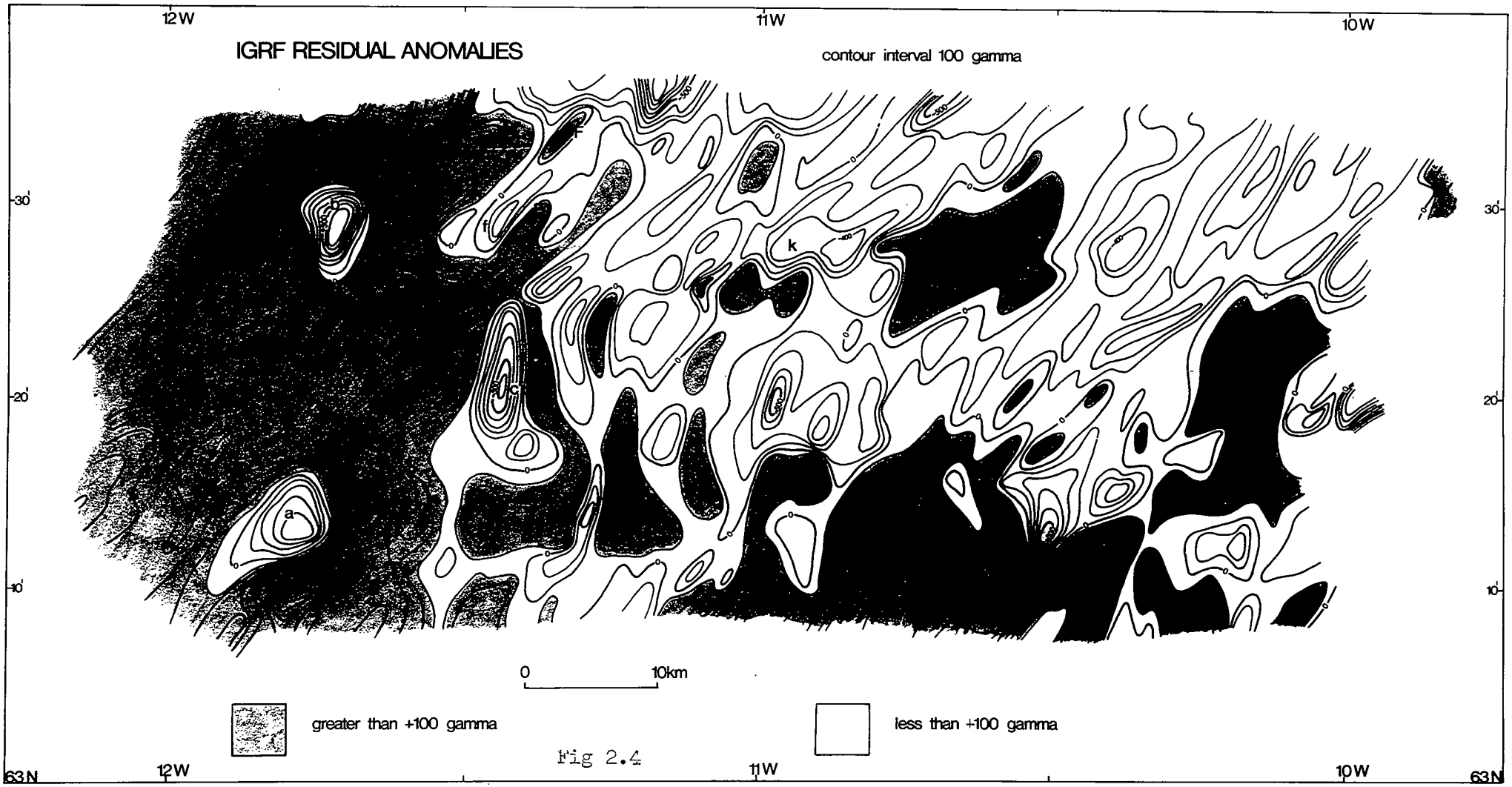
12W
11W
10W
IGRF RESIDUAL ANOMALIES
contour interval 100 gamma
30'
20'
10'
63N
a
b
c
f
k
0
10km
greater than +100 gamma
less than +100 gamma

Fig 2.4

To the north of anomaly G, anomalies B, b, E, f and F form an E - W en echelon system of positives and negatives. Each anomaly has a closed form with elongation N - S or NNE - SSW in ratios 2:1 to 5:1. Anomaly F is of greater elongation but may consist of two smaller parallel anomalies of NE - SW trend (fig 2.4). The continuation of high B wraps round the northern end of low b, while to the south of anomaly G, high A wraps round the southern and eastern edges of low a, and achieve maximum amplitude when aligned in a NE - SW direction.

Apart from low amplitude superimposed anomalies, such as those of high G, the regional high appear to have a magnetic unity as a sub area, with the high amplitude anomalies in close association. Anomalies of the type B, b, A, a and E are not found over the central and eastern sections of the area, and the association with the regional high is probably geological as well as one of location. Low c and high F are located on the eastern margin of the regional high; both are more elongate N - S or NNE - SSW, and may characterise the transitional zone between the two main levels in magnetic field. High D is also of marked elongation in a N - S direction and may be association with c and F, although it lies further to the east. Between anomalies c and D there is a band of alternating highs and lows of N - S trend. It may be of significance that anomalies c and D approximately cover the latitudes for which high amplitude anomalies are lacking on the regional high.

East of high D, the area may be subdivided into a northern

and a southern subarea about an E - W line that is approximately on the latitude of line 6. The northern subarea is characterised by the development of broad areas, such as high I, that are elongated in a NE - SW direction. These features are more evident on the residual map (fig 2.4) where they appear as bands of alternating positive and negative anomalies of width 10 - 15km. The widths show a tendency to decrease towards the west and the regional high. On fig 2.4, anomalies F and f appear to form part of this NE - SW system that interferes with the rise of the field values towards the regional high. In the southern subarea, and just to the east of the regional high, the NE - SW striking system of anomalies realign N - S to include c and D. Further east, however, the southern subarea contains a number of trends and local sharp anomalies (fig 2.3). A N - S trend is present in places, and in the southeast corner, a number of features strike NE - SW.

There is another difference between the northern and southern subareas in the distribution (by area) of positive and negative anomalies, with predominantly negative to the north and positive to the south, though this may be a local peculiarity of the small survey area. This change in relative distribution may occur about a NW - SE feature and not about an E - W line. A series of magnetic 'cols' and a deep low centred about $63^{\circ}12'N$, $10^{\circ}30'W$ (fig 2.3) appear to have a continuation to the northwest into low k; the system may extend NW - SE across the whole of the survey area. On the residual map (fig 2.4), this feature is represented by a

locus of 'offsets' in the NE - SW system of anomalies. In the direction of the NE - SW trend, the position of the transverse feature is marked by the junction of anomalies of different sign. Johnson and Tanner (1971) noted a strong NW - SE lineament in the same area, and although the feature with the same trend in the data of the present survey is discontinuous, it does appear to be persistent, with local steep gradients. Thus on the contour map of Johnson and Tanner, which was based on a more widely separated lines, the NW - SE trend could have a certain dominance with respect to anomalies of greater wavelength than the minimum that was resolved in the present survey data. This would be the case if the feature did represent a persistent line of offsets in NE - SW anomaly system, and two anomalies of like sign were contoured as one from the data of a survey of inadequate resolution.

The status of high H is uncertain; its most prominent trend of N - S or NNE - SSW, which is more typical of the high amplitude anomalies to the west of the survey area. The presence of NE - SW anomalies to the north and south of high H produces a sigmoid pattern in the magnetic field at the eastern margin of the area. A similar pattern is present over high B, and the relation of the regional high to anomaly configuration of the rest of the survey area produces a half sigmoid pattern on a larger scale.

Reference to the available bathymetry for the area (fig 2.5) indicates that the southern part of high H is associated with local bathymetric ridge. The bathymetric data of RRV John Murray

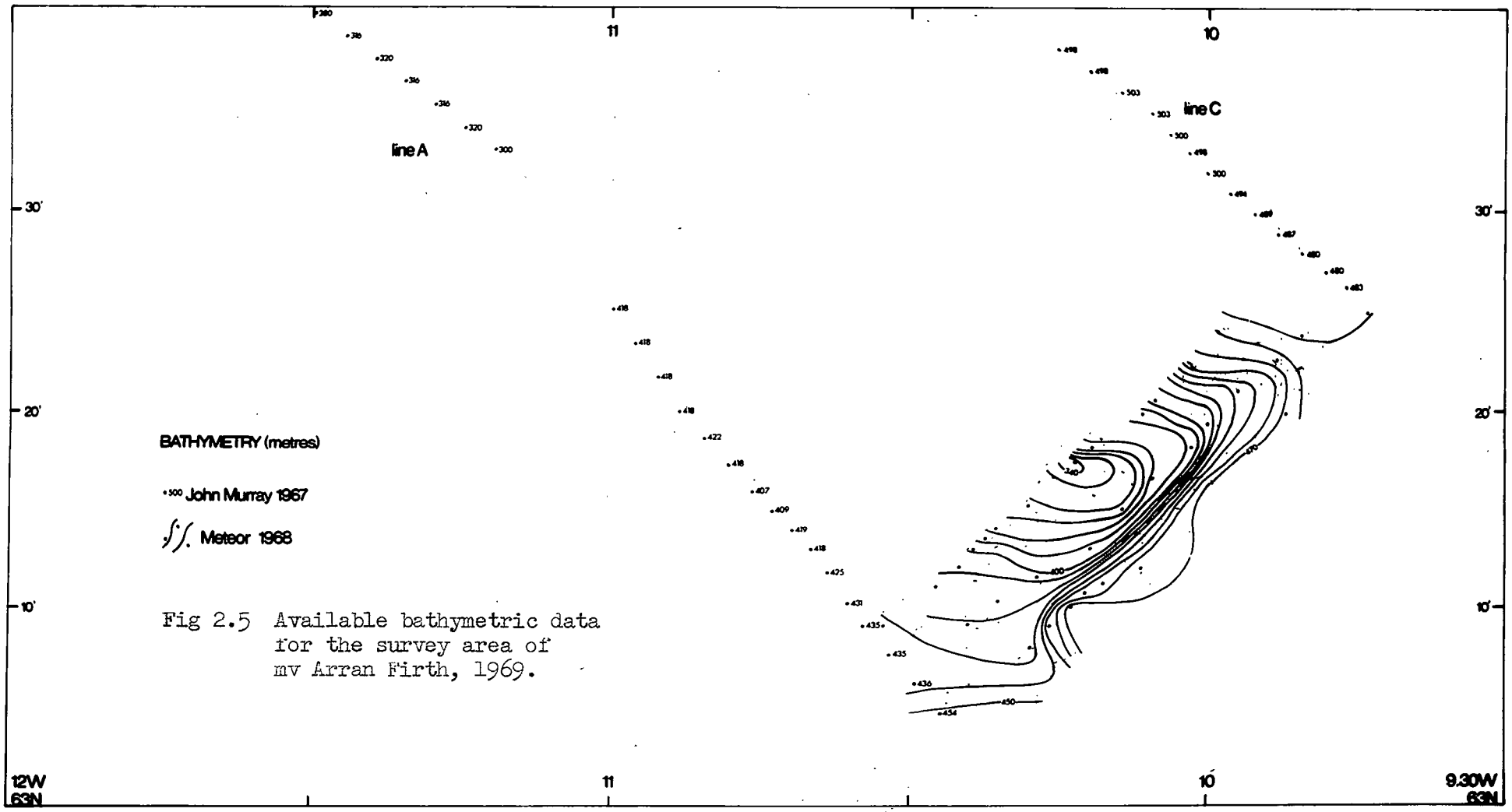

Fig 2.5 Available bathymetric data for the survey area of mv Arran Firth, 1969.

also indicate shallower water at the north end of the regional high. A further comparison, that of the aeromagnetic map (fig 1.3) with the regional bathymetry (fig 1.4), indicates that the N - S trend in the magnetic anomalies is associated with relatively shallow water on a regional scale. The conclusion is that the general sigmoid pattern of the aeromagnetic anomalies (Avery et al., 1968) over the Iceland-Faeroes Rise is the response of a survey, based on widely spaced flight lines and with an inherent upward continuation, to an anomaly configuration which, in detail, consists of a number of local realignments on several smaller scales.

2.3.3 Summary and discussion of trends.

The main trends observed in the data of the survey area are as follows:

a) N - S or NNE - SSW; elongation of some major anomalies and the eastern margin of the regional high, also a major bathymetric trend on the north-west flank of the Iceland-Faeroes Rise (fig 1.4).

b) NE - SW; bands of alternating positive and negative anomalies in the north-eastern section of the survey area and of high and low positive anomalies on the western margin, also a minor bathymetric trend (fig 2.5).

c) NW - SE; trend of the locus of apparent offsets in the NE - SW anomaly system, also a minor bathymetric trend (fig 1.5), i.e. from "Meteor" data.

d) E - W; a trend of uncertain significance which may

affect the magnetic regional field in a N - S direction; also the trend of the bathymetric scarp for much of the northern side of the Faeroes shelf.

The N - S anomalous trend that characterises the magnetic anomalies over the crest of the Iceland-Faeroes Rise is also present over the Faeroes Bank, both on the aeromagnetic map (fig 1.3) and from the results of a shipborne survey (Dobinson, 1970). Dobinson described two large positive anomalies with this trend on the east and west sides of the bank, with amplitudes of 1000 gamma and widths 10 - 20km, and some lesser anomalies of NE - SW trend. In other areas, magnetic anomalies of this trend have been observed in the Norwegian Sea and west of the South Jan Mayen Ridge (Avery et al., 1968), and in Iceland north of 65°N (Gudmundsson, 1966; Serson et al., 1968). The same strike direction is associated with the eastern branch of the Neo-volcanic Zone in northern Iceland and with the earthquake epicentre belt on the northern Icelandic Shelf (Johnson and Heezen, 1967).

The NE - SW trend is that of the Raff-Mason type of magnetic anomalies associated with spreading from the Reykjanes Ridge (Heirtzler et al., 1966), and of magnetic anomalies in the southern half of Iceland (Serson et al., 1968).

A strike direction NW - SE is the regional structural trend of the Greenland-Iceland-Faeroes lateral ridge system, and is also the direction of Faeroes fjord system which is considered to parallel the fissures from which the lavas were erupted (Rasmussen and Noe-Nygaard, 1966).

The trend of E - W or ESE - WNW has deep structural

associations; this is the trend direction of the components of the Jan Mayen Fracture Zone (Johnson and Heezen, 1967), and the postulated fractures across central (Sigurdsson, 1970) and southern Iceland (Ward et al., 1969). The same trend has been noted in association with fracture zones to the south of Iceland at 53°N (Johnson, 1967).

Thus, the trends evident in the present survey data indicate the presence of structural controls from most sections of the northeast Atlantic. This variety of control is in keeping with the status of the Iceland-Faeroes Rise as a zone of separation between two ocean basins with different histories of evolution.

CHAPTER THREE

METHODS FOR THE INTERPRETATION OF MAGNETIC DATA.

All interpretation methods used in the present work are based on a two-dimensional approximation; the anomalous body is assumed to extend to infinity in both directions perpendicular to the plane of the anomaly profile, with the same cross-section that is produced when the body is cut by this plane. The programmed versions of the methods were written for use on the NUMAC IBM 360/67.

The intensity and direction of magnetisation of an anomalous body are composite quantities which are the vector sums of induced and remanent components.

3.1 Methods developed by previous workers.

Interpretation methods for magnetic anomalies may be divided into the categories of indirect and direct. The indirect method derives a solution by trial and error; a likely anomaly source is used as a starting point, and successive 'manual' readjustments are made to the parameters defining the source body until agreement between calculated and observed anomaly curves is deemed to be satisfactory. Due to the inherent ambiguity in the magnetic method, the model body produced by this method is just one of a very large number of solutions that satisfy both the anomaly and geological feasibility.

By use of a direct method, a solution for the anomalous

source is obtained directly from the observed anomaly. In the present work, this category is used to include iterative methods which automatically perform adjustments to the source body model. The solution obtained by use of a direct method of interpretation is derived by prior assumption of one or more of the magnetisation parameters and shape, or the limits within which these quantities will satisfy the observed anomaly.

3.1.1 The indirect method.

The computer program used in this method is MAGN (Bott, 1969b) which calculates the horizontal, vertical and total field magnetic anomalies for two dimensional bodies of polygonal cross-section. In the present work, MAGN was used for four purposes:

a) The production of anomalies due to bodies of relatively simple geometry for the purpose of testing programs under development.

b) Incorporation, in modified form, as a subroutine in other programs.

c) Simulation of broad geological situations for comparison of magnetic anomaly amplitude, gradient and phase relations.

d) Basic interpretation of magnetic anomalies where interfering effects due to a number of source bodies reduce the effectiveness of automated methods.

The equivalent routine for gravity interpretation, the program GRAVN (Bott, 1969a), was used in the first two of the situations listed above.

3.1.2 Non-linear optimisation, a direct method.

The development of the application of non-linear optimisation techniques to the interpretation of magnetic anomalies is due mainly to M. Al-Chalabi (Al-Chalabi, 1970a). A complete explanation of the theory of optimisation routines, together with examples of their application to geophysics, is given by Al-Chalabi (1970b). The full theory will not be presented here as the programmed versions for magnetic interpretation were used in the original form developed by Al-Chalabi.

Basically, non-linear optimisation applied to magnetic interpretation proceeds to solve for parameters describing an anomalous body by minimising the residual discrepancies between observed and calculated magnetic anomaly. The criterion used in the magnetic programs of Al-Chalabi is that the sum of the squares of residuals should be minimised by successive adjustments to the defining parameters. Thus, for an anomaly profile of n station points, and where Ai and Ci are the observed and calculated anomaly values at the ith station point, the function f which is to be minimised is given by,

$$f = \sum_{i=1}^{n} (Ai - Ci)^2$$

The function f is known as the objective function. If m variable parameters are used to describe the anomalous body, the objective function may be represented geometrically, in an m-dimensional space, by constructing a Euclidean hyperspace based on m mutually orthogonal axes. Within this hyperspace

the objective function is completely representable by means of contours of equal value, and its behaviour may be described qualitatively in terms of topographic nomenclature such as peaks and valleys.

In magnetic interpretation, the variable parameters describing the body are the background field, the horizontal and vertical components of magnetisation in the plane of the anomaly profile, and the cartesian coordinates defining a two dimensional polygonal body. For the purposes of optimisation, these parameters may be divided into adjustable and non-adjustable types. The non-adjustable parameters are those specified at known values and are held constant throughout the optimisation process. Adjustable parameters are the unknowns which require solution, and form the m variable parameters which dimension the hyperspace of the objective function. The programs of Al-Chalabi are capable of dealing with a system consisting entirely of adjustable parameters. At program input, the adjustable parameters are specified by a likely starting point value and upper and lower numerical bounds which define the range of adjustment by optimisation. Two of the programs were used in the present work: one derives a geometric solution based on just one pair of horizontal and vertical magnetisation components (MAGOP); the second program (MULTIJ) has the additional scope of solving for a source body with a distinct pair of magnetisation components associated with each side of the polygon. The distribution of sides with magnetisation components in common may be specified by the user of MULTIJ.

Al-Chalabi (1970b) has shown that the ambiguity that is inherent in all practical interpretations of potential field data (including magnetics) may be represented graphically by contoured cross-sections in the hyperspace of the objective function. The minimum of the objective function is located, on the contour plot, in an elongate 'valley' within which subsidiary minima are present. The subsidiary minima are associated with alternative model solutions which are acceptable within the limits of resolution of the interpretation. Limits of resolution are imposed by an incomplete knowledge of the length of the anomaly, the representation of a continuous anomaly by a sequence of digitised points, containing observational errors in measurement and values of finite numerical precision, and by the representation of an anomalous source by a relatively simple model. Each subsidiary minimum in the hyperspace corresponds to an acceptable solution in terms of the emphasis of some part of the more detailed structure on the simplified model used to represent a geological situation.

3.1.3 The linear inverse method, a direct method.

This method solves for a lateral distribution of anomalous magnetisation or density, within a layer of specified shape, to satisfy a given magnetic or gravity anomaly profile. The specification of shape and the configuration and number of components of the distribution makes the solution unambiguous. The distribution is obtained as a sequence of discrete values by solution of a set of simultaneous equations containing the digitised anomaly values, the unknown anomalous property

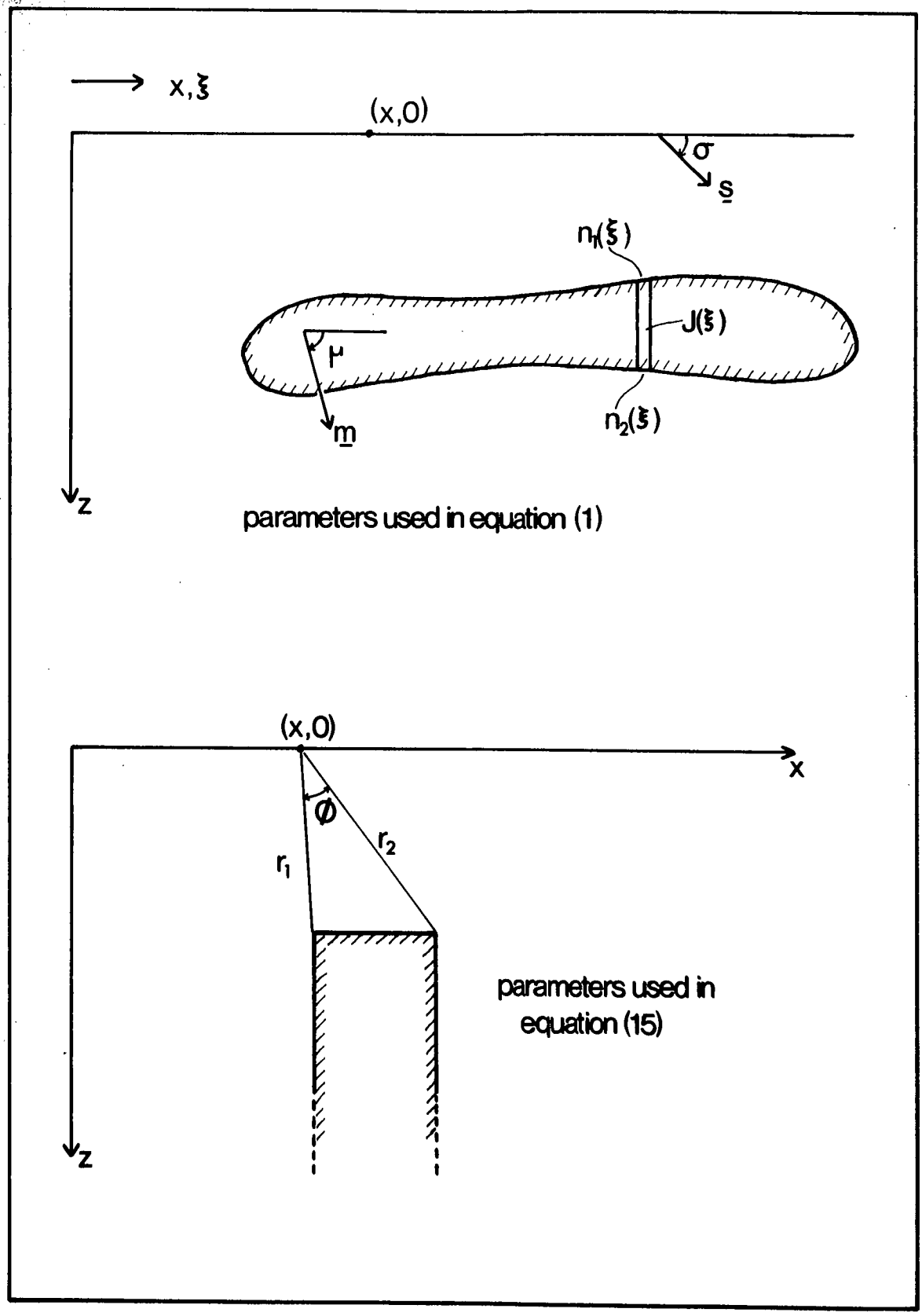

Fig 3.1 Parameter definition.

variable parameters and a coefficient set. The theory of the linear inverse method has been presented several times previously (Bott, 1967; Tanner, 1967; Emilia and Bodvarsson, 1969; Bott and Hutton, 1970b; Hutton, 1970), but the basic equations will be repeated here as they form the basis for further development of the method.

For two-dimensional interpretation, the theory followed is that of Bott (1967). The two dimensions are defined by cartesian coordinates in the xz-plane, where the x-axis is horizontal and z-axis is vertical and positive downwards. A magnetic anomaly A(x,o), measured along the x-axis, is considered to be caused by a two-dimensional distribution of magnetisation in the positive half-space $z > 0$, with its strike direction perpendicular to the x-axis, and with a constant specified direction of magnetisation (fig 3.1). The direction of magnetisation is given by $\underline{m}(\cos\mu\ ,\ \sin\mu\ )$, and that of the measured component of the anomaly by $\underline{s}(\cos\sigma\ ,\ \sin\sigma\ )$, both of which are assumed to lie in the xz-plane. The distribution of magnetisation may be represented by a closed body or a system of closed bodies whose surfaces are cut twice or not at all by any vertical line. ξ is the x-coordinate of a point on or in the system of bodies, of which the upper and lower surfaces are at depths $z = n_1(\xi)$ and $z = n_2(\xi)$ respectively. The intensity of magnetisation $J(\xi)$ is assumed to be a function of ξ alone within the bodies and zero without.

The magnetic anomaly is then given by the convolution integral,

$$A(x, o) = \int_{-\infty}^{+\infty} J(\xi) \, K(n_1, n_2, B, (x-\xi)) \, d\xi \qquad (1)$$

where $B = \mu + \sigma$, and K is the kernel function of the magnetic relation.

If the directions of magnetisation and measured anomaly component do not lie in the xz-plane a transformation may be used to bring them into the plane. In the form of Bott (1969c), the transformation is given by,

$$\mu = \arctan(\tan Im / \cos am)$$

$$\sigma = \arctan(\tan Ie / \cos ae)$$

where Im and Ie are the inclinations of magnetisation and the measured anomaly component respectively, and am and ae are their respective azimuths as measured from the x-axis. If $\underline{J}$ is the body magnetisation in the direction defined by Im and am, a fictitious intensity of magnetisation J^1 in the direction $\underline{m}$ may be defined by,

$$J^1 = |\underline{J}| \, (\sin^2 Im + \cos^2 Im \cos^2 am)^{\frac{1}{2}} . \, (\sin^2 Ie + \cos^2 Ie \cos^2 ae)^{\frac{1}{2}}$$

The magnetic anomaly in the direction defined by (Ie, ae) caused by magnetisation $\underline{J}$(Im, am) is then identical to the magnetic anomaly component in the direction $\underline{s}$ caused by magnetisation $\underline{J}^1$ in a direction $\underline{m}$.

In equation (1), $J(\xi)$ stands outside the kernel function and is in linear relationship to the magnetic anomaly provided

that $J(\xi)$ is a function of ξ only,

The anomaly A(x,o) may be replaced by a sequence of n digitised station points of value $Ai(i = 1,2,.....,^{n})$, and the source distribution can be approximated by a layer of m finite two-dimensional block elements, within each of which the intensity of magnetisation is assumed to be a constant $Jj(j = 1,2,...,m)$. Thus the integral of equation (1) may be approximated by the following summation (Bott, 1967; Tanner, 1967),

$$Ai = \sum_{j-1}^{m} KijJj \qquad (i = 1.....n) \qquad (2)$$

where Kij is a kernel coefficient and is the contribution to the ith anomaly value by the jth block element for unit of specified intensity of magnetisation. The relationship is one between anomalous quantities and assumes the prior removal of a background field. Equation (2) represents a system of n linear equations which may be solved for the m values of J provided that $n \geqslant m$. Direct solution is possible if n = m, and a solution is obtainable by least-squares, for the overdetermined case where $n > m$.

In matrix notation, equation (2) may be written as

$$\underline{A} = K\underline{J} \qquad (3)$$

where K is the n x m kernel matrix and $\underline{A}$ and $\underline{J}$ are column vectors of length n and m respectively. The solution for $\underline{J}$ in the overdetermined case is

$$\underline{J} = (K^T K)^{-1} K^T \underline{A} \qquad (4)$$

(Bott, 1967; Tanner, 1967)

where K^T denotes the transpose of K.

Application of programmed versions of this method to the interpretation of magnetic anomalies has been quite extensive (Bott, 1967; Emilia and Bodvarrson, 1969; Bott and Hutton, 1970b; Hutton, 1970), and its limitations with respect to resolution and data quality have been discussed (Bott and Hutton, 1970a; Hutton, 1970). In its most versatile form, the method has been programmed to deal with a magnetic layer composed of elements of polygonal cross-section (Hutton, 1970). The programs of Hutton, and the developments of the linear inverse method, described below, perform the least squares operation by a call to subroutine LLSQ (IBM, 1968).

The linear inverse technique is a direct method of interpretation as it produces a solution, in terms of a lateral distribution of intensities of magnetisation, directly from the observed anomaly. This solution is unique for a given anomaly and a specified block element configuration within the magnetic layer.

For interpretation of data from the survey of 1969, which lacked reflection seismic and detailed bathymetric control, and data from the survey of 1967, for which seismic reflection control was lacking, a simple magnetic layer of rectangular block elements was used with constant depths to parallel upper and lower surfaces. Deviations of this simple equivalent layer from the real geological situation are to be expected

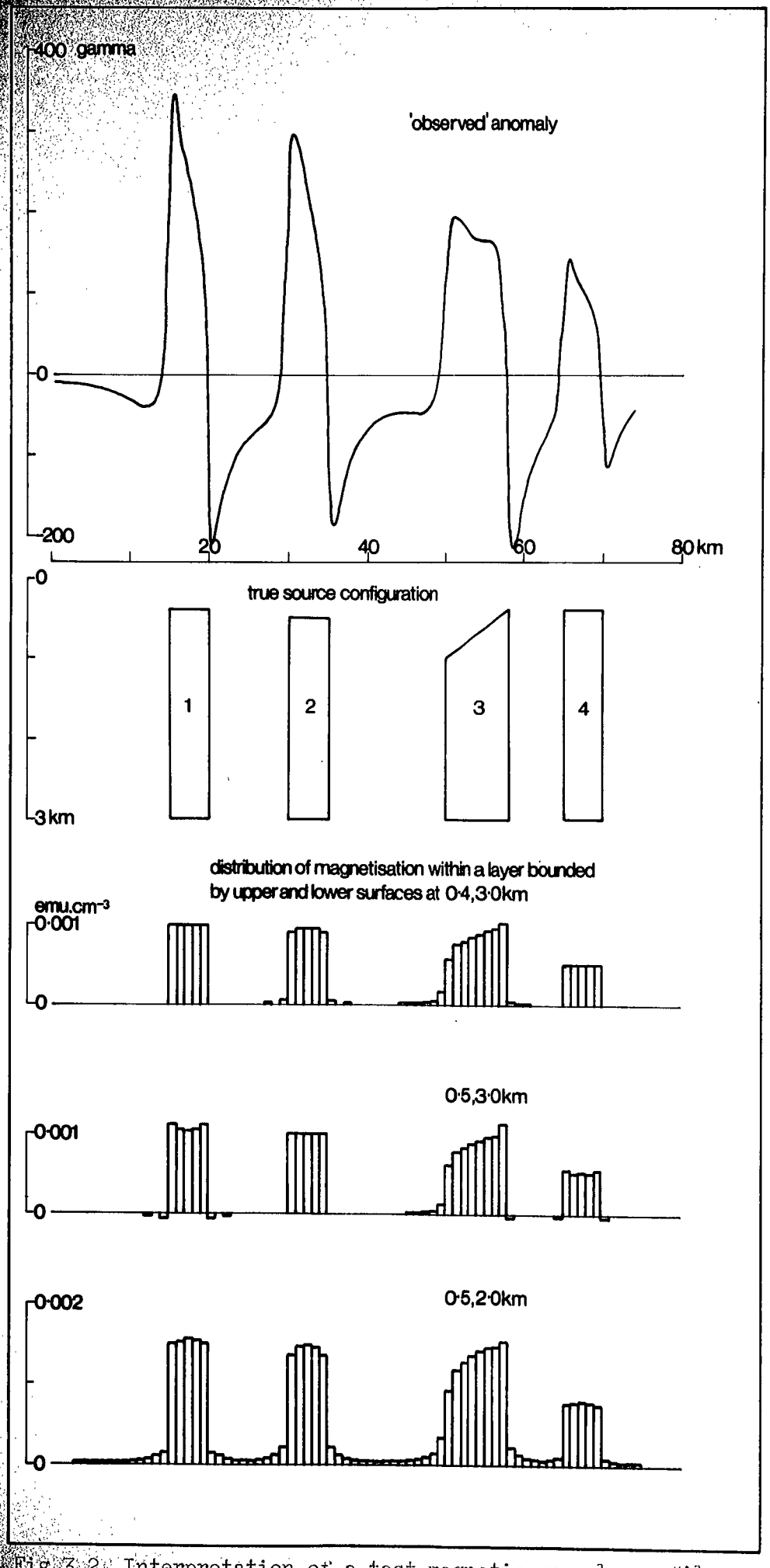

Fig 3.2 Interpretation of a test magnetic anomaly profile by use of the linear inverse method.

as additional spurious magnetisations in the solutions. The affect on the solution of an inadequately representative, or inaccurately positioned equivalent layer is shown in fig 3.2. The response of the method to placing either or both of the upper and lower surfaces of the layer at too great a depth, with respect to the configuration of the true source, is to cause instability by emphasis of short wavelengths in the solution. The opposite case, of surfaces not being deep enough, causes a response to suppress the short wavelengths as a smoothing of the solution.

3.2 The development of methods for the joint analysis of gravity and magnetic anomalies by the linear inverse technique.

In this section, the theory and development is presented of an extension to the linear inverse method to perform transformations from gravity to magnetic anomalies (and vice versa), to solve for the ratio of anomalous properties (magnetisation/density), and to determine the angle of magnetisation of a source body. The anomaly transformations are also used in the study of magnetic anomalies to separate those due to body geometry from those due to variations in magnetisation alone.

Equation (1) shows that the magnetic anomaly is produced by convolution of the magnetisation and a kernel function, which itself is a function of source shape and location. Similarly, the gravity anomaly is produced by convolution of

density and a term which is a function of shape and location. Thus, if a body causes a gravity and a magnetic anomaly, a joint analysis of both anomaly types may be performed to eliminate the unknown shape term (Garland, 1951), and to derive the relation between anomalous properties, density and magnetisation. In analytical terms, the gravity and magnetic anomalies may be compared without consideration of the source body shape if the gravity anomaly is differentiated with respect to the space coordinates (Lundbak, 1956).

3.2.1 The Poisson formula and its application.

A formula due to Poisson relates the gravitational and magnetic potentials of a source body:

$$V = (\frac{1}{Gp})\underline{J}.\underline{\nabla}U \qquad (5)$$

where V is the magnetic potential, U is the gravitational potential, $\underline{J}$ and p are the body magnetisation vector and density, G is the gravitational constant and $\underline{\nabla}$ the Laplacian differential operator. A simple formula obtained from equation (5) relates the vertical magnetic anomaly component Z to the gravity anomaly g. Differentiating both sides of equation (5) with respect to z:

$$Z = (\frac{1}{Gp})\underline{J} \cdot \underline{\nabla}(g)$$

where $g = \frac{dU}{dz}$

For a two-dimensional coordinate system as defined for equation

(1), where μ is the angle of magnetisation and $J = |\underline{J}|$,

$$Z = \left(\frac{J}{Gp}\right)\left(\frac{dg}{dx}\cos\mu + \frac{dg}{dz}\sin\mu\right) \qquad (6)$$

Equation (6) was used by Garland (1951) to determine the ratio J/p in an area from which both gravity and magnetic data had been obtained. This ratio was then used as a parameter diagnostic of the concealed rock type. Using a three-dimensional form of equation (6), Lundbak (1956) calculated values of J/p and angles of magnetisation. A more general form of the equation which relates the magnetic anomaly component A, measured in the direction $\underline{s}$, to the derivatives of the gravity anomaly, for a two-dimensional system is,

$$A = \left(\frac{J}{Gp}\right)\left(\frac{dg}{dx}\sin B - \frac{dg}{dz}\cos B\right) \qquad (7)$$

(Bott, 1969c)

where $B = \mu + \sigma$, and has been defined above (equation (1)).

The theory of pseudo-gravity anomalies was developed by Baranov (1957) from equation (5). The pseudo-gravity anomaly was calculated from the total field anomaly using a conventional density of p=J/G. It is the real gravity anomaly for a particular body if this conventional relation between density and magnetisation exists in the real situation, but whatever the ~~time~~ true relation between J and p, the pseudo-gravity anomaly behaves as a real gravity anomaly in that the anomaly peaks are located more easily, and may be interpreted by the simpler methods of gravity interpretation.

The original method of Baranov was developed for a three-dimensional anomaly system for which the source body magnetisation was assumed to be in the direction of the earth's field. An extension of the method for two-dimensional bodies by Bott et al., (1966) does not require this assumption. Bott et al., (1966) present also a method for estimating the direction of magnetisation, based on the use of the pseudo-gravity anomaly, with assumptions that direction of magnetisation is the same at every point in the body and that intensity of magnetisation has the same sign throughout the body. From the second assumption it follows that the computed pseudo-gravity anomaly at every point above the body must have the same sign. Estimates of ranges of possible directions of magnetisation were made by Bott et al. to satisfy this condition.

Recent applications of the Poisson formula and its derivative forms of equation (6) have been made from two main approaches. Wilson (1970) used a least-squares technique to derive the parameters (Jx/p), (Jz/p) and a from the system of n linear equations

$$Z_i = a + (Jx/p)\ (dg/dx)_i + (Jz/p)\ (dg/dz)_i \qquad (i = 1.. \ldots\ldots\ldots n)$$

Where Jx and Jz are the horizontal and vertical components of magnetisation $\underline{J}$. Kanasewich and Agarwal (1970) performed calculations for J/p in the wavenumber domain, by use of a theoretical vertical magnetic anomaly calculated from equation

(6) and a transformation of the observed total field magnetic anomaly to the magnetic pole (Baranov, 1957). Individual values of J/p associated with selected wavenumbers or bands of wavenumbers, were computed directly from the corresponding sections of the amplitude spectra of the transformed and theoretical vertical magnetic anomalies. Acceptability of the ratio values was based on the value of a coherence coefficient, calculated as a function of the auto- and cross-power spectra of the vertical anomalies for the selected wavenumber bands. The method was used by Kanasewich and Argarwal with the assumption that high coherence did indicate a common source from the transformed magnetic anomaly and the theoretical magnetic anomaly calculated from gravity data.

3.2.2 Development of the linear inverse method to perform Poisson type analyses.

An advantage of using an analysis of the Poisson type is that information on the source of a gravity and magnetic anomaly, such as the ratio J/p, may be obtained without assumptions concerning the shape of the source body. All the necessary information is contained in the waveforms of the two anomalies. Therefore, any distribution of density and magnetisation that satisfies the two observed anomalies must also permit the determination of the true ratio of anomalous properties. The inherent ambiguity of potential field interpretation implies that the effect of an anomalous body may be represented by a distribution of density of magnetisation

within an equivalent layer (Skeels, 1947; Peters, 1949; Bott, 1967; Tanner, 1967; Dampney, 1969). This equivalent source may be a layer of finite thickness or it may be a horizontal plane on which the distribution of the anomalous property is in the form of a variable coating of density or magnetisation per unit area. Moreover, for a given anomaly and a specified equivalent layer, and, in the case of magnetic interpretation, a specified direction of magnetisation, the distribution of the anomalous property is unique (Roy, 1962). The uniqueness for a specified layer is essential to the numerical approximation of the linear inverse method, as used by Bott (1967) to derive distributions of magnetisation that satisfy observed marine magnetic anomalies. When used in this way, the equivalent layer is also assumed to approximate the true source body shape and position so that the intensities of magnetisation in the solution are of the correct order of magnitude. In the extension of the linear inverse method to perform Poisson type analyses, the equivalent layer of finite block elements has only to satisfy the gravity and magnetic anomalies in terms of an adequate distribution of density and magnetisation which is unique for the specified layer. Adequacy of the distribution, for a given horizontal extent of the true body, depends on the relative thickness of the equivalent layer to that of the true body. Complete representation of an anomalous body, of finite thickness, by a coating of density or magnetisation on an equivalent plane requires that the plane be of infinite extent. In the practical case, of a thin equivalent layer of

block elements, the requirement is that the blocks are extended beyond the horizontal limits of the true body to a distance that depends on their thickness relative to that of the body.

3.2.2.1 The transformation of anomalies.

A simple extension of the linear inverse method enables a transformation to be made, in either direction, between gravity and magnetic anomalies. For a transformation from the magnetic to the gravity anomaly, an equivalent layer is used to represent a body in which the ratio J/p is assumed to remain constant, and for which a direction of magnetisation is specified. The distribution of intensities of magnetisation within the equivalent layer is given by equation (4) for the overdetermined case,

$$\underline{J} = (K^T K)^{-1} K^T \underline{A} \qquad (4)$$

The method now calculates the gravity anomaly which would be caused by the same body for a density p, where p = fJ, and f is a constant. For each block element of the equivalent layer, the relation is

$$pj = fJj \qquad (j = 1.....m)$$

or for the whole layer

$$\underline{p} = f\underline{J} \qquad (8)$$

Equation (8) holds if the equivalent layer is an adequate

representation of the observed anomaly source.

If C denotes the kernel matrix for the gravity anomaly $\underline{g}$, then

$$\underline{g} = C\underline{p} \tag{9}$$

By substituting the right hand side of (4) in (8) and then (8) in (9), the transformation from the total field magnetic anomaly to the gravity anomaly becomes

$$\underline{g} = Cf(K^TK)^{-1} K^T\underline{A} \tag{10}$$

Similarly, the transformation from gravity to the magnetic anomaly is given by

$$\underline{A} = Kh(C^TC)^{-1} C^T \underline{g} \tag{11}$$

where h is a constant and, if equation (11) is used on the gravity anomaly caused by the same body as that represented in equation (8), it is the reciprocal of f.

In equation (8), the constant f can take any value in the range $-\infty \leqslant f \leqslant +\infty$; it implies one or more coincident sources for gravity and magnetic anomalies with a constant ratio p/J.

The method is useful for computing one anomaly, gravity or magnetic, from the other by use of a conventional value $f = h = 1$, and comparing the anomaly produced by transformation with the observed anomaly of the same type. The hypothesis

of coincident sources for the two observed anomalies may be accepted or rejected on the basis of this comparison. The actual comparison may be made after scaling the anomaly produced by transformation, the pseudo-anomaly, by multiplying the whole profile by the ratio of maximum amplitudes of observed anomaly/pseudo-anomaly.

3.2.2.2 The direct calculation of the ratio p/J or J/p.

A more general situation than that represented by equation (8) is that of an anomaly source consisting of a lateral distribution of m elements within each of which density and intensity of magnetisation are assumed uniform but which may differ for successive elements. Thus, for each element there is an individual constant of proportionality fj such that the density and intensity of magnetisation for each element are related by

$$pj = fjJj \qquad (j = 1.....m) \qquad (12)$$

If the direction of magnetisation is the same for all the elements, and is specified, the individual values of fj (pj/Jj) may be calculated.

The solution for the individual values fj is obtained as follows, starting from the solution of a distribution of intensity of magnetisation.

$$\underline{J} = (K^T K)^{-1} K^T \underline{A} \qquad (4)$$

A new kernel matrix C_f is now formed from the gravity

kernel C and the individual components of $\underline{J}$ in the following way,

$$C_f(i,j) = C(i,j)Jj$$

Thus $C_f(i,j)$ is the contribution to the gravity anomaly at the ith station point due to the jth block element for a conventional ratio value of pj/Jj = 1, and with the assumption that density and magnetisation within each block are constant values. A matrix equation may now be written to represent the case when p/j = 1,

$$\underline{g} = C_f \underline{f}$$

where $\underline{g}$ is a column vector of length n, $\underline{f}$ is a column vector of length m and C_f is an nxm matrix. The solution for $\underline{f}$ in the overdetermined case is given by

$$\underline{f} = (C_f^T C_f)^{-1} C_f^T \underline{g} \qquad (13)$$

Thus the individual values of p/J are determined directly from the gravity anomaly. For completeness, there is a similar equation for the derivation of the reciprocal ratio values,

$$\underline{h} = (K_h^T K_h)^{-1} K_h^T \underline{A} \qquad (14)$$

where the ith, and jth element of matrix K_h is the contribution

to the magnetic anomaly at the ith station point by the jth block for a conventional ratio value of Jj/pj = 1.

This is just one way of deriving the individual ratio values associated with each block element. Another method would solve for the distributions of density and magnetisation independently, and directly from the observed anomalies, and then divide one of the distributions by the other, block by block, so that the numerator and denominator are of the same subscript (j = 1.....m). There is little to choose between the two methods as both require the two types of observed anomaly, and both require two calls to the least-squares routine. For programmed versions, the method represented by equation (13) and (14) has a slight advantage in that only one array of length m is required in storage, as the same array can be used to store magnetisation or density and the ratio values successively.

Interpretation using this technique is aided by a knowledge of the distribution of one of the anomalous properties, density or magnetisation, and the programmed version includes an intermediate print-out of the first stage solution for one of these distributions, as represented by equation (4).

3.2.2.3 Calculation of the angle of magnetisation.

If it is assumed that the observed gravity and magnetic anomalies are caused by a common source, homogeneous with respect to J/p, or a number of common sources with identical values of the ratio J/p, and that the direction of magnetisation

is everywhere constant, the angle of magnetisation can be determined.

The method makes use of an expression for the magnetic effect due to a two-dimensional vertical dyke with a sloping upper surface and of infinite extent downwards. This expression, which is due to Bott (personal communication), is used in the calculation of the kernel matrix elements. This expression for a dyke with a horizontal upper surface is of the form

$$F = r(r_1, r_2) \sin B - q(\phi) \cos B \qquad (15)$$

where F is the total field magnetic anomaly, B is the composite angle defined for equation (1), and r_1, r_2 are defined as shown in fig 3.1. To calculate the effect of a block element of finite thickness, the separate effect due to a vertical dyke of infinite extent downwards, with its upper surface at the depth of the lower surface of the block, is subtracted from that due to a similar dyke, with upper surface at the depth of the finite block upper surface. Thus the element of the kernel matrix K corresponding to the ith station point and the jth block is given by

$$K(i,j) = R(i,j) \sin B - Q(i,j) \cos B \qquad (16)$$

and the elements of the matrices R and Q are the difference in magnetic effect between the two dyke bodies described above.

To solve for the angle B the procedure starts from the

observed gravity anomaly, and is as follows:

$$\underline{g} = C\underline{p}$$

for which the solution in the overdetermined case is,

$$\underline{p} = (C^T C)^{-1} C^T \underline{g} \qquad (17)$$

The individual elements of matrices R and Q are now multiplied by the solutions of equation (17) and the new values are summed over all values of j to produce an (n x 2) matrix K_B. The complete process to derive the elements of K_B is given by,

$$K_B(i,1) = \sum_{j=1}^{m} R(i,j)p(j) \qquad (18)$$

$$K_B(i,2) = \sum_{j=1}^{m} Q(i,j)p(j) \qquad (19)$$

$$(i = 1.....n)$$

Thus, the magnetic anomaly at the ith station point is given by,

$$A(i) = K_B(i,1)h \sin B \mp K_B(i,2)h \cos B \qquad (20)$$

where h is a constant value of the true ratio J/p. The matrix equation is

$$\underline{A} = K_B\underline{b} \qquad (21)$$

where $\underline{A}$ is a column vector of length n, and $\underline{b}$ is a column vector of length 2. The solution for the overdetermined case is given by

$$\underline{b} = (K_B^T K_B)^{-1} K_B^T \underline{A} \qquad (22)$$

and the angle B is calculated from the two elements of $\underline{b}$ as,

$$B = \arctan (b(1)/b(2)) = \arctan (h \sin B / h \cos B) \qquad (23)$$

which also eliminates h. The angle σ' of the measured anomaly component is known in the relation $B = \mu + \sigma'$, and hence the angle of magnetisation μ is obtained.

The value of h, the ratio J/p, is obtained from

$$h = (b(1)^2 + b(2)^2)^{\frac{1}{2}} = (h^2 \sin^2 B + h^2 \cos^2 B)^{\frac{1}{2}} \qquad (24)$$

A further extension to this method would enable an individual value for angle B to be calculated for each block element of the equivalent layer. In this case the kernel matrix corresponding to K_B in equation (21) would be of dimension (n x 2m) and the vector $\underline{b}$ would be of length 2m, with a condition for solution of $n \geqslant 2m$ that imposes severe practical limitations on the method. A dense cover of precisely determined anomaly values is required unless the equivalent layer is divided into relatively few block elements of large width, this would usually render the distribution of density and magnetisation inadequate to

represent the anomalies, or unless the block elements are grouped into units each with a common magnetisation direction. For the case of an individual magnetisation angle associated with each of a moderate number of block elements, the resolution of the least-squares method is severely tested, as additional digital sampling of the anomaly, to satisfy the condition for solution, is effected without an improvement in error control. In addition, the condition of the kernel matrix increases as the number of columns (Anderssen, 1969), and consequently the accuracy to which the elements of the solution vector can be determined, decreases.

This additional extension was programmed, but meaningful distributions of magnetisation angle were obtained only when ideallised test anomalies were used, and when the equivalent layer approximated the shape of the 'true' body very closely. Thus, the application of the linear inverse method to calculate an individual magnetisation angle for each block element is not justified in practical situations.

3.2.3 The programmed versions of the methods and their application to test models.

The developments of the linear inverse method were programmed in the language of PL1 for use on the NUMAC IBM 360/67 computer. Programs with input specifications are described in the appendix. For the interpretation of data associated with this thesis, the joint gravity/magnetics analysis programs were used mainly on the long profiles from the survey of RRV John Murray in 1967, and the solutions were interpreted in a

semi-qualitative manner. For this type of use, simplified gravity and magnetic kernel functions are adequate to define an equivalent layer composed of two-dimensional rectangular block elements of constant width and thickness. The use of a simple equivalent layer makes available additional computer core space which enables long anomaly profiles to be processed as a single unit. Calculation of the kernel matrix elements involves several stages that are common to both gravity and magnetics, but core space was saved at the expense of time, and the kernels were computed sequentially. For calculation of the gravity kernel a version of GRAVN (section 3.1.1) was used in the modified form of G.J. Laving (1971); calculation of the magnetics kernel was based on equation (17), but one program, GJ/RAT, includes a kernel calculation based on a modified version of MAGN (section 3.1.1).

3.2.3.1 Basic transform programs, TR/GM and TR/MG.

The two transformation programs are TR/GM (gravity to magnetics) and TR/MG (magnetics to gravity), and listings of these are contained in appendices B and C. The programs perform the following operations:

a) Complete input: observed anomaly; inclination and azimuth angles of the earth's field and body magnetisation vectors; equivalent layer configuration.

b) Transformation of magnetic angles into the plane of the anomaly profile.

c) Calculation of the kernel elements appropriate to the anomaly type of the observed anomaly.

d) Calculation of the distribution of anomalous property, density or magnetisation, within the equivalent layer to satisfy the observed anomaly.

e) Calculation of the kernel elements appropriate to an anomaly of the other type.

f) Calculation of an anomaly of the other type for a conventional value of J/p = 1.

Tests on the transform programs used the gravity and magnetic anomalies caused by the simple body shown in fig 3.3. Tables 3.1 and 3.2 contain the results of the transformations for an equivalent layer at the same depth and thickness as the true body; tables 3.3 and 3.4 contain the results of transformations using a thin equivalent layer (0.1km) at the depth of the true body. The calculated anomalies have been scaled by multiplying by the true ratio J/p or p/J. Residual anomalies (observed magnetic minus pseudo-magnetic) for the transformation gravity to magnetics are also plotted in fig 3.3.

A difference in style of residuals between the two directions of transformation is to be anticipated from a consideration of the process represented by the two-kernel operation in the programs. It is evident from equation (7)

$$A = (J/Gp)\left(\frac{dg}{dx}\sin B - \frac{dg}{dz}\cos B\right) \qquad (7)$$

that the transformation gravity to magnetics is a differential operation, and as with derivative filters, short wavelength 'error' components are amplified (table 3.4; fig 3.3). The source of errors responsible for the oscillations is

probably limited definition of the gravity anomaly and limited numerical precision of the values at low amplitudes away from the main peak. Other contributory factors are the approximation to a continuous density distribution by a sequence of discrete values for the blocks, and the presence of a small step to the end point anomaly values, due to the finite length of the profile.

The transformation magnetics to gravity is an integration operation, and the small almost constant residual (table 3.3) is due to the finite length of the integration process; in terms of the present method, it is due to the finite length of the anomaly profile and restriction of the horizontal extent of the equivalent layer to the same length.

The method can be used to discriminate between source bodies which differ in the value of the ratio J/p. Fig 3.4 shows the results of transform operations on the gravity and magnetic anomalies caused by two discrete bodies. The two transformations are unscaled, but both components are resolved for the correct values of J/p to be determined from the ratios of the peak values observed/calculated. This method of determining J/p from the peak values of the observed anomaly is analogous to that of Kanasewich and Agarwal (1970), except that these authors compared amplitudes from selected sections of the spectra of the observed and calculated anomalies.

Fig. 3.3.

A: Observed anomaly curves caused by shaded body.

B: Magnetisation and density distributions within a thin equivalent layer.

C: Residuals, observed minus scaled pseudo - magnetic anomaly, for the gravity to magnetics transformation using a thin equivalent layer.

Origin at south end of profile.

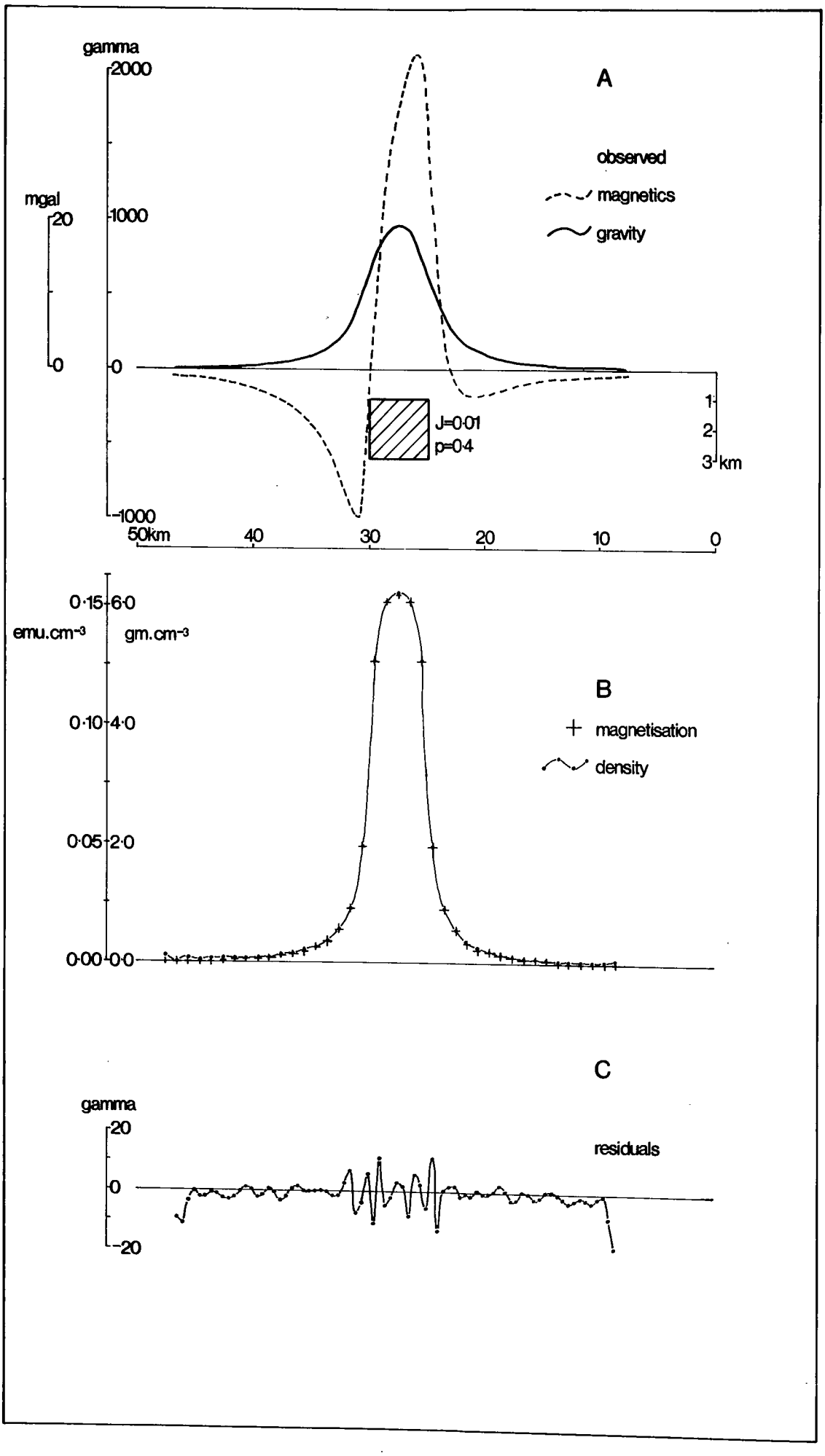
gamma
2000
1000
0
-1000
A
observed
magnetics
gravity
mgal
20
0
J=0·01
p=0·4
1
2
3
km
50km
40
30
20
10
0
0·15
6·0
emu.cm⁻³
gm.cm⁻³
0·10
4·0
0·05
2·0
0·00
0·0
B
magnetisation
density
C
gamma
20
0
-20
residuals

TABLE 3.1 TRANSFORMATION MAGNETICS TO GRAVITY, FULL DEPTH LAYER.

Distance	Observed (Mgal)	Calculated * 40.0	Residuals
8.5	0.30	0.30	0.00
9.0	0.31	0.31	0.00
9.5	0.33	0.33	0.00
10.0	0.35	0.35	0.00
10.5	0.37	0.37	0.00
11.0	0.39	0.39	0.00
11.5	0.42	0.42	0.00
12.0	0.45	0.44	+ 0.01
12.5	0.48	0.48	0.00
13.0	0.51	0.51	0.00
13.5	0.55	0.55	0.00
14.0	0.59	0.59	0.00
14.5	0.63	0.64	- 0.01
15.0	0.69	0.69	0.00
15.5	0.75	0.74	+ 0.01
16.0	0.81	0.81	0.00
16.5	0.89	0.89	0.00
17.0	0.98	0.98	0.00
17.5	1.08	1.08	0.00
18.0	1.19	1.19	0.00
18.5	1.33	1.33	0.00
19.0	1.49	1.49	0.00
19.5	1.68	1.68	0.00
20.0	1.92	1.92	0.00
20.5	2.20	2.20	0.00
21.0	2.55	2.55	0.00
21.5	2.99	2.99	0.00
22.0	3.55	3.54	+ 0.01

TABLE 3.1 continued

Distance	Observed (Mgal)	Calculated * 40.0	Residuals
22.5	4.26	4.26	0.00
23.0	5.20	5.20	0.00
23.5	6.45	6.44	+ 0.01
24.0	8.10	8.10	0.00
24.5	10.23	10.22	+ 0.01
25.0	12.73	12.73	0.00
25.5	15.18	15.18	0.00
26.0	17.12	17.12	0.00
26.5	18.45	18.44	+ 0.01
27.0	19.20	19.20	0.00
27.5	19.44	19.44	0.00
28.0	19.20	19.20	0.00
28.5	18.45	18.44	+ 0.01
29.0	17.12	17.12	0.00
29.5	15.18	15.18	0.00
30.0	12.74	12.73	+ 0.01
30.5	10.23	10.22	+ 0.01
31.0	8.10	8.10	0.00
31.5	6.45	6.44	+ 0.01
32.0	5.20	5.20	0.00
32.5	4.26	4.26	0.00
33.0	3.55	3.54	+ 0.01
33.5	2.99	2.99	0.00
34.0	2.55	2.55	0.00
34.5	2.20	2.20	0.00
35.0	1.92	1.92	0.00
35.5	1.68	1.68	0.00
36.0	1.49	1.49	0.00
36.5	1.33	1.33	0.00

TABLE 3.2 continued

Distance	Observed (gamma)	Calculated/40.0	Residuals
36.50	-248.5	-250.1	+1.6
37.00	-222.6	-220.9	-1.7
37.50	-200.4	-197.7	-2.7
38.00	-181.2	-181.3	+0.1
38.50	-164.6	-166.0	+1.5
39.00	-150.2	-149.7	-0.5
39.50	-137.5	-136.5	-1.0
40.00	-126.3	-127.4	+1.1
40.50	-116.4	-118.5	+2.1
41.00	-107.6	-108.2	+0.6
41.50	- 99.8	- 99.0	-0.8
42.00	- 92.8	- 92.2	-0.6
42.50	- 86.5	- 86.1	-0.4
43.00	- 80.8	- 80.5	-0.3
43.50	- 75.6	- 76.6	+1.0
44.00	- 70.9	- 74.2	+3.3
44.50	- 66.7	- 69.3	+2.6
45.00	- 62.8	- 62.7	-0.1
45.50	- 59.2	- 61.7	+2.5
46.00	- 55.9	- 65.0	+9.1
46.50	- 52.9	- 57.4	+4.5

TABLE 3.1 continued

Distance	Observed (Mgal)	Calculated * 40.0	Residuals
37.0	1.19	1.19	0.00
37.5	1.08	1.08	0.00
38.0	0.98	0.98	0.00
38.5	0.89	0.89	0.00
39.0	0.81	0.81	0.00
39.5	0.75	0.74	+ 0.01
40.0	0.69	0.69	0.00
40.5	0.63	0.64	- 0.01
41.0	0.59	0.59	0.00
41.5	0.55	0.55	0.00
42.0	0.51	0.51	0.00
42.5	0.48	0.48	0.00
43.0	0.45	0.44	+ 0.01
43.5	0.42	0.42	0.00
44.0	0.39	0.39	0.00
44.5	0.37	0.37	0.00
45.0	0.35	0.35	0.00
45.5	0.33	0.33	0.00
46.0	0.31	0.31	0.00
46.5	0.30	0.30	0.00

TABLE 3.2 TRANSFORMATION GRAVITY TO MAGNETICS, FULL DEPTH LAYER.

Distance	Observed (gamma)	Calculated/40.0	Residuals
8.50	-41.2	-41.2	-1.0
9.00	-43.2	-43.7	+0.5
9.50	-45.4	-46.3	+0.9
10.00	-47.7	-48.5	+0.8
10.50	-50.3	-50.8	+0.5
11.00	-53.0	-53.2	+0.2
11.50	-55.9	-55.5	-0.4
12.00	-59.1	-57.9	-1.2
12.50	-62.5	-61.1	-1.4
13.00	-66.3	-65.6	-0.7
13.50	-70.4	-71.0	+0.6
14.00	-74.8	-76.5	+1.7
14.50	-79.6	-80.6	+1.0
15.00	-84.9	-83.9	-1.0
15.50	-90.6	-89.4	-1.2
16.00	-96.9	-97.5	+0.6
16.50	-103.7	-104.3	+0.6
17.00	-111.1	-109.3	-1.8
17.50	-119.2	-117.3	-1.9
18.00	-127.9	-129.3	+1.4
18.50	-137.1	-140.0	+2.9
19.00	-146.8	-147.4	+0.6
19.50	-156.6	-155.9	-0.7
20.00	-165.9	-166.4	+0.5
20.50	-173.8	-174.5	+0.7
21.00	-178.4	-177.1	-1.3
21.50	-176.2	-174.7	-1.5
22.00	-161.2	-162.1	+0.9

TABLE 3.2 continued

Distance	Observed (gamma)	Calculated/40.0	Residuals
22.50	-122.5	-124.6	+2.1
23.00	- 40.1	- 40.7	+0.6
23.50	121.4	123.2	-1.8
24.00	420.8	423.7	-2.9
24.50	923.1	924.1	-1.0
25.00	1558.6	1555.7	+2.9
25.50	1997.7	1994.6	+3.1
26.00	2105.2	2105.8	-0.6
26.50	2029.2	2031.4	-2.2
27.00	1886.1	1885.8	+0.3
27.50	1716.6	1715.2	+1.4
28.00	1517.4	1518.7	-0.3
28.50	1259.9	1260.5	-0.6
29.00	881.4	879.9	+1.5
29.50	315.7	314.5	+1.2
30.00	-370.3	-367.8	-2.5
30.50	-850.4	-846.5	-3.9
31.00	-992.9	-992.2	-0.7
31.50	-950.6	-952.9	+2.3
32.00	-847.2	-849.6	+2.4
32.50	-735.2	-736.0	+0.8
33.00	-632.9	-631.9	-1.0
33.50	-544.9	-543.8	-1.1
34.00	-470.9	-471.5	+0.6
34.50	-409.3	-410.4	+1.1
35.00	-358.0	-358.0	0.0
35.50	-315.1	-315.3	+0.2
36.00	-279.0	-281.7	+2.7

TABLE 3.3 TRANSFORMATION ~~GRAVITY TO MAGNETICS~~ MAGNETICS TO GRAVITY, THIN LAYER.

Distance	Observed (Mgal)	Calculated x 40.0	Residuals
8.5	0.30	0.20	0.10
9.0	0.31	0.22	0.09
9.5	0.33	0.24	0.09
10.0	0.35	0.26	0.09
10.5	0.37	0.29	0.08
11.0	0.39	0.31	0.08
11.5	0.42	0.34	0.08
12.0	0.45	0.36	0.09
12.5	0.48	0.40	0.08
13.0	0.51	0.43	0.08
13.5	0.55	0.47	0.08
14.0	0.59	0.51	0.08
14.5	0.63	0.56	0.07
15.0	0.69	0.61	0.08
15.5	0.75	0.67	0.08
16.0	0.81	0.74	0.07
16.5	0.89	0.82	0.07
17.0	0.98	0.90	0.08
17.5	1.08	1.00	0.08
18.0	1.19	1.12	0.07
18.5	1.33	1.26	0.07
19.0	1.49	1.42	0.07
19.5	1.68	1.62	0.06
20.0	1.92	1.85	0.07
20.5	2.20	2.13	0.07
21.0	2.55	2.48	0.07
21.5	2.99	2.92	0.07
22.0	3.55	3.48	0.07

TABLE 3.3 continued

Distance	Observed (Mgal)	Calculated x 40.0	Residuals
22.5	4.26	4.20	0.06
23.0	5.20	5.13	0.07
23.5	6.45	6.38	0.07
24.0	8.10	8.04	0.06
24.5	10.23	10.16	0.07
25.0	12.73	12.67	0.06
25.5	15.18	15.12	0.06
26.0	17.12	17.05	0.07
26.5	18.45	18.38	0.07
27.0	19.20	19.14	0.06
27.5	19.44	19.38	0.06
28.0	19.20	19.14	0.06
28.5	18.45	18.38	0.07
29.0	17.12	17.05	0.07
29.5	15.18	15.12	0.06
30.0	12.74	12.67	0.07
30.5	10.23	10.16	0.07
31.0	8.10	8.04	0.06
31.5	6.45	6.38	0.07
32.0	5.20	5.14	0.06
32.5	4.26	4.20	0.06
33.0	3.55	3.48	0.07
33.5	2.99	2.92	0.07
34.0	2.55	2.49	0.06
34.5	2.20	2.14	0.06
35.0	1.92	1.86	0.06
35.5	1.68	1.62	0.06
36.0	1.49	1.43	0.06

TABLE 3,3 continued

Distance	Observed (Mgal)	Calculated x 40.0	Residuals
36.5	1.33	1.27	0.06
37.0	1.19	1.13	0.06
37.5	1.08	1.01	0.07
38.0	0.98	0.91	0.07
38.5	0.89	0.82	0.07
39.0	0.81	0.75	0.06
39.5	0.75	0.68	0.07
40.0	0.69	0.62	0.07
40.5	0.63	0.57	0.06
41.0	0.59	0.52	0.07
41.5	0.55	0.48	0.07
42.0	0.51	0.44	0.07
42.5	0.48	0.41	0.07
43.0	0.45	0.38	0.07
43.5	0.42	0.35	0.07
44.0	0.39	0.32	0.07
44.5	0.37	0.30	0.07
45.0	0.35	0.28	0.07
45.5	0.33	0.26	0.07
46.0	0.31	0.24	0.07
46.5	0.30	0.22	0.08

TABLE 3.4 TRANSFORMATION GRAVITY TO MAGNETICS, THIN LAYER.

Distance	Observed (gamma)	Calculated/40.0	Residuals
8.5	- 41.2	- 23.0	-18.2
9.0	- 43.2	- 35 1	- 8.1
9.5	- 45.4	- 44.5	- 0.9
10.0	- 47.7	- 45.9	- 1.8
10.5	- 50.3	- 47.1	- 3.2
11.0	- 53.0	- 50.9	- 2.1
11.5	- 55.9	- 54.4	- 1.5
12.0	- 59.1	- 56.4	- 2.7
12.5	- 62.5	- 59.5	- 3.0
13.0	- 66.3	- 64.4	- 1.9
13.5	- 70.4	- 70.0	- 0.4
14.0	- 74.8	- 75.5	+ 0.7
14.5	- 79.6	- 79.9	+ 0.3
15.0	- 84.9	- 83.0	- 1.9
15.5	- 90.6	- 88.5	- 2.1
16.0	- 96.9	- 96.5	- 0.4
16.5	-103.7	-103.7	0.0
17.0	-111.1	-108.7	- 2.4
17.5	-119.2	-116.7	- 2.5
18.0	-127.9	-128.3	+ 0.4
18.5	-137.1	-139.3	+ 2.2
19.0	-146.8	-147.0	+ 0.2
19.5	-156.6	-155.9	- 0.7
20.0	-165.9	-165.2	- 0.7
20.5	-173.8	-173.9	+ 0.1
21.0	-178.4	-177.1	- 1.3
21.5	-176.2	-175.3	- 0.9
22.0	-161.2	-159.4	- 1.8

TABLE 3.4 continued

Distance	Observed (gamma)	Calculated/40.0	Residuals
22.5	-122.5	-124.3	+ 1.8
23.0	- 40.1	- 41.8	+ 1.7
23.5	121.4	121.1	+ 0.3
24.0	420.8	434.3	-13.5
24.5	923.1	911.9	+11.2
25.0	1558.6	1564.2	- 5.9
25.5	1997.7	1995.5	+ 2.2
26.0	1105.2	2100.2	+ 5.2
26.5	2029.2	2037.9	- 8.7
27.0	1886.1	1884.4	+ 1.7
27.5	1716.6	1713.8	+ 2.8
28.0	1518.4	1520.5	- 2.1
28.5	1259.9	1264.9	- 5.0
29.0	881.4	870.3	+11.1
29.5	315.7	327.4	-11.7
30.0	- 370.3	- 375.8	+ 5.5
30.5	- 850.4	- 846.1	- 4.3
31.0	- 992.9	- 985.2	- 7.7
31.5	- 950.6	- 957.4	+ 6.8
32.0	- 847.2	- 849.5	+ 2.3
32.5	- 735.2	- 733.5	- 1.7
33.0	- 632.9	- 631.1	- 1.8
33.5	- 544.9	- 544.5	- 0.4
34.0	- 470.9	- 470.9	0.0
34.5	- 409.3	- 409.1	- 0.2
35.0	- 358.0	- 357.6	- 0.4
35.5	- 315.1	- 315.1	0.0
36.0	- 279.0	- 280.3	+ 1.3

TABLE 3.4 continued

Distance	Observed (gamma)	Calculated/40.0	Residuals
36.5	-248.5	-249.0	+ 0.5
37.0	-222.6	-220.2	- 2.4
37.5	-200.4	-197.1	- 3.3
38.0	-181.2	-180.5	- 0.7
38.5	-164.6	-164.9	+ 0.3
39.0	-150.2	-148.7	- 1.5
39.5	-137.5	-135.4	- 2.1
40.0	-126.3	-126.2	+ 0.1
40.5	-116.4	-117.2	+ 0.8
41.0	-107.6	-107.1	- 0.5
41.5	- 99.8	- 99.6	- 2.2
42.0	- 92.8	- 89.7	- 3.1
42.5	- 86.5	- 83.7	- 2.8
43.0	- 80.8	- 79.5	- 1.3
43.5	- 75.6	- 74.6	- 1.0
44.0	- 70.9	- 68.6	- 2.3
44.5	- 66.7	- 64.4	- 2.3
45.0	- 62.8	- 62.0	- 0.8
45.5	- 59.2	- 55.5	- 3.7
46.0	- 55.9	+ 44.6	-11.3
46.5	- 52.9	- 43.1	- 9.8

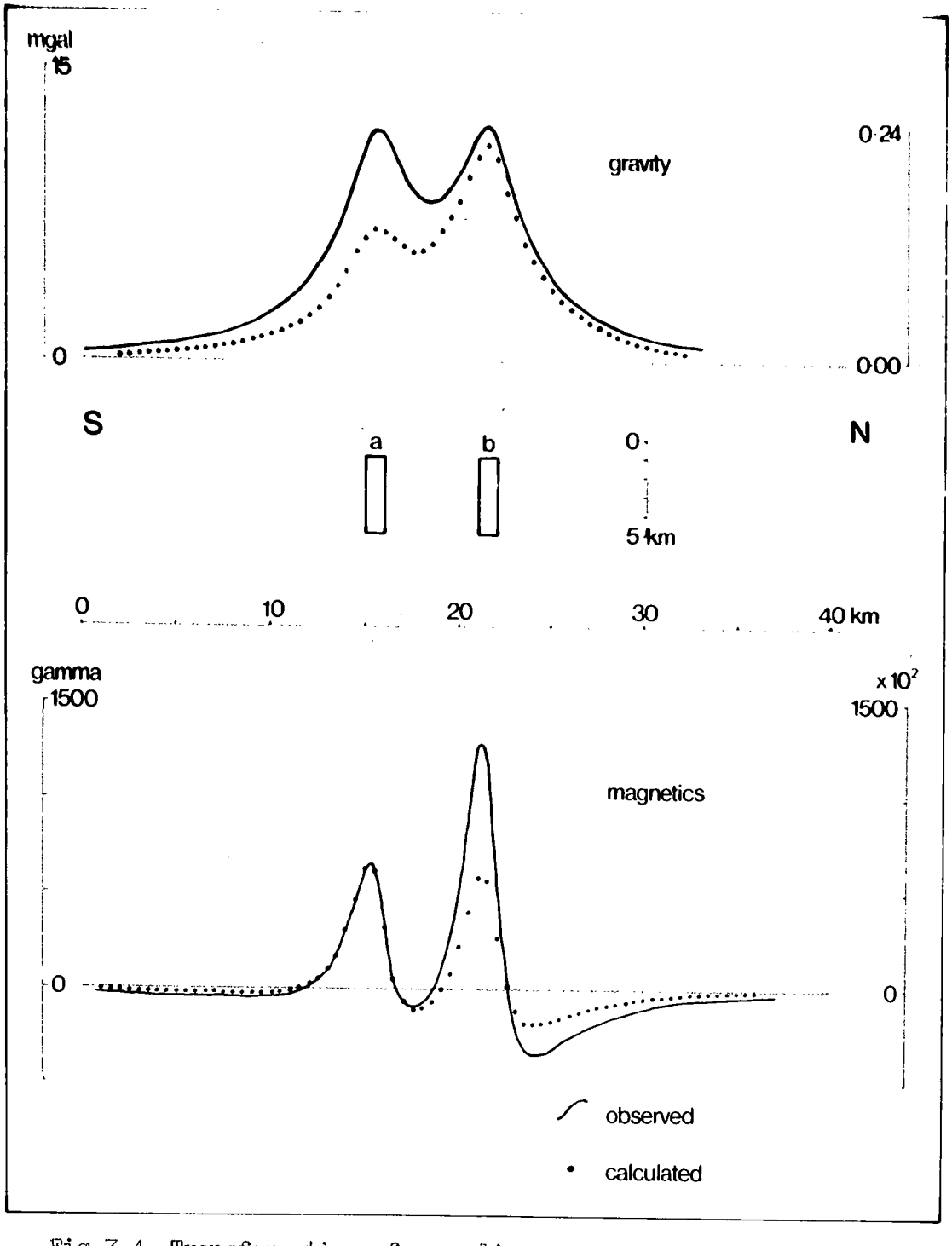

Fig 3.4 Transformation of anomalies caused by two bodies, a and b, of different J/p ratio value.

3.2.3.2 Direct calculation of J/p and p/J by use of programs JG/RAT and GJ/RAT.

These programs calculate the individual ratios of anomalous properties J/p (JG/RAT) and p/J (GJ/RAT) for each block element of the equivalent layer. The calculation requires both types of observed anomaly at input, and uses the first to derive a distribution of magnetisation or density which is then used in solution against the second type of observed anomaly for the individual ratio values, with the initial assumption that each of these is equal to unity. A listing of JG/RAT is included in appendix D.

When used with an equivalent layer that approximates the true source body in shape and size, the programs can be used to obtain individual block ratio values of the correct order or magnitude. Use of the programs in this manner is closely analogous to deriving distributions of magnetisation or density alone, and considerations apply which are similar to those discussed in connection with fig 3.2.

Alternatively, a thin equivalent layer can be used to obtain a single estimate of the ratio value directly from anomalies which are considered to be caused by a single homogeneous source, or a number of homogeneous sources for which the ratio J/p is the same. Figs 3.5, 3.6 and 3.7 show the results of tests applied to anomalies due to the simple body of fig 3.3, a body of inward dipping lower surface and an asymmetrical body with outward dipping upper surface. The results of these tests demonstrate that, although it is necessary to extend the equivalent layer some distance beyond the horizontal limits of

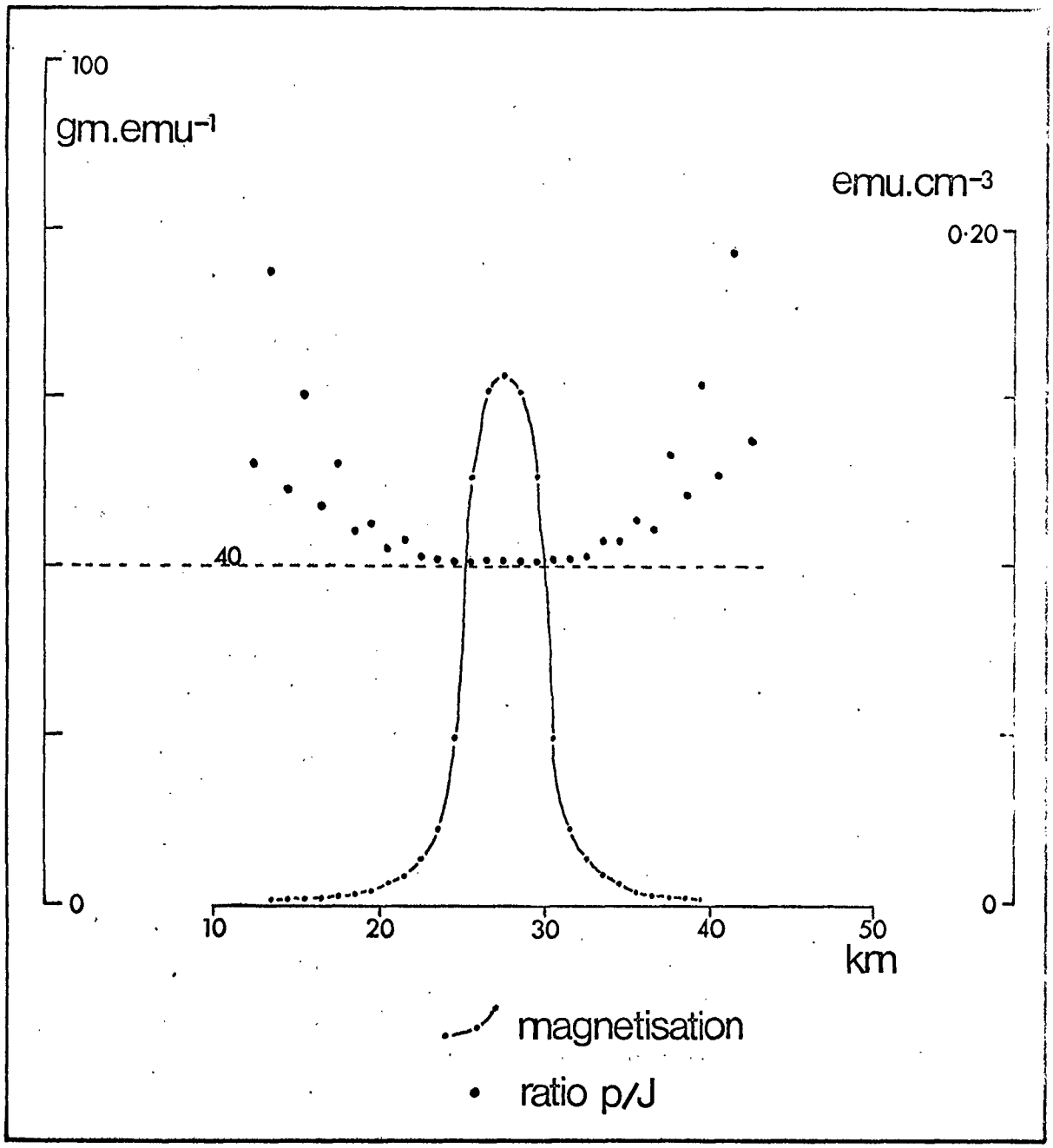

Fig 3.5 Distribution of p/J ratio values in a thin equivalent layer; for the anomalies caused by a two-dimensional body of rectangular cross section.

Fig. 3.6.

A: Observed anomaly curves caused by shaded body. Dashed curve, magnetics.

B: J/p and density plots for a thin equivalent layer with upper surface at 0.5km, and lower surface as indicated at the bottom of the figure. The higher scale calibration for density refers to the thinner of the two layers used. The values for the thinner layer are for the two cases of a full horizontal extent and a layer restricted to the width of the true body. The thicker layer is restricted horizontally.

C: Plot of magnetisation and ratio J/p in a restricted thin equivalent layer.

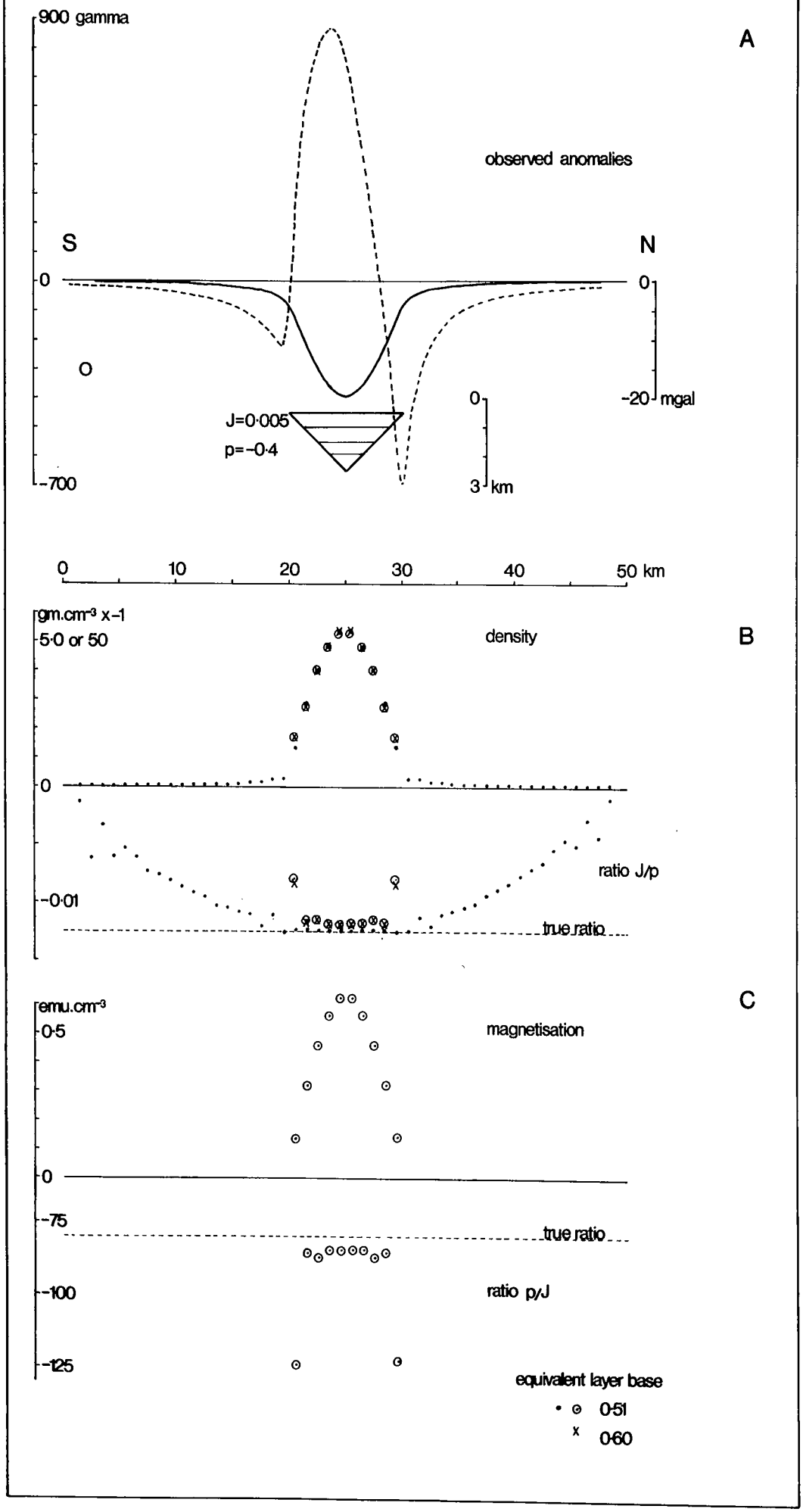
900 gamma
A
observed anomalies
S
N
0
0
O
-20 mgal
J=0·005
p=-0·4
0
3 km
-700
0
10
20
30
40
50 km
gm.cm⁻³ x-1
5·0 or 50
density
B
0
ratio J/p
-0·01
true ratio
emu.cm⁻³
0·5
magnetisation
C
0
-75
true ratio
-100
ratio p/J
-125
equivalent layer base
0·51
0·60

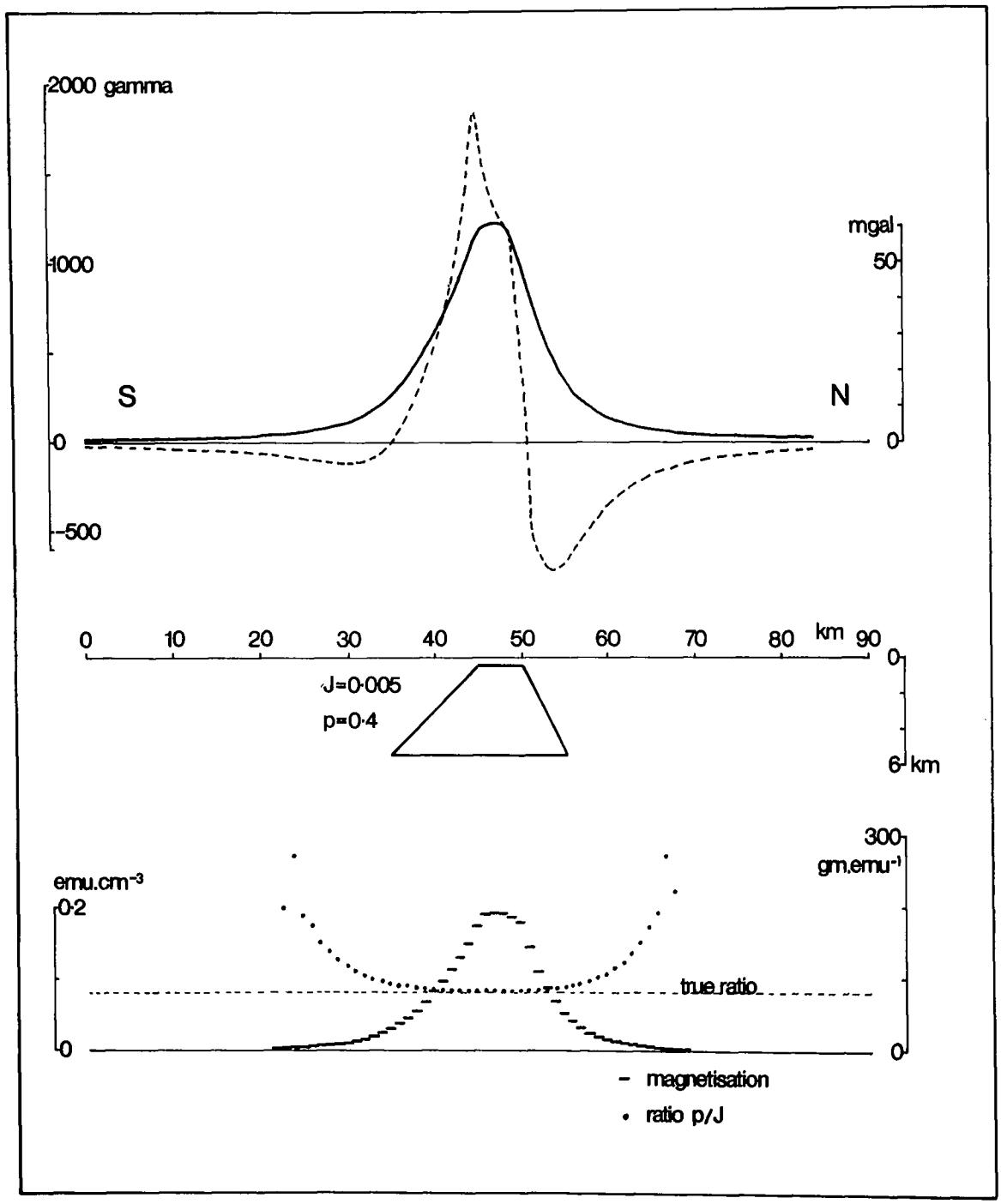

Fig 3.7 Derivation of the distribution of p/J values within a thin equivalent layer. Test anomalies caused by anomalous body as shown.

the true source body for an accurate estimate of the ratio value, a good approximation to the value may be obtained with the layer restricted horizontally to the limits of the body, or to the region of the main anomaly peaks. In fig 3.6 there is a discrepancy of about 4% of the true value of J/p between that and the best value on the plot for a restricted thin layer; for p/J the discrepancy is about 6%. For the variable upper surface body of fig 3.7, the estimate is not as good, with a p/J discrepancy of 20% for a restricted layer.

Bott and Hutton (1970a) discussed the resolution of the linear inverse method to derive distributions of magnetisation and density with respect to the block width/depth to upper surface ratio. These authors concluded that instability due to amplification of short wavelength errors set in when this ratio was less than 0.6. This value is one for good quality data and generally, the limiting value is somewhat higher; a ratio of 1.0 usually ensures stability. In calculations for J/p by the linear inverse method, the two calls to the least-squares procedure produce a greater amplification of errors in limiting conditions and a width/depth ratio of 1.0 should be the minimum value for stability when a full thickness equivalent layer is used. For a thin layer applied to the model and anomalies of fig 3.7 a minimum ratio value of 1.5 - 2.0 was found to be the necessary limit.

3.2.3.3 Calculation of the angle of magnetisation, program SBETA.

SBETA computes a single angle of magnetisation for the whole profile represented by an equivalent layer. A listing of the program is contained in appendix E.

Table 3.5 lists the solutions obtained by SBETA for different configurations of the equivalent layer applied to the anomalies caused by the body of fig 3.7. The depths, thicknesses and horizontal extent of the equivalent layers may be compared with the extent of the true model between horizontal limits of 35km and 55km, and vertical limits of 0.5km and 5.5km; the computed angles of magnetisation may be compared with the true angle of 75°.

TABLE 3.5 SOLUTION OF ANGLES OF MAGNETISATION BY PROGRAM SBETA

Equivalent layer configuration				Magnetisation angle.
upper surface.	lower surface.	blodk width.	layer extension.	inclination.
depth (km)	depth (km)	(km)	(km)	(degrees)
0.50	0.51	1.0	30 - 60	75.3
0.50	0.51	1.0	35 - 55	75.5
0.50	5.50	5.0	35 - 55	76.0
0.45	0.46	1.0	35 - 55	76.1
0.50	0.51	5.0	35 - 55	77.2

Definition of the solutions to the first decimal place is made in table 3.5, only to indicate the trend of accuracy for different layer configurations. In the treatment of real data, a solution quoted to such precision would not be justified; from the spread of values in table 3.5, a minimum error of 2° would be expected in the treatment of well defined and relatively isolated anomalies.

The use of SBETA in the treatment of anomalies caused by

bodies with a negative ratio J/p (fig 3.6) produces solutions of approximately (μ - 180°), where μ is the true angle of magnetisation.

The solutions in table 3.5 indicate considerable stability for the process, and if the assumptions made at the beginning of section 3.2.2.3 are a good approximation to the geological situation, little else need be known about the true source body.

The variation in solutions obtained by SBETA may be compared with the corresponding variation in solutions obtained by the method of Bott et al. (1966). The method is based on determining the range of angles of magnetisation for which the pseudo-gravity anomaly is positive for a positive magnetisation of the source body. A range of possible values was calculated by Bott et al. for successive pseudo-gravity stations and the final range of values to delimit the angle of magnetisation was that which was common to the individual ranges. The precision to which the angle can be estimated depends on the number of individual ranges used and the accuracy to which the integrals defining each individual range could be evaluated. The integrals are

$$I_r = \int_{-\infty}^{+\infty} T(x^1, 0) \log r \, dx^1$$

$$I_\theta = \int_{-\infty}^{+\infty} T(x^1, 0) \, \theta \, dx^1$$

where $T(x^1,0)$ is the total field magnetic anomaly on the plane of measurement (the x-axis in Bott et al., 1966), and r and θ are the polar coordinates of $(x^1,0)$ from the pseudo-gravity

station (x,z). Thus, for complete definition of the permissible ranges of magnetisation angles, a complete knowledge of the magnetic anomaly on the x-axis is required. The practical definition of the ranges by a numerical integration over a finite length of profile in the method of Bott et al., is strictly analogous to the lateral extent of the thin equivalent layer in the present method by the linear inverse technique. The latter method achieves greater precision as the solution is controlled by the whole waveform of the gravity anomaly and not by its sign only. The final solution is slowly changing for different equivalent layer extensions, as was the mean value of the common range in the method of Bott et al. for different lengths for the numerical integration.

The response of the linear inverse method to different equivalent layer configurations is seen in fig. 3.8 which contains plots of the two columns of matrix K_B (equations (18) and (19)) for the 1st, 3rd and 5th test treatments of table 3.5. The widely differing waveforms in fig 3.8 produce values for the angle of magnetisation which differ by a maximum of 2° and have in common only a phase correspondence for long wavelength components. The plots of fig 3.8 emphasise the importance of long wavelength components in the definition of a magnetic anomaly and the difficulty encountered in solving for a magnetisation angle for each block element if the equivalent layer is not a close approximation to the shape of the true body.

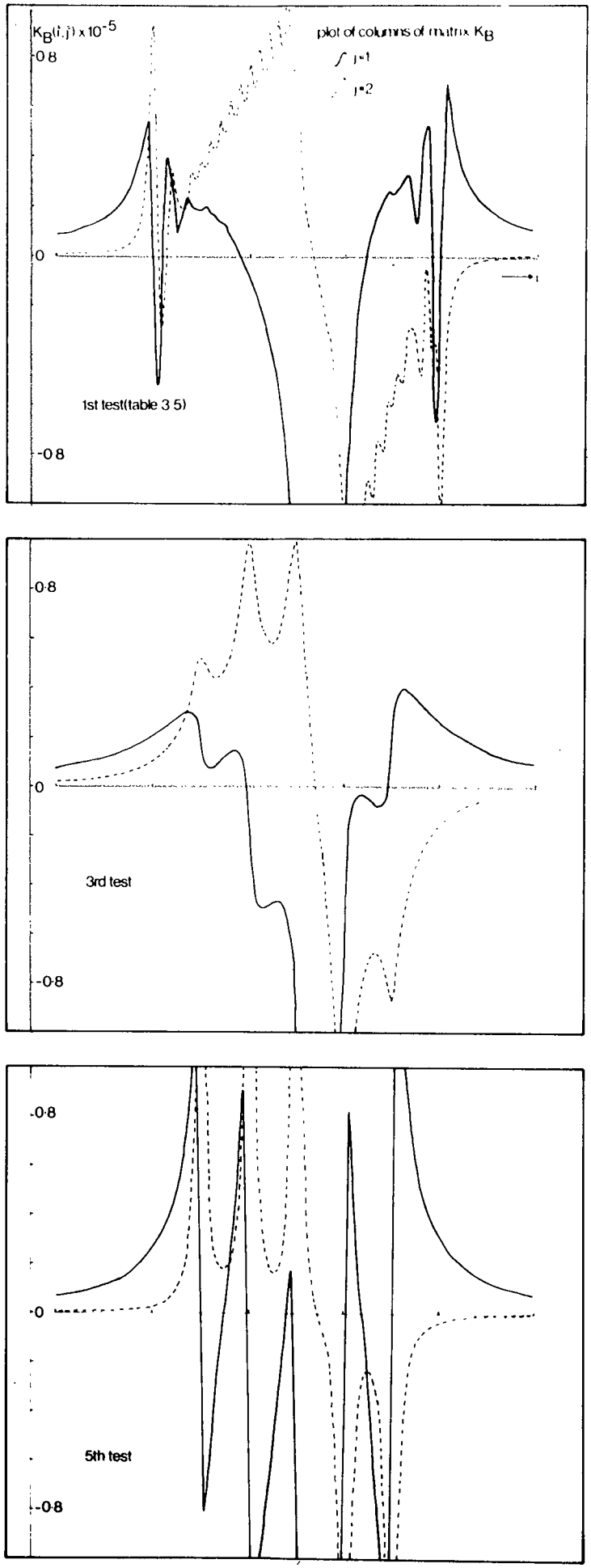

Fig 3.8 Plot of the columns of matrix K_B for three of the test operations of table 3.5.

3.2.4 Application of the transformation programs to separate magnetic anomalies.

This section is concerned with methods for separating the component of a magnetic anomaly that is caused by the shape and topographic relief of a source body from the component that is caused by a change in intensity of magnetisation alone. The methods depend on the use of the gravity anomaly as representative of the component due to shape, thus the separation is effected between magnetisation changes which are associated with a change in density and those which are not.

In outline, the procedure is as follows:

a) Transformation of observed gravity anomaly to a pseudo-magnetic anomaly, using a specified direction of magnetisation.

b) Point for point calculation of the ratio observed/pseudo-magnetic anomaly.

c) Derivation of the variation in the ratios of step b) that corresponds to topographic changes only; this variation will be called the regional variation.

d) Scaling of the pseudo-magnetic anomaly by product with the regional variation value at each point.

e) Subtraction of the scaled pseudo-magnetic anomaly from the observed magnetic anomaly.

One method of performing step c) is to fit a curve to the individual ratio values by least-squares. Where topography of magnetically active bodies is relatively simple a line with the equation ($y = a + bx$) is a good approximation. For an idealised least-squares fit to the observed/pseudo-anomaly ratios due to a source body of uniform J/p, the gradient 'b' is

zero and the intercept 'a' provides an accurate estimate of the ratio J/p. A test on the anomalies caused by the simple body of fig 3.3., using a thin equivalent layer, produced a small but significant value for the gradient b due to the inclusion of the profile end point observed/pseudo-magnetic anomaly ratio values in the least-squares process. These end point ratio values are oscillatory due to truncation of the anomaly profile within a finite length and to the use of a thin equivalent layer which is responsive to high wavenumber components over the whole profile. The gradient was effectively reduced to zero by excluding the end points from the least-squares process or by using a thick equivalent layer.

The standard model used for testing anomaly separation applications of the joint analysis methods is shown in fig 3.9, and contains a central section with an intensity of magnetisation double that for the rest of the body, but with the same magnetisation direction. To test the effectiveness of the separation of magnetic anomaly components based on a linear representation of the regional scaling ratio, an additional set of statements was added to program TR/GM to compute the individual observed/pseudo-anomaly ratio values, to make an additional call to subroutine LLSQ and to perform the scaling and subtraction. This is the form of TR/GM in appendix B, where the additional statements are optional.

Results of the separation process, using a thin equivalent layer, are shown in fig 3.9; the true ratio, J/p = 0.01, for the main part of the body is indicated by the line tt, and the least-squares scaling equation by line ee. The symmetry of line ee about tt within the length of the profile, and the intersection

Fig. 3.9.

A: Continuous curve, observed magnetic anomaly; dotted curve, magnetic anomaly due to additional intensity of magnetisation of the shaded body section, relative to the intensity of magnetisation of the main body.

B: Residual anomaly separated from scaled pseudo - magnetic anomaly; to be compared with dotted curve above.

C: Plot of ratios observed/pseudo - magnetic anomaly. Least - squares fitted scaling line ee and true J/p ratio value tt.

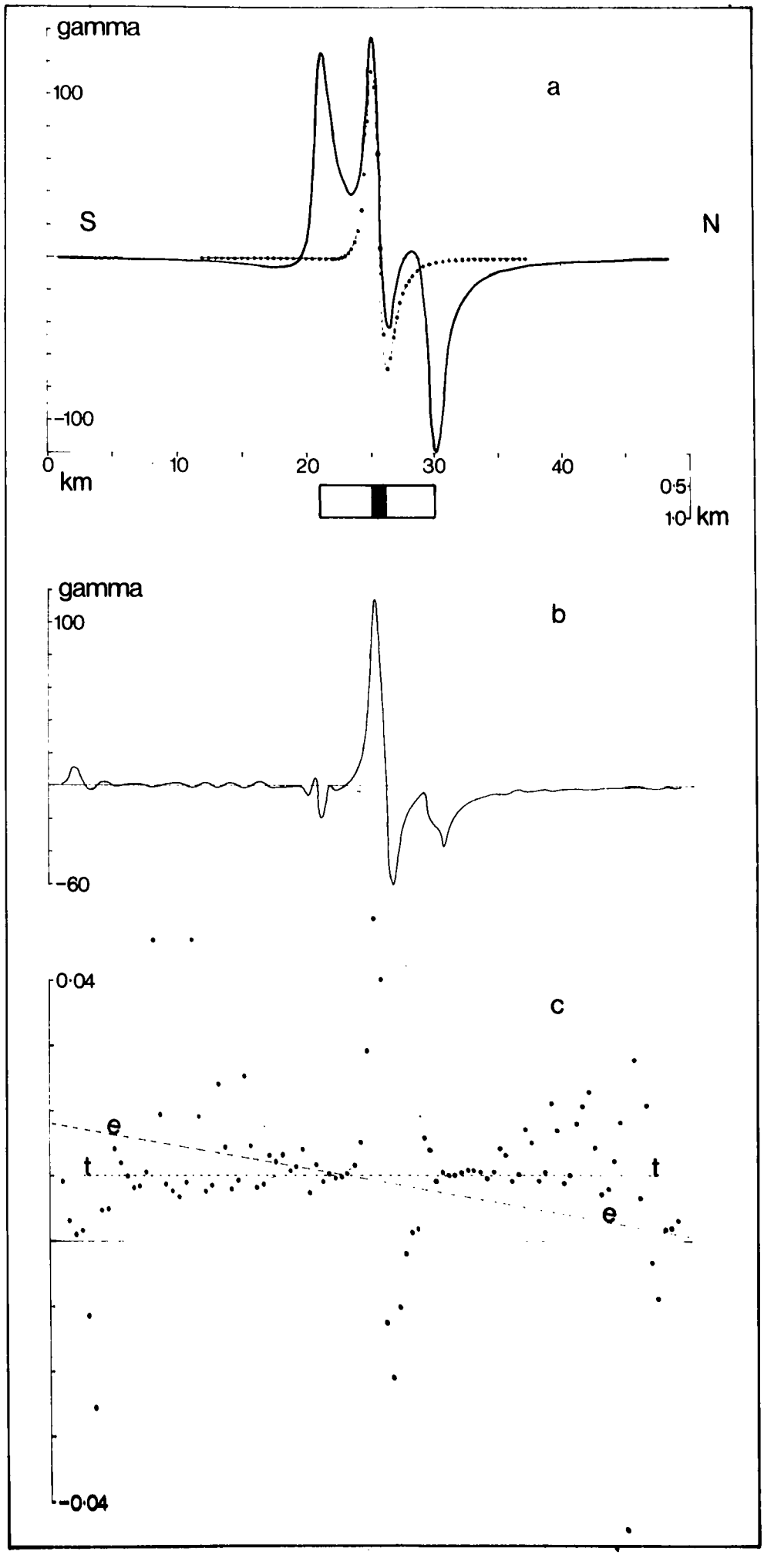
gamma
100
-100
a
S
N
0
10
20
30
40
km
0·5
1·0
km
gamma
100
-60
b
0·04
-0·04
c
e
t
t
e

of the two lines over that part of the body which is of higher intensity of magnetisation, illustrates that within practical limitations, induced by use of a finite profile length, the gradient of line ee is due entirely to the additional magnetic anomaly component which is not represented in the observed gravity anomaly. At the profile ends, where the effect of difference in location between the sources of the two anomaly components is much reduced, the difference in the ordinates of lines tt and ee approaches the value of the difference in the two values of J/p for the body.

Resolution of the anomaly due to a higher intensity of magnetisation in the centre of the body, termed the residual anomaly, is accurate to within 3 gamma for the main peak (fig 3.9). This accuracy is obtainable as the intersection of lines tt and ee is located over the part of the body that is of higher intensity of magnetisation; thus in this section of the profile the pseudo-magnetic anomaly is scaled by the correct regional value J/p = 0.01. The spurious lobes on the residual anomaly profile (fig 3.9) at 21km and 30km are due to divergence of line ee from line tt in a section where anomaly amplitudes are still relatively high, but these are instantly recognised by the presence of sharp discontinuities.

Any method to separate magnetic anomaly components, of different relation to the associated gravity anomaly, is an approximation if it is based on the transformation technique. Scaling of the pseudo-magnetic anomaly is based on the observed anomaly which contains both components, and success of the method requires that the section of the body that is of

different intensity of magnetisation should form only a small part of the whole.

The same limitations apply to the alternative method of scaling by normalisation. Normalisation has been used in magnetic interpretation to compare observed magnetic anomalies with standard anomalies due to known body shapes with known directions of magnetisation (Gay, 1963). It is performed by dividing each anomaly value by the mean absolute value for the profile. For the present purpose, after calculation of the mean observed and mean pseudo-magnetic anomaly, the method proceeds as:

a) Product of the pseudo-magnetic anomaly by the ratio (mean observed)/(mean pseudo-anomaly).

b) Subtraction of the scaled pseudo-magnetic anomaly from the observed anomaly to produce the residual anomaly.

This method was adopted in program NUFIL. The program is basically a version of TR/GM that calculates the mean values for normalisation, and performs the product and subtraction. In addition, fully normalised anomaly values are calculated which are in the form suitable for correlation analysis, and, as a final stage, a distribution of magnetisation appropriate to the residual anomaly is calculated. Another feature of NUFIL is a subroutine to preform cosine tapering of the profile ends, based closely on a subroutine included in the fast fourier analysis program COOL, which was written at the Australian National University. Where tapering was considered to be necessary in data inputs for other programs, a temporary

routine was inserted to achieve this. A listing of program NUFIL is contained in appendix F.

The residual anomaly associated with the body of fig 3.9 was not so well resolved by NUFIL due to the use of a constant scaling ratio which was slightly higher than the main body ratio of J/p. However, the main advantage of normalisation is that a constant signal to noise ratio is maintained on the plot of the residual anomaly, whereas noise is progressively amplified by the divergence of lines ee and tt (fig 3.9) in the least-squares method.

For an input specification of an estimated full thickness equivalent layer, the apparent variation within distributions of J/p which is caused by unrepresented body to topography is generally quite gentle, whereas changes in intensity of magnetisation alone cause sharp variations in the J/p plot. This provides another, but less precise and more subjective method of separating the two anomaly components. A polynomial is fitted to those J/p ratio values which are considered to form part of the gentle variations, and deviations from this polynomial in the J/p plot are assumed to represent changes in magnetisation only. The method produced accurate results for the test anomalies of fig 3.9, and is illustrated by an example from the Scottish Shelf in chapter five.

3.2.5 The importance of the regional field.

Of critical importance in the use of these joint analysis gravity/magnetics methods is the prior removal of a representative background field from both sets of data. This is of particular

relevance to the gravity field which, in most cases, must be cleared of all but upper crustal effects if it is to be used in conjection with magnetic data. For data from marine surveys, if isostatic equilibrium can be assumed, the free-air gravity anomalies are often the most suitable; the IGRF is often suitable as a background field for magnetic anomalies. The uncertainty of what constitutes a representative background field, for each of the two types of anomaly which are considered to be caused by the same structure, is one main limitation of the methods as interpretation techniques.

3.3 The two-dimensional approximation in quantitative interpretation.

A synopsis and reassessment of the magnitude of errors introduced into interpretations by assuming a two-dimensional structure has recently been presented by Lehmann (1971). Lehmann's examples, of simple source bodies causing complex anomalies, are taken from extreme situations where inclination of the earth's field is low (about 20°). Over the Iceland-Faeroes Rise, where the field inclination is approximately 75°, these effects should be reduced. However, errors in depth calculations will still exist, especially in the interpretation of anomalies Aa, based on profiles taken from E - W lines in the detailed survey area (fig 2.3). The error in this case may be as high as Lehmann's estimated 20% for prismatic and tabular bodies. Elsewhere, the ratio of strike-length/width of anomaly is significantly higher, and the errors due to the assumption of

assumption of a two-dimensional structure should be much below 20%.

CHAPTER FOUR

INTERPRETATION OF DATA FROM THE ICELAND-FAEROES RISE

Interpretation in this chapter is divided into two sections; the first section deals with magnetic data from the detailed survey of m.v. Arran Firth in 1969, and the second section with gravity and magnetic data obtained in 1967 from RRS John Murray. As the data used in the first section is based on short survey lines, the interpretation of local features is emphasized, in terms of body shapes and intensities of magnetisation. In the second section, data from the longer survey lines is used in a discussion of the regional upper crustal structure of the Iceland-Faeroes Rise.

4.1 Interpretation of magnetic data from the survey of m.v. Arran Firth, 1969.

It is evident from the contour maps (figs. 2.3 and 2.4) that the west of the survey area differs in magnetic anomaly style from the rest of the area. The western regional high contrasts with the variable positive and negative anomalies to the east, and dominates the field to such an extent that the average IGRF residual anomaly for the whole survey area is + 130 gamma. Thus, the survey area has a net positive anomaly which demonstrates a dominance of positive magnetisation by volume relative to the IGRF.

The least-squares regional fields, calculated directly from the data for each line, reflect the broad magnetic structure of

the area directly. Fig. 4.1 shows a plot of E - W regional field gradients for the twelve lines individually, together with the E - W gradient of the plane-fitted regional. All gradients are positive, which reflects the development of the 'regional high' in the west; the general northward increase in gradient values is due to the presence of anomalies B, E, F and to increasingly large areas of negative anomalies in the central and eastern sections of the area (fig. 2.4).

Several problems were investigated in the survey area:

a) The nature of the structure causing the broad N - S magnetic high in the west of the area, and its relation to magnetic sources in the east.

b) The nature of structures causing high amplitude anomalies A, a, B, b, and their relation to the regional high.

c) The nature of the structure causing anomaly H (fig.2.3).

d) The intensity of magnetisation required to produce the positive and negative anomalies in the central and eastern sections of the area.

4.1.1 The regional magnetic high in the west of the survey area.

The IGRF residual map (fig. 2.4) indicates that the regional magnetic high is associated with a long wavelength change from 400 - 500 gamma in the west to approximately zero in the east. The distance over which this change takes place is approximately 30km, and thus, the regional high in the west of the area may be considered as a positive anomaly of wavelength 60km. An estimate of the intensity of magnetisation required to produce

Fig 4.1
E-W least-squares regional gradients, lines 1-12.
pf, E-W gradient of plane fitted to data.

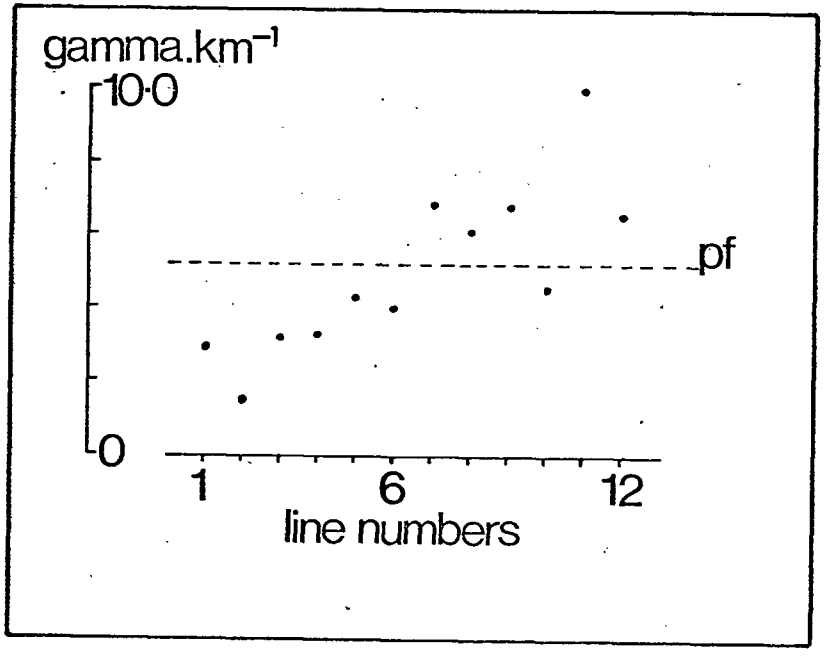

Fig 4.2
Amplitude spectra, line 5.
Solid: western profile.
Dashed: eastern profile.

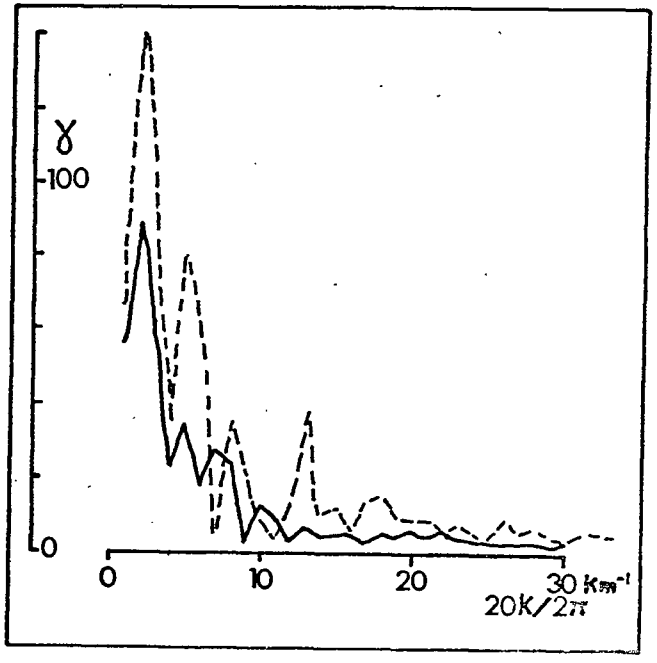

this change may now be made.

The estimate is made by considering a single fourier component of two-dimensional magnetic anomalies, and by use of the formula which relates the gravity and magnetic anomalies of a two-dimensional body for a certain ratio J/p,

$$A = \frac{J^1}{Gp} \left(\frac{dg}{dx} \sin B - \frac{dg}{dz} \cos B\right)$$

(Bott, 1969c).

where A is the magnetic anomaly, g is the gravity anomaly, G the gravitational constant, p is density and J^1 is the intensity of magnetisation transformed into the plane of the profile, and with a direction specified by the composite angle B, as defined for equation (1) in chapter three. Now consider a sine series gravity anomaly of wavenumber k, which may be interpreted as caused by a sine series surface distribution of density at a depth z, and written down as,

$$g = G \sigma_o \sin kx. e^{-kz}$$

(Bott, personal communication)

where $\sigma = \sigma_o \sin kx$ is the distribution of mass per unit area with wavenumber k. Thus, the magnetic anomaly fourier component of wavenumber k may be obtained by differentiating the gravity anomaly with respect to x and z to give

$$A = - J^1 k e^{-kz} \sin(kx - B)$$

where J^1 is the magnetic moment per unit area. The amplitude of magnetic moment is related to the amplitude of the magnetic anomaly by

$$|A| = |J^1| \, k e^{-kz} \qquad (4.1)$$

(Bott, personal communication)

For small values of kz, this relationship does not depend critically on the depth z as the exponential term tends to unity. For an equivalent layer of thickness Δz, equation (4.1) may be written as,

$$|A| = |J| \, k e^{-kz} \Delta z \qquad (4.2)$$

Where J is the magnetic moment per unit volume, or the intensity of magnetisation.

Equation (4.2) may now be applied to the long wavelength magnetic anomaly over the regional high in the west of the present survey area. The anomaly amplitude, for a wavelength λ of approximately 60km, is at most 500 gamma; the wavenumber, $k = 2\pi/\lambda$, has an approximate value of $0.1 km^{-1}$; for an equivalent layer of thickness 2km (the average thickness of oceanic layer 2), the estimated value of J is 0.025 cgs. If an amplitude for the long wavelength component is taken to be 300 gamma, the magnitude of J is 0.015 cgs.

The results of this estimate may now be compared with the full distribution of magnetisation derived by the linear inverse method for the whole of line 8 (fig. 4.3). An equivalent layer

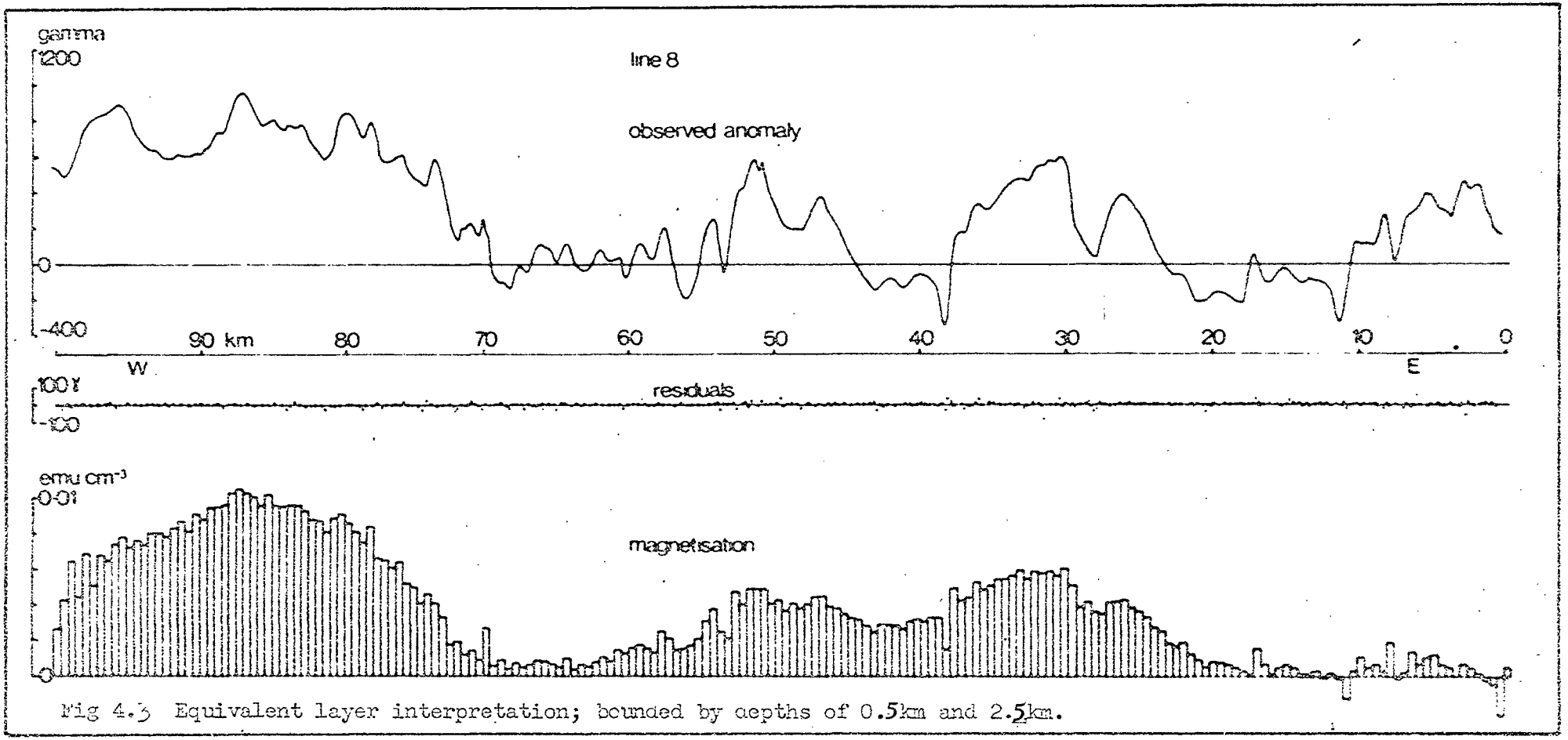

Fig 4.3 Equivalent layer interpretation; bounded by depths of 0.5km and 2.5km.

of thickness 2.0km was used, at a depth of 0.5km, and the direction of magnetisation was specified as true north, for an inclination of 75°. The distribution in fig. 4.3 is dominated by long wavelength components which obscure detail over both the western regional high and from 20km to 70km, over two large positive anomalies in the centre of the profile. For the former, the change in magnetisation is of the order 0.01 cgs, and for the latter it is approximately 0.005cgs. These values are differences in magnetisation, and for the specified equivalent layer configuration, they are not altered by adjustments to the background field. The results of the estimates, and of the more specific computations by the linear inverse method, show that this part of the Iceland-Faeroes Rise is associated with high amplitude effective lateral changes in magnetisation.

For comparison with other areas in the north-east Atlantic, the values obtained above may be converted to the form of magnetic moment per unit area, by multiplying by the thickness of the equivalent layer. In this form, the two values are proportional to *0.02 cgs and *0.01 cgs, and may be compared with *0.015 cgs and *0.006 cgs obtained by treating in the same way the interpretations of Vogt et al. (1970) for the axial zone and flanks of the Iceland - Jan Mayen Ridge. Corresponding values for the axial zone and the flanks of the Reykjanes Ridge were calculated from the models of Talwani et al. (1971) as 0.01 cgs and 0.005 cgs., and from the models of Godby et al. (1968) as 0.02 cgs. and 0.01 cgs. Thus, in terms of magnetic moment per unit area, the section of the Iceland-Faeroes Rise

* or, magnitudes quoted * 10^5 c.g.s

within the detailed survey area is comparable to active mid-ocean ridges in the north-east Atlantic.

However, in terms of wavelength, the distribution of magnetisation for line 8 (fig. 4.3) is unusual. The width of the zone of high intensity magnetisation on the Reykjanes Ridge (Talwani et al., 1971) is about 20km*, in contrast to the 30-40km for the regional high in the present survey area. Thus, the area is dominated by an E-W high amplitude change in magnetisation of anomalously long wavelength for its setting in the north-east Atlantic. An interpretation based purely on sea-floor spreading would imply a spreading rate for the present area that is at least twice that on the Reykjanes Ridge, and in a different direction.

If a sudden change in sea-floor spreading parameters is considered unacceptable, then alternative interpretations are required, and which imply a fundamental change in configuration or composition of the magnetic basement from west to east. This condition is illustrated by the amplitude spectra for two 20km anomaly profile lengths from line 5; one profile covers the western regional high and the other is located just to the east of the high. The length of 20km is the maximum for an anomaly profile restricted entirely to the regional high in a location where high amplitude anomalies such as B, b (fig. 2.3) are absent. The spectra for the two profiles(fig. 4.2) are very different in character, and the immediate interpretation is that magnetic basement to the west is located at a greater depth than that to the east. The actual

* also a general maximum width of anomalies and bands of magnetisation of one polarity.

depth difference may be calculated for selected wavenumbers by use of the method described in appendix G, and with the assumption that the attenuation of spectral components in the western profile is due entirely to the greater depth to the basement. Depth differences of 0.5km to 1.5km were calculated for the higher wavenumbers by this method. Consideration of the available bathymetric data (figs. 1.4 and 2.5) suggests that even for a depth difference of 0.5km, the magnetic basement in the west must be buried if the difference in amplitude spectra is to be explained in this way. Furthermore, if the seismic reflection results of Jones et al. (1970) are assumed to be representative of the western part of the crestal plateau, then little or no sediment can be present, and the magnetic basement in the west must be buried beneath a non-magnetic basement. Although an upper non-magnetic basement is feasible, and this is discussed below in connection with high amplitude anomalies a and b, it is considered unlikely, for the main structure in the west of the Iceland-Faeroes Rise was produced by sea-floor spreading (Bott et al., 1971). The conclusion is that the anomaly field in the west contains much of its energy in wavelength components which are longer than the 20km permitted by data cover for the spectra in fig.4.2. This supports the qualitative study made above. Thus, the difference in amplitude spectra is explained by a fundamental difference in the properties of two igneous basements at outcrop. The difference in anomaly style between east and west supports this conclusion.

4.1.1.1 An interpretation in terms of body geometry.

As an alternative to the distribution of magnetisation shown in fig. 4.3, magnetically equivalent geometric models were produced as interpretations of the regional high in the west of the area. Anomaly clusters A, a and B, b (fig. 2.3) will be identified in an interpretation described below, as intrusive centres, and as these appear to be confined to the structure that causes the magnetic regional high (fig. 2.4), then an interpretation of the latter is of importance.

Figs. 4.4 to 4.7 show a first series of optimization models for the structure causing the regional magnetic high. The optimization models are in the form of simple basement uplifts and provide approximate depth estimates for further interpretation. The profile from line 7 (fig. 4.7) was included for comparison with those over the regional high in the west, and shows the development of high H (fig. 2.3). A depth of 0.4km to the model for high H correlates with a depth of 0.35 km recorded just to the south by FS Meteor (fig. 2.5). Generally, the available bathymetric data indicates that 0.4km to 0.5km is an average depth to the sea floor in the area, and the models in figs. 4.4 to 4.7 reach this depth in places.

The optimization process produced also a vertical and horizontal component of magnetisation intensity for each model. Palaeomagnetic studies in the Faeroe Islands (Tarling and Gale, 1968) have determined normal and reversed stable remanent magnetisations in north - northeast and south - southeast directions respectively. Inclination of magnetisation in the

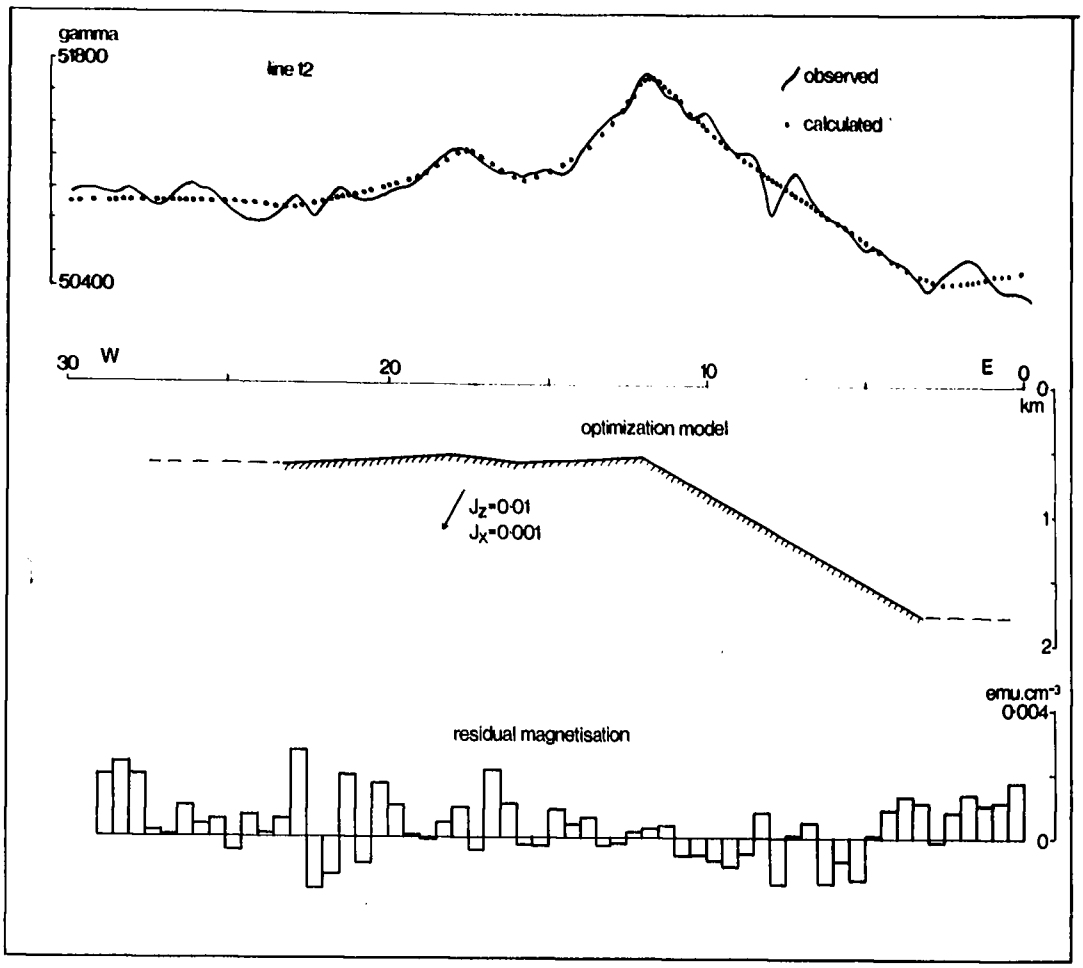

Figs 4.4 and 4.5 First optimisation series, western regional high.

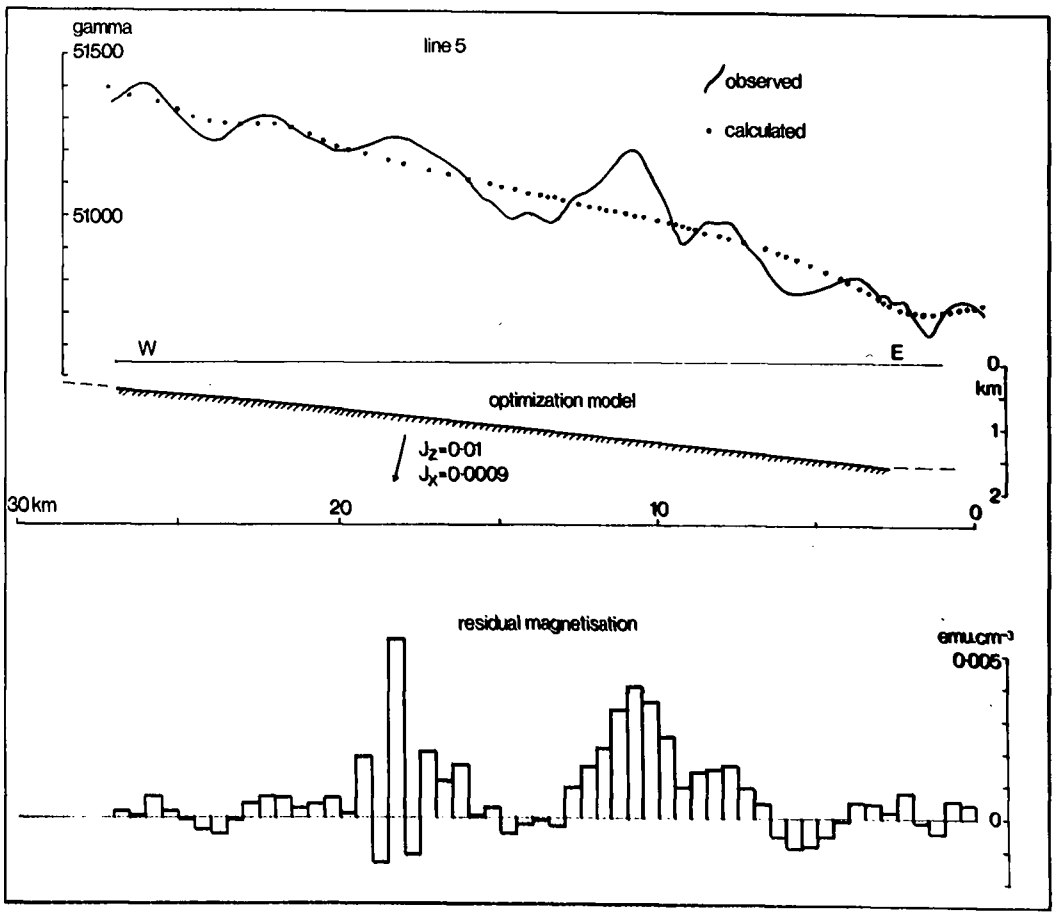

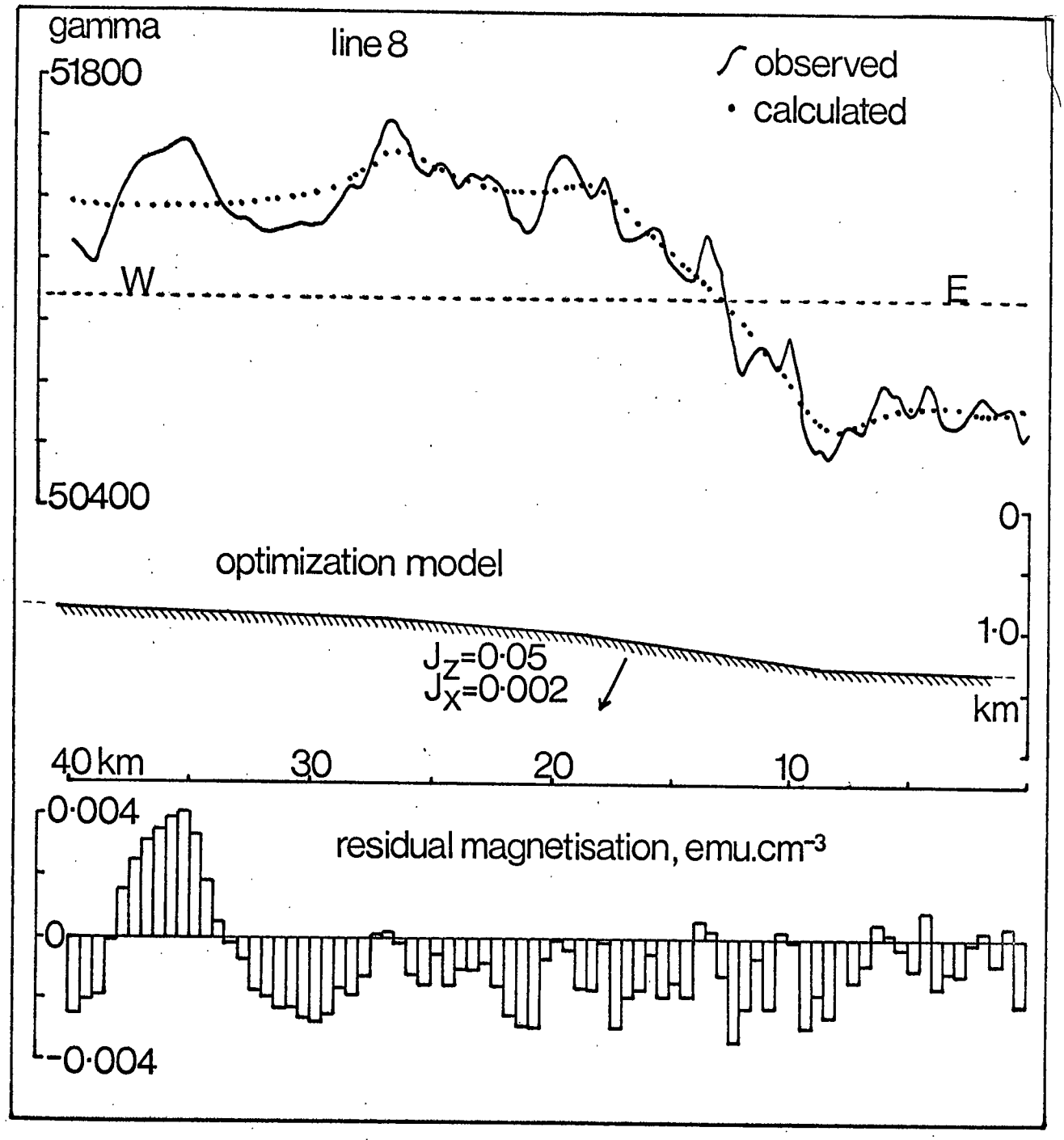

Fig 4.6 First optimisation series, western regional high.

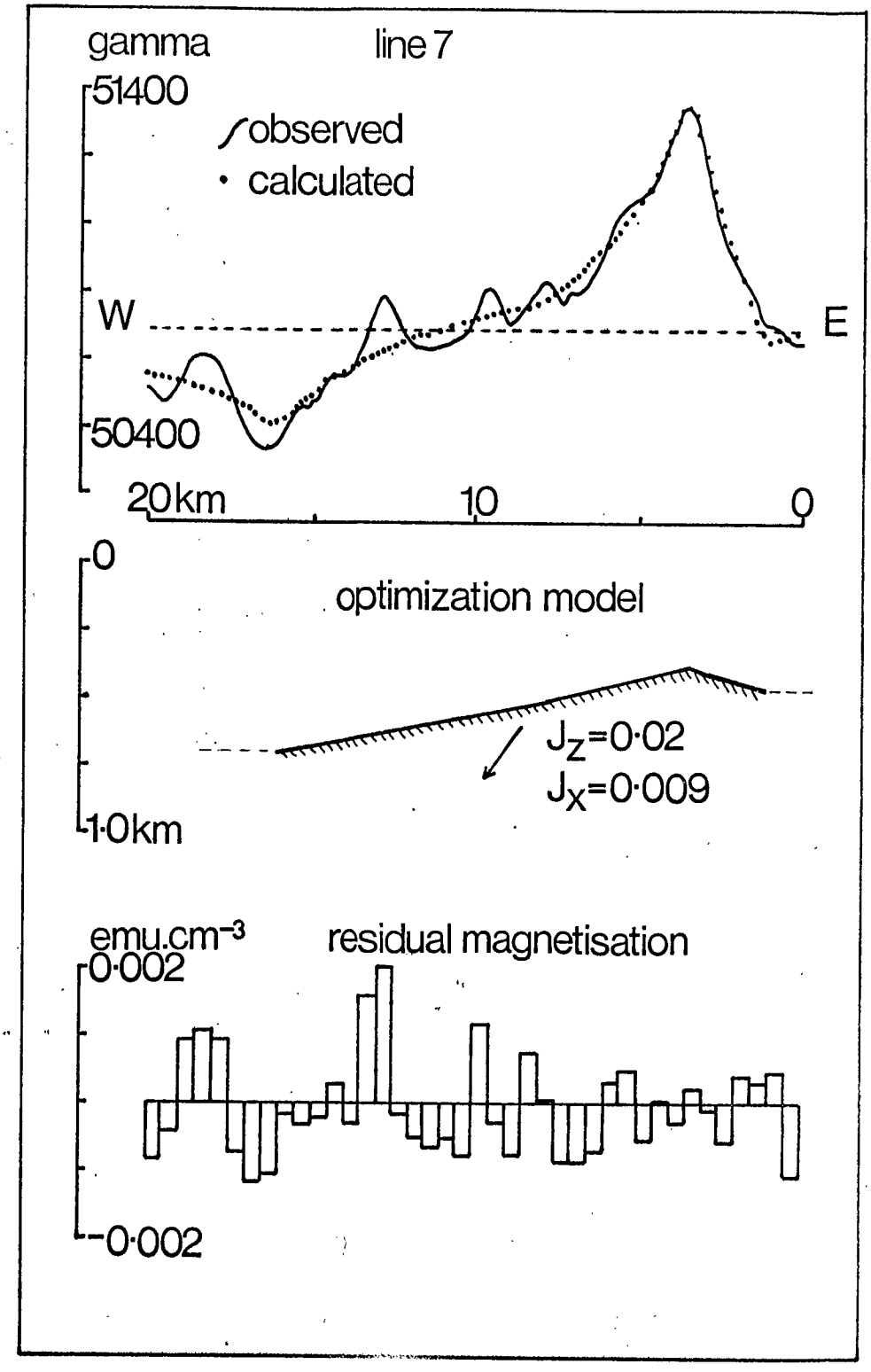

Fig 4.7 First optimisation series, anomaly H.

Faeroes is on the average ~~± 70°~~ +70° or -110°. If these results can be extrapolated to the present survey area, then the inclination defined by the 'optimum' components of magnetisation in figs. 4.4 to 4.7, and which is as low as 30° for line 7 (fig. 4.7), is not of palaeomagnetic significance, but is due to over-simplified models in the optimization process.

Residuals, observed anomaly minus calculated anomaly, from the optimization process were interpreted using the linear inverse technique to derive a residual distribution of magnetisation. The magnetisation distributions (figs. 4.4 to 4.7) are those for rectangular two-dimensional prisms contained within an equivalent layer, for which a depth of 0.4km to the upper surface corresponds to the estimated average bathymetry for the survey area. The depth of 0.6km to the lower surface is approximately that of the shallower plateau regions of the models produced by optimization. An alternative would have been to section the optimization model into a sequence of vertical sided trapezoids and to solve for a residual distribution of magnetisation within these. The residual magnetisation distributions of figs. 4.4 to 4.7 show two sections where oscillatory instability is much reduced; one of these is located on line 8 (fig. 4.6), in a position where the depth of the optimization model is of the same order as the depth to the lower surface of the equivalent layer; the other is located on line 5 (fig. 4.5) in a position where the optimization model is much deeper than the equivalent layer. Apparent stability within sections of a distribution of magnetisation is not a reliable criterion for establishing the vertical bounds of magnetic sources,

but on line 5 (fig. 4.5) it may indicate the existence of an independent weak and shallow source of magnetic anomalies.

The first series of optimization models (figs. 4.4 to 4.7) provides interpretations for the regional magnetic high and high H which are relatively objective. More specific interpretations for the same four profiles were obtained in the form of a single magnetic layer of variable upper and lower surface topography, and of uniform intensity and direction of magnetisation. This second series of geometrical interpretations was obtained by a two-stage procedure for each profile. In the first stage, an upper surface topography was produced by trial and error, program MAGN, and was based approximately on the optimization models of figs. 4.4. to 4.7, but included more detail. For this stage, a conventional lower surface was placed at a constant depth of 5km and a magnetisation intensity of 0.005 cgs was used, with an inclination of 75° (inclination of present earth's field) in the direction of true north. The trial and error stage was terminated when steep gradients, and local peak to trough gamma amplitudes had been produced in correct phase relations for the most prominent local anomalies and inflections. In the second stage, lower surface relief and final values for the vertical and horizontal components of magnetisation were derived by optimization; upper surface co-ordinates, obtained by the indirect method in the first stage, were retained as fixed 'known' co-ordinates through the second stage optimization. The final models are shown in figs. 4.8 and 4.9. In order to maintain continuous gradients and levels of

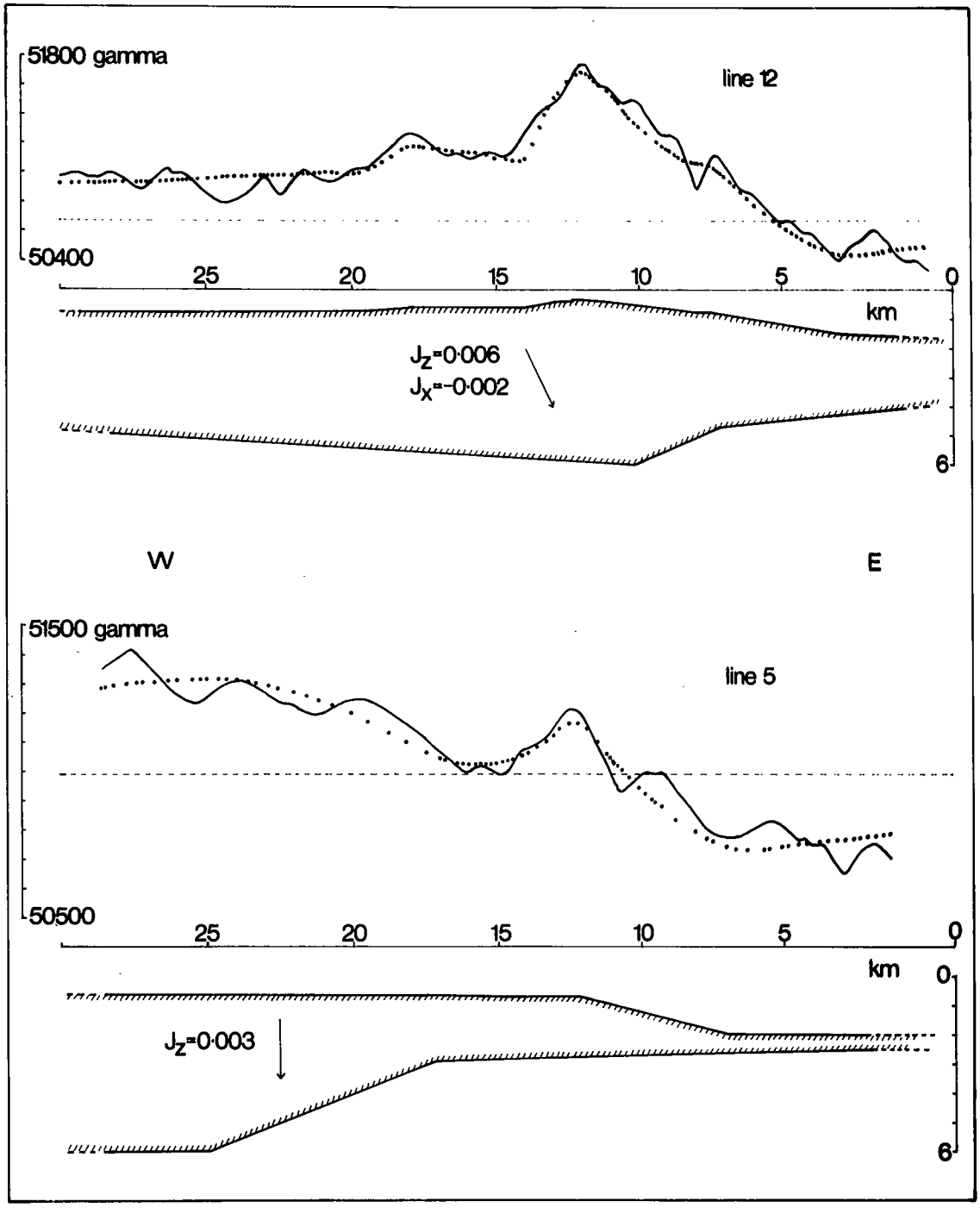

Fig 4.8 Interpretation of the western regional high as a magnetic layer of variable topography.
Solid curve: observed anomaly. Dashed curve: calculated anomaly.

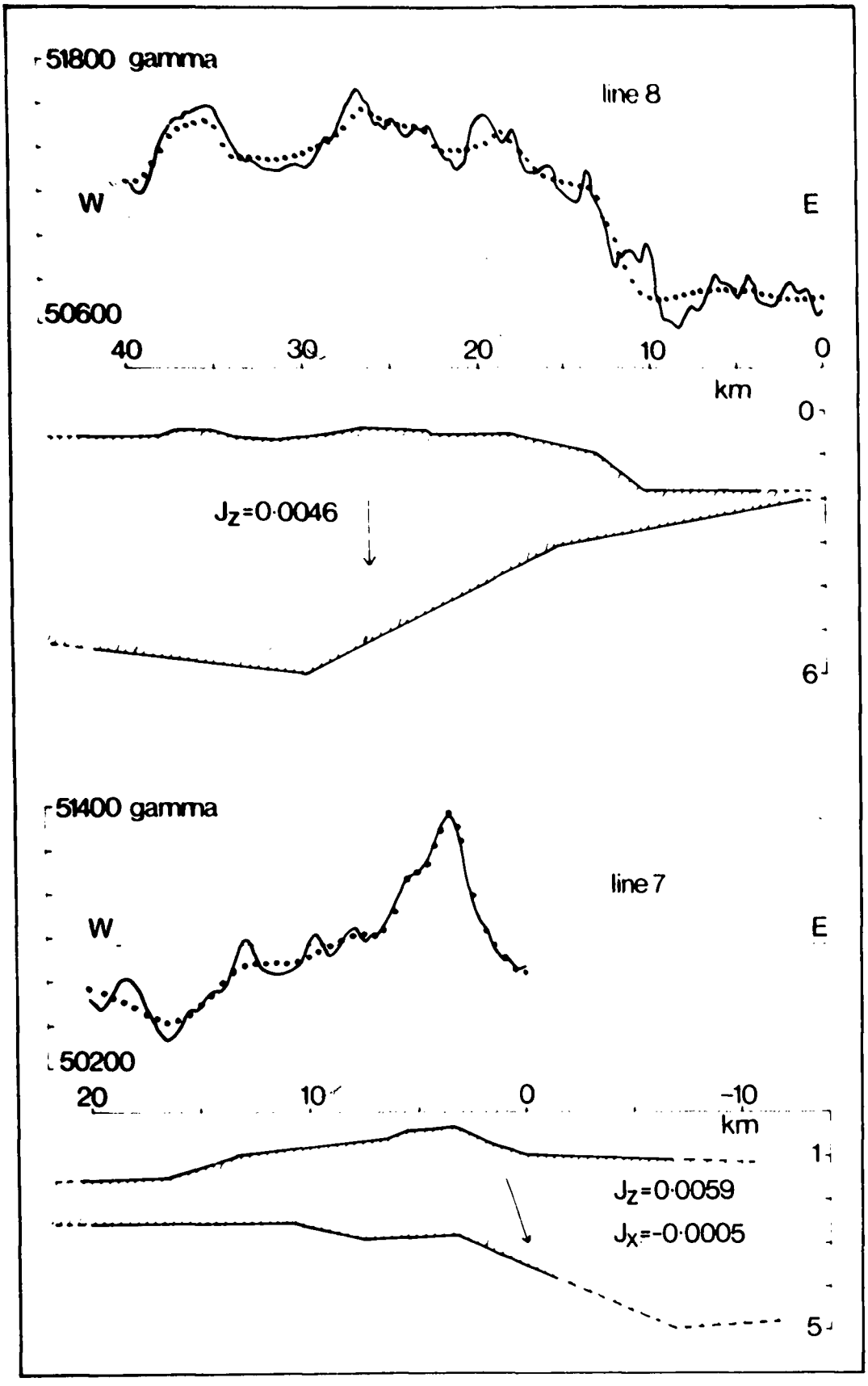

Fig 4.9 Interpretation of the western regional high and anomaly H. Solid curve: observed anomaly. Dotted curve: calculated anomaly.

the calculated anomaly at the profile ends, to match those of the observed anomaly, the models were extended slightly beyond the profile ends. This accounts for the thickening of the model layer beyond the eastern end of the profile from line 7 (fig. 4.9), and the rapid thinning of the layer at the eastern ends of the profiles from lines 5 and 8 (figs. 4.8 and 4.9).

Generally, the model magnetic layers (figs. 4.8 and 4.9) develop maximum thickness beneath sections of smallest depth to the upper surface. Again, from the estimated average bathymetry for the area, the model upper surfaces probably reach the sea floor on the western and eastern margins of the survey area, but towards the centre of the area, the model upper surface is considerably deeper than the estimated bathymetry.

Apart from their significance as individual interpretations, the models in figs. 4.8 and 4.9 are useful in that they are standardized by the use of a common intensity of magnetisation and depth to lower surface in the first stage of their production. Thus, these models, and any magnetic equivalents, may be compared systematically from profile to profile. For example, intensities of magnetisation are of the same order for models of profiles 5, 8 and 12 (figs. 4.8 and 4.9), but lower surface relief on the model for line 8 is more exaggerated than on the other two models; the profile from line 8 is close to high amplitude anomalies B, b (fig. 2.3), and the exaggerated model may represent directly the greater development of the regional magnetic high source structure in this sub area. The profile

from line 5 contains lesser gradients and lower amplitudes than those of line 8, and its proximity to the anomaly cluster A, a may indicate that activity associated with this cluster is older, deeper, or less well developed than in the area of B, b. A similar comparison of high H (fig. 4.9) with the western profiles shows that if a similar structure is present, then it must be on a smaller scale than that responsible for the regional magnetic high in the west, not only in terms of area, but also in thickness.

Interpretation of the regional magnetic high by models of the type obtained for lines 12, 8 and 5 (figs. 4.8 and 4.9) receives support from the interpretation of seismic refraction results by Bott et al. (1971). Seismic refraction line 69/3 of Bott et al. is shown in fig. 1.4, and the south-eastern end of this reversed line is located within the eastern quarter of the present survey area. A full table of the refraction results for south-eastern end of line 69/3 is included in section 4.1.3 of this present work, but it is sufficient here to note that Bott et al. recorded an uparching of layer 2 rocks, of P - velocity 5.7km/s, which crossed line 69/3 in the form of a ridge surrounded by rocks of lower P - velocity, just to the north of the present survey area. Thus, it is appropriate to identify the structure causing the regional magnetic high in the west with a similar ridge of layer 2 rocks, but of approximately N - S trend.

The topographic relief on the upper surface of the models for the western anomaly profiles in figs. 4.8 and 4.9 is

approximately 1.5km to 2.0km, or of the same order as that of the layer 2 ridge defined by Bott et al. The depth of the base of layer 2 was calculated for line 69/3 as 7.25 $\pm$ 1.28km, and thus the models of figs. 4.8 and 4.9 may be of approximately the correct dimensions, and the intensity of 0.005cgs may be a realistic estimate of the average intensity of magnetisation of the postulated layer 2 ridge in the survey area. The models for profiles 12, 8 and 5 (figs. 4.8 and 4.9) must not be taken too literally, and it is very dangerous to equate the thinning towards the east in these models with a thinning of layer 2 in the same direction. If any interpretation is to be assigned to model lower surface relief, then an apparent change in magnetisation, away from the postulated ridge, within the layer 2 rocks is all that can be suggested.

The identification of the western regional high with a ridge of layer 2 rocks is in agreement with the explanation of the difference in amplitude spectra for profiles from line 5, as being due to a fundamental difference in basement; to the west, the basement is formed by layer 2 rocks which differs from the basement of the central and eastern sections of the survey area.

Features such as the N - S regional high in the west of the survey area would dominate the magnetic field if they were common on the Iceland-Faeroes Rise, and the N - S trend on the aeromagnetic map of Avery et al. (1968), which is shown in fig. 1.3, may indicate a wide variability in the type of basement at outcrop which is controlled by significant topography within the upper seismic layers.

4.1.2 The interpretation of high amplitude, relatively isolated anomalies.

A qualitative comparison of the anomaly patterns superimposed on the regional magnetic high in the west of the survey area with the I.G.S. aeromagnetic maps, covering the Tertiary volcanic centres of North-west Scotland, suggest that the circular, or semi-circular configurations of anomaly clusters A, a and B, b (fig. 2.3) mark the sites of volcanic/intrusive centres. Kristjansson (1970) quotes a personal communication from Th. Sigurgeirsson concerning the presence of large aeromagnetic anomalies over intrusive complexes within the Tertiary basalts of Iceland, and deduces that similar anomalies over other parts of the Tertiary area are caused by intrusive centres beneath the basalts; some of these centres may be reversely magnetised.

In this context, high amplitude anomalies such as A, a, B, b and E (fig. 2.3) mark the sites of the components of two such centres, as volcanic superstructure, intrusive apophyses and subsidiary intrusions. Simple models, produced by optimization, indicate that these individual components reach the estimated depth of the sea floor at 0.4 - 0.5km (figs. 4.10 to 4.13), although the model for high A alone (fig. 4.10) is unreliable as the assumption of a two-dimensional structure is a poor approximation for the profile from line 2 (fig. 2.3).

Of particular importance are the negative anomalies a and b (fig. 2.4). At the high latitudes of the survey area, these features are certainly caused by bodies which are distinct from those that cause the high amplitude positive anomalies A

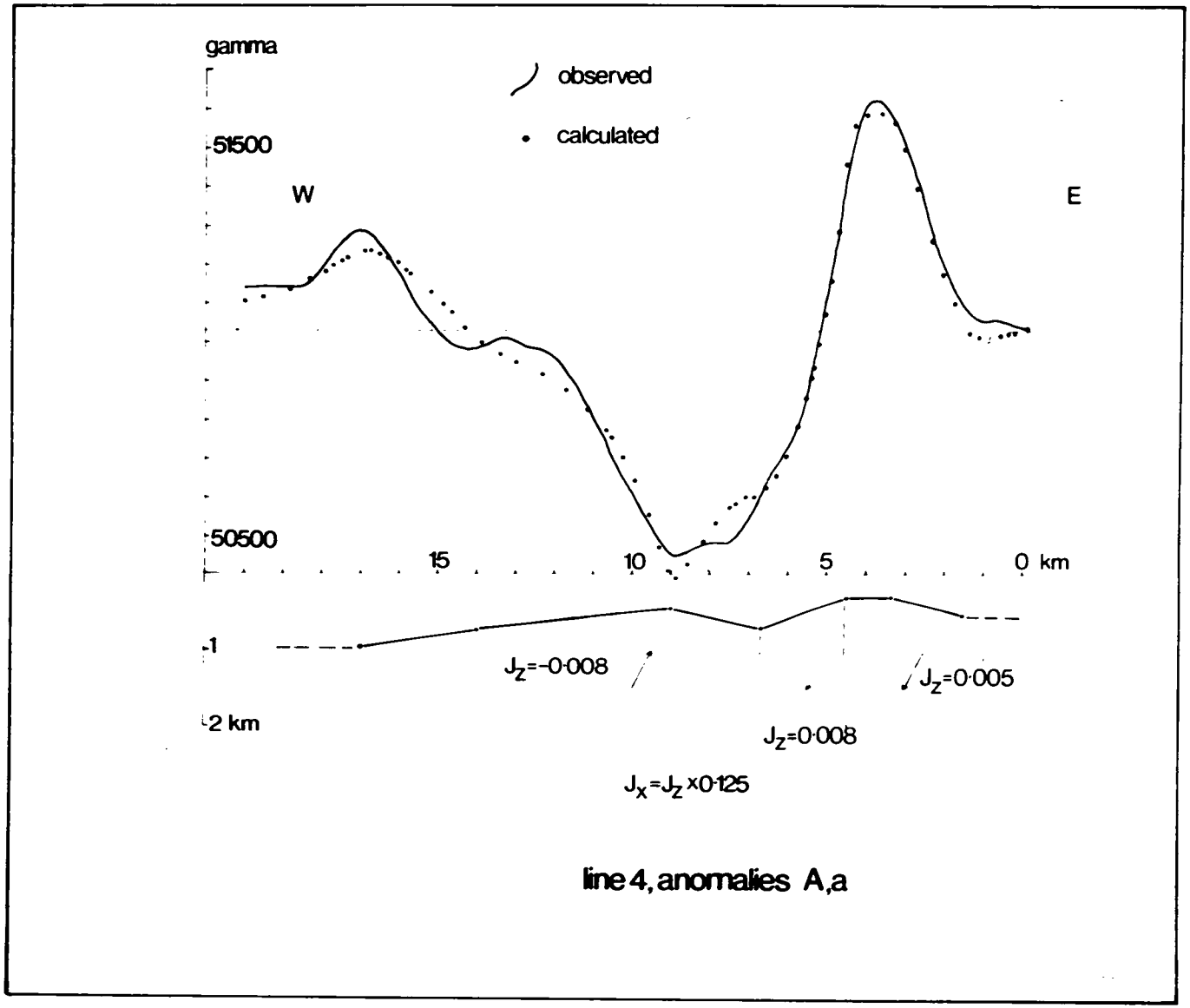

Fig 4.12

Optimisation model, anomalies A,a.

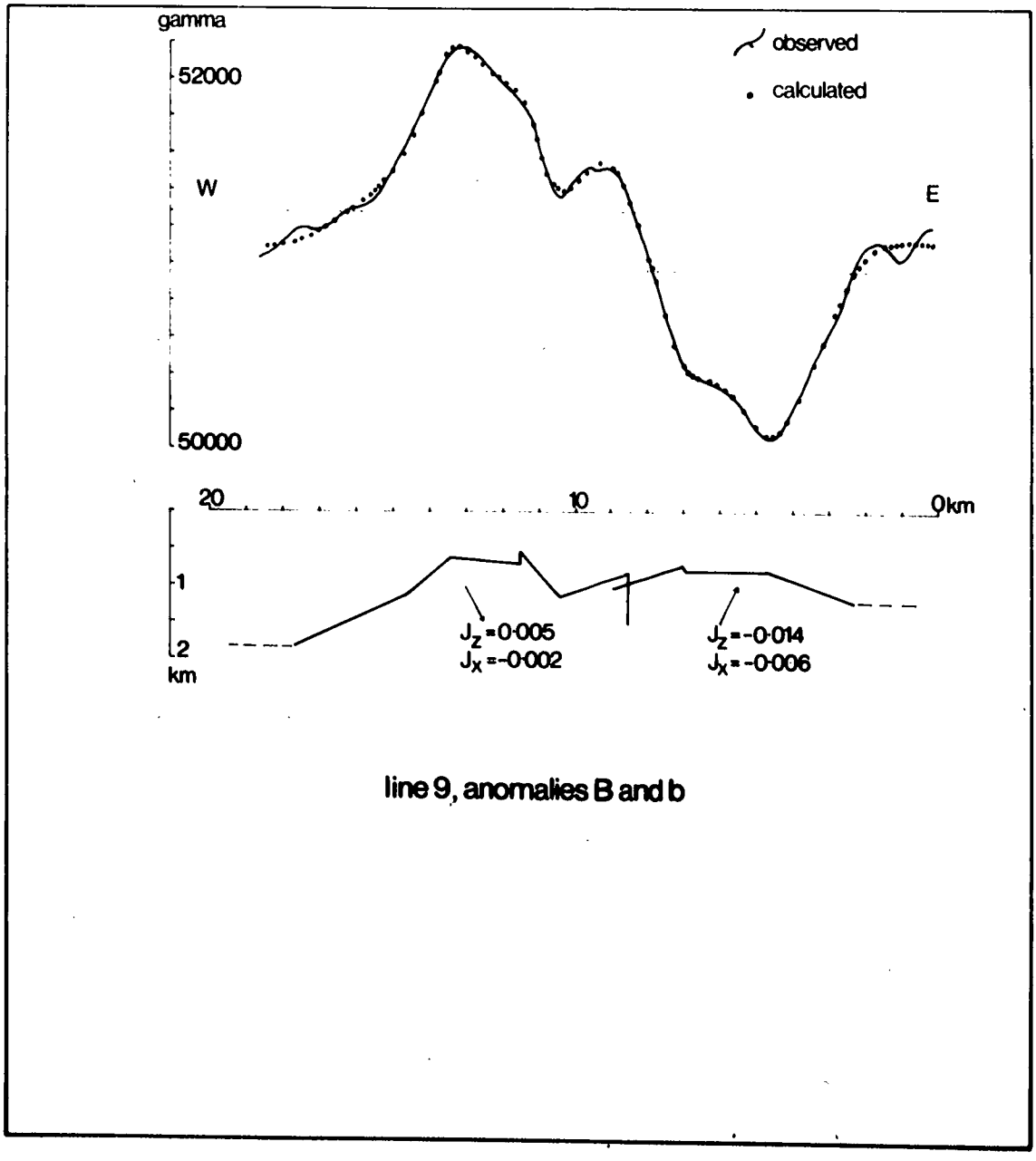

Fig 4.13 Optimisation model, anomalies B,b.

and B. On the total field map (fig. 2.3), the amplitudes of A and a are approximately equal with respect to the estimated background field, and the emplitude of b is greater than that of B. That A, a and B, b are coupled positive and negative lobes of anomalies produced by a single body in each case, with a very low magnetisation inclination, is refuted by the steep gradients that define a and b, and especially as B appears to be separated from b on the contour map (fig. 2.3). Thus A and a, B and b are to be interpreted as four individual structural components.

The geometrical models produced by use of the indirect method (program MAGN) show that the bodies causing anomalies a and b are negatively magnetised relative to the source bodies of A and B, and to the 'country rocks' generally (figs. 4.14 and 4.15). However, lateral distributions of magnetisation within equivalent layers of constant thickness (fig. 4.16) show that, relative to the IGRF, the change in magnetisation that is responsible for low b is one from positive high intensity to very low intensity and not necessarily to one of reversed polarity. Thus, in the absence of a knowledge of the true configuration of anomalous bodies, it is safer to discuss the bodies responsible for a and b in terms of a low intensity of magnetisation relative to that of the 'country rocks'. There are several ways in which this change in magnetisation can be explained.

One explanation is that the bodies causing anomalies a and b were intruded or extruded at a different time from that

of the formation of the rest of the volcanic/intrusive centres and the layer 2 ridge. The relatively low intensities of magnetisation are thermo-remanent components acquired under different geomagnetic field conditions. A similar situation has been described by Hamilton and Richardson (1971), in which a magnetic anomaly over a seamount in the Tyrrhenian Sea may be explained by a normally magnetised central feeder surrounded by reversely magnetised material. However, the uniqueness of anomalies a and b, and their apparent central location in the two postulated centres of activity, suggest that they are associated with a distinctive rock type, as well as with a low intensity of magnetisation.

The distinctive rock type may represent an original difference in petrology, or may be an alteration product in which the magnetisation was effectively destroyed. The hydrothermal aureole of the volcanic centres of Thingmuli (Carmichael, 1964) and Breiddalur (Walker, 1963), in eastern Iceland, is of wide extent, and of radially decreasing intensity away from the volcanic cores. This situation does not agree with the relatively narrow width and sharp definition of anomalies a and b, especially b. If alteration is to be invoked, then it must be associated with a local rock type, such as a loose agglomerate, that is especially permeable to hydrothermal fluids; some magnetic lows in Iceland have been explained by this mechanism (Saemundsson, 1971).

The preferred interpretation of anomalies a and b is one that suits the sharp definition of these features on the contour

map (fig. 2.3) as well as their apparent simplicity, and is that they are caused by the presence of relatively non-magnetic granitic rocks at the centre of intrusive complexes. Acid intrusions and lavas are found in the core of Thingmuli in Iceland (Carmichael, 1964), and granophyres occur in the centres of Mull and Ardnamurchan (Richey, 1961). The I.G.S. aeromagnetic maps show that the granophyres of Mull and Ardnamurchan, and also the granites of Skye, are associated with negative magnetic anomalies. Thus, the anomalies A, a, B, b, are considered to be due to basic and acid petrological components within the two volcanic/intrusive centres on the ridge of layer 2 rocks. The semi-circular configuration of positive anomalies round low a and low b may be due to partial ring-dyke development.

Saemundsson (1971) discusses such centres in Iceland as central volcano/fissure swarm units, and gives the dimensions of a typical unit as 10-25km across and 50-100km along the axis. These dimensions are comparable to those of the N - S trending regional high. There is little indication of the presence of dykes in fissures, or of swarms of these, on the postulated layer 2 ridge as is normal in Iceland (Walker, 1963; Carmichael, 1964; Saemundsson, 1967), but fissures are not so common in some parts of Iceland such as the volcanic zone of Snaefellsnes (Sigurdsson, 1967). In addition, Kristjansson (1970) suggests that dykes do not cause any major magnetic anomalies in Iceland, in comparison with those caused by lavas and large intrusions.

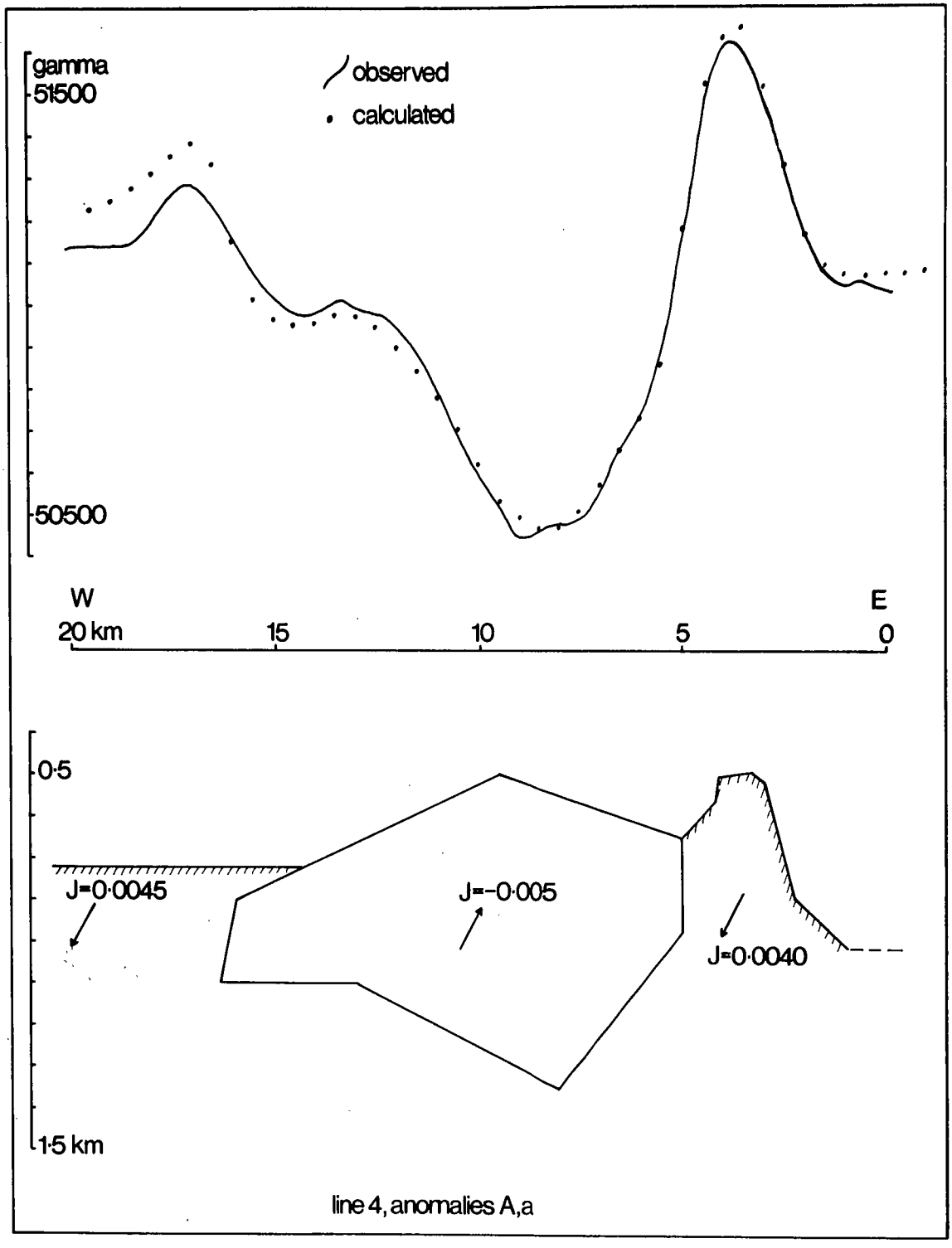

Fig 4.14 Interpretation of anomalies A,a by the indirect method.

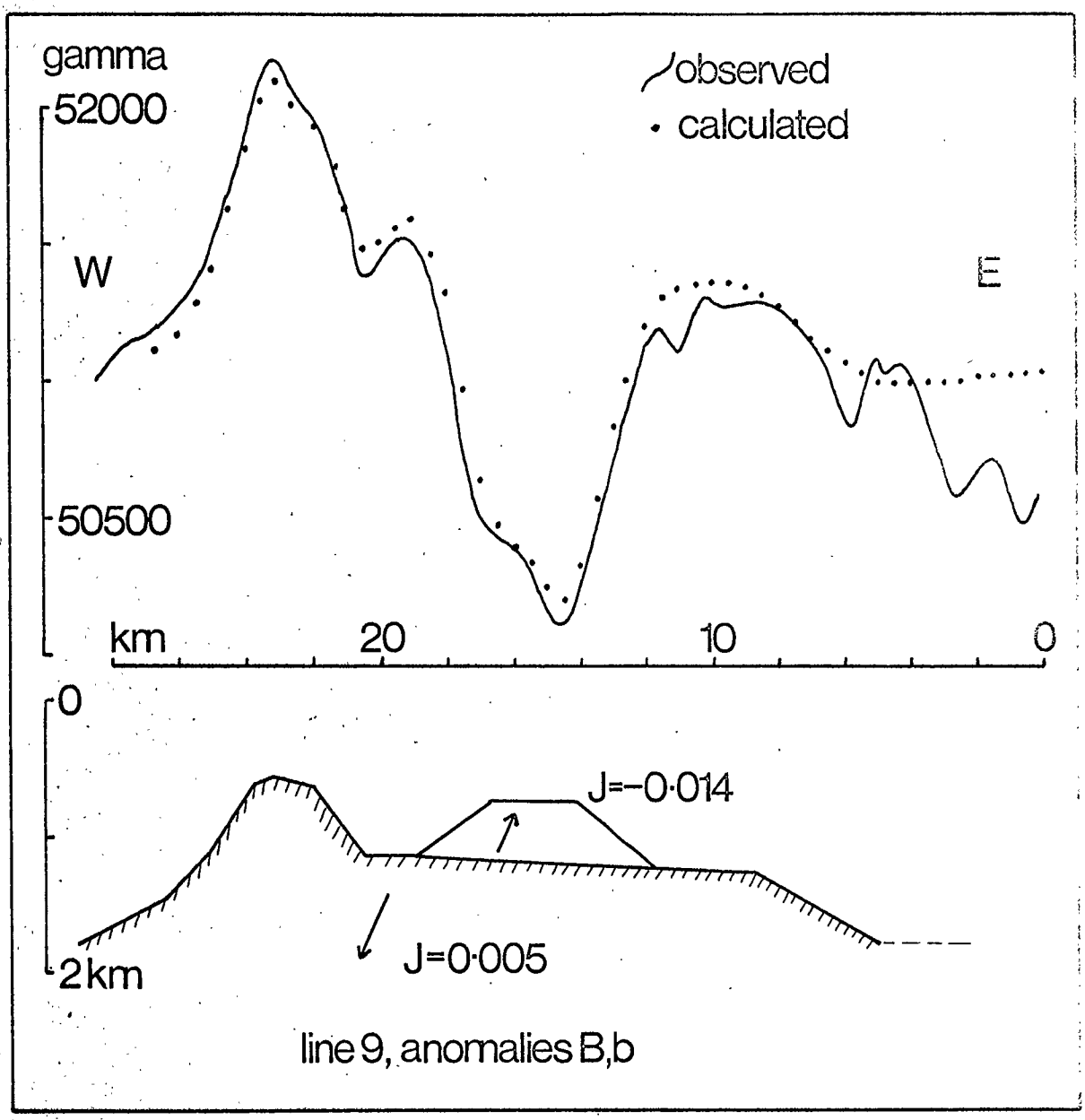

Fig 4.15 Interpretation of anomalies B,b by the indirect method.

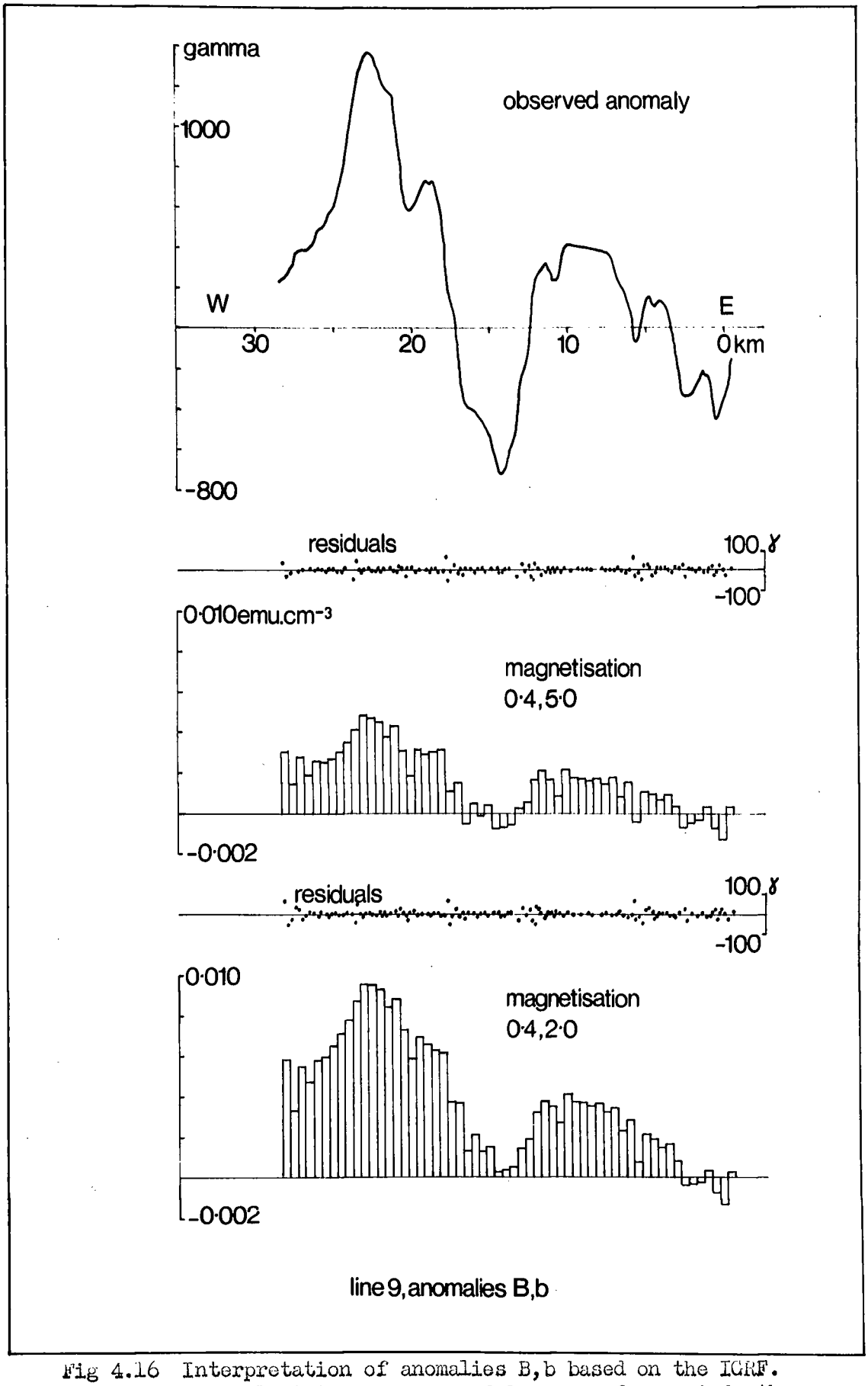

Fig 4.16 Interpretation of anomalies B,b based on the IGRF. Equivalent layer upper and lower surfaces at depths indicated for each distribution of magnetisation.

4.1.3 The eastern section of variable magnetic anomalies.

Whatever the true situation represented by the models for the regional high in figs. 4.8 and 4.9, the steep field gradients at the eastern margin of this feature are interpreted as steep upper surface scarps which descend to depths between 1km and 2km, or on average 1.5km. Optimization for the dimensions of a tabular body to satisfy an anomaly profile over low c (fig. 2.3) produced a solution contained between depths of 0.4km and 1.5km. This anomaly will be discussed below, but the depth range of the tabular model is considered to be significant. Although it is not possible to resolve a vertical distribution of magnetic sources, there is strong seismic refraction evidence for a layer interface at approximately 2km. The south-eastern end of seismic refraction line 69/3 of Bott et al. (1971) lies just to the west of high H (fig. 2.3). The seismic structure beneath the south-eastern end of line 69/3 is interpreted by Bott et al. as follows:

Layer	P - velocity (km/s)	Layer thickness (km)	Depth to top (km)
water	1.48*	0.4	-
1a	3.68*	0.57	0.40
1b	4.47**	1.63	0.97 ± 0.24
2	5.74	4.65	2.60 ± 0.52
3	6.80	-	7.25 ± 1.28

* assumed ** assumed horizontal

The layer numbers of Bott et al. are based on the convention

of Palmason (1970) for similar seismic velocities in Iceland. The velocity for layer 1a is that observed at the north-western end of line 69/3, and the thickness of this layer at the south-eastern end of the line, where it was not observed directly, was calculated from the time intercept on the distance - time plot for layer 1b, which is greater than would be expected for a first refraction at the sea floor. The seismic results tabled above indicate that the layer 1/layer 2 interface occurs at a minimum depth of 2km, which is in partial agreement with the average depth of 1.5km noted at the beginning of this section. Thus, the mixed and variable anomaly field east of the regional magnetic high (fig. 2.3) is probably caused mainly by sources contained within layer 1a and 1b of Bott et al. (1971). On this hypothesis, layers 1a and 1b are underlain either by relatively non-magnetic material, or by material within which the intensity of magnetisation is slowly varying in a lateral sense, so that it is effectively uniform over distances of 10-20km, as in the case of the regional high in the west. This interpretation is a tentative one, but suits the change in anomaly style from west to east, and is supported by the results of reversed refraction line 69/3.

Lateral distributions of magnetisation, obtained by use of the linear inverse technique for an equivalent layer bounded by depths of 0.4km and 1.5km, contain changes in intensity that are quite consistent in absolute magnitude for magnetic anomalies of 5-15km wavelength over most of the central and eastern sections of the survey area. Fig. 4.17 shows two of these distributions of magnetisation; one is for an anomaly profile

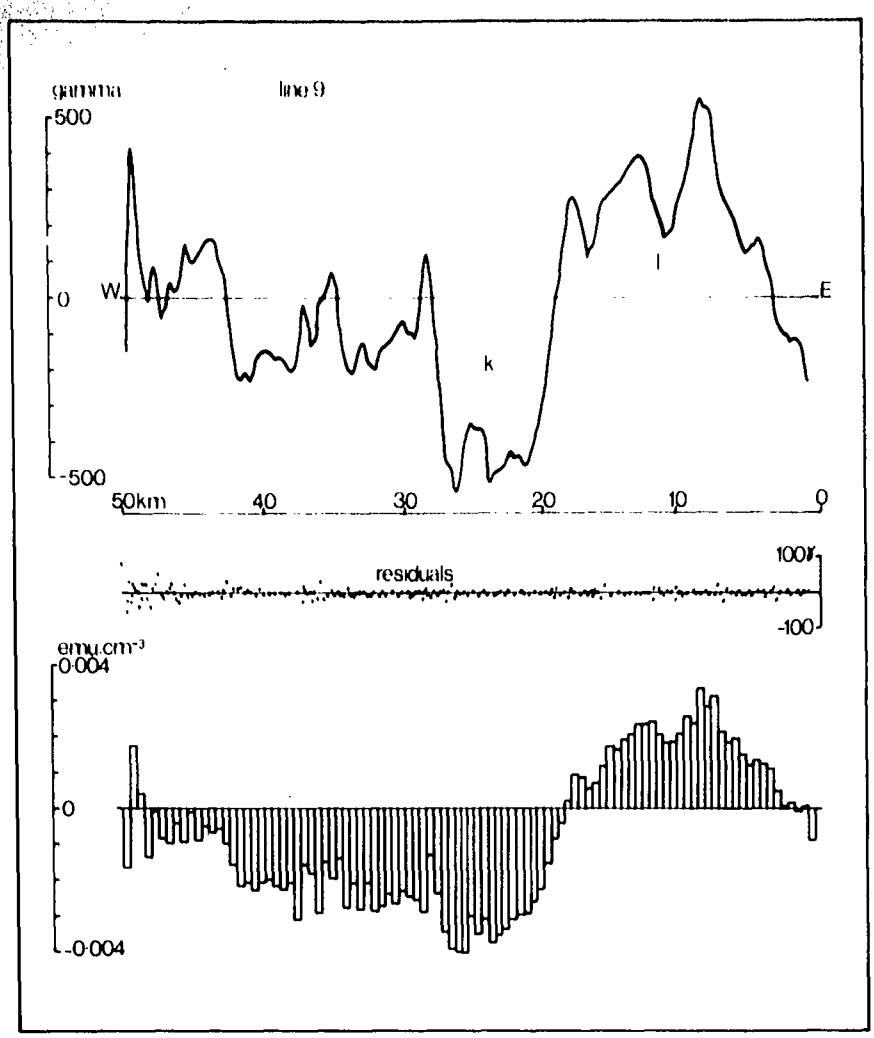

Fig 4.17 Interpretations by use of an equivalent layer between depths of 0.4km and 1.5km.

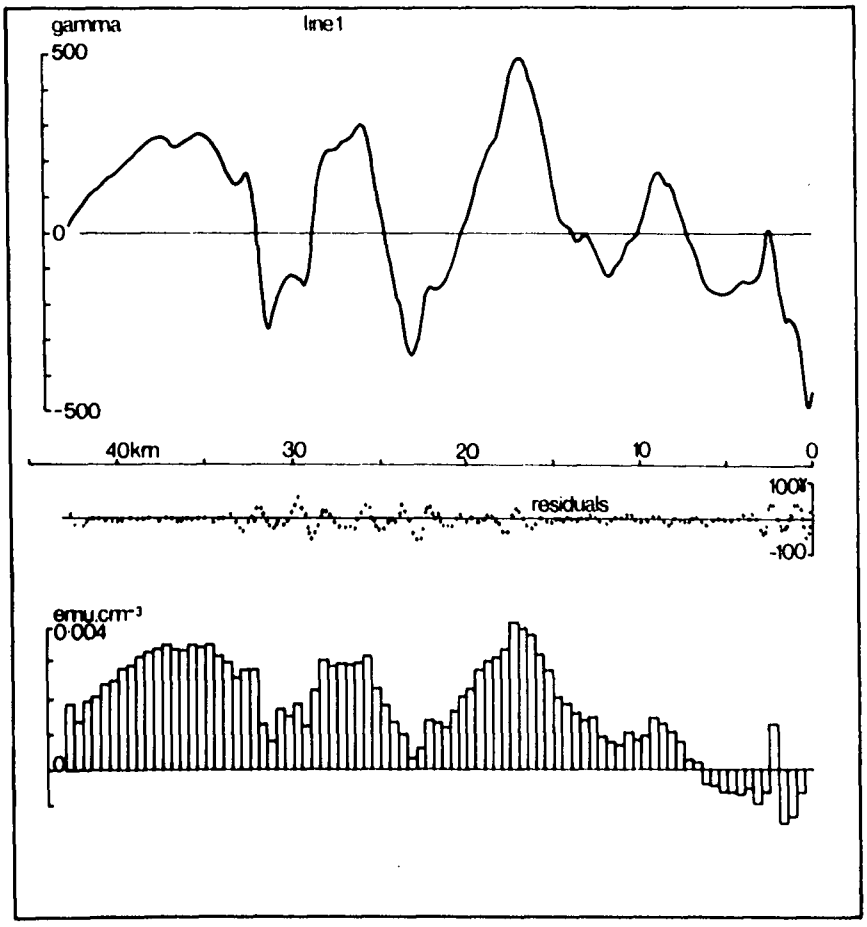

from line 9, based on the IGRF, and the other is for a profile from line 1, based on a least - squares regional. The E - W least - squares regional gradient is very slight for line 1 (fig. 4.1), due to a lower amplitude for the western 'regional high' and to the presence of a long wavelength positive anomaly in the centre of the line (fig. 2.4). Both distributions in fig. 4.17 include local changes in intensity over distances of 5-10km of the order $\pm$ 0.003cgs.

The interpretation of low c (fig. 2.3) by optimization, and high D (fig. 2.3) by the linear inverse method indicates intensities of magnetisation of the same order as those derived for local anomalies on the profiles from lines 1 and 9 (fig. 4.17). However, the regular form and trend of anomalies c and D distinguishes them from the general anomaly field east of the regional high (fig. 2.3). The tabular body produced for low c is of width 3km and of intensity of magnetisation -0.003cgs; the width is too great for a single dyke and the absolute intensity seems rather high for a dyke swarm, when compared to measured intensities on samples from dykes in Iceland (kristjansson, 1970), unless individual dykes are closely packed to form an effectively homogeneous intrusion of moderate size. Alternatively, the regular form of anomaly c may be explained by a lens of lava built up over a N - S fissure; a similar interpretation could account for anomaly D. Certainly, the N - S trend of anomalies c and D (fig. 2.3) identifies them more closely with the 'regional high' than with the mixed anomaly field in which they are set. If these features are associated with fissure - controlled intrusion or

extrusion on the flanks of the postulated layer 2 ridge, then the development of fissures would appear to be very limited.

Of equal uncertainty is the interpretation of high H figs. 2.3, 4.8 and 4.9). Again, there is a certain simplicity and a suggestion of a N - S trend that associates this feature with the regional magnetic high in the west. It may be caused by another, smaller ridge of layer 2 rocks, and if it contains a volcanic centre, this may be poorly developed or buried by younger basalts, such as the central volcano of Husafell in south-west Iceland (Saemundsson, 1967).

A NW - SE trend is poorly developed in the present survey area, and is only recognisable in low k and its continuations as the locus of relatively low and negative anomalies (figs. 2.3 and 2.4). From fig. 4.17, it appears that low k is associated with a negative magnetisation of greater absolute intensity than that for adjacent anomalies. This may indicate a greater depth extent for the source of low k and a possible association with deep fractures; the steep gradients of low k on line 9 (fig. 4.17) could support this, but the interpretation is uncertain. However, it is noted that the major fjord system of the Faeroe Islands is aligned NW - SE, and that this is also one of the two suggested conjugate fault directions that control the present outline of Iceland (Tr. Einarsson, 1965).

4.1.4 Discussion.

Before the results of interpretations presented above are discussed, it should be noted that a long wavelength component from layer 3 may be present in the magnetic data of the detailed

survey area. The typical oceanic layer 3 is considered to contribute little to the observed magnetic field (Bott, 1967; Luyendyk, 1969; Talwani et al., 1971), but in south-west Iceland (Kristjansson, 1970; Kristjansson, 1971) highly altered basalts with a remanent magnetisation of 0.06cgs have been sampled from a borehole sunk in an area where seismic data indicates a depth to layer 3 of only a few hundred metres (Palmason, 1970). Seismic refraction studies in Iceland (Palmason, 1970) have also shown that the depth to layer 3 is sharply reduced by as much as 4km beneath Tertiary volcanic centres. If such a situation is present beneath the regional magnetic high in the west of the present survey area, then the effects will be of greatest influence in the models of figs. 4.8 and 4.9. Interpretation of high amplitude anomalies A, a and B, b should not be affected.

The relatively quiet anomaly field over sections of the regional magnetic high in the west suggests that the postulated ridge of layer 2 rocks is composed of thick units of large areal extent. The presence of volcanic/intrusive centres A, a and B, b indicate that former magma reservoirs at a high level in the crust are to be expected, and, thus, a likely composition for the ridge of layer 2 rocks in the west of the area is of thick basalt formations and gabbroic intrusions. If, as was noted in section 4.1.1.1, the intensities of magnetisation for the models for the regional high in figs. 4.8 and 4.9 are average intensities of the correct order of magnitude, then a tentative correlation may be made with the intensities of sampled gabbros and the more highly magnetic Tertiary basalts

in Iceland (Kristjansson, 1970). Interpretation of the regional magnetic high is appropriate to the ridge of layer 2 rocks only, and should not be extrapolated to include the whole of the thick layer 2 that seems to be characteristic of the Iceland - Faeroes Rise (Bott et al., 1971). However, it has been proposed (Kristjansson, 1970) that an extensive substratum of gabbro is present beneath Iceland to account for the widespread occurrence of gabbroic nodules in basalts.

Another problem is whether other ridges of layer 2 rocks on the Iceland - Faeroes Rise (Bott et al., 1971) are closely associated with volcanic/intrusive centres, as appears to be the case in the present survey area. If such a close association is the general rule, then it may be indicative of a prolonged or a very intense activity for the formation of layer 2 in distinct stages. During the first stage an extensive thickness of basalts, probably of submarine pillow form, was built up from numerous fissures, while activity became localised to centres during a second stage. These two stages may represent separate phases in time, or may be different contemporaneous aspects of one period of activity in a particular area.

The dominant positive polarity of the regional magnetic high (fig. 2.4) also suggests either prolonged activity during a lengthy geomagnetic epoch of normal polarity, or rapid extrusion and intrusion during a period of intense activity.

The style of activity which has been associated with the western part of the survey area contrasts sharply with that which seems to have occurred in the eastern and central sections. The variable anomaly field east of the regional high contains

both positive and negative anomalies which, when based on the IGRF, are explained by positive and negative magnetisations (Fig. 4.17). This situation is indicative of igneous activity over a long interval, during which the ambient geomagnetic field changed polarity at least once, but probably several times. The generally irregular nature of the anomaly field in this sub-area suggests, in addition, that the igneous activity was mainly extrusive in character.

The sources of magnetic anomalies within this sub-area have been identified as contained within seismic layers 1a and 1b of Bott et al. (1971). Layer 1a is poorly defined at the south-eastern end of line 69/3, and it appears that layer 1 is composed mainly of the 1b rock type in the present survey area. In Iceland, seismic layers 1 and 2 are composed of Tertiary basalts (Palmason, 1970) of very similar petrological and magnetic properties, and, thus, the intensities of magnetisation of 0.003-0.004cgs computed for lines 9 and 1 (fig. 4.17) are probably of the correct order when compared to slightly higher, but comparable intensities associated with the models for the regional high in figs. 4.8 and 4.9. In this context, the W - E high amplitude, long wavelength change in magnetisation that characterises the present survey area is explained as a change from basement formed by the style of igneous activity associated with a thick ridge of layer 2 rocks to that of a thinner layer 1.

Bott et al. (1971) have drawn the general conclusion that the crust of the Iceland-Faeroes Rise bears strong similarities to that of Iceland, in terms of both upper crustal variability and total crustal thickness. Thus, it may be valid to equate the apparent W - E change in style of igneous activity, in the

present survey area, to eruption in shallower water or in sub-aerial conditions. It was also considered by Bott et al. that a local V - shaped gravity anomaly, on the south-east section of the Iceland - Faeroes Rise, is caused by a V - shaped valley which is now buried by sediment, and which had been cut sub-aerially when the crest of the Rise stood above sea level. Emergence of the Iceland - Faeroes may be reflected in the change in style of igneous activity as mentioned above, and possibly also in the topographic form of some minor feature. Many of the geometric models for the sources of some isolated anomalies in the present survey area show a break in slope below the shallowest 100-300m of the bodies (figs. 4.10 to 4.13). This break in slope may mark the change from pillow basalts to tephra in the postulated series; pillow structures, breccias and tuff, and plateau basalts; a series that indicates the transition from eruption in deep water through eruption in shallow water, to quiet subaerial extrusion. This series has been deduced from the study of extrusion forms in and around Iceland (Jones, 1966; Kjartansson, 1967; Jones, 1970). A major difficulty in applying this hypothetical series to the present area is that the emergent tephra stage on Surtsey has a weak magnetisation compared with that of the presumed pillow basalts of the totally submarine volcano Surtla (Sigurgeirsson, 1966), while the models in figs. 4.10 to 4.13 are associated with a high intensity of magnetisation.

Indirect evidence of a former elevation of the Iceland-Faeroes Rise, at least within the marked influence of wave action, is provided by the lack of significant bathymetric

relief on the crestal plateau. The crestal plateau has been shown from seismic results (Bott et al., 1971) to be formed of a very variable upper crust with considerable topography on the layer interfaces, and the present work has shown the existance of a number of discrete volcanic centres. Thus, the smooth crestal plateau may be the result of marine peneplanation when igneous activity had ceased, possibly accompanied by gradual subsidence. However, the effect of bottom current activity must not be underestimated in this respect (Jones et al., 1970), and this may have been more intense during the period of lower sea level associated with the Pleistocene glaciations.

There is a strong indication of a former sub-aerial status for the western part of the Faeroes shelf area in the thickening towards the west of the Eocene coal series on Sudheroy (Rasmussen and Noe - Nygaard, 1970).

4.1.5 Summary of conclusions.

a) The magnetic structure of this section of the Iceland-Faeroes Rise is anomalous when compared to that of typical oceanic crust in the North-east Atlantic.

b) A long wavelength positive magnetic anomaly in the west of the area is interpreted as caused by a ridge of thick basalts and gabbro intrusions that is associated with the thick seismic layer 2 (P - velocity 5.7km/s), which is characteristic of the Iceland-Faeroes Rise.

c) The ridge of layer 2 contains volcanic/intrusive centres which are associated with basic and acid rocks, as component intrusions or volcanic superstructure.

d) Much of the magnetic anomaly field east of the layer 2 ridge is due to magnetisations within seismic layer 1, of thickness approximately 2km. This layer is composed almost exclusively of extruded material of variable character.

e) There is slight and uncertain evidence for the former elevation of the Iceland-Faeroes Rise up to, or above sea level.

4.2 Interpretation of data from the survey of RRS John Murray, 1967.

Profiles from lines K and C (fig. 1.4) were interpreted using the basic linear inverse method and the joint analysis gravity/magnetic programs to determine the crustal relation of magnetisation to anomalous density.

4.2.1 Interpretation of line K.

By the use of gravity data (fig. 4.18) and the results of seismic refraction lines 69/2 and 69/3 (fig. 1.4), Bott et al. (1971) concluded that the Iceland-Faeroes Rise is approximately in isostatic equilibrium, with compensation of the Airy type by crustal thickening to a depth of 20km. The present study of line K is to investigate the sources of magnetic anomalies and their relation to local gravity anomalies.

In terms of magnetic anomalies, the situation on line K is similar to that of the detailed survey area of section 4.1. Here again, a central section of variable high wavenumber anomalies is contained between two flanking anomalies, centred about 100km and 300km (fig. 4.18), which contain long wavelength components of significant amplitude. The outer sections of the

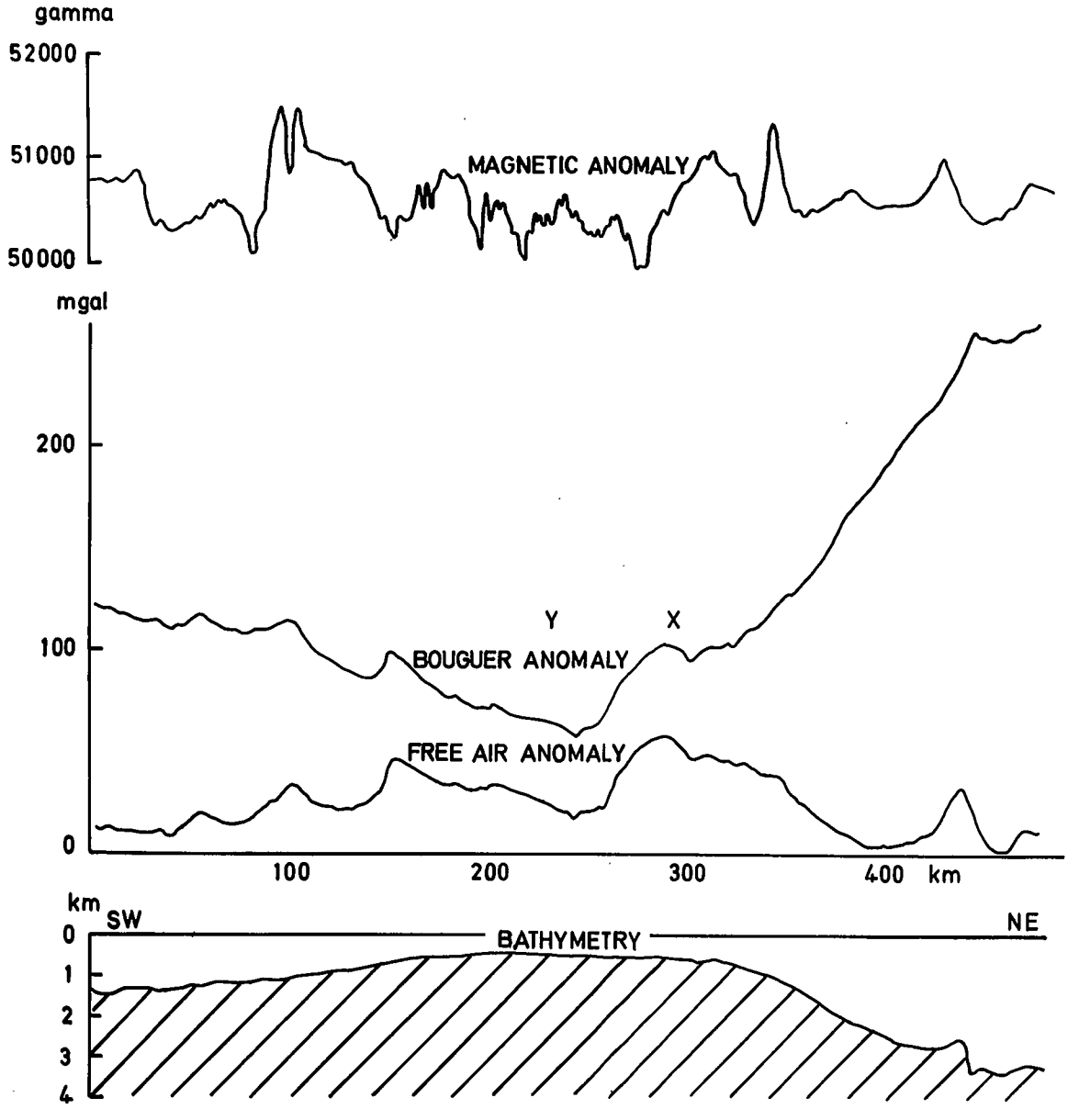

Fig 4.18 Line K: magnetic, gravimetric and bathymetric profiles.

magnetic profile are probably of little use in two-dimensional interpretation, as south-west and north-east of the two major flanking anomalies, the data profile is probably sub-parallel to the strike of magnetic anomalies (fig. 1.3).

The central section of high wavenumber magnetic anomalies is associated with a relative low of 30-40mgal in the gravity field, gravity anomaly Y in fig. 4.18. This low is part of a depression in the free air gravity field, of approximately N - S or NNW - SSE trend, which is terminated just to the north of the detailed survey area by an E - W gravity high (fig. 1.5).

The approximate centres of the south-west and north-east flanking magnetic highs on line K (fig. 4.18) are located at 62°20'N, 11°20'W and 63°30'N, 08°20'W. In fig. 1.3, the south-west flanking high forms part of a N - S or NNW - SSE band of high field values that includes also the western 'regional high' of the detailed survey area. Continuity of the north-~~west~~ east flanking high on line K is more obscure, but it may form part of a band of anomalies striking N - S from the north-western edge of the Faeroes 'shelf', with a change in trend to NE - SW at approximately 62°50'N.

A lateral distribution of magnetisation within an equivalent layer bounded by depths of 0.5km and 5.0km indicates a change in intensity of approximately 0.006cgs, from the central section to the north-east flanking high. This is of the same order as was obtained from the intensity of magnetisation of models for the 'regional high' in the detailed survey area (figs. 4.8 and 4.9), with vertical dimensions approximately those of the equivalent layer used here. Intensities of

magnetisation associated with the south-west flanking high on line K are somewhat higher, and this difference will be discussed below, but there is some indication of a general structural similarity, and possibly continuity between the detailed survey area in the north and line K in the south.

4.2.1.1. Transformation of anomalies and the ratio p/J.

Program TR/GM was used to transform the free air gravity anomaly profile (fig. 4.18) to pseudo-magnetic anomalies. Some features of the observed magnetic anomaly profile were reproduced in correct phase relation, but generally the results were unsatisfactory.

Program TR/MG was used to produce the pseudo-gravity anomaly profiles shown in fig. 4.19 from the observed magnetic anomalies, based on the IGRF, and for two different magnetisation inclinations in the direction of true north. The pseudo-gravity profiles show a striking difference between the north-east and south-west sections. To the north-east, the positive anomaly X on the gravity profile (fig. 4.18) is reproduced quite accurately on the pseudo-gravity profile (fig. 4.19) with the exception that slight phase discrepancies exist and that the pseudo-gravity profile does not quite match the steep gradients between anomalies X and Y, from high to low. However, the general agreement between observed free air and pseudo-gravity profiles is very close for the section of anomalies X and Y.

In contrast, the south-western half of line K is dominated by a high amplitude long wavelength component in the pseudo-gravity anomaly. Local features in the observed free air

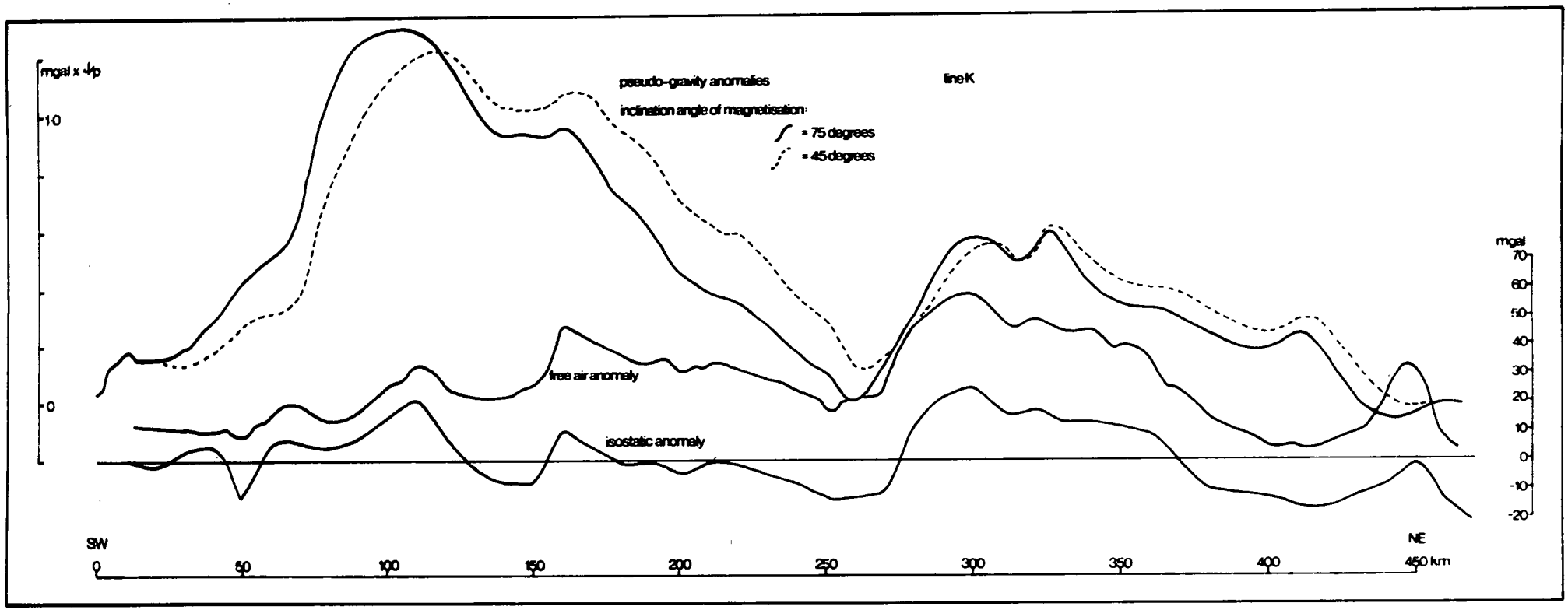

Fig 4.19 Line K: pseudo-gravity transformations.

gravity profile are represented as inflections and secondary peaks and troughs, superimposed on a broad positive pseudo-gravity anomaly.

The ratio of the amplitudes of the two major pseudo-gravity anomalies on line K is approximately 2:1, and this contrasts with the situation on the observed free air gravity profile, and with that on the isostatic anomaly computed from the Airy model of Bott et al. (1971). The amplitude ratio is not significantly affected by a change in the specified angle of inclination of the magnetisation vector, as is shown by the two pseudo-gravity profiles of fig. 4.19. The immediate conclusion to be drawn from the pseudo-gravity profiles of line K is that a relation does exist between gravity and magnetic anomalies, but that this is obscured in part by a long wavelength effective change in the value of the ratio p/J.

The NW - SE seismic refraction line 69/2 of Bott et al. (1971) crosses line K just to the south-west of gravity high X (figs. 1.4 and 1.5), and interpretation of the seismic data includes another step or ridge in layer 2. Thus, the correspondence of inflections and peaks in the pseudo-gravity profile is identified with topography on the layer 1/layer 2 interface.

Gravity anomaly Y (fig. 4.20B) is an important feature in this correspondence between magnetic and gravity anomalies. Bott et al. (1971) noted that the steep gravity gradients between anomalies X and Y necessitates that the associated density contrast occurs at or close to the sea floor. The plot of anomalous density in fig. 4.20C, as derived from the Airy isostatic anomaly and defined by an equivalent layer between

Fig. 4.2D: Line K.

A: Observed magnetic anomalies based on IGRF.

B: Observed free air gravity anomaly; dashed line is satellite derived regional of +20mgal.

C: Isostatic anomaly calculated from Airy type model of Bott et. al. (1971). Density distribution in an equivalent layer between 0.5km and 2.5km.

D: Distribution of magnetisation (dotted) and ratio p/J (histogram) derived from anomalies of A and B.

E: Distribution of ratio p/J derived from anomalies A and C.

F: Upper; 'correct' magnetic anomaly profile. Lower; distribution of magnetisation (dotted) and ratio p/J (histogram) derived from anomalies of B and F.

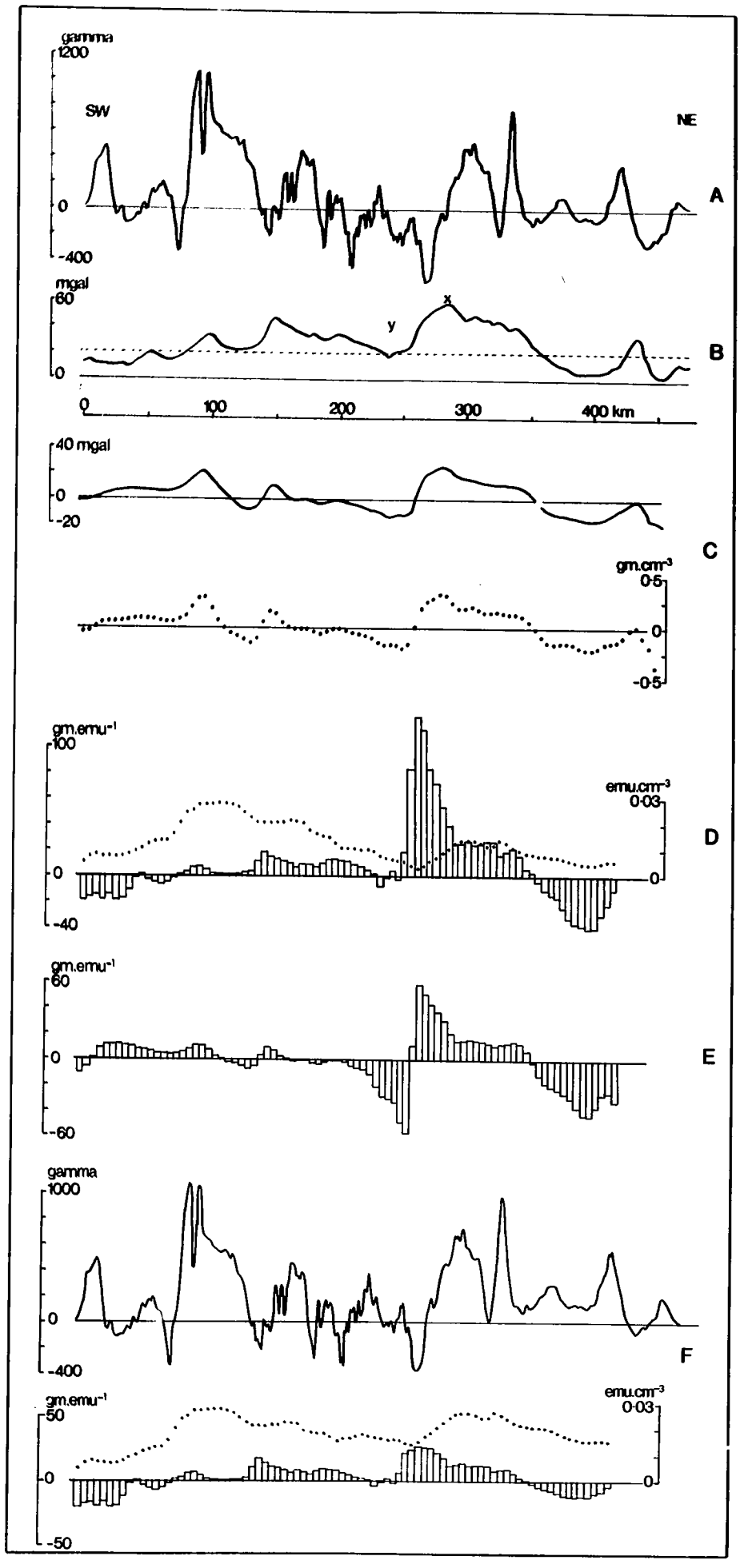
gamma
1200
SW
NE
0
-400
A
mgal
60
x
y
B
0
0
100
200
300
400 km
40 mgal
0
-20
C
gm.cm⁻³
0·5
0
-0·5
gm.emu⁻¹
100
emu.cm⁻³
0·03
0
-40
D
gm.emu⁻¹
60
0
-60
E
gamma
1000
0
-400
F
gm.emu⁻¹
50
emu.cm⁻³
0·03
0
-50

depths of 0.5 and 2.5km, shows that the magnitude of this density contrast is 0.5gm/cm^3. Although this contrast would seem to be rather high, confidence in the value is provided by the interpretation of seismic refraction line 69/2 by Bott et al. (1971). The intersection of line K with the north-western end of refraction line 69/2 occurs at the minimum value for free air gravity anomaly Y at +20mgal. The upper crustal interpretation at the north-western end of seismic line 69/2 is for a thick trough of layer 1 rocks overlying layer 2. Layer 1 has been identified here to consist entirely of the 1a type, of P-velocity 3.24 $\pm$ 0.35km/s, and for a seismic model containing a 'hidden' layer 3, these low velocity rocks are contained between depths of 0.5km and 3.32 $\pm$ 0.63km (Browitt, 1971), or approximately within the dimensions of the equivalent layer used here. Even for an equivalent layer base at 3.5km the density contrast is as high as 0.35gm/cm^3. Thus a density contrast of the order 0.5gm/cm^3 may be identified with the layer 1a/layer 2 interface, and with considerable significance.

All seismic velocities on the Iceland-Faeroes Rise (Bott et al., 1971) show a correlation with those of Iceland (Palmason, 1970), except that the Icelandic velocities are slightly lower, which may reflect the younger age. In this context, and in view of the high density contrast between layers 1a and 2, a lithological correlation may be made between layer 1a on the Iceland-Faeroes Rise and layer 0 in Iceland, for which Palmason (1970) has suggested a density contrast with layer 2 of 0.2 - 0.7gm/cm^3. In Iceland, layer 0 is restricted to the Neo-volcanic Zone, and is composed of thin lava flows, volcanic breccias and tuffs, of maximum thickness 1.5km. Thus, the

layer 1a trough of Bott et al. (1971) appears to be a wholly Tertiary lithological equivalent of the Neo-volcanic Zone in Iceland. A pyroclastic source structure was also suggested, to explain the high wavenumber magnetic anomalies in association with the free air gravity trough, by Dr. U. Fleischer of Deutsches Hydrographisches Institut (personal communication, 1969).

An equivalence in overall structure of the Iceland-Faeroes Rise to Iceland was concluded by Bott et al. (1971), with a possibly thicker crust for the former. A greater total crustal thickness, and a thicker zone of low-velocity pyroclastics may indicate that, whatever the mechanism responsible for the igneous activity on Iceland, the Iceland-Faeroes Rise represents an equivalent structure, in association with which, the activity was more intense, or reached a more advanced stage in development than that observed in present day Iceland.

The long wavelength effect.

The long wavelength effect that obscures the gravity and magnetics correspondence in the pseudo-gravity profile for line K (fig. 4.19) is evident in the plot of magnetic anomalies based on the IGRF (fig. 4.20A). The drastic effect of this component on the distribution of magnetisation in an equivalent layer is shown in fig. 4.20D, where the intensities associated with the south-western flanking magnetic high are dominant.

The sharply peaked sections of the two p/J distributions (figs. 4.20D and 4.20E) correspond in position with gradient discrepancies and slight phase discrepancies, at low anomaly values, in the correspondence of the free air and pseudo-

gravity profiles (fig. 4.19).

To estimate the magnitude of the effect of the long wavelength magnetic anomaly component on the distributions of magnetisation and p/J, a 'corrected' magnetic anomaly profile was prepared. The anomaly profile of Fig. 4.20A was used, and the IGRF background field was retained from 0km to 180km; from 280km to the north-eastern end of the profile, a background field 200 gamma lower than the IGRF was specified, or lower by the estimated amplitude of the disturbing long wavelength component. Continuity between the two background levels was obtained by use of a cosine taper over the intervening 100km. The 'corrected' anomaly profile is shown in fig. 4.20F. Although this is a somewhat arbitrary construction, it may be seen that in the 'corrected' distributions, the intensity of magnetisation is approximately equal for both large flanking highs, a condition that is suggested by the density distribution (fig. 4.20C) for a strict correspondence between gravity and magnetic anomalies. In addition, the sharp peak in the p/J distribution is much reduced.

A tentative conclusion drawn from the results of this approximate test, is that the effective change in p/J that is evident on the pseudo-gravity profile (fig. 4.19) is due to a long wavelength change in magnetisation, rather than to major changes in depth or thickness of the principal source layers. This conclusion is supported by the results of fourier analysis.

Energy spectra and amplitude spectra were computed directly for two partly overlapping sections of the magnetic anomaly

profile of line K. Each section contained one of the two major flanking anomalies plus the central region of high wavenumber anomalies. The graphs in fig. 4.21 provide a qualitative and semi-quantitative assessment of the source depth distribution. The upper graph of fig. 4.21 shows a log-plot of the energy spectra. According to Spector and Grant (1970), the depth to the source of a band of magnetic anomaly wavenumbers varies with wavenumber and as the gradient of the log-plot energy spectrum. The plot for the north-eastern anomaly section (fig. 4.21) appears to have a steeper gradient for lower wavenumbers than that for the south-western section. This may indicate the onset of sediment on the eastern parts of the Iceland-Faeroes Rise (Jones et al., 1970), but both log-plot energy spectra are rather flat and imply that there are significant energy contributions which are not related to differences in source depth.

The two-layer upper crustal structure for the Iceland-Faeroes Rise (Bott et al., 1971) makes the use of fourier spectra rather dangerous in depth of source analyses when both layer 1 and layer 2 contribute significantly to the observed magnetic field. This consideration applies to the energy spectra and to the plot of depth differences (fig. 4.2[illegible]), calculated from the amplitude spectra of the two anomaly sections of line K, by the method described in appendix G. However, the main feature of the depth-difference plot (fig. 4.2[illegible]) is the discontinuity at lower wavenumbers, which is considered to be caused by the influence of a long wavelength magnetisation change which is not related to changes in topography. The same feature is represented by coincidence for the two anomaly

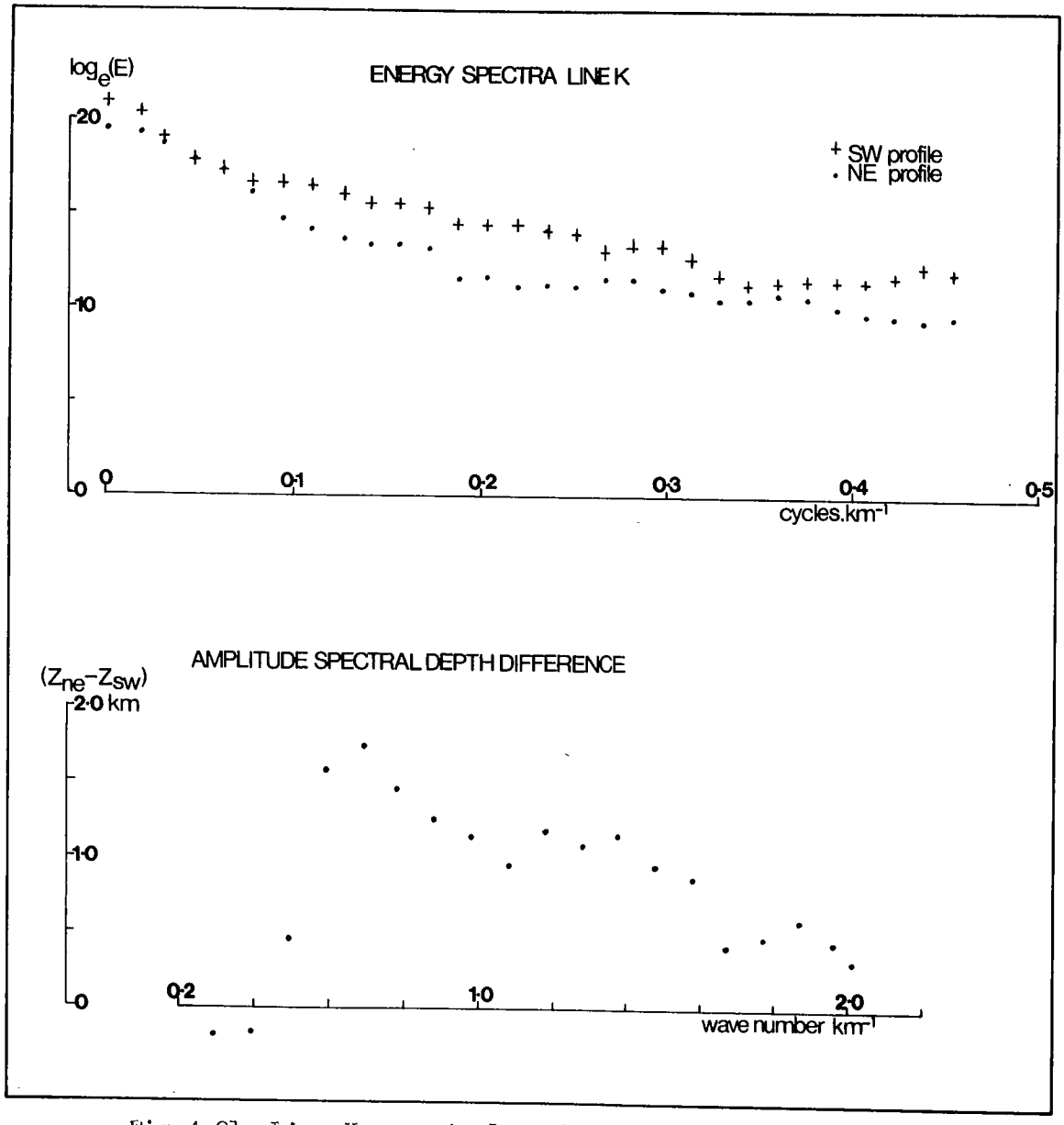

Fig 4.21 Line K: spectral analysis(see text).

sections at low wavenumbers on the log-plot energy spectra.

Thus, there are indications of a long wavelength change in magnetisation on line K that is independent of topography and lithology.

4.2.2 Interpretation of data from line C.

Line C is of NW - SE trend (fig. 1.4), and gravity, magnetic and bathymetric profiles are shown in fig. 4.22. A long wavelength component in the gravity profiles has been attributed by Bott et al. (1971) to a change in depth to layer 3, from about 7km north-west of 130km (fig. 4.22) to about 12km in the south-east. Local gravity anomalies are presumably related to differences in lithology at the sea floor, such as represented by sediment, layer 1a, layer 1b and layer 2.

A pseudo-gravity anomaly profile was computed from the IGRF residual magnetic anomalies, and is shown together with the free air anomaly in fig. 4.23. The pseudo-gravity anomaly shows wide variation in the value of the ratio J/ρ; in view of this, and of the variability and complexity of upper crustal structure, a qualitative correlation was made of the pseudo-gravity profile with the observed free air profile. Correlation was based on phase relations and amplitude polarity with respect to the local background field. In fig. 4.23, the digit '1' denotes in-phase correlation, and the digit '0' denotes anti-phase correlation. There are two sets of correlation in fig. 4.23; the lower one is based on broad features and groups of anomalies, while the upper correlation is more detailed and includes some inflections as well as peaks

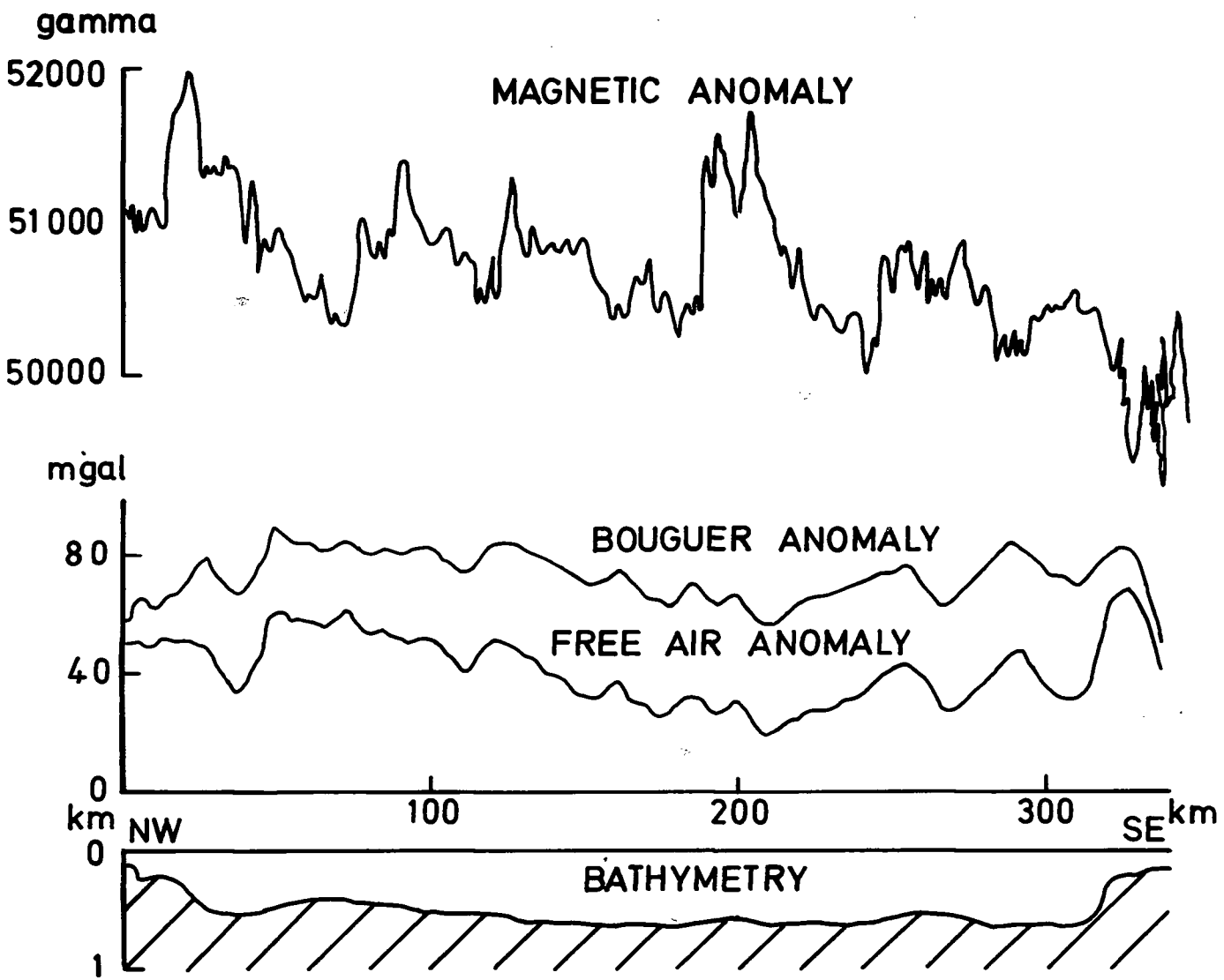

Fig 4.22

LINE C

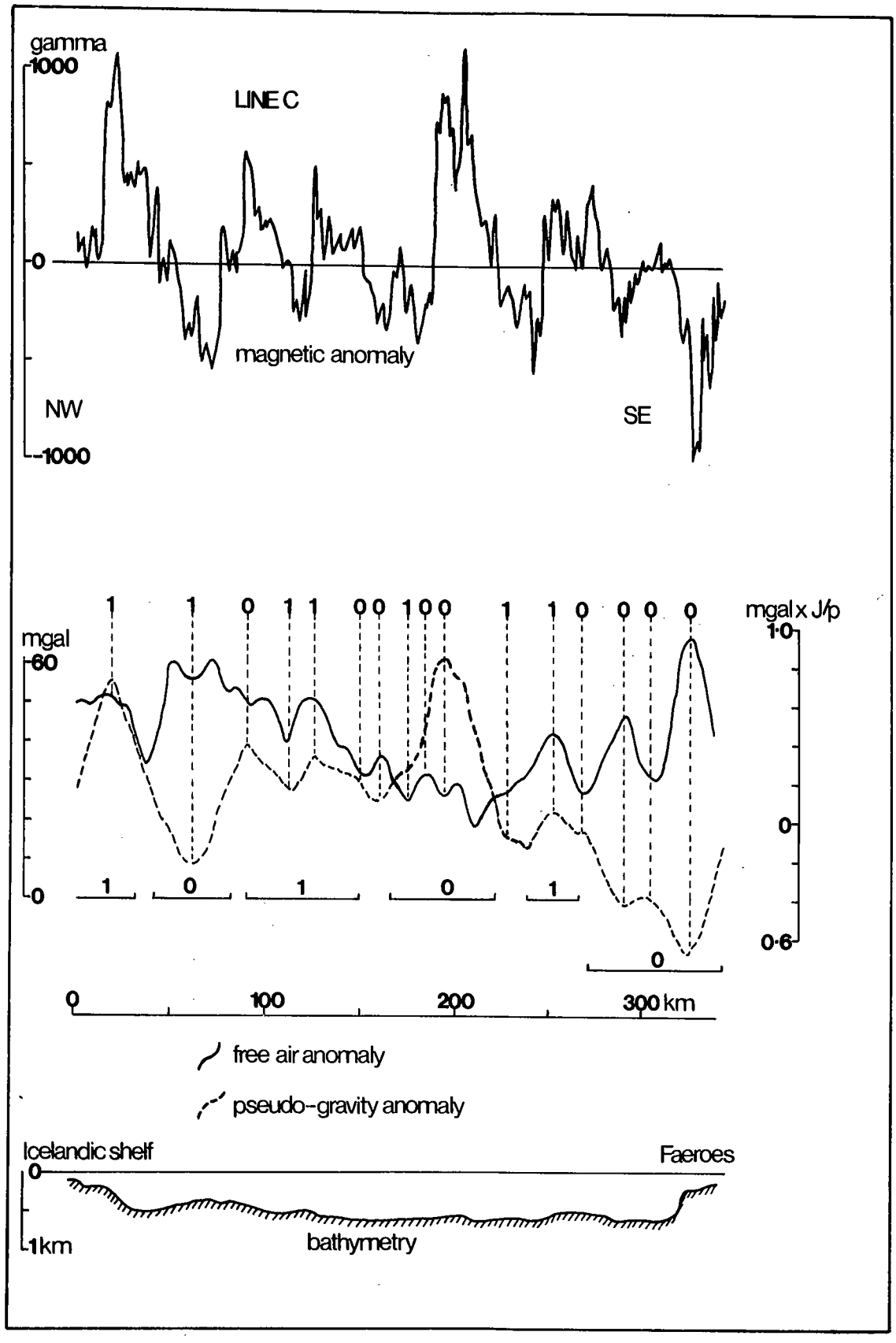

Fig 4.23 Line C: gravity anomaly correlation.

and troughs, but is somewhat more uncertain.

It is considered that the alternating bands of in-phase and anti-phase correlations must in part represent magnetisation changes that are independent of lithology and topography. These changes are also identified with the very long wavelength magnetic anomaly component on line K, and thus the strike of the magnetisation changes is subparallel to the trend of line K, or approximately NE - SW. This is also the trend of magnetic anomalies in the north-eastern section of the detailed survey area (fig. 2.4), and approximately that of the Raff-Mason type anomalies south of Iceland that are associated with sea-floor spreading from the Reykjanes Ridge.

Thus, the magnetic anomaly field of the Iceland-Faeroes Rise may contain contributions from NE - SW zones of magnetisation, each of which reflect the ambient geomagnetic field at the time of formation of that part of the crust. This conclusion supports the conclusion of Bott et al. (1971) that the Iceland-Faeroes Rise was formed by sea-floor spreading, albeit of an anomalous type.

4.2.3 Conclusions.

a) The magnetic anomaly field on NE - SW profiles is controlled mainly by the layer 1/layer 2 interface.

b) A thick trough of low P - velocity volcanic rocks, similar in lithology to layer 0 of the Neo-volcanic Zone in Iceland, is present on the crest of the Iceland-Faeroes Rise, and is of N - S or NNW - SSE strike direction.

c) NE - SW zones of remanent magnetisation may exist

as indicative of an anomalous type of sea-floor spreading, by which process the Iceland-Faeroes Rise was formed.

4.3 General discussion and recommendations.

The Iceland-Faeroes Rise is almost certainly younger than the basalt formation of the Faeroe Island. This is supported indirectly by a reconstruction of the pre-drift continental fit between Greenland and Europe, including the Faeroe Islands (Bott and Watts, 1970b). The considerable quantities of positive magnetisation in the interpretations of this work differentiate the Iceland-Faeroes Rise from the basalt pile of the Faeroe Islands, which is considered to be mainly of reversed magnetisation (Abrahamsen, 1967; Tarling and Gale, 1968).

If the NE - SW zones of magnetisation changes are closely associated with an anomalous type of sea-floor spreading, then this process would appear to have taken place in a direction at a significant angle to the structural trend of the upper crust, as defined by the eastern margin of the regional high (fig. 2.4) and the main trend of aeromagnetic anomalies (fig. 1.3) In the formation of crustal units of N - S trend, in chronological units of NE - SW trend, NW - SE fractures which parallel the Faeroes fjord system, and which might be represented in the detailed survey area by low k (figs. 2.3 and 2.4), could have played a significant role. Hald et al. (1969) concluded that the thick Kakksvik flow in the Faeroes was built up in units produced from individual centres of activity on NW - SE fissures at different times. However, the extent and significance of the NW - SE fractures remains uncertain, both in Iceland and the

Faeroe Islands.

If the trough of low P - velocity volcanic rocks on the Iceland-Faeroes Rise is a true Tertiary equivalent of the Neo-volcanic Zone in Iceland, then there are serious difficulties in the hypothesis of a continuous spreading relation between the two (Bott et al., 1971). The presence of such a feature is indicative of at least one major discontinuity of spreading in the area, after which the axis of activity migrated to the site of present day Iceland. This major discontinuity may have been associated with the migration of the spreading axis in the north, from the east side to the west side of the South Jan Mayen Ridge (Vogt et al., 1970).

At the northern end of the Iceland-Faeroes Rise, the aeromagnetic map (fig. 1.3) shows that the short wavelength magnetic anomalies, except those on the Icelandic shelf area, are associated with an apparent northward continuation to the east of the aseismic South Jan Mayen Ridge. These latitudes, at 64^{o}N and 65^{o}N, have been associated with major E - W transform faults in Iceland (Ward et al., 1969; Sigurdsson, 1970). The whole lateral ridge system, from Greenland to Scotland, is probably constructed on a number of such faults, many of which may have lost their former function.

Generally, the uncertainty in the present interpretations is due to a lack of control and supporting data, and the following investigations are recommended:

a) Detailed gravity, magnetic and seismic measurements in the Greenland-Iceland region.

b) Investigation of the region of junction of Iceland with the Iceland-Faeroes Rise by gravity, seismic reflection

and refraction methods.

c) Investigations of the proposed E - W transform faults east and south-east of Iceland, including a bathymetric feature which crosses the whole area in fig. 1.4 at 63°N, and is approximately of WNW - ESE trend.

d) Investigation of the areal extent of Tertiary igneous activity between western Britain and the Wyville-Thompson Ridge.

e) Theoretical studies on stress and plastic flow conditions at the base of the thickened crust beneath mountain chains, when these are cut obliquely by developing oceans. The Caledonian Front crosses the break in slope at the continental edge on the latitude of the Faeroes in the pre-drift reconstruction of Bott and Watts (1970b).

CHAPTER FIVE

GRAVITY AND MAGNETIC ANOMALIES OF THE SCOTTISH CONTINENTAL SHELF AREA

This chapter deals with data collected by the Durham group during geophysical surveys in 1967, 1968 and 1970. All anomaly profiles described in this chapter have been presented previously by other authors, but they provide further testing of the joint analysis programs with real data in the light of existing interpretations.

5.1 The Faeroes-Shetland Channel

The Faeroes-Shetland Channel is a NE - SW region of deep water, average depth 900-1000 metres, which separates the Hebridean-Shetland continental shelf from the Faeroes 'shelf' area (fig 1.1). On the aeromagnetic map (Avery et al., 1968), the Faeroes-Shetland Channel is characterised by broad magnetic anomalies of general strike direction parallel to the bathymetric trend.

The measured gravity, magnetic and bathymetric profiles shown in fig 5.1 have been presented and discussed by Bott and Watts (1970b). These authors interpreted the regional high Bouguer gravity values over the centre of the Faeroes-Shetland Channel as caused by crustal thinning to 19km, or by about 6km relative to the thickness of the crust beneath the shelf areas on both sides.

An investigation of the relation between gravity and

magnetic anomalies over the Faeroes-Shetland Channel should assist in determining the origin of this feature. If the magnetic anomalies show a significant independence of the local gravity anomalies the interpretation may be that the former reflect changes in intensity of magnetisation only, which are unrelated to lateral density changes; in this case, the Faeroes-Shetland Channel may be of oceanic origin, with a formation due to sea-floor spreading from an axis that ceased activity or migrated soon after its initial development. The crustal thickness (Bott and Watts, 1970b) suggests that if spreading did take place, it was anomalous in character, such as that responsible for the Iceland-Faeroes Rise (Bott et al., 1971). Bidston (1970) made a study of the magnetic anomalies in the Faeroes-Shetland Channel, and concluded that the basement could be compared to that of adjacent continental areas.

In the present study, program TR/MG was used to produce a pseudo-gravity anomaly from the observed magnetic anomaly (fig 5.1). The anomaly profiles of fig 5.1 are not ideal for this purpose as they do not include significant local gravity and magnetic anomalies which are present in the data of the more northerly Durham traverses across the Faeroes-Shetland Channel. Unfortunately, magnetic data from the other traverses were not available, and the present study is rather limited due to the low amplitude of local anomalies on the profiles in fig 5.1

Both types of anomaly are affected by sediment distribution; the short wavelength components in the observed magnetic anomaly are attenuated on the Faeroes 'shelf' as the basaltic basement dips south-east beneath a thickening wedge of sediment from

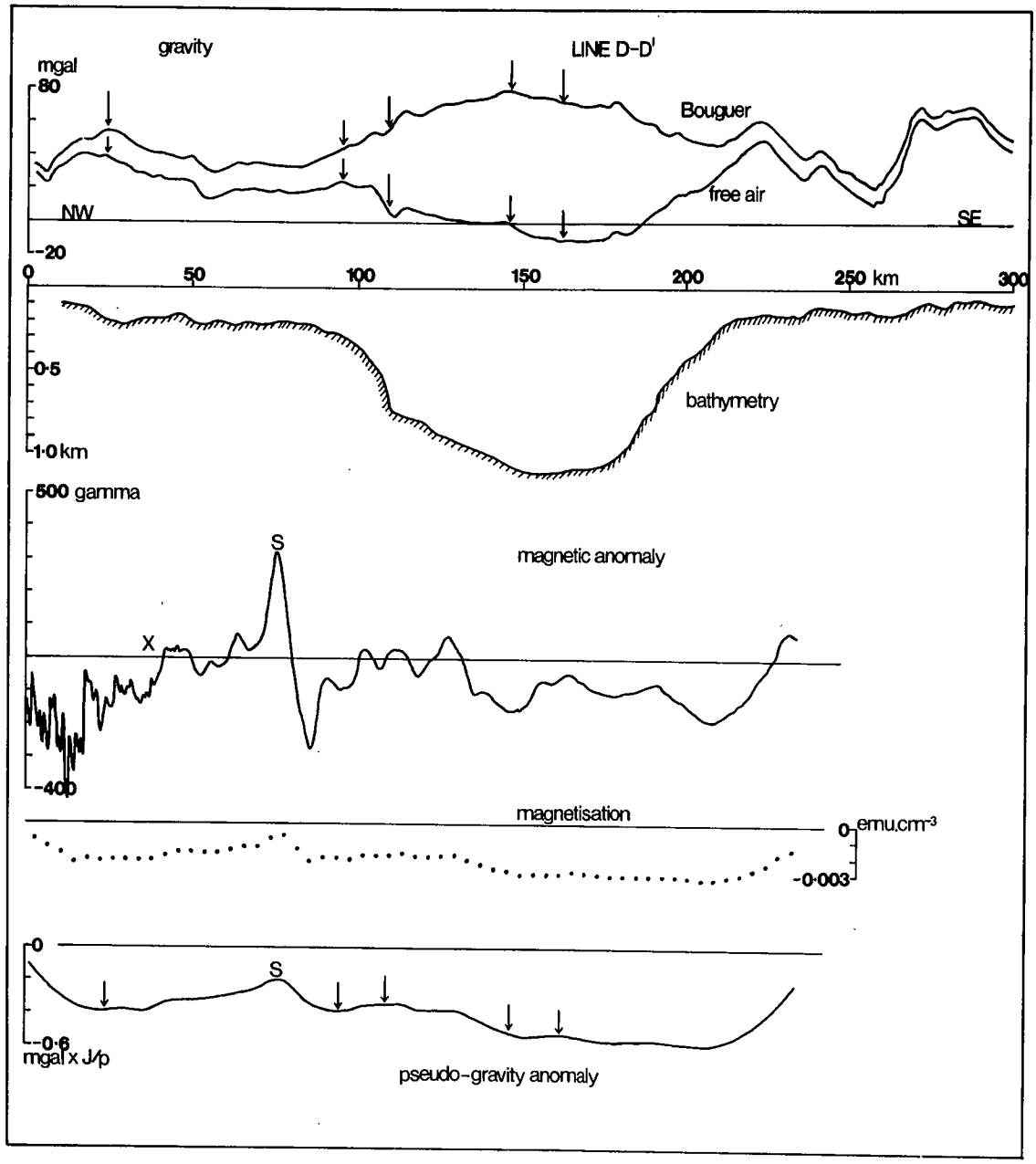

Fig 5.1 Pseudo-gravity transformation of line D-D', Faeroe-Shetland Channel.

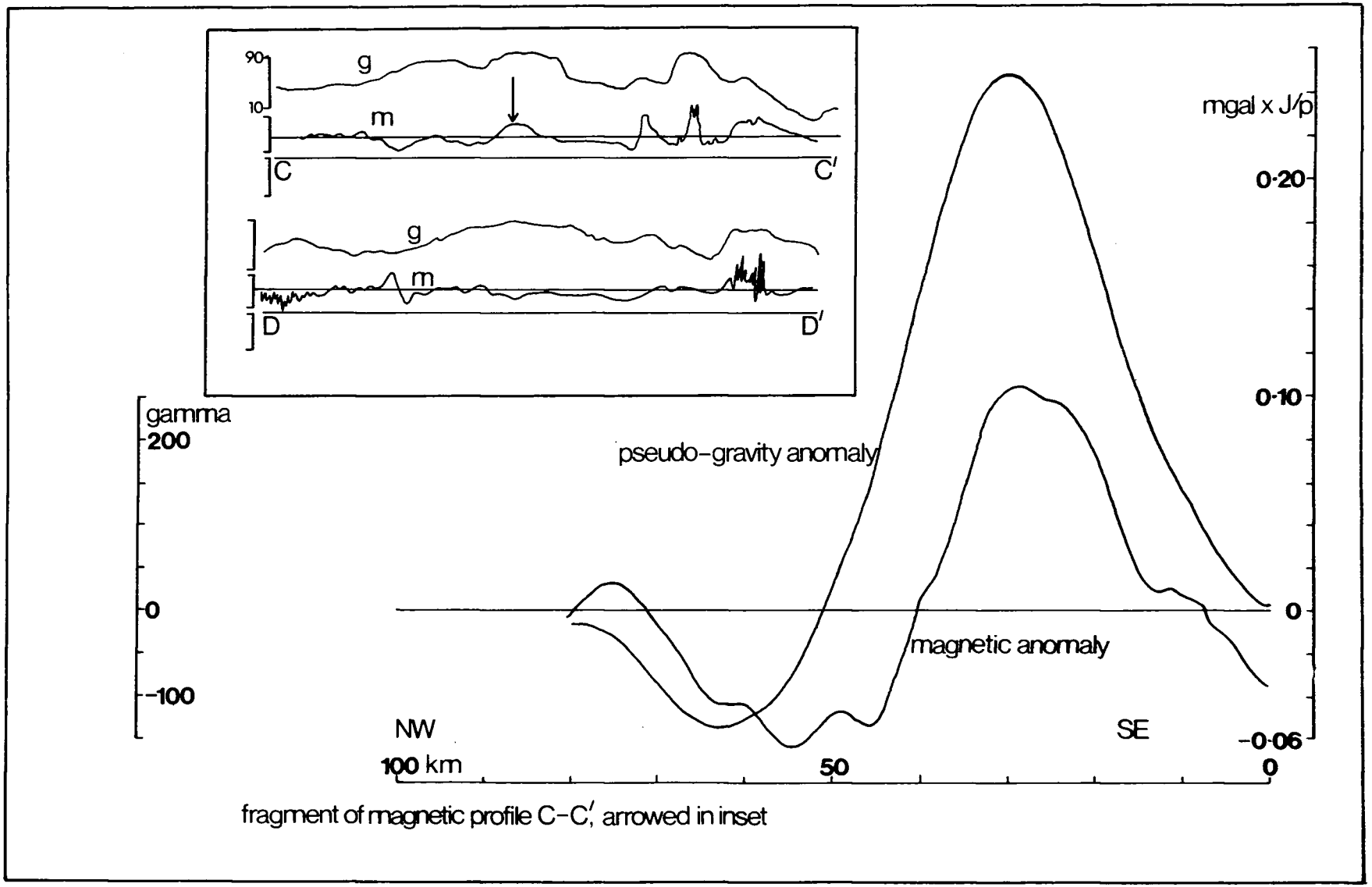

Fig 5.2 Pseudo-gravity transformation of line C-C', Faeroe-Shetland Channel.

point X in fig 5.1 (Bott and Watts, 1970b). Thick sediment is also present on the Hebridean continental slope (Stride et al., 1969). In the centre of the Channel, sediment thickness is uncertain.

As the observed magnetic anomaly is predominantly of negative sign relative to the IGRF, and particularly for the long wavelength components, the unscaled pseudo-gravity anomaly is wholly negative (fig 5.1). Close inspection reveals that local features on the pseudo-gravity profile mirror image similar features on the observed free-air and Bouguer gravity profile; these are indicated by arrow in fig 5.1. Thus, the pseudo-gravity anomaly indicates that topography on a negatively magnetised basement is the major source of magnetic anomalies on this profile across the Faeroes-Shetland Channel, and in this respect, the results here are evidence in support of Bidston (1970).

Magnetic anomaly 'S' (fig 5.1) produces a large pseudo-gravity anomaly, but is not represented on the observed free-air gravity profile, and thus the density contrast associated with this change in magnetisation must be very small. If a small depression of 2-3mgal in the observed free-air gravity field is assumed to be the gravitational expression of magnetic anomaly S, then a minimum value for J/p is -0.1, in contrast to approximately -0.005 for other features on the profile. Magnetic anomaly S may have chronological significance, either as the magnetisation contrast between rock suites of different ages on the inner and outer sections of the Faeroes shelf, or as a small local intrusion in the basement. The evidence here is limited, but in view of the high value J/p, it is

certain that the magnetisation contrast is not associated with a rock type that differs significantly in density from that of the main basement on the Faeroes shelf.

Although full data for other traverses were not available, a fragment from the adjacent profile to the north was obtained. This magnetic data includes one of the prominant local anomalies that are present on three of the five Durham traverses across the Faeroe-Shetland Channel. This anomaly and its pseudo-gravity transformation are shown in fig 5.2 together with a copy of the small scale plot of the whole profile, taken from Watts (1970). Detailed gravity data was not available, but it can be seen that although the pseudo-gravity anomaly is of the same width as the observed local Bouguer anomaly, it does not match the flat-topped shape of the latter. Thus, it seems that gravity and magnetic sources are not strictly coincident for this feature. For an estimated local gravity amplitude of 30 - 40mgal, the J/p ratio value is approximately +0.007, and this positive correlation of density and magnetisation differs from the negative correlation for the more southerly profile (fig 5.1).

The limited evidence from the available data does not permit any firm conclusion, ~~but it is likely that the Faeroes-Shetland Channel is underlain by rocks of several ages~~. A continental or oceanic origin is not resolved.

5.2 The Hebridean-Shetland Shelf gravity high 'A'

The gravity map of the Hebridean-Shetland continental shelf region, presented by Bott and Watts (1970b), shows a large gravity high of NE - SW or NNE - SSW trend, west of the

Shetland Islands, and which meets the 100 fathom bathymetric contour at an angle of 10-15° north of the Shetlands. The anomaly is 40km to 50km wide and was interpreted as caused by the presence of high density Lewisian basement rocks outcropping at the sea floor (Bott and Watts, 1970b), similar in properties to the pyroxene granulites of Scourie on the mainland of north-west Scotland (Watts, 1970).

Gravity and magnetic profiles across this feature, high 'A', are shown in figs 5.3 and 5.4. The magnetic field is particularly active over high 'A' and behaves in a special way; the rapid attenuation of magnetic anomalies away from gravity maxima, particularly on the more northerly traverse (fig 5.4), and the general predominance of short wavelength components indicate that the distribution of magnetisation is confined to the uppermost sections of the body causing the gravity anomaly, or alternatively, that the magnetic anomalies are caused by ~~this~~ thin vertical strips of moderately high intensity or magnetisation within a main structure of lesser magnetisation. In either case, the geological situation is unusual in continental terrain. The thin vertical strip interpretation was adopted for further study as this is convenient for methods based on the linear inverse technique. On both profiles (figs 5.3 and 5.4), there is a subsidiary gravity high to the west of the main high 'A', from which it is separated by low E, one of the postulated shelf sedimentary basins (Bott and Watts, 1970a). Low 'E' has been interpreted as a basin extending to a maximum depth of approximately 5km (Watts, 1970), and this depth was used as the base of the equivalent layer.

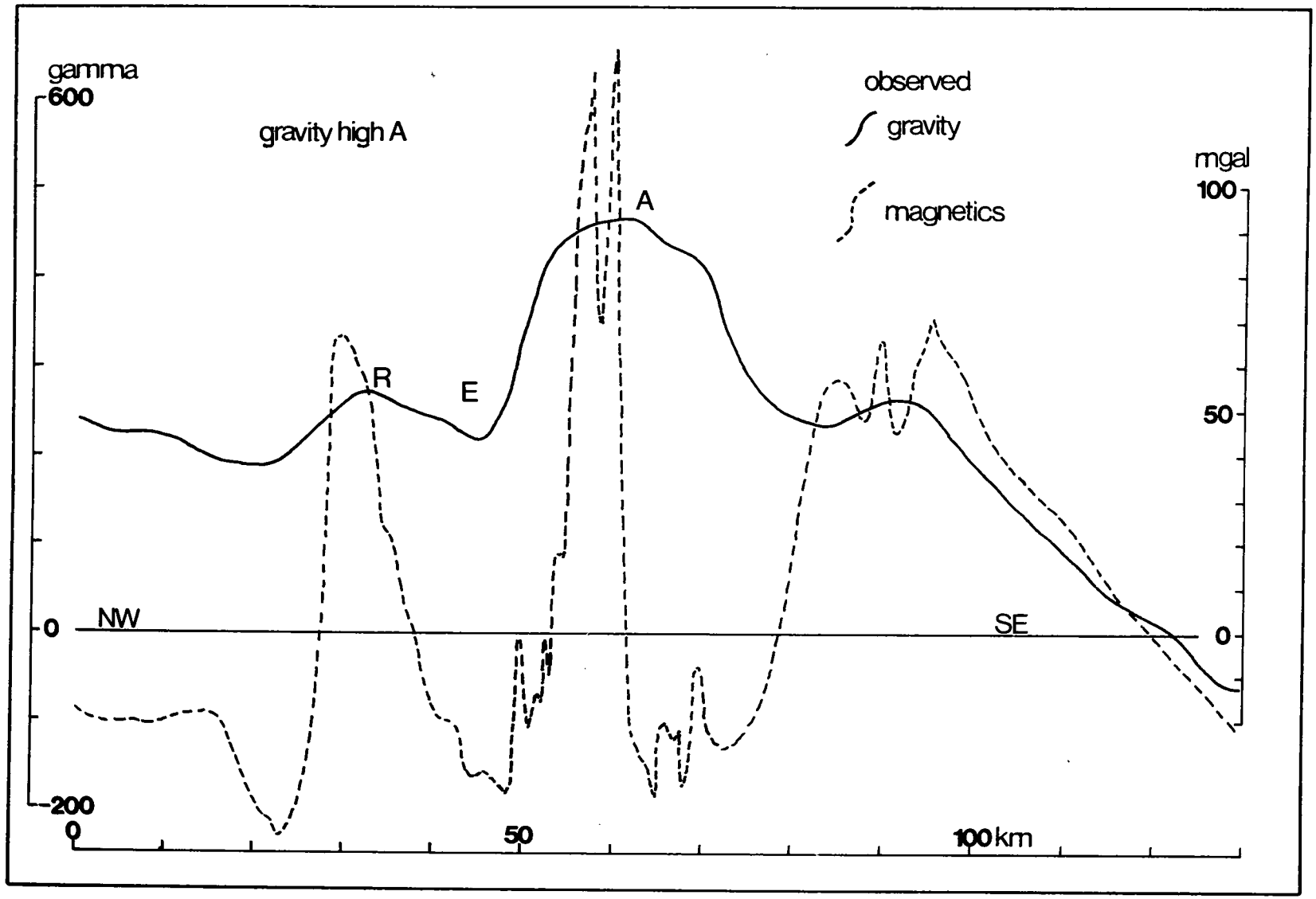

Fig 5.3 Hebridean-Shetland Shelf, part of line C-C'.

Fig. 5.4. Gravity high A.

A: Observed gravity and magnetic anomalies.

B: Density distribution.

C: Distribution of J/p values; values between dashed vertical lines, except those circled, used in fitting a second order polynomial by least squares.

D: J/p polynomial values; topographic component.

E: Values of magnetisation corresponding to polynomial distribution of J/p.

F: Residual distribution of magnetisation, non - topographic component.

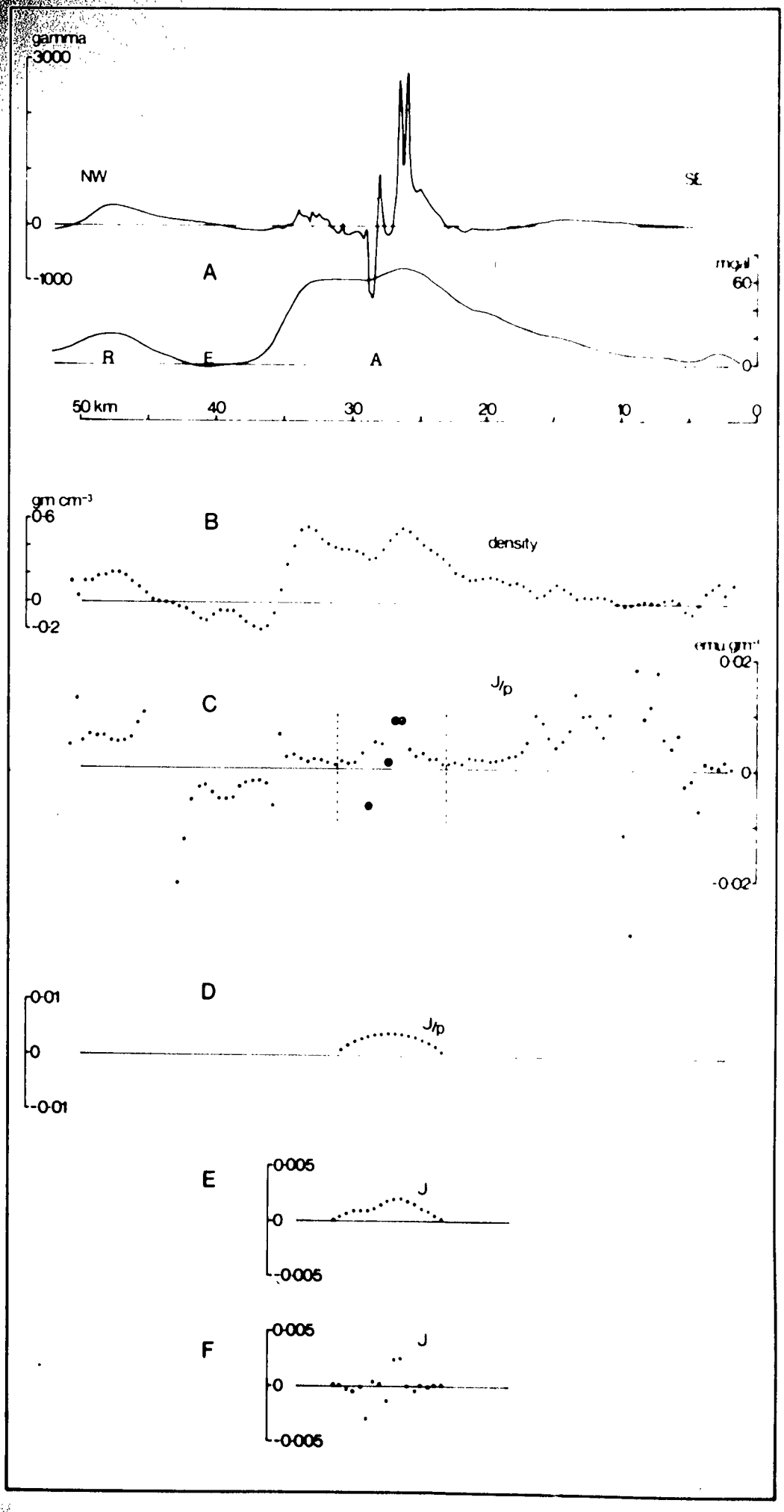
gamma
3000
NW
SE
0
-1000
A
60
R
E
A
50 km
40
30
20
10
0
gm cm⁻³
0·6
B
density
0
-0·2
C
J/p
0·02
0
-0·02
0·01
D
J/p
0
-0·01
E
0·005
J
0
-0·005
F
0·005
J
0
-0·005

Program SBETA was used to obtain the angle of magnetisation from the profiles in fig 5.3, assuming a single value of J/p for the whole structure. An average magnetisation inclination of 80° was obtained in association with an average value of 0.004 for J/p. If the direction of magnetisation is that of true north, then the inclination in this direction is approximately 77°, or close to the 74° inclination of the present earth's field west of Shetland. This angle was used in further computations.

The Bouguer gravity anomaly profile in fig 5.4 is based on a background field that approximately produces only positive anomalies and is assumed to reflect lateral variations in density above the 5km base level of the postulated sedimentary basin beneath low E.

There is considerable oscillation in the J/p values over sections of low anomaly amplitudes (fig 5.4C), but the distribution is relatively stable over high A and the subsidiary gravity high to the west, high R. The J/p ratio value for high A lies in the range 0.001-0.002 for the bulk of the structure, and is approximately 0.005 for high R. Intensities of magnetisation, computed from these values and the associated density values (fig 5.4B), are 0.001cgs for high R, and in the range 0.005 - 0.001cgs for the main part of high A. Thus, high A and high R may be caused by ridges of the same rock type, but at a greater depth beneath the latter anomaly. In the same way, the more highly magnetic sections of high A are associated with positive and negative J/p ratio values of at least 0.008, and the intensity of magnetisation is calculated

at 0.005cgs. Thus, if the high amplitude, short wavelength magnetic anomaly over gravity high A (fig 5.4A) is due to narrow zones of higher intensity of magnetisation, this is approximately five times that of the intensity of the main structure.

An additional estimate of the relative intensities of magnetisation within the structure causing high A was made by an automated method. It was noted in chapter three that the equivalent layer distribution of J/p for simple bodies such as that in figs 3.6 and 3.9 could be approximated quite accurately by the fit of a second order polynomial. In the present case, a polynomial was fitted to the J/p values between the dashed vertical lines in fig 5.4C, but excluding the circled values. The J/p polynomial values are shown in fig 5.4D, and the corresponding magnetisation values are shown in fig 5.4E. If these distributions are assumed to reflect the effects of topography that is not represented in the equivalent layer, then the residual distribution of magnetisation (fig 5.4F) contains the extra intensities which are not related to lateral variations in density. Here, the residual magnetisations are of the order ± 0.003cgs; this is probably a minimum value as the distributions of J/p and p/J tend to flatten over the region of the true body (figs 3.6 and 3.7).

Thus, the sources of short wavelength magnetic anomalies in figs 5.4A are from two to five times as magnetic as the main structure of high A.

A feasible geological explanation of this situation, within the general metamorphic concept for high A, is difficult. A possibility is that the higher magnetisations are associated

with small lenses of basic and ultrabasic ortho-gneiss at a high level in the basement, as have been recognised in north-west Scotland (Phemister, 1960).

5.3 Gravity low 'F', south-west of Shetland.

In July, 1970, as part of a geophysical survey conducted by the Durham group from RRS John Murray, a study was made of an area immediately south-west of the main island of Shetland. Seismic refraction and reflection lines, and gravity and magnetic measurements were made in the region of a NNE - SSW gravity low, low 'F', south of the Walls Peninsula, and west of the Walls Boundary Fault and the Dunrossness Peninsula. The gravity low has been presented previously (Bott and Watts, 1970b), and with interpretation (Browitt, 1971).

West of the N - S Walls Boundary Fault, on the main island of Shetland, granite sheets and diorite intrude a synform of Old Red Sandstone Rocks on the Walls Peninsula, and according to Finlay (1930) the whole Walls Peninsula complex is underlain by granite, grading downwards into gabbro. McQuillin and Brooks (1967) suggest, on the basis of gravity and magnetic data, that the Walls Boundary Fault is a major tear fault.

East of the Walls Boundary Fault, and west of the sub-parallel Whalsey-Clift Sound Dislocation, is a region of schists, migmatites and gneisses, while further south-east on the Dunrossness Peninsula, the predominant rock type is phyllite, with Old Red Sandstone and granite.

Thus, the southern part of Shetland is composed of these

three geological units in N - S or NNE - SSW zones.

The data from a partly reversed seismic refraction line, recorded along the strike of the NNE - SSW gravity low, have been interpreted by Browitt (1971) in terms of a layer of thickness 1.2km, underlain by material with a P-velocity of 5.16km/s. Browitt's interpretation ~~identified~~ identified the upper layer as a basin of Permian and post-Permian sediments, and the lower layer was considered to be consistent with granite containing blocks of Old Red Sandstone, or an extrapolation of the exposed geology of the Walls Peninsula.

The seismic refraction interpretation is similar to that inferred from seismic reflection (fig 5.5B), gravity and magnetic data (fig 5.5), collected on an E - W line perpendicular to the trend of gravity low, between coordinates 59°48'N, 00°57'W and 59°46'N, 02°16'W, and passing about 10km south of Sumburgh Head at its eastern end. The notation on the seismic reflection summary is that of Browitt (1971), and used 'sed' for sections of the record that show continuous sedimentary layering, 'base' for a structureless reflector which presumably represents basement outcrop and 'int' for sections of the record which show intermittent layering within material with basement features. The category 'int' was considered by Browitt to represent blocks of sedimentary strata surrounded by granite. The zone of apparent vertical banding, denoted by 'm' was considered by the same author to be the mylonitised zone of the southward continuation of the Walls Boundary Fault. The density model (fig 5.5D) is also due to Browitt who attributed the subsidiary gravity low in the east to a basin of

Fig. 5.5. South-west Shetland.

A: Observed gravity and magnetic anomalies.

B: Seismic reflection summary (after Browitt, 1971).

C: Bathymetry.

D: Density model, interpretation of the observed gravity anomaly (after Browitt, 1971).

E: Block distribution of density and J/p values within an equivalent layer.

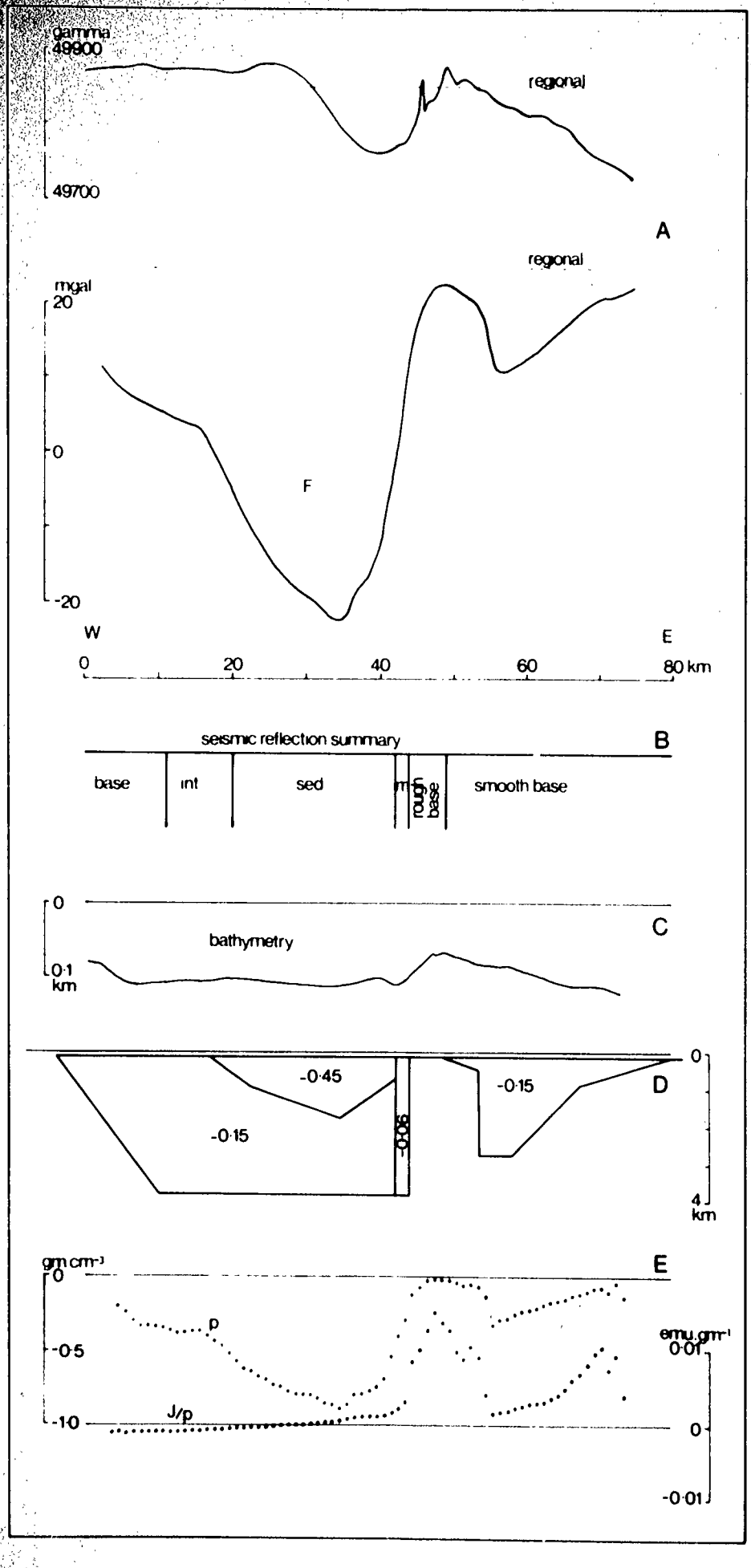
gamma
49900
49700
regional
A
regional
mgal
20
0
-20
F
W
E
0
20
40
60
80 km
seismic reflection summary
B
base
int
sed
rough base
smooth base
0
0·1
km
bathymetry
C
-0·45
-0·15
-0·15
-0·06
D
0
4
km
gm cm⁻³
0
-0·5
-1·0
p
J/p
E
emu gm⁻¹
0·01
0
-0·01

Old Red Sandstone rocks.

Fig 5.5E shows plots of density and J/p within an equivalent layer extending to a depth of 1.5km, or to the depth of the low density basin west of the mylonite zone (fig 5.5D). The character of the J/p plot is significantly different on either side of the mylonitised zone; to the east the J/p distribution varies in the same way as that of density, while to the west, values of J/p remain very low and are independent of density variations. There is no distinction on the J/p plot between seismic reflection 'sed' and 'base' categories west of the mylonite zone. Thus, in the absence of prior interpretations, the conclusion would be reached that the mylonite zone separated two geological areas of fundamentally different basement rocks; the basement to the east might be interpreted as of basic igneous or metamorphic origin, and that to the west as ancient sediments or, as in section 4.1.2, of granitic composition. This is a controlled demonstration of how the J/p and density plots can be used for a semi-quantitative structural interpretation. Values of density depend on the configuration of the equivalent layer, and the general use of J/p values as rock type diagnostic tools depends on sufficient use of the method in areas of good geological control to provide a supply of calibrating values.

REFERENCES

ABRAHAMSEN, N. 1967. Some palaeomagnetic investigations in the Faeroe Islands. Medd. Dansk Geol Foren., 17, 371 - 384.

AL-CHALABI, M. 1970a. Interpretation of two-dimensional magnetic profiles by non-linear optimisation. Boll. Geof. Teo. ed Applic., 12, 3 - 20.

_____ 1970b. The application of non-linear optimisation techniques in geophysics. Unpublished Ph.d. Thesis. University of Durham. 198pp.

ANDERSSEN, R.S. 1969. On the solution of certain overdetermined systems of linear equations that arise in geophysics. J. Geophys. Red., 74, 1045 - 1051.

AVERY, O.E. 1968. An aeromagnetic survey of the
BURTON, G.D. and Norwegian Sea. J. Geophys. Red., 73,
HEIRTZLER, J.R. 4583 - 4600.

BARANOV, V. 1957. A new method for interpretation of aeromagnetic maps; pseudo-gravimetric anomalies. Geophysics, 22, 359 - 383.

BARTELS, J. 1957. Geomagnetic measures for the time-variations of solar corpuscular radiation. I.G.Y. Annals, 4, London: Pergamon Press. 227 - 236.

BATH, M. 1960. Crustal structure of Iceland. J. Geophys. Red. 65, 1793 - 1807.

BIDSTON, B.J. 1970. A geophysical investigation of the Faeroes-Shetland Channel. Unpublished M.Sc dissertation. University of Durham. 22pp.

BOTT, M.H.P. 1967. Solution of the linear inverse problem in magnetic interpretation with application to oceanic magnetic anomalies. Geophys. J.R. astr. Soc. 13, 313 - 323.

_____ 1969a. Durham University Geophysical computer program No. 1. GRAVN.

_____ 1969b. Durham University Geophysical computer program No. 2. MAGN.

_____ 1969c. Computation of the magnetic anomalies caused by two-dimensional bodies. Geophys. J.R. astro. Soc. 18, 251 - 256.

BOTT, M.H.P. BROWITT, C.W.A. and STACEY, A.P. 1971. Crustal structure of the Iceland-Faeroes Rise from seismic refraction and gravity measurements. Mar. Geophys. Res. (in the press).

BOTT, M.H.P. and HUTTON, M.A. 1970a. Limitations on the resolution possible in the direct interpretation of marine magnetic anomalies. Earth Planet. Sci. Lett. 8, 317 - 319.

_____ 1970b. A matrix method for interpreting oceanic magnetic anomalies. Geophys. J.R. astr. Soc. 20, 149 - 157.

BOTT, M.H.P., SMITH, R.A. and STACEY, R.A. 1966. Estimation of the direction of magnetisation of a body causing a magnetic anomaly using a pseudo-gravity transformation. Geophysics 31, 803 - 811.

BOTT, M.H.P. and STACEY, A.P. 1967. Geophysical evidence on the origin of the Faero Bank Channel - II. A gravity and magnetic profile. Deep-sea Res. 14, 7 - 11.

BOTT, M.H.P. and WATTS, A.B. 1970a. Deep sedimentary basins proved in the Shetland-Hebridean Continental Shelf and margin. Nature, Lond. 225, 265 - 268.

_____ 1970b. Deep structure of the continental margin adjacent to the British Isles. Rep. No. 70/14, Inst. Geol. Sci. 93 - 109.

BROWITT, C.W.A. 1971. Seismic refraction experiments between Iceland and Scotland. Unpublished Ph.D. thesis. University of Durham. 128pp.

BULLARD, E.C. EVERETT, J.E. and SMITH, A.G. 1965. The fit of the continents around the Atlantic. Phil. Trans. R. Soc. Lond. 258A, 41 - 51.

BULLARD, E.C. and MASON, R.G. 1963. The magnetic field over oceans. M.N. Hill (ed) The Sea. Interscience, New York, 3, 175 - 217.

CANN, J.R. and VINE, F.J. 1966. An area on the crest of the Carlsberg Ridge: petrology and magnetic survey. Phil. Trans. R. Soc. Lond. 259A, 198 - 217.

CARMICHAEL, I.S.E. 1964. The petrology of Thingmuli, a Tertiary volcano in eastern Iceland. J. Petrol. 5, 435 - 460.

CHAYES, F. 1964. Petrographic distinction between Cenozoic volcanics in and around open oceans. J. Geophys. Res. 69, 1573.

DAMPNEY, C.N.G. 1969. The equivalent source technique. Geophysics 34, 39 - 53.

DICKSON, G.O. PITMAN, W.C. and HEIRTZLER, J.R. 1968. Magnetic anomalies in the South Atlantic and ocean floor spreading. J. Geophys. Res. 73, 2087 - 2100.

DOBINSON, A. 1970. 1. The development of a marine seismic recording system. 2. A magnetic survey of the Faeroe Bank. Unpublished Ph.D. thesis. University of Durham. 127pp.

EINARSSON, Tr. 1954. A survey of gravity in Iceland. Soc. Sci. Islandica 30, 1 - 22.

_____ 1965. Remarks on crustal structure in Iceland. Geophys. J.R. astr. Soc. 10, 283 - 288.

EMILIA, D.A. and BÖDVARSSON, G. 1969. Numerical methods in the direct interpretation of marine magnetic anomalies. Earth Planet. Sci. Lett. 7, 194 - 200.

EWING, J. and EWING, M. 1967. Sediment distribution on the mid-ocean ridges with respect to spreading of the sea-floor. Science 156, 1590 - 1592.

FINLAY, T.M. 1930. The Old Red Sandstone of Shetland Part 2. North-Western Area. Trans. R. Soc. Edin. 56, 671 - 694.

GARLAND, G.D. 1951. Combined analysis of gravity and magnetic anomalies. Geophysics 16, 51 - 62.

GAY, S.P. 1963. Standard curves for interpretation of magnetic anomalies over long tabular bodies. Geophysics 28, 161 - 200.

GODBY, E.A. HOOD, P.J. and BOWER, M.E. 1968. Aeromagnetic profiles across the Reykjanes Ridge southwest of Iceland. J. Geophys. Res. 73, 7637 - 7649.

GUDMUNDSSON, G. 1967, Magnetic anomalies. Soc. Sci. Islandica 38, 97 - 105.

HALD, N. NOE-NYGAARD, A. and WAAGSTEIN, R. 1969. On extrusive forms in plateau basalts. 2. The Klakksvik Flow, Faeroe Islands. Medd. Dansk Geol. Foren. 19, 2 - 7.

HAMILTON, N. and RICHARDSON, A. 1971. Magnetisation of a seamount in the Tyrrhenian Sea. Paper SG - 11, First European Earth and Planetary Physics Colloquium. Reading, 30th March - 2nd April, 1971.

HEIRTZLER, J.R. DICKSON, G.O. HERRON, E.M. PITMAN, W.C. and LE PICHON, X. 1968. Marine magnetic anomalies; geomagnetic field reversals and motions of the ocean floor and continents. J. Geophysics. Res. 73, 2119 - 2136.

HEIRTZLER, J.R. and HAYES, D.E. 1967. Magnetic boundaries in the North Atlantic Ocean. Science 1957, 185 - 187.

HEIRTZLER, J.R. LE PICHON, X and BARON, J.G. 1966. Magnetic anomalies over the Reykjanes Ridge. Deep-Sea Res. 13, 427 - 443.

HUTTON, M.A. 1970. Interpretation of oceanic magnetic anomalies using a linear inverse technique. Unpublished Ph.D. thesis. University of Durham. 139pp.

I.A.G.A. 1969. International geomagnetic reference field. 1965 - O. J. Geophys. Res. 74, 4407 - 4408.

I.B.M, 1968. System/360, scientific subroutine package (360-CM-03X). Version III. Programmers manual. New York. I.B.M.

JOHNSON, G.L. 1967. North Atlantic fracture zones near 53°N. Earth Planet. Sci. Lett. 2, 445 - 448.

JOHNSON, G.L. and HEEZEN, B.C. 1967. The morphology and evolution of the Norwegian-Greenland Sea. Deep-Sea Res. 14, 755 - 771.

JOHNSON, G.L. and TANNER, B. 1971. Geophysical observations on the Iceland-Faeroe Ridge. Jokull (in the press).

JONES, E.J.W., EWING, M. EWING, J.I. and EITTREIM, SL. 1970. Influences of Norwegian Sea overflow water on sedimentation in the northern Atlantic and Labrador Sea. J. Geophys. Res. 75, 1655 - 1680.

JONES, J.G. 1966. Intraglacial volcanoes of S.W. Iceland and their significance in the interpretation of the form of marine basalt volcanoes. Nature, Lond. 212, 586 - 588.

_____ 1970. The intraglacial volcanoes of the Laugarvatn region, southwest Iceland. II. J. Geol. 78, 127 - 140.

KANASEWICH, E.R. and AGARWAL, R.G. 1970. Analysis of combined gravity and magnetic fields in the wave number domain. J. Geophys. Res. 75, 5702 - 5712.

KJARTANSSON, G. 1967. Volcanic forms at the sea bottom. Soc. Sci. Islandica 38, 53 - 64.

KRISTJANSSON, L. 1970. Palaeomagnetism and magnetic surveys in Iceland. Earth Planet. Sci. Lett. 8, 101 - 108.

_____ 1971. Studies of drill cores from an unusual magnetic high in S.W.Iceland. Paper 01 - 19. First European Earth and Planetary Physics Colloguium. Reading, 30th March - 2nd April, 1971.

LAUGHTON, A.S. 1971. South Labrador Sea and the evolution of the North Atlantic. Nature, Lond. 232, 612 - 617.

LAVING, G.J. 1971. Ph.D. thesis. University of Durham. (In preparation).

LEHMANN, H.J. 1971. A control of two-dimensional magnetic interpretation by three-dimensional model body anomalies. Geoph. Prosp. 19, 133 - 155.

LE PICHON, X. and HEIRTZLER, J.R. 1968. Magnetic anomalies in the Indian Ocean and sea-floor spreading. J. Geophys. Res. 73, 3661 - 3697.

LE PICHON, X. HOUTZ, R.E. DRAKE, C.L. and NAFE, J.E. 1965. Crustal structure of the mid-ocean ridges. 1. Seismic refraction measurements. J. Geophys. Res. 70 319 - 339.

LE PICHON, X. HYNDMAN, R. and PAUTOT, G. 1971. A geophysical study of the opening of the Labrador Sea. J. Geophys. Res. 76, 4724.

LUNDBAK, A. 1956. Combined analysis of gravimetric and magnetic anomalies and some palaeomagnetic results. Geoph. Prosp. 4, 226 - 235.

LUYENDYK, B.P. 1969. Origin of short wavelength magnetic lineations observed near the ocean bottom. J. Geophys. Res. 74, 4869 - 4881.

MASON, R.G. 1958. A magnetic survey off the west coast of the United States between Latitudes 32° and 36°N, longitudes 121° and 128°W. Geophys. J.R. astr. Soc. 1, 320 - 329.

MASON, R.G. and RAFF, A.D. 1961. Magnetic survey off the west coast of North America, 32°N latitude to 42°N latitude. Bull. Geol. Soc. Am. 72, 1259 - 1266.

McQUILLIN, R. and BROOKS, M. 1967. Geophysical surveys in the Shetland Islands. Geophysical paper No. 2, H.M.S.O., 22pp.

MENARD, H.W. and ATWATER, T. 1968. Changes in direction in sea-floor spreading. Nature, Lond. 219, 463 - 467.

MOORBATH, S. SIGURDSSON, H. and GOODWIN, R. 1968. K-Ar ages of the oldest exposed rocks in Iceland. Earth Planet. Sci. Lett. 4, 197 - 205.

MOORBATH, S. and WELKE, H. 1969a. Isotopic evidence for the continental affinity of Rockall Bank, North Atlantic. Earth Planet. Sci Lett. 5, 211 - 216.

_____ 1969b. Lead isotope studies on igneous rocks from the Isle of Skye, Northwest Scotland. Earth Planet, Sci. Lett. 5, 217 - 230.

NOE-NYGAARD, A. AND RASMUSSEN, J. 1968. Petrology of a 3,000 metre sequence of basaltic lavas in the Faeroe Islands. Lithos 1, 286 - 304.

PALMASON, G. 1965. Seismic refraction measurements of the basalt lavas of the Faeroe Islands. Tectonophysics 2, 475 - 482.

_____ 1967. Upper crustal structure in Iceland. Soc. Sci. Islandica 38, 67 - 78.

_____ 1970. Crustal structure in Iceland from explosion seismology. Science Institute, University of Iceland, 239pp.

PETERS, L.J. 1949. The direct approach to magnetic interpretation and its practical application. Geophysics 14, 290 - 320.

PHEMISTER, J. 1960. British Regional Geology. Scotland: The Northern Highlands. Third Edition. H.M.S.O., 104pp.

PITMAN, W.C. and HEIRTZLER, J.R. 1966. Magnetic anomalies over the Pacific-Antarctic Ridge. Science 154, 1164 - 1171.

PITMAN, W.C. HERRON, E.M. and HEIRTZLER, J.R. 1968. Magnetic anomalies in the Pacific and sea-floor spreading. J. Geophys. Res. 73, 2069 - 2085.

RASMUSSEN, J. and NOE-NYGAARD, A. 1966. New data on the geological age of the Faeroes. Nature, Lond. 209, 1229 - 1230.

_____ 1970. Geology of the Faeroe Islands. Geological Survey of Denmark I, Series No. 25. Copenhagen, 1970.

RICHEY, J.E. 1961. British Regional Geology. Scotland: The Tertiary Volcanic Districts. Third Edition, revised by A.G. MacGregor and F.W. Anderson, H.M.S.O. 120pp.

ROW, A. 1962. Ambiguity in geophysical interpretation. Geophysics 27, 90 - 99.

SAEMUNDSSON, K. 1967. An outline of the structure of S.W. Iceland. Soc. Sci. Islandica 38, 151 - 159.

_____ 1971. Relation between geological structure of Iceland and some geophysical anomalies. Paper 01 - 16. First European Earth and Planetary Physics Colloquium. Reading, 30th March - 2nd April, 1971.

SARGINSON, M.K. 1969. Forschungsschiff "Meteor". Fahrt nr. 14. Berichts under die wissenschaftlichen Arbeiten. Geology. Deutsches Hydrographisches Institut, Hamburg.

SERSON, P.H. HANNAFORD, W.L. and HAINES, G.V. 1968. Magnetic anomalies over Iceland. Science 162. 355 - 356.

SIGURGEIRSSON, Th. 1966. Geophysical measurements in Surtsey carried out during the year of 1965. In: Surtsey Research Progress Report, II, 181 - 185.

SIGURDSSON, H. 1967. The Icelandic basalt plateau and the question of sial. A review. Soc. Sci. Islandica 38, 32 - 46.

_____ 1970. Structural origin and plate tectonics of the Snaefellsnes volcanic zone, western Iceland. Earth Planet. Sci. Lett. 10, 129 - 135.

SKEELS, D.C. 1947. Ambiguity in gravity interpretation. Geophysics 12, 43 - 56.

SPECTOR, A. and GRANT, F.S. 1970. Statistical models for interpreting aeromagnetic data. Geophysics 35, 293 - 302.

STRIDE, A.H. CURRAY, J.R. MOOR, D.G. and BELDERSON, R.H. 1969. Marine geology of the Atlantic continental margin of Europe. Phil. Trans. R. Soc. Lond. 264A, 31 - 75.

TALWANI, M., WINDISCH, C.C. and LANGSETH, M.G. 1971. Reykjanes Ridge Crest: a detailed geophysical study, J. Geophys. Res. 76 473 - 517.

TANNER, J.G. 1967. An automated method of gravity interpretation. Geophys. J.R. astr. Soc. 13, 339 - 347

TARLING, D.H. and GALE, N.H. 1968. Isotopic dating and palaeomagnetic polarity in the Faeroe Islands. Nature, Lond. 218, 1043 - 1044.

TRYGGVASON, E. 1962. Crustal structure of the Iceland region from dispersion of surface waves. Bull. Seism. Soc. Am. 52, 359 - 388.

VINE, F.G. and MATTHEWS, D.H. 1963. Magnetic anomalies over oceanic ridges. Nature. Lond. 199, 947 - 949.

VOGT, P.R., AVERY, O.E. MORGAN, W.J. and HIGGS, R.H. 1969. Morphology, magnetic anomalies and evolution of the Northeast Atlantic and Labrador Sea. Part III - Evolution Trans. Amer. Geophys. Un. 50, 184 (abstract)

VOGT, P.R. OSTENSO, N.A. and JOHNSON, G.L. 1970. Magnetic and bathymetric data bearing on sea-floor spreading north of Iceland. J. Geophys. Res. 75, 903 - 920.

WALKER, G.P.L. 1963. The Breiddalur central volcano, eastern Iceland. Quart. J. Geol. Soc. Lond. 119, 29 - 63.

WARD, P.L. PALMASON, G. and DRAKE, C.L. 1969. Microearthquake survey and the Mid-Atlantic Ridge in Iceland. J. Geophys. Res. 74, 665 - 684.

WATTS, A.B. 1970. Geophysical investigations in the Faeroes to Scotland region, Northeast Atlantic. Unpublished Ph.D. thesis. University of Durham.

WILSON, C.D.V. 1970. The use of the Poisson relationship for separating the anomalies due to neighbouring bodies and for recognising inhomogeneities and structural deformation. Boll. Geof. Teo. ed Applic. 12, 158 - 182.

WILSON, J.T. 1963. Hypothesis of Earth's behaviour. Nature, Lond. 198, 925 - 929.

_____ 1965. A new class of faults and their bearing on continental drift. Nature, Lond. 207, 343 - 347.

APPENDIX A

The computer program SPHEL (standard form).

A marine magnetic data reduction program, written in PL/1 for use on the N.U.M.A.C. IBM 360/67.

Input and declaration structure.

L, M are the dimensions of arrays used in the least-squares derivation of a regional field, and are of unspecified at this stage.

BEGIN; L,M are assigned as dimensions of arrays in succeeding declarations. At this stage L, M are still unspecified but are designated as controlled (CTL), and are fixed at a later stage.

LA: counting navigation fixes as read in.

LI: reading in navigation cards with:

- A(I) time as an integer day and a decimal fraction of a day
- SLA(I) latitude.
- SLO(I) longitude.
- WR(I) IGRF at fix (SLA(I), SLO(I)).

L2: total number of navigation fixes.

L3: magnetic data block headings with:

- TD1, TD2 day number at start and finish of block.
- TH1, TH2 time in hours at start and finish of block.
- TMi, TM2 time in minutes at start and finish of block.

L4: reading in digitised total field magnetic data.

- GAM measured total field.

FRAC decimal fraction of time duration of block.

General procedure.

L5, L6, L7, L8, L9: assignment of geographical coordinates and a value of the IGRF to each digitised station point. The assignment is effected by linear interpolation to correlate the start and finish of each data block with the navigation fix record, thence each digitised point is supplied with coordinates by use of the decimal fraction of the total duration of the block. The IGRF is subtracted from each measured total field value to produce a residual anomaly.

L10: total number of digitised anomaly values. Variables L and M are fixed, and the values are allocated to dimension the dependent arrays. Calculation of distances and azimuths of anomaly stations by a calll to subroutine DISAZ.

L11: setting up arrays for least-squares subroutine. Calculation of a second set of residual anomalies by fitting a line to the measured total field data reduced to a base level of 50,000 gamma. Line fitted by a call to the least-squares subroutine LLSQ. Printout of data and punched card output.

Subroutine DISAZ.

DISAZ was written by Hutton (1970) and computes the distance and azimuth on the spheroid between two given points of latitude and longitude. The procedure is based on the formulation given in the Admiralty Manual of Hydrographic Surveying, Vol. 1,

1965. The figure of the earth is taken from that given by Hayford (1910).

Subroutine LLSQ (IBM, 1968).

A standard subroutine of the IBM. Scientific Subroutine Package to obtain the solution of linear least-squares problems. In general form, a solution is required to the system of equations defined by

$$A * X = B$$

where A is a real m by n matrix of rank $n(m \geq n)$, B is a system of column vectors of dimension m, and X is a system of column vectors of dimension m to be determined such that the sum of residuals

$$\| Bj - A * Xj \| = \sqrt{\sum_{i=1}^{m} r^2_i} \qquad \text{is a minimum;}$$

where j = 1.....K, the number of column vectors.

The general call to LLSQ is,

CALL LLSQ (A,B,M,N,L,X,IPIV,EPS,IER,AUX)

A (M xN) coefficient matrix, destroyed in LLSQ.

B (M x L) right hand side matrix, destroyed in LLSQ.

X (N x L) solution matrix.

IPIV integer output vector of dimension N of which the last N - K elements denote the useless columns of matrix A, where K is the rank of matrix A when found to be less than N but greater than 0.

EPS input parameter specifying relative tolerance for

determination of the rank of matrix A.

IER error parameter.

AUX auxiliary storage array of dimension (2 * N, L).

LLSQ is a Fortran subroutine, and its use in a PL/1 calling program necessitates that rows and columns of arrays be interchanged to suit the Fortran storage mode.

```
PHEL: PROC OPTIONS(MAIN);

T
      SPHEL: PROC OPTIONS(MAIN);
      DCL (L,M) FIXED BIN(31);
      BEGIN;
      DCL (I,J,K,N,COUNT,IQ,IW) FIXED BIN(31);
      DCL (TD1,TD2,TH1,TH2,TM1,TM2) FLOAT;
      DCL (RD,XX,F1,F2,FRAC,T1,T2,TT,DLA1,DLO1,FR1,RLA1,RLO1,DLA2,DLO2,
      FR2,RLA2,RLC2,LAT,LON,EPS,IER,GAM) FLOAT;
      DCL (A,SLO,SLA)(100) FLOAT;
      DCL (GLA,GLO,AUA)(1200) FLOAT;
      DCL (ANOM,AC,X)(L) CTL;
      DCL (AR(M,L),S(M),XPIV(M),AUX(2*M)) CTL;
      DCL (DWR1,DWR2,RWR1,RWR2,WWR) FLOAT;
      DCL GRR(1200) FLOAT;
      DCL WR(100);
      DCL IN FIXED BIN(31);
      DCL NAME CHAR(25);
      DCL (ANY) FILE OUTPUT STREAM;
      GET LIST(NAME);
      I=0;
   LA:I=I+1;
   L1:GET LIST(A(I),SLA(I),SLO(I),WR(I));
      IF A(I)<0 THEN GO TO L2;
      ELSE DO;
      PUT SKIP LIST(A(I),SLA(I),SLO(I),WR(I));
      GO TO LA; END;
   L2:I=I-1;
      N=I;
      COUNT=0;
      PUT PAGE EDIT('LAT','LONG','GAMMA')(SKIP(2),X(17),A,X(6),A,X(6),
      A);
      PUT SKIP(2);
   L3:GET LIST(TD1,TH1,TM1,TD2,TH2,TM2,XF1,XF2);
      IF TD1=0 THEN GO TO L10;
      ELSE GO TO L4;
   L4:GET LIST(GAM,FRAC);
      IF GAM=0 & ((FRAC-0.000001)<0) THEN GO TO L3;
      ELSE DO;
      COUNT=COUNT+1;
      T1=TD1+TH1/24+TM1/1440;
      T2=TD2+TH2/24+TM2/1440;
      TT=T1+((T2-T1)*FRAC);
      J=0;
      K=0;
   L5:J=J+1;
      IF ABS(A(J)-T1)<0.0001 THEN GO TO L6;
      ELSE IF A(J)<T1 THEN GO TO L5;
      ELSE IF T1<A(J) THEN DO;
      DLA1=SLA(J)-SLA(J-1);
      DLO1=SLO(J)-SLO(J-1);
      DWR1=WR(J)-WR(J-1);
      FR1=(T1-A(J-1))/(A(J)-A(J-1));
      RLA1=SLA(J-1)+(FR1*DLA1);
      RLO1=SLO(J-1)+(FR1*DLO1);
      RWR1=WR(J-1)+(FR1*DWR1);
      GO TO L7;
      END;
```

```
HEL: PROC OPTIONS(MAIN);



      ELSE PUT EDIT('ERROR IN SORTING ARRAY')(SKIP,X(2),A(24));
   L6:RLA1=SLA(J);
      RLO1=SLO(J);
      RWR1=WR(J);
   L7:K=K+1;
      IF ABS(A(K)-T2)<0.0001 THEN GO TO L8;
      ELSE IF A(K)<T2 THEN GO TO L7;
      ELSE IF T2<A(K) THEN DO;
      DLA2=SLA(K)-SLA(K-1);
      DLO2=SLO(K)-SLO(K-1);
      DWR2=WR(K)-WR(K-1);
      FR2=(T2-A(K-1))/(A(K)-A(K-1));
      RLA2=SLA(K-1)+(FR2*DLA2);
      RLO2=SLO(K-1)+(FR2*DLO2);
      RWR2=WR(K-1)+(FR2*DWR2);
      GO TO L9;
      END;
      ELSE PUT EDIT('ERROR IN SORTING ARRAY')(SKIP,X(2),A(24));
   L8:RLA2=SLA(K);
      RLO2=SLO(K);
      RWR2=WR(K);
   L9:LAT=RLA1+(FRAC*(RLA2-RLA1));
      LON=RLO1+(FRAC*(RLO2-RLO1));
      WWR=RWR1+(FRAC*(RWR2-RWR1));
      AUA(COUNT)=GAM;
      GLA(COUNT)=LAT;
      GLO(COUNT)=LON;
      GRR(COUNT)=GAM-WWR;
      PUT SKIP EDIT(LAT,LON,GAM,WWR)(X(13),F(10,5),F(10,5),F(7,0),X(3),
      F(7,0));
      GO TO L4;
      END;
  L10:L=COUNT;  M=2;
      ALLOCATE ANOM,X;
      ALLOCATE AR,S,XPIV,AUX,AC;
      DO I=1 TO L;
      ANOM(I)=AUA(I);
      END;
      PUT PAGE LIST(NAME);
      PUT SKIP(1);
      /* CALCULATION OF DISTANCES BETWEEN STATIONS */
      PUT SKIP(2);
      X=0;
      DO I=2 TO L;  XX=0;
      CALL DISAZ(GLA(I-1),GLO(I-1),GLA(I),GLO(I),XX);
      X(I)=X(I-1)+XX;
      END;
      PUT SKIP(2);
      /* EVALUATION OF LEAST-SQUARES REGIONAL */
  L11:AR(1,*)=1;
      DO I=1 TO L;
      AR(2,I)=X(I);
      AC(I)=ANOM(I);
      END;
```

```
HEL: PROC OPTIONS(MAIN);



      IQ=2;  IW=1;  EPS=0.0001;
      PUT LIST(TIME)SKIP;
      CALL LLSQ(AR(1,1),ANOM(1),L,IQ,IW,S(1),XPIV(1),EPS,IER,AUX(1));
      PUT LIST(TIME)SKIP;
      PUT LIST(IER)SKIP;
      PUT LIST(S)SKIP;
      PUT EDIT('DISTANCE','TOTAL INTENSITY','REGIONAL','RESIDUAL')(SKIP(
      2),X(7),A,X(3),A,X(3),A,X(4),A);
      DO I=1 TO L;
      RD=S(1)+S(2)*X(I);
      RESID=AC(I)-RD;
      PUT EDIT(I,X(I),AC(I),RD,RESID,GRR(I))(SKIP,F(4),X(3),F(8,3),
      X(7),F(7,1),X(8),F(7,1),X(4),F(7,1),X(4),F(7,1));
      PUT FILE (ANY) EDIT(I,X(I),GLA(I),GLO(I),AC(I),RESID,GRR(I))
      (X(2),F(4),F(8,3),F(14,6),F(14,6),F(9),F(9),F(9));
      END;
      PUT EDIT('REGIONAL AT FALSE ORIGIN=',S(1))(SKIP(2),A,F(8,1));
      PUT EDIT('REGIONAL GRADIENT ALONG X AXIS=',S(2))(SKIP,A,F(11,6));
      GO TO FIN;
      DISAZ: PROCEDURE(ALAT,ALON,BLAT,BLON,DIS);
      DECLARE (AB,ALAT,ALON,AZ,BLAT,BLON,CA,CHORD,DIS,GB,P,R,SA,UA,UB,V,
      XA,XB,YA,YB,ZA,ZB);
      UA=ATAN(0.996633*TAND(ALAT));
      UB=ATAN(0.996633*TAND(BLAT));
      GB=((0.99327733*TAN(UB))/TAN(UA))+((0.00672267)*COS(UA))/COS(UB);
      AZ=ATAND((SIND(ALON-BLON)),(SIND(ALAT)*(COSD(ALON-BLON)-(GB))));
      PUT LIST(AZ);
      SA=SIND(AZ);
      CA=COSD(AZ);
      XA=(6378388)*COS(UA)*COSD(ALON);
      YA=(6378388)*COS(UA)*SIND(ALON);
      ZA=(6356912)*SIN(UA);
      XB=(6378388)*COS(UB)*COSD(BLON);
      YB=(6378388)*COS(UB)*SIND(BLON);
      ZB=(6356912)*SIN(UB);
      CHORD=SQRT((XA-XB)**2+(YA-YB)**2+(ZA-ZB)**2);
      AB=SIND((ALAT+BLAT)/2);
      V=(6378388)/SQRT(1-(0.00672267)*(AB**2));
      P=((V)*(1-0.0672267))/(1-(0.00672267)*(AB**2));
      R=((P)*(V))/(P*(SA**2)+V*(CA**2));
      DIS=(((CHORD)**3)/(24*((R)**2)))+(3*((CHORD)**5))/(640*((R)**4));
      DIS=DIS+CHORD;  DIS=DIS/1000;  END DISAZ;
FIN:END;  /* END-BEGIN */
      END SPHEL;
```

APPENDIX B

The computer program TR/GM.

TR/GM transforms a gravity anomaly into a magnetic anomaly. The program is written in PL/1 for use on the N.U.M.A.C. IBM 360/67.

Input and declaration structure.

N number of station points.

M number of block edges, number of blocks minus one.

BEGIN; arrays are dimensioned by the input values of N and M

LI: HM, HE, ALFM, ALFE are the dips and azimuths of body magnetisation and the earth's filed; measured in degrees. Inclinations are measured positive from the horizontal, with increasing distance, downwards; azimuths are measured positive from the strike of the body, assumed perpendicular to the anomaly profile, towards the positive x - axis (anticlockwise).

These angles are then transformed into the plane of the anomaly profile to produce the compositie angle B.

L2:

ZS anomaly station height, sea level = 0.

SDAT -1; regularly spaced stations.

SDAT 1; irregularly spaced stations.

XO anomaly station origin.

XSTEP anomaly station spacing.

XS calculated or input array of anomaly station distances.

DG array of observed gravity anomaly values.

L3:

ZT depth to upper surface of equivalent layer.

ZB depth to lower surface of equivalent layer.

BXO origin on x - axis of equivalent layer.

BSTEP width of block elements of equivalent layer.

BX calculated array of x - coordinates for block edges.

IJF = -1; program terminates after effecting transformation gravity to magnetics.

IJF = 1; separation of magnetic anomaly components by use of a least-squares scaling equation.

Calculation of gravity kernel matrix elements.

L4:

GK gravity kernel matrix of dimension (M - 1, N), initially set to zero.

The calculation is based on program GRAVN (Bott, 1969a) in the modified form due to Laving (1971).

Solving for a block distribution of density.

L5;

EPS, IW, IQ tolerance parameter and dimensions of arrays in LLSQ (see appendix A).

A density distribution is obtained by a call to LLSQ.

SS solution array of length (M - 1), containing values for the density distribution.

Calculation of the pseudo - magnetic anomaly.

L6: The set of statements to calculate the magnetic kernel matrix elements are those of Hutton (1970), but modified for the simpler situation of an equivalent layer divided into block elements of rectangular cross - section.

GK magnetic kernel matrix of dimension (M - 1, N).

The elements of the kernel matrix are then multiplied by the elements or array SS and summed to produce a pseudo - magnetic anomaly at each station point for a conventional value of J/ρ 1.

Separation of magnetic anomaly components.

L7: IJF = 1: proceed with separation.

DB array of observed magnetic anomalies.

RR array of ratios observed/pseudo - magnetic anomalies.

A line is now fitted to the values of RR with distance by a call to the least-squares subroutine LLSQ.

SR array of length (2) containing intercept and gradient of scaling operation.

RAT scaling parameter at each station point.

CALC value of the scaled pseudo - magnetic anomaly at each point.

RES value of residual anomaly, observed minus scaled pseudo - magnetic anomaly at each point.

```
1: PROC OPTIONS(MAIN);


    TR/GM: PROC OPTIONS(MAIN);
    /* A.INGLES,1970, GRAVITY-MAGNETICS TRANSFORM.                    */
    DCL (I,J,K,L,M,N) FIXED BIN(31);
    DCL NAME CHAR(25);
    GET LIST (NAME);
    PUT PAGE LIST (NAME);
    GET LIST(N,M);
    BEGIN;
    DCL ((XS,DG)(N),GK(M-1,N),(X,Z)(5),(S,C)(4),BX(M),
    (SS,IPIV)(M-1),AUX(2*(M-1))) FLOAT;
    DCL ((DB,RR)(N),B(2,N),(SR,IPAV)(2),AAX(4)) FLOAT;
    DCL (RAT,CALC,RES) FLOAT;
    DCL (HM,HE,ALFM,ALFE,A,HHE,HHM,BETA,CBETA,SBETA,SDAT,XO,XSTEP,ZS,
    ZT,ZB,BXO,BSTEP,GOH,X1,Z1,R1,FI1,X2,Z2,R2,FI2,H,W,CA,CB,SX,XSA,
    XSB,ZSA,CC,EE,RA,RB,TA,TB,TT,TBA,THETA,MAG) FLOAT;
    DCL KK FIXED BIN(31);
    DCL EPS FLOAT;
    DCL(IER,IQ,IW) FIXED BIN(31);
    DCL IJF FIXED BIN(31);
    DCL LINK LABEL;
L1: GET LIST(HM,HE,ALFM,ALFE);
    A=SQRT((((COSD(HE))**2)*((SIND(ALFE))**2)+(SIND(HE))**2)*(((COSD(
    HM))**2)*((SIND(ALFM))**2)+(SIND(HM))**2));
    HHE=ATAND(SIND(HE),COSD(HE)*SIND(ALFE));
    HHM=ATAND(SIND(HM),COSD(HM)*SIND(ALFM));
    BETA=(HHE+HHM);
    CBETA=200000.0*COSD(BETA);
    SBETA=200000.0*SIND(BETA);
    PUT EDIT('BETA=',BETA)(SKIP(2),A(5),F(7,2));
    /*                                                               */
L2: GET LIST(ZS,SDAT);
    IF SDAT<0 THEN DO;
    GET LIST(XO,XSTEP);
    DO I=1 TO N;
    XS(I)=XO+(I-1)*XSTEP;
    GET LIST(DG(I));
    PUT LIST(DG(I));
    END;
    END;
    ELSE DO I=1 TO N;
    GET LIST (XS(I),DG(I));
    END;
L3: GET LIST(ZT,ZB,BXO,BSTEP);
    DO J=1 TO M;
    BX(J)=BXO+(J-1)*BSTEP;
    END;
    PUT EDIT('BLOCK-LAYER REPRESENTATION')(SKIP(2),X(10),A);
    PUT SKIP(1);
    DO J=1 TO M;
    PUT SKIP EDIT(J,BX(J),ZT,ZB)(X(5),F(5,0),F(10,4),F(10,4),F(10,4));
    END;
    GET LIST(IJF);
    /*                                                               */
    /* COMPUTATION OF GRAVITY KERNEL MATRIX                          */
L4: GK=C;
    GOH=0.013328;
```

```
GM: PROC OPTIONS(MAIN);


      DO J=1 TO M-1;
      X(1),X(2),X(5)=BX(J);
      X(3),X(4)=BX(J+1);
      Z(1),Z(4),Z(5)=ZT-ZS;
      Z(2),Z(3)=ZB-ZS;
      DO I=1 TO N;
      X1=X(1)-XS(I);
      Z1=Z(1);
      R1=X1**2+Z1**2;
      FI1=(1.5708-ATAN(X1,Z1));
      DO K=1 TO 4;
      X2=X(K+1)-XS(I);
      Z2=Z(K+1);
      R2=X2**2+Z2**2;
      FI2=(1.5708-ATAN(X2,Z2));
      H=SQRT((X(K)-X(K+1))**2+(Z(K+1)-Z(K))**2);
      S(K)=(Z(K+1)-Z(K))/H;
      C(K)=(X(K)-X(K+1))/H;
      W=0.5*S(K)*LOG(R2/R1)+C(K)*(FI2-FI1);
      GK(J,I)=GK(J,I)+GOH*(Z2*FI2-Z1*FI1-W*(X1*S(K)+Z1*C(K)));
      GK(J,I)=GK(J,I)*1000.0;
      X1=X2;  Z1=Z2;  R1=R2;  FI1=FI2;
      END;              /* K-LOOP */
      END;              /* I-LOOP */
      END;              /* J-LOOP */
      /*                                                          */
      /* SOLUTION OF EQUATIONS BY LLSQ                            */
  L5: EPS=0.0001;
      IW=M-1;
      IQ=1;
      PUT SKIP EDIT('IN-LLSQ')(X(20),A(7));
      CALL LLSQ(GK(1,1),DG(1),N,IW,IQ,SS(1),IPIV(1),EPS,IER,AUX(1));
      PUT LIST (IER)SKIP(2);
      PUT LIST(SS);
      PUT SKIP(2);
      GK=0;
      /*                                                          */
      /* CALCULATION POINT FOR POINT OF MAGNETIC ANOMALY          */
      PUT EDIT ('NO','DISTANCE','GAMMA')(X(5),A(2),X(10),A(8),X(10),
      A(5));
  L6: CA=0.5*SBETA;
      CB=-CBETA;
      DO I=1 TO N;
      SX=XS(I);
      DO J=1 TO M-1;
      XSA=BX(J)-SX;
      XSB=BX(J+1)-SX;
      ZSA=ZT-ZS;
      LINK=PT1;
      GO TO DK;
 PT1:DD=EE;
      ZSA=ZB-ZS;
      LINK=PT2;
  DK:RA=XSA*XSA+ZSA*ZSA;
```

```
/GM: PROC OPTIONS(MAIN);



      RB=XSB*XSB+ZSA*ZSA;
      TA=XSA/ZSA;
      TB=XSB/ZSA;
      TT=1+TA*TB;
      TBA=TB-TA;
      THETA=ATAN(TBA,TT);
      EE=THETA*CB+LOG(RB/RA)*CA;
      GO TO LINK;
  PT2:GK(J,I)=(DD-EE)*A;
      END;
      END;
      /* PRODUCT OF KERNEL ELEMENTS AND SOLUTIONS OF MLSQ                */
      DO I=1 TO N;
      MAG=0;
      DO J=1 TO M-1;
      MAG=MAG+(GK(J,I)*SS(J));
      END;
      DG(I)=MAG;
      PUT EDIT (I,XS(I),DG(I))(SKIP(1),X(4),F(3,0),X(10),F(8,4),X(5),
      F(11,4));
      END;
      DO I=1 TO N;
   L7: IF IJF<0 THEN GO TO LE;
      ELSE DO I=1 TO N;
      GET LIST(DB(I));
      END;
      DO I=1 TO N;
      RR(I)=DB(I)/DG(I);
      END;
      PUT SKIP(2);
      PUT LIST(RR);
      PUT SKIP(2);
      IQ=2;
      IW=1;
      EPS=0.0001;
      I=1;
      DO J=1 TO N;
      B(I,J)=1.0;
      B(I+1,J)=XS(J);
      END;
      DO J=1 TO 6;
      RR(J)=0.0250;
      END;
      DO J=N-5 TO N;
      RR(J)=0.0250;
      END;
      PUT SKIP(2);
      DO J=1 TO N;
      PUT LIST(RR(J));
      END;
      PUT SKIP(1);
      KK=N;
      PUT LIST(TIME)SKIP;
      CALL LLSQ(B(1,1),RR(1),KK,IQ,IW,SR(1),IPAV(1),EPS,IER,AAX(1));
```

```
GM: PROC OPTIONS(MAIN);


      PUT SKIP LIST(IER);
      PUT EDIT('SCALING PARAMETERS,AT ORIGIN AND ALONG PROFILE')(SKIP(2)
      ,X(10),A);
      PUT SKIP LIST(SR);
      PUT EDIT('NO','X','OBS','CALC','RESID')(SKIP(2),X(5),A,X(10),
      A,X(10),A,X(10),A,X(10),A);
      DO I=1 TO N;
      RAT=SR(1)+SR(2)*XS(I);
      CALC=RAT*DG(I);
      RES=DB(I)-CALC;
      /** RES DUE TO MAGNETIC VARIATIONS ONLY **/
      PUT SKIP EDIT(I,XS(I),DB(I),CALC,RES)(X(2),F(5,0),X(3),F(8,3),
      X(6),F(7,1),X(7),F(7,1),X(8),F(7,1));
      END;
   LE: END;    /* END BEGIN */
      END TR/GM;
```

APPENDIX C

The computer program TR/MG.

This program performs the transformation magnetic anomaly to gravity anomaly and is written in PL/1 for use on the N.U.M.A.C. IBM 360/67.

The procedure is essentially that of TR/GM in reverse.

L4:

S array of length (M - 1) containing values for block distribution of magnetisation.

L5: DA array of length (N) containing unscaled pseudo - gravity anomalies.

```
MG£ PROC OPTIONS(MAIN)£


    TR/MG£ PROC OPTIONS(MAIN)£
    /* A.INGLES,1970, MAGNETICS TO GRAVITY TRANSFORM                    */
    DCL (I,J,K,L,M,N) FIXED BIN(31)£
    DCL NAME CHAR(25)£
    GET LIST(NAME)£
    PUT PAGE LIST(NAME)£
    GET LIST(N,M)£
    BEGIN£
    DCL ((XS,DA)(N),GK(M-1,N),(X,Z)(5),(SS,CC)(4),BX(M)) FLOAT£
    DCL DB(N) FLOAT£
    DCL (HM,HE,ALFM,ALFE,A,HHE,HHM,BETA,CBETA,SBETA,SDAT,XO,XSTEP,ZS,
    ZT,ZB,BXO,BSTEP,GOH,X1,Z1,R1,FI1,X2,Z2,R2,FI2,H,W,CA,CB,SX,XSA,
    XSB,ZSA,DD,EE,RA,RB,TA,TB,TT,TBA,THETA,MGAL,EPS) FLOAT£
    DCL (IER,IQ,IW) FIXED BIN(31)£
    DCL (AUX(2*(M-1)),(S,IPIV)(M-1)) FLOAT£
    DCL IN FIXED BIN(31)£
    DCL LINK LABEL£
    /**************                                    **************/
L1£GET LIST(HM,HE,ALFM,ALFE)£
    A=SQRT((((COSD(HE))**2)*((SIND(ALFE))**2)+(SIND(HE))**2)*(((COSD(
    HM))**2)*((SIND(ALFM))**2)+(SIND(HM))**2))£
    HHE=ATAND(SIND(HE),COSD(HE)*SIND(ALFE))£
    HHM=ATAND(SIND(HM),COSD(HM)*SIND(ALFM))£
    BETA=(HHE+HHM)£
    CBETA=200000.0*COSD(BETA)£
    SBETA=200000.0*SIND(BETA)£
    PUT EDIT('BETA=',BETA)(SKIP(2),A(5),F(7,2))£
L2£GET LIST(ZS,SDAT)£
    IF SDAT£0 THEN DO£
    GET LIST(XO,XSTEP)£
    DO I=1 TO N£
    XS(I)=XO+(I-1)*XSTEP£
    GET LIST(DA(I))£
    DB(I)=DA(I)£
    END£
    END£
    ELSE DO I=1 TO N£
    GET LIST(XS(I),DA(I))£
    END£
L3£GET LIST(ZT,ZB,BXO,BSTEP)£
    DO J=1 TO M£
    BX(J)=BXO+(J-1)*BSTEP£
    END£
    PUT EDIT('BLOCK-LAYER REPRESENTATION')(SKIP(2),X(10),A)£
    DO J=1 TO M£
    PUT SKIP EDIT(J,BX(J),ZT,ZB)(X(5),F(5,0),F(10,4),F(10,4),F(10,4))£
    END£
    /**************                                    **************/
    /* CALCULATION OF MAGNETIC KERNEL MATRIX                          */
    GK=0£
    CA=0.5*SBETA£
    CB=-CBETA£
    DO I=1 TO N£
    SX=XS(I)£
    DO J=1 TO M-1£
    XSA=BX(J)-SX£
```

```
/MG£ PROC OPTIONS(MAIN)£


      XSB=BX(J+1)-SX£
      ZSA=ZT-ZS£
      LINK=PT1£
      GO TO DK£
   PT1£DD=EE£
      ZSA=ZB-ZS£
      LINK=PT2£
    DK£RA=XSA*XSA+ZSA*ZSA£
      RB=XSB*XSB+ZSA*ZSA£
      TA=XSA/ZSA£
      TB=XSB/ZSA£
      TT=1+TA*TB£
      TBA=TB-TA£
      THETA=ATAN(TBA,TT)£
      EE=THETA*CB+LOG(RB/RA)*CA£
      GO TO LINK£
   PT2£GK(J,I)=(DD-EE)*A£
      END£
      ENC£
      /**************                                    **************/
      /* SOLUTION BY LEAST SQUARES                                    */
      EPS=0.0001£
      IW=M-1£
      IQ=1£  PUT SKIP(2)£ PUT LIST('IN-LLSQ')£ PUT SKIP(2)£
      CALL LLSQ(GK(1,1),DA(1),N,IW,IQ,S(1),IPIV(1),EPS,IER,AUX(1))£
      PUT LIST(IER)£
      PUT SKIP(2)£
      IF IER£=0 THEN BEGIN£
      S=0£
      PUT LIST('SSP FAILED')£
      PUT SKIP(1)£
      END£
      PUT SKIP(1)£
    L4£ DO J=1 TO M-1£
      PUT LIST(S(J))£
      END£
      PUT SKIP(1)£
      /**************                                    **************/
      /* CALCULATION OF GRAVITY ANOMALY,POINT FOR POINT               */
      GK=0£
      CA=0£
      GOH=0.013328£
      DO J=1 TO M-1£
      X(1),X(2),X(5)=BX(J)£
      X(3),X(4)=BX(J+1)£
      Z(1),Z(4),Z(5)=ZT-ZS£
      Z(2),Z(3)=ZB-ZS£
      DO I=1 TO N£
      X1=X(1)-XS(I)£
      Z1=Z(1)£
      R1=X1**2+Z1**2£
      FI1=(1.5708-ATAN(X1,Z1))£
      DO K=1 TO 4£
      X2=X(K+1)-XS(I)£
```

```
R/MG£ PROC OPTIONS(MAIN)£

T

      Z2=Z(K+1)£
      R2=X2**2+Z2**2£
      FI2=(1.5708-ATAN(X2,Z2))£
      H=SQRT((X(K)-X(K+1))**2+(Z(K+1)-Z(K))**2)£
      SS(K)=(Z(K+1)-Z(K))/H£
      CC(K)=(X(K)-X(K+1))/H£
      W=0.5*SS(K)*LOG(R2/R1)+CC(K)*(FI2-FI1)£
      GK(J,I)=GK(J,I)+GOH*(Z2*FI2-Z1*FI1-W*(X1*SS(K)+Z1*CC(K)))£
      X1=X2£  Z1=Z2£  R1=R2£  FI1=FI2£
      END£              /* K-LCOP */
      END£              /* I-LCOP */
      END£              /* J-LCOP */
      PUT EDIT('NO','DISTANCE','MGALS')(X(5),A(2),X(10),A(8),X(10),A(5))
      £
      DO I=1 TO N£
      MGAL=0£
   L5£ DO J=1 TO M-1£
      MGAL=MGAL+(GK(J,I)*S(J))£
      END£
      DA(I)=MGAL*1000.0£
      END£
      DO I=1 TO N£
      PUT EDIT(I,XS(I),DA(I),DB(I))(SKIP(1),X(4),F(3,0),X(10),F(8,4),
      X(5),F(10,4),X(5),F(10,2))£
      END£
   LE£ END£  /* END BEGIN */
      END TR/MG£
```

APPENDIX D

The computer program JG/RAT.

This program computes a distribution of values for the ratio J/p directly from the observed gravity and magnetic anomalies. The program is written in PL/1 for use on the N.U.M.A.C. IBM 360/67.

Input and the first part of the program are essentially the same as for TR/GM.

L5: S1 array of length (M - 1) containing values for a block distribution of density.

L6: read in observed magnetic anomaly values.

L7: product of magnetic kernal matrix elements with elements of array S1.

L8: derivation of a distribution of values for J/p by a call to least-squares subroutine LLSQ.

S2 array of length (M - 1) containing values for the block distribution of J/p.

```
G/RAT: PROC OPTIONS(MAIN);


      JG/RAT: PROC OPTIONS(MAIN);
      /*************                                          *************/
      DCL NAME CHAR(25);
      DCL (I,J,K,L,M,N) FIXED BIN(31);
      GET LIST(NAME);
      PUT PAGE LIST (NAME);
      GET LIST(N,M);
      BEGIN;
      DCL ((XS,DA)(N),GK(M-1,N),(X,Z)(5),(SS,CC)(4),BX(M),(S1,S2)(M-1),
      AUX(2*(M-1)),IPIV(M-1)) FLOAT;
      DCL (HM,HE,ALFM,ALFE,A,HHE,HHM,BETA,CBETA,SBETA,SDAT,XO,XSTEP,ZS,
      ZT,ZB,BXO,BSTEP,GOH,X1,Z1,R1,FI1,X2,Z2,R2,FI2,H,W,CA,CB,SX,XSA,XSB
      ,ZSA,DD,EE,RA,RB,TA,TB,TT,TBA,THETA,MAG,EPS) FLOAT;
      DCL (IER,IQ,IW) FIXED BIN(31);
      DCL MM FIXED BIN(31);
      DCL LINK LABEL;
      /*************                                          *************/
   L1:GET LIST(HM,HE,ALFM,ALFE);
      A=SQRT((((COSD(HE))**2)*((SIND(ALFE))**2)+(SIND(HE))**2)*(((COSD(
      HM))**2)*((SIND(ALFM))**2)+(SIND(HM))**2));
      HHE=ATAND(SIND(HE),COSD(HE)*SIND(ALFE));
      HHM=ATAND(SIND(HM),COSD(HM)*SIND(ALFM));
      BETA=(HHE+HHM);
      CBETA=200000.0*COSD(BETA);
      SBETA=200000.0*SIND(BETA);
      PUT EDIT('BETA=',BETA)(SKIP(2),A(5),F(7,2));
   L2:GET LIST(ZS,SDAT);
      IF SDAT<0 THEN DO;
      GET LIST(XO,XSTEP);
      DO I=1 TO N;
      XS(I)=XO+(I-1)*XSTEP;
      GET LIST(DA(I));
      END;
      END;
      ELSE DO I=1 TO N;
      GET LIST(XS(I),DA(I));
      END;
   L3:GET LIST(ZT,ZB,BXO,BSTEP);
      DO J=1 TO M;
      BX(J)=BXO+(J-1)*BSTEP;
      END;
      PUT EDIT('INITIAL FIELD VALUES')(SKIP(2),X(10),A(20));
      DO I=1 TO N;
      PUT SKIP EDIT(I,XS(I),DA(I))(X(10),F(5,0),F(10,4),X(5),F(10,2));
      END;
      PUT EDIT('BLOCK-LAYER REPRESENTATION')(SKIP(2),X(10),A);
      DO J=1 TO M;
      PUT SKIP EDIT(J,BX(J),ZT,ZB)(X(10),F(5,0),F(10,4),F(10,4),F(10,4))
      ;
      END;
      /*************                                          *************/
      /* COMPUTATION OF FIRST KERNEL MATRIX                                */
      GOH=0.013328;
      GK=0;
      DO J=1 TO M-1;
      X(1),X(2),X(5)=BX(J);
```

```
/RAT: PROC OPTIONS(MAIN);


      X(3),X(4)=BX(J+1);
      Z(1),Z(4),Z(5)=ZT-ZS;
      Z(2),Z(3)=ZB-ZS;
      DO I=1 TO N;
      X1=X(1)-XS(I);
      Z1=Z(1);
      R1=X1**2+Z1**2;
      FI1=(1.5708-ATAN(X1,Z1));
      DO K=1 TO 4;
      X2=X(K+1)-XS(I);
      Z2=Z(K+1);
      R2=X2**2+Z2**2;
      FI2=(1.5708-ATAN(X2,Z2));
      H=SQRT((X(K)-X(K+1))**2+(Z(K+1)-Z(K))**2);
      SS(K)=(Z(K+1)-Z(K))/H;
      CC(K)=(X(K)-X(K+1))/H;
      W=0.5*SS(K)*LOG(R2/R1)+CC(K)*(FI2-FI1);
      GK(J,I)=GK(J,I)+GOH*(Z2*FI2-Z1*FI1-W*(X1*SS(K)+Z1*CC(K)));
      GK(J,I)=GK(J,I)*1000.0;
      X1=X2;  Z1=Z2;  R1=R2;  FI1=FI2;
      END;          /* K-LCOP */
      END;          /* I-LCOP */
      END;          /* J-LOOP */
      PUT SKIP(1);
      /*************                                          *************/
      /* SOLUTION BY LEAST SQUARES                                        */
      EPS=0.0001;
      IW=M-1;
      IQ=1;
      PUT SKIP EDIT('IN-LLSQ')(X(10),A);
      CALL LLSQ(GK(1,1),DA(1),N,IW,IQ,S1(1),IPIV(1),EPS,IER,AUX(1));
      PUT SKIP LIST(IER);
      IF IER¬=0 THEN DO;
      PUT EDIT('SSP FAILED')(SKIP(1),A);
      GO TO LE;  END;
      ELSE DO;
      PUT EDIT('SOLUTIONS OF DENSITY DISTRIBUTION')(SKIP(2),X(10),A);
      PUT SKIP(1);
      PUT LIST(S1);
      END;
      /*************                                          *************/
      /* CALCULATION OF SECOND KERNEL MATRIX                              */
      GK=0;
      DA=0;
      DO I=N BY -1 TO 1;
      GET LIST(DA(I));
      GK(J,I)=GK(J,I)*S1(J);
      CA=0.5*SBETA;
      CB=-CBETA;
      DO I=1 TO N;
      SX=XS(I);
      DO J=1 TO M-1;
      XSA=BX(J)-SX;
      XSB=BX(J+1)-SX;
```

```
G/RAT: PROC OPTIONS(MAIN);

T

      ZSA=ZT-ZS;
      LINK=PT1;
      GO TO DK;
PT1:  DD=EE;
      ZSA=ZB-ZS;
      LINK=PT2;
 DK:  RA=XSA*XSA+ZSA*ZSA;
      RB=XSB*XSB+ZSA*ZSA;
      TA=XSA/ZSA;
      TB=XSB/ZSA;
      TT=1+TA*TB;
      TBA=TB-TA;
      THETA=ATAN(TBA,TT);
      EE=THETA*CB+LOG(RB/RA)*CA;
      GO TO LINK;
PT2:  GK(J,I)=(DD-EE)*A;
      END;
      END;
      PUT SKIP(1);
      DO J=1 TO M-1;
      DO I=1 TO N;
      GK(J,I)=GK(J,I)*S1(J)*0.001;
      END;
      END;
      /**************                                          **************/
      /* SOLUTION OF J-RHO RATIO BY LLSQ                                    */
      PUT EDIT('IN LLSQ')(SKIP(2),X(10),A);
      CALL LLSQ(GK(1,1),DA(1),N,Iw,IQ,S2(1),IPIV(1),EPS,IER,AUX(1));
      PUT SKIP LIST(IER);
      IF IER¬=0 THEN DO;
      PUT EDIT('SSP FAILED')(SKIP(1),A);
      GO TO LE;  END;
      ELSE DO;
      PUT EDIT('DISTRIBUTION OF J/RHO')(SKIP(2),X(10),A);
      DO J=1 TO M-1;
      PUT EDIT(J,S2(J))(SKIP(1),X(10),F(5,0),X(5),F(14,6));
      END;
      END;
 LE:  END;          /* END-BEGIN */
      END JG/RAT;
```

APPENDIX E

The computer program SBETA.

This program solves for the composite angle B (Chapter three, equation (1)) and thereby calculates an angle of magnetisation for the whole profile which lies in the plane of the profile. The program is written in PL/1 for use on the N.U.M.A.C. IBM 360/67.

Input to SBETA is essentially that to TR/GM except that angles HM, ALFM are omitted.

L5: S1 array of length (M - 1) containing values for the block distribution of desnity.

L6: MK a magnetic kernel matrix of dimension (2,N) which corresponds to the (N x 2) matrix K_B of equations (18) and (19) in Chapter three.

L7: DA array of length (N) containing observed magnetic anomaly values.

L8: S2 array of length (2) containing the values hcos B and hsin B, where h is the ratio J/p.

```
BETA:PROC OPTIONS(MAIN);  /* A.INGLES,1970  */

T
      SBETA:PROC OPTIONS(MAIN);  /* A.INGLES,1970  */
      DCL (N,M,L) FIXED BIN(31);
      DCL NAME CHAR(25);
      GET LIST(NAME);
      PUT PAGE LIST(NAME);
      GET LIST(N,M);
      L=2;
      BEGIN;
      DCL ((XS,DA)(N),BX(M+1),GK(M,N),MK(L,N),(S1,IPIV)(M),(S2,IPAV)(L),
      AUX(2*M),AAX(2*L),(X,Z)(5),(SS,CC)(4)) FLOAT;
      DCL (ZS,SDAT,XO,XSTEP,BXO,BSTEP,ZT,ZB,HE,ALFE,HHE,HHM,X1,Z1,R1,FI1
      ,X2,Z2,R2,FI2,H,W,GCH,EPS,SM1,SM2,CA,CB,CD1,CD2,EE1,EE2,TA,TB,TT,
      TBA,THETA) FLOAT;
      DCL (I,J,K,IW,IQ,IER) FIXED BIN(31);
      DCL MM FIXED BIN(31);
      DCL LINK LABEL;
      /*************  DERIVATION OF SINGLE VALUE OF BETA  *************/
   L1: GET LIST(HE,ALFE);
   L2: GET LIST(ZS,SDAT);
      IF SDAT<0 THEN DO;
   L3: GET LIST(XO,XSTEP);
      DO I=1 TO N;
      XS(I)=XO+(I-1)*XSTEP;
      GET LIST(DA(I));
      END; END;
      ELSE DO I=1 TO N;
      GET LIST(XS(I),DA(I));
      END;
   L4: GET LIST(BXO,BSTEP,ZT,ZB);
      DO J=1 TO M+1;
      BX(J)=BXO+(J-1)*BSTEP;
      END;
      PUT EDIT('INITIAL FIELD VALUES')(SKIP(2),X(10),A);
      DO I=1 TO N;
      PUT SKIP EDIT(I,XS(I),DA(I))(X(10),F(5,0),F(10,4),X(5),F(10,2));
      END;
      PUT EDIT('BLOCK-LAYER REPRESENTATION')(SKIP(2),X(10),A);
      DO J=1 TO M+1;
      PUT SKIP EDIT(J,BX(J),ZT,ZB)(X(10),F(5,0),F(10,4),F(10,4),F(10,4))
      ;
      END;
      /*************   GRAVITY MATRIX                    *************/
      GK=C;
      GOH=0.013328;
      DO J=1 TO M;
      X(1),X(2),X(5)=BX(J);
      X(3),X(4)=BX(J+1);
      Z(1),Z(4),Z(5)=ZT-ZS;
      Z(2),Z(3)=ZB-ZS;
      DO I=1 TO N;
      X1=X(1)-XS(I);
      Z1=Z(1);
      R1=X1**2+Z1**2;
      FI1=(1.5708-ATAN(X1,Z1));
      DO K=1 TO 4;
      X2=X(K+1)-XS(I);
```

```
TA:PROC OPTIONS(MAIN);  /* A.INGLES,1970  */



      Z2=Z(K+1);
      R2=X2**2+Z2**2;
      FI2=(1.5708-ATAN(X2,Z2));
      H=SQRT((X(K)-X(K+1))**2+(Z(K+1)-Z(K))**2);
      SS(K)=(Z(K+1)-Z(K))/H;
      CC(K)=(X(K)-X(K+1))/H;
      W=0.5*SS(K)*LOG(R2/R1)+CC(K)*(FI2-FI1);
      GK(J,I)=GK(J,I)+1000.0*GCH*(Z2*FI2-Z1*FI1-W*(X1*SS(K)+Z1*CC(K)));
      X1=X2;  Z1=Z2;  R1=R2;  FI1=FI2;
      END;  END;  END;
      /*************  SOLUTION OF DENSITY DISTRIBUTION    *************/
      EPS=0.0001;
      IW=M;
      IQ=1;
      PUT SKIP EDIT('IN-LLSQ')(X(10),A);
      CALL LLSQ(GK(1,1),DA(1),N,IW,IQ,S1(1),IPIV(1),EPS,IER,AUX(1));
      PUT SKIP LIST(IER);
      PUT SKIP EDIT('SOLUTION OF DENSITY DISTRIBUTION')(X(10),A);
      PUT SKIP(1);
   L5: PUT LIST(S1);
      PUT SKIP(1);
      /************* MAGNETIC MATRIX                          *************/
      CA=1CC0CC.0;
      CB=-200000.0;
      MK=0;
      DO I=1 TO N;  SM1=0;  SM2=0;
      DO J=1 TO M;
      X1=BX(J)-XS(I);
      X2=BX(J+1)-XS(I);
      Z1=ZT-ZS;
      LINK=PT1;
      GO TO DK;
  PT1:DD1=EE1;
      DD2=EE2;
      Z1=ZB-ZS;
      LINK=PT2;
   DK:R1=X1**2+Z1**2;
      R2=X2**2+Z1**2;
      TA=X1/Z1;
      TB=X2/Z1;
      TT=1+TA*TB;
      TBA=TB-TA;
      THETA=ATAN(TBA,TT);
      EE1=THETA*CB;
      EE2=LOG(R2/R1)*CA;
      GO TO LINK;
  PT2:SM1=SM1+(DD1-EE1)*S1(J);
      SM2=SM2+(DD2-EE2)*S1(J);
      END;
   L6: MK(1,I)=SM1;
      MK(2,I)=SM2;
      END;
      /************* REDUCED MATRIX AND SOLUTION OF VECTOR VALUES *****/
      PUT EDIT('REDUCED MAGNETIC MATRIX')(SKIP(2),X(10),A);
```

```
SBETA:PROC OPTIONS(MAIN);  /* A.INGLES,1970  */

NEST

            PUT EDIT('SYMMETRIC COMPONENTS')(SKIP(1),X(10),A);
            PUT SKIP(1);
            DO I=1 TO N;
1           PUT LIST(MK(1,I));
1           END;
            PUT EDIT('ASSYMMETRIC COMPONENTS')(SKIP(2),X(10),A);
            PUT SKIP(1);
            DO I=1 TO N;
1           PUT LIST(MK(2,I));
1           END;
            DA=0;
            DO I=1 TO N;
1       L7: GET LIST(DA(I));
1           END;
            PUT EDIT('ASSOCIATED FIELD VALUES')(SKIP(2),X(10),A);
            DO I=1 TO N;
1           PUT SKIP EDIT(I,XS(I),DA(I))(X(10),F(5,0),F(10,4),X(5),F(10,2));
1           END;
            IQ=2;  IW=1;
            PUT EDIT('IN-LLSQ')(SKIP(1),X(10),A);
            CALL LLSQ(MK(1,1),DA(1),N,IQ,IW,S2(1),IPAV(1),EPS,IER,AAX(1));
            PUT SKIP LIST(IER);
            PUT EDIT('*COS(BETA) & *SIN(BETA)')(SKIP(2),X(10),A);
        L8: PUT SKIP LIST(S2(1),S2(2));
            TB=ATAND(S2(2),S2(1));
            PUT EDIT('BETA=',TB)(SKIP(1),X(10),A(5),F(7,2));
            HHE=ATAND(SIND(HE),COSD(HE)*SIND(ALFE));
            HHM=TB-HHE;
            PUT EDIT('MU=',HHM)(SKIP(1),X(12),A(3),F(7,2));
            HH=SQRT((S2(1)**2)+(S2(2)**2));
            PUT EDIT('J/P=',HH)(SKIP(2),X(10),A(4),F(14,8));
            END;  /* END BEGIN */
            END SBETA;
```

APPENDIX F

The computer program NUFIL.

This program compares observed and pseudo - magnetic anomalies after normalization by the mean absolute anomaly values in each case. The program is written in PL/1 for use on the N.U.M.A.C. IBM 360/67.

N number of anomaly station points.

M number of block edges in equivalent layer.

NO number of anomaly values at each end of the profile to take part in cosine tapering.

The first part of the program is a transformation gravity to pseudo - magnetic anomaly with the additions:

L8: cosine tapering of observed gravity anomaly.

L9: cosine tapering of observed magnetic anomaly.

Thence,

L10: array DA refilled with values of pseudo - magnetic anomaly.

L11: calculation of mean absolute values of pseudo - magnetic anomaly.

L12: calculation of mean absolute value of observed magnetic anomaly.

L13: printout of normalized observed magnetic anomaly.

L14: printout of normalized pseudo - magnetic anomaly.

L15: scaling of normalized pseudo - magnetic anomaly by product with the mean absolute observed magnetic anomaly.

L16: DC array of length (N) containing values of the residual magnetic anomaly (observed minus scaled pseudo - magnetic anomaly).

L17: S array of length (M - 1) containing values of the block distribution of intensity of magnetisation to satisfy the residual anomaly.

Subroutine GSUB: Calculates the gravity kernel matrix elements.

Subroutine MSUB: Calculates the magnetic kernel matrix elements.

Subroutine TAPSUB: Performs cosine tapering on the NO end values of the observed gravity and magnetic anomaly profiles.

```
FIL:PRCC OPTIONS(MAIN);  /* A.INGLES,APRIL 1971 */


     MUFIL:PROC OPTIONS(MAIN);  /* A.INGLES,APRIL 1971 */
     DCL NAME CHAR(30);
     DCL (N,M,NO,NN) FIXED BIN(31);
     GET LIST(NAME);
     PUT PAGE LIST(NAME);
     GET LIST(N,M,NO);
     NN=2*NO;
     BEGIN;
     DCL (GK(M-1,N),(XS,DA,DB,DC)(N),BX(M),(S,IPIV)(M-1),AUX(2*(M-1)),
     TX(NN)) FLOAT;
     DCL (HM,HE,ALFM,ALFE,ZS,SDAT,XO,XSTEP,BXO,BSTEP,ZT,ZB,A,HHE,HHM,
     BETA,CBETA,SBETA,CA,CB,GOH,EPS,TO1,TO2,YN,YCBA,YOBA) FLOAT;
     DCL (I,J,II,JJ,IQ,IW,IER) FIXED BIN(31);
     /*COMPARISON OF OBSERVED AND CALCULATED MAGNETIC ANOMALIES      */
     /*                  BY NORMALIZATION                            */
  L1:GET LIST(HM,HE,ALFM,ALFE);
  L2:GET LIST(ZS,SDAT);
     IF SDAT<0 THEN DO;
 AL3:GET LIST(XO,XSTEP);
     DO I=1 TO N;
     XS(I)=XO+(I-1)*XSTEP;
     END;
     DO I=1 TO N;
 AL4:GET LIST(DA(I));                    /* GRAVITY */
     END;
     END;
     ELSE DO I=1 TO N;
 BL5:GET LIST(XS(I),DA(I));
     END;
  L6:GET LIST(BXO,BSTEP,ZT,ZB);
     ZT=ZT-ZS;
     ZB=ZB-ZS;
     DO J=1 TO M;
     BX(J)=BXO+(J-1)*BSTEP;
     END;
  L7: DO I=1 TO N;
     GET LIST(DB(I));
     END;
     A=SQRT(((COSD(HE))**2)*((SIND(ALFE))**2)+(SIND(HE))**2)*(((COSD(
     HM))**2)*((SIND(ALFM))**2)+(SIND(HM))**2));
     HHE=ATAND(SIND(HE),COSD(HE)*SIND(ALFE));
     HHM=ATAND(SIND(HM),COSD(HM)*SIND(ALFM));
     BETA=HHE+HHM;
     CBETA=200000.0*COSD(BETA);
     SBETA=200000.0*SIND(BETA);
     CA=0.5*SBETA;
     CB=-CBETA;
     GOH=0.013328;
     PUT EDIT('INCLINATION-BODY MAGNETISATION',HM)(SKIP,X(10),A,F(6,1))
     ;
     PUT EDIT('INCLINATION-EARTHS FIELD',HE)(SKIP,X(10),A,X(6),F(6,1));
     PUT EDIT('AZIMUTH-BODY MAGNETISATION',ALFM)(SKIP,X(10),A,X(4),
     F(6,1));
     PUT EDIT('AZIMUTH-EARTHS FIELD',ALFE)(SKIP,X(10),A,X(10),F(6,1));
     PUT EDIT('SIGMA',HHE)(SKIP,X(10),A,F(8,1));
     PUT EDIT('MU',HHM)(SKIP,X(10),A,X(3),F(8,1));
```

```
UFIL:PROC OPTIONS(MAIN);  /* A.INGLES,APRIL 1971 */

T

      PUT SKIP(2);
      PUT SKIP EDIT('OBSERVED GRAVITY AND MAGNETIC ANOMALIES')(X(10),A);
      DO I=1 TO N;
      PUT SKIP EDIT(I,XS(I),ZS,DA(I),DB(I))(X(10),F(5,0),F(10,4),X(5),
      F(3,1),X(5),F(10,1),X(5),F(10,1));
      END;
      PUT SKIP(2);
      PUT SKIP EDIT('BLOCK CONFIGURATION')(X(10),A);
      DO J=1 TO M;
      PUT SKIP EDIT(J,BX(J),ZT,ZB)(X(10),F(5,0),F(10,4),F(10,4),F(10,4))
      ;
      END;
      DO I=1 TO NC;
      TX(I)=DA(I);
      II=N-NO+I;
      JJ=NO+I;
      TX(JJ)=DA(II);
      END;
   L8: CALL TAPSUB(TX,NN,NO);
      DO I=1 TO NO;
      DA(I)=TX(I);
      II=N-NO+I;
      JJ=NO+I;
      DA(II)=TX(JJ);
      END;
      PUT SKIP EDIT('TAPERED',NO,'GRAVITY VALUES')(X(10),A,X(1),F(2),
      X(1),A);
      PUT SKIP(1);
      DO I=1 TO NN;
      PUT EDIT(TX(I))(F(10,1));
      END;
      DO I=1 TO NC;
      TX(I)=DB(I);
      II=N-NO+I;
      JJ=NO+I;
      TX(JJ)=DB(II);
      END;
   L9: CALL TAPSUB(TX,NN,NO);
      DO I=1 TO NO;
      DB(I)=TX(I);
      II=N-NO+I;
      JJ=NO+I;
      DB(II)=TX(JJ);
      END;
      PUT SKIP EDIT('TAPERED',NO,'MAGNETIC VALUES')(X(10),A,X(1),F(2),
      X(1),A);
      PUT SKIP(1);
      DO I=1 TO NN;
      PUT EDIT(TX(I))(F(10,1));
      END;
      GK=0;
      CALL GSUB(GK,XS,BX,ZT,ZB,GOH,N,M);
      DO J=1 TO M-1;
      DO I=1 TO N;
```

```
NUFIL:PROC OPTIONS(MAIN);  /* A.INGLES,APRIL 1971 */

NEST

  2          GK(J,I)=GK(J,I)*1000.0;
  2          END;
  1          END;
             EPS=C.0001;
             IW=M-1;
             IQ=1;
             PUT SKIP EDIT('IN-LLSQ')(A);
             CALL LLSQ(GK(1,1),DA(1),N,IW,IQ,S(1),IPIV(1),EPS,IER,AUX(1));
             PUT SKIP LIST(IER);
             IF IER¬=0 THEN DO;
  1          PUT EDIT('FAILURE IN LLSQ')(SKIP,A);
  1          GO TO LE;
  1          END;
             ELSE;
             PUT EDIT('DENSITY DISTRIBUTION')(SKIP(2),A);
             PUT SKIP(1);
             DO J=1 TO M-1;
  1          PUT EDIT(S(J))(X(6),F(14,6));
  1          END;
          L10: DA=0;
             GK=0;
             CALL MSUB(GK,XS,BX,ZT,ZB,CA,CB,A,N,M);
             DO I=1 TO N;
  1          DO J=1 TO M-1;
  2          DA(I)=DA(I)+(GK(J,I)*S(J));
  2          END;
  1          END;
          L11: TO1=0;
             DO I=1 TO N;
  1          TC1=TO1+ABS(DA(I));
  1          END;
             YN=N*1.0;
             YCBA=TO1/YN;
          L12: TO2=0;
             DO I=1 TO N;
  1          TO2=TO2+ABS(DB(I));
  1          END;
             YOBA=TO2/YN;
             DO I=1 TO N;
  1          DC(I)=DB(I)/YOBA;
  1          END;
             PUT EDIT('NORMALIZED OBSERVED MAGNETIC ANOMALY')(SKIP(2),A);
             PUT SKIP(1);
          L13: DC I=1 TO N;
  1          PUT EDIT(I,DC(I))(X(2),F(3),X(3),F(12,4));
  1          END;
             DO I=1 TO N;
  1          DA(I)=DA(I)/YCBA;
  1          END;
             PUT EDIT('NORMALIZED CALCULATED MAGNETIC ANOMALY')(SKIP(2),A);
             PUT SKIP(1);
          L14: DO I=1 TO N;
  1          PUT EDIT(I,DA(I))(X(2),F(3),X(3),F(12,4));
  1          END;
```

```
NUFIL:PROC OPTIONS(MAIN);  /* A.INGLES,APRIL 1971 */

ST

      L15: DO I=1 TO N;
1        DA(I)=DA(I)*YOBA;
1        END;
         PUT EDIT('OBSERVED,SCALED CALCULATED AND RESIDUAL ANOMALIES')
         (SKIP(2),A);
      L16: DO I=1 TO N;
1        DC(I)=DB(I)-DA(I);
1        END;
         DO I=1 TO N;
1        PUT SKIP EDIT(I,XS(I),DB(I),DA(I),DC(I))(F(5),X(5),F(8,3),
         X(5),F(10,2),F(10,2),F(10,2));
1        END;
         S=0;
         CALL LLSQ(GK(1,1),DC(1),N,IW,IQ,S(1),IPIV(1),EPS,IER,AUX(1));
         PUT SKIP LIST(IER);
         IF IER¬=0 THEN DO;
1        PUT SKIP EDIT('FAILURE IN LLSQ')(A);
1        GO TO LE;
1        END;
         ELSE;
         PUT EDIT('DISTRIBUTION OF MAGNETISATION DUE TO RESIDUALS')(SKIP(2)
         ,A);
      L17: DO J=1 TO M-1;
1        PUT SKIP EDIT(J,S(J))(X(5),F(5),X(5),F(10,6));
1        END;
         GO TO LE;
         GSUB:PROCEDURE(GK,XS,BX,ZT,ZB,GOH,N,M);
         DCL (GK(M-1,N),XS(N),BX(M)) FLOAT;
         DCL ((X,Z)(5),(SS,CC)(4)) FLOAT;
         DCL (X1,Z1,R1,FI1,X2,Z2,R2,FI2,H,W) FLOAT;
         DCL (I,J,K,M,N) FIXED BIN(31);
         DO J=1 TO M-1;
1        X(1),X(2),X(5)=BX(J);
1        X(3),X(4)=BX(J+1);
1        Z(1),Z(4),Z(5)=ZT;
1        Z(2),Z(3)=ZB;
1        DO I=1 TO N;
2        X1=X(1)-XS(I);
2        Z1=Z(1);
2        R1=X1**2+Z1**2;
2        FI1=(1.5708-ATAN(X1,Z1));
2        DO K=1 TO 4;
3        X2=X(K+1)-XS(I);
3        Z2=Z(K+1);
3        R2=X2**2+Z2**2;
3        FI2=(1.5708-ATAN(X2,Z2));
3        H=SQRT((X(K)-X(K+1))**2+(Z(K+1)-Z(K))**2);
3        SS(K)=(Z(K+1)-Z(K))/H;
3        CC(K)=(X(K)-X(K+1))/H;
3        W=0.5*SS(K)*LOG(R2/R1)+CC(K)*(FI2-FI1);
3        GK(J,I)=GK(J,I)+GOH*(Z2*FI2-Z1*FI1-W*(X1*SS(K)+Z1*CC(K)));
3        X1=X2;  Z1=Z2;  R1=R2;  FI1=FI2;
3        END;
2        END;
```

```
NUFIL:PROC OPTIONS(MAIN);  /* A.INGLES,APRIL 1971 */

NEST

1           END;
            END GSUB;
            MSUB:PROCEDURE(GK,XS,BX,ZT,ZB,CA,CB,A,N,M);
            DCL (GK(M-1,N),XS(N),BX(M)) FLOAT;
            DCL (X1,X2,Z1,DD,EE,R1,R2,T1,T2,TT,TBA,THETA) FLOAT;
            DCL (I,J,M,N) FIXED BIN(31);
            DCL LINK LABEL;
            DO I=1 TO N;
1           DO J=1 TO M-1;
2           X1=BX(J)-XS(I);
2           X2=BX(J+1)-XS(I);
2           Z1=ZT;
2           LINK=LS1;
2           GO TO LS2;
2       LS1:DD=EE;
2           Z1=ZB;
2           LINK=LS3;
2       LS2:R1=X1**2+Z1**2;
2           R2=X2**2+Z1**2;
2           T1=X1/Z1;
2           T2=X2/Z1;
2           TT=1+T1*T2;
2           TBA=T2-T1;
2           THETA=ATAN(TBA,TT);
2           EE=THETA*CB+LOG(R2/R1)*CA;
2           GO TO LINK;
2       LS3:GK(J,I)=(DD-EE)*A;
2           END;
1           END;
            END MSUB;
            TAPSUB:PROCEDURE(TX,NN,NO);
            DCL TX(NN) FLOAT;
            DCL (NN,NO,I,IA,IN) FIXED BIN(31);
            DCL (PI,ANO,PHI,CPHI,SPHI,CTHET1,STHET1,CTHET2,STHET2) FLOAT;
            PI=4.0*ATAN(1.0);
            ANO=(NO-1)*1.0;
            PHI=PI/ANO;
            CPHI=COS(PHI);
            SPHI=SIN(PHI);
            CTHET1=1.0;
            STHET1=0.0;
            CTHET2=1.0;
            STHET2=0.0;
            DO I=1 TO NO;
1           IA=NN-I+1;
1           IN=I;
1           TX(IN)=0.5*TX(IN)*(1.0-CTHET2);
1           TX(IA)=0.5*TX(IA)*(1.0-CTHET2);
1           CTHET2=CTHET1*CPHI-STHET1*SPHI;
1           STHET2=STHET1*CPHI+CTHET1*SPHI;
1           CTHET1=CTHET2;
1           STHET1=STHET2;
1           END;
            END TAPSUB;
```

```
NUFIL:PROC OPTIONS(MAIN);  /* A.INGLES,APRIL 1971 */

STMT LEVEL NEST

265    2          LE:END;  END NUFIL;
```

APPENDIX G.

THE DIFFERENCE IN DEPTH TO MAGNETIC SOURCES.

If a two-dimensional magnetic anomaly fourier component has an amplitude A_o, as measured on the x - axis, and a wavelength $\lambda = 2\pi/k$, it may be written down as a solution to Laplace's Equation as,

$$A(x) = A_o \sin kx$$

and at a depth of z, for positive z and k, as

$$A(x,z) = A_o e^{kz} \sin kx \qquad \text{(G.1.)}$$

(Bott and Stacey, 1967).

Now, if two identical sources at different z_1 and z_2 produce magnetic fourier component amplitudes A_1 and A_2 as measured at z = 0, then the depth difference may be calculated from

$$\frac{A_1}{A_2} = e^{k(z_1 - z_2)}$$

or

$$(z_1 - z_2) = \frac{1}{k} \log_e \left(\frac{A_1}{A_2}\right) \qquad \text{(G.2)}$$